

¹ **Biotransformations from and to
² methylated flavonoids**

³ Dissertation

⁴ zur Erlangung des Doktorgrades der
⁵ Naturwissenschaften
⁶ (Dr. rer. nat)

⁷ der

⁸ Naturwissenschaftlichen Fakultät II
⁹ Chemie, Physik und Mathematik

¹⁰ der Martin-Luther-Universität
¹¹ Halle-Wittenberg

¹² vorgelegt von
¹³ Herr Benjamin Weigel
¹⁴ geb. am 06. April 1986 in Bernburg (Saale)

¹⁵ Gutachter:
¹⁶ 1. Prof. Dr. Ludger A. Wessjohann (Martin-Luther Universität Halle-
¹⁷ Wittenberg)
¹⁸ 2. zweiter Gutachter

¹⁹ Halle (Saale), November 2, 2015

1

It is what it is. Accept it and move on.

2

– *unknown* –

Contents

2	Contents	iii
3	List of Figures	vii
4	List of Tables	xiv
5	List of Schemes	xvii
6	I Preface	1
7		—
8	1 Abstracts	2
9	1.1 English Abstract	2
10	1.2 Deutsche Zusammenfassung	3
11	2 List of Publications	5
12	II Thesis	6
13		—
14	3 Introduction and Motivation	7
15	3.1 Flavonoids	7
16	3.1.1 Overview	7
17	3.1.2 The phenyl propanoid pathway	9
18	3.1.3 Biological activity	9
19	3.2 Methyl transferases (MTs)	10
20	3.2.1 Overview	10
21	3.2.2 S-Adenosyl-L-methionine	14
22	3.2.3 Methyl transferase mechanisms	15
23	3.2.4 Plant O-methyl transferases (O-MTs)	17
24	3.3 Alkylation and biotransformations	19
25	3.3.1 Overview	19
26	3.3.2 Methyl transferases for industrial use	20
27	3.3.3 Artificial SAM analogues	22
28	3.4 Motivation	23

1	4 Material And Methods	25
2	4.1 Materials	25
3	4.1.1 Chemicals	25
4	4.1.2 Commonly used solutions and buffers	25
5	4.1.3 Culture media used to grow bacteria	26
6	4.1.4 Bacterial strains	27
7	4.1.5 Plasmids	28
8	4.1.6 Oligonucleotides and synthetic genes	28
9	4.1.7 Instruments	28
10	4.1.8 Software	29
11	4.2 Molecular Biology	30
12	4.2.1 Golden Gate Cloning	30
13	4.2.2 Subcloning of genes	31
14	4.2.3 Transformation of electrocompetent <i>Agrobacterium</i> <i>tumefaciens</i> cells	32
15	4.3 Treatment of plant material	32
16	4.3.1 Infiltration of <i>Nicotiana benthamiana</i>	32
17	4.3.2 Plant material harvest	33
18	4.3.3 Extraction of flavonoids from <i>N. benthamiana</i> leaves .	33
19	4.4 Protein biochemistry	33
20	4.4.1 Determination of protein concentration	34
21	4.4.2 Protein production test (expression test)	34
22	4.4.3 Protein subfractionation	35
23	4.4.4 Protein sample concentration by TCA precipitation .	35
24	4.4.5 Preparation of periplasmic protein	36
25	4.4.6 Discontinuous SDS-polyacrylamide gel electrophoresis (SDS-PAGE)	36
26	4.4.7 Buffer change of protein samples	37
27	4.4.8 Production of recombinant protein	37
28	4.4.9 Preparation of inclusion bodies (IBs)	38
29	4.4.10 Purification of His-tagged proteins using immobilized metal affinity chromatography (IMAC)	39
30	4.4.11 Refolding of SOMT-2 on a micro scale using design of experiments (DoE)	39
31	4.4.12 Enzymatic production of SAM and SAE	41
32	4.5 Crystallographic Procedures	42
33	4.5.1 Crystallization of proteins	42
34	4.5.2 Data collection and processing	43
35	4.5.3 Structure solution	44
36	4.5.4 Model building, refinement and validation	44
37	4.5.5 <i>In silico</i> substrate docking	45
38	4.6 Analytics	45
39	4.6.1 Recording of growth curves	45
40	4.6.2 <i>In vitro</i> determination of glucose	46
41	4.6.3 <i>In vitro</i> O-methyl transferase (O-MT) assay	46

1	4.6.4 Photospectrometric assay for the methylation of catecholic moieties	49
3	4.6.5 Concentration of SOMT-2 using hydrophobic interaction chromatography (HIC)	49
5	4.6.6 Analytical gel filtration.	50
7	4.6.7 Binding experiments using Isothermal Titration Calorimetry (ITC)	50
9	4.6.8 High-performance liquid chromatography (HPLC) analytics	50
10	4.6.9 Liquid chromatography-tandem mass spectrometry (LC-MS/MS) measurements	51
12	5 Engineering of phenylpropanoid and flavonoid O-methyl transferase (PFOMT)	53
14	5.1 Introduction	54
15	5.2 Crystallization of PFOMT	56
16	5.3 Substrate binding studies using ITC.	59
17	5.4 Study of variants for long-chain alkylations	61
18	5.5 Conclusion/Discussion	63
19	5.6 Contributions	65
20	6 Tandem mass-spectrometry studies of flavonoids	66
21	6.1 Introduction	67
22	6.2 Fragmentation of flavanones	69
23	6.3 Fragmentation of flavones	72
24	6.4 Fragmentation of flavonols	78
25	6.5 Conclusions	83
26	6.6 Contributions	84
27	7 Enzymatic methylation of non-catechols	85
28	7.1 Introduction	86
29	7.2 SOMT-2.	87
30	7.2.1 <i>In vivo</i> biotransformation in <i>Nicotiana benthamiana</i> .	87
31	7.2.2 <i>In vivo</i> biotransformation in <i>E. coli</i>	89
32	7.2.3 <i>In vitro</i> studies using recombinantly produced SOMT-2	93
33	7.3 PFOMT	100
34	7.3.1 Phenolic hydroxyls	100
35	7.3.2 PFOMT pH-profiles are influenced by Mg ²⁺	101
36	7.3.3 Methylation of different chemical motifs.	106
37	7.4 Conclusion	111
38	8 Summary	113
39	9 Acknowledgements	115
40	10 Affidavit	116

III Appendix

117

3A Engineering of PFOMT	118
4B Tandem mass-spectrometry studies of flavonoids	120
5C Enzymatic methylation of non-catechols	124
6 C.1 SOMT expression studies	124
7 C.2 Conversion of non-catechols by PFOMT	128
8 C.2.1 Modelling and shrinkage of catechols subset (pH profile)	128
9 C.3 Identification of products from conversion of non-catechols	
10 by PFOMT	129
11 C.3.1 <i>p</i> -Coumaric acid methylester	129
12 C.3.2 <i>iso</i> -Ferulic acid esters and caffeic acid dimethylether .	130
13 C.3.3 3',4'-dimethyl eriodictyol	130
14 C.3.4 3',4'-dimethyl luteolin	132
15D Additional information	134
16 Bibliography	156
17 Acronyms	157
18 Glossary	161

List of Figures

2 3.1 The central feature of the flavonoids is the chromane ring. The 3 names of the different groups of flavonoids are derived from 4 the substitution of this moiety. From a biosynthetic point of 5 view, flavonoids are built up from phenylpropanoid (blue) and 6 acetate derived moieties (orange).	8
7 3.2 General pathways in the biosynthesis of flavonoids. PAL – 8 phenylalanin ammonia lyase, C4H – cinnamate-4-hydroxylase, 9 4CL – 4-coumarate:CoA ligase, CHS – chalcone synthase, CHI 10 – chalcone isomerase, F3H – flavanone-3-hydroxylase, FLS – 11 flavonol synthase, FNS – flavone synthase, IFS – isoflavone 12 synthase.	10
13 3.3 Topology plots of the five major structural classes of methyl 14 transferases and radical SAM methyl transferases (RSMTs) 15 (modified and extended from Schubert <i>et al.</i> [174]). Helices are 16 depicted as circles and β -strands as triangles. The SAM bind- 17 ing site is depicted as a flag. Radical SAM methyl transferases 18 all share a common “radical SAM”-domain, which cotains the 19 iron sulfur cluster (red checker). The individual radical SAM 20 methyl transferase classes are differentiated according to the 21 other domains they contain.	12
22 3.4 Reactions catalyzed by methyl transferases (MTs). Different 23 shades of gray were used to differantiate between different 24 groups of compounds and methyl transferases. In contrast to 25 other methyl transferases, the group of radical SAM methyl 26 transferases also requires additional co-factors to SAM. . . .	13

1	3.5 Mechanism of the methyl transfer reaction catalyzed by methyl 2 transferases. Non-radical S-adenosyl-L-methionine dependent 3 methyl transferases catalyze the nucleophilic transfer of a 4 methyl group from the donor S-adenosyl-L-methionine to a nu- 5 cleophile (Nu; e.g. O,N,C,S). A proton (H^+) is usually abstracted 6 through a general base (B), to achieve activation of the nucle- 7 ophile. The proton is later transferred to the aqueous medium. 8 The S_N2 reaction proceeds via a single transition state, during 9 which the methyl-carbon is sp^2 hybridized. After transfer of 10 the methyl to the nucleophile the carbon's configuration is 11 inverted.	15
12	3.6 Bioenzymatic synthesis of chiral acetate, the precursor for the 13 synthesis of SAM carrying an assymetrical methyl, as used 14 by Woodward <i>et al.</i> [223]. Ring hydroxyls of hexoses and 15 pentoses are omitted for easier reading. HK – hexokinase, 16 PGI – phosphoglucose isomerase, PFK – phosphofructokinase, 17 ALD – aldolase, TIM –triose phosphate isomerase, G3PDH – 18 glyceraldehyde-3-phosphate dehydrogenase, PGM – phos- 19 phoglycerate mutase, ENO – enolase, Glu – glucose, F1,6BP – 20 fructose-1,6-bisphosphate, 3PG – 3-phosphoglycerate, PEP – 21 phosphoenol pyruvate	16
22	3.7 Natural products synthesized with the help of methyl trans- 23 ferases. O-methyl transferases were used for the synthe- 24 sis of ermanine (1), 7-O-methyl-aromadendrin (2) and 3,5- 25 dimethoxy-4'-fluorostilbene (3). N-MT catalyze the production 26 of epinephrine (4) and N-methyltetrahydroisoquinoline (5), 27 whereas 3-(benzoylamino)-8-methylumbelliferone (6) and 28 furfuryl-methyl-sulfide (7) can be produced by C-methyl 29 transferase (C-MT) and S-methyl transferase (S-MT)	21
30	3.8 Labelling of macromolecules by using a combination of novel 31 alkine-derivatized S-adenosyl-L-methionine analogues and 32 Cu ^I -catalyzed azide-alkyne 1,3-dipolar cycloaddition (CuAAC). 33 Depending on the type of label used, it can be employed 34 for detection (e.g. through fluorophores, coupled assays) or 35 affinity purification (e.g. biotin). This technique might also be 36 also feasable for use in activity based protein profiling (ABPP) 37 approaches.	22
38	4.1 Golden Gate cloning scheme for SOMT-2	31
39	4.2 Pruned <i>N. benthamiana</i> plant, with two bottom and one top 40 leaf, ready to be infiltrated.	33

1	4.3 Oxidation of the reporter substrate <i>o</i> -dianisidine. Consecutive	
2	one-electron transfers lead to the fully oxidized diimine form of	
3	<i>o</i> -dianisidine. The first electron transfer is believed to produce	
4	a charge transfer complex intermediate. [31, 91]	47
5	5.1 Some crystal and pseudo-crystal shapes that were observed	
6	during the crytsallization screen. a – high $(\text{NH}_4)_2\text{SO}_4$, b-c –	
7	CaCl_2 , PEG-4000, e – LiCl , PEG-6000	56
8	5.2 An overview of the features in the <i>apo</i> -PFOMT structure. a	
9	– The assymetric unit of <i>apo</i> -PFOMT consists of two homod-	
10	imers (4 monomers). Individual monomers are rainbow colored	
11	from N- (blue) to C-terminus (red). b – Comparison of 3C3Y	
12	(steelblue) and <i>apo</i> -PFOMT (green). The N-terminus of <i>apo</i> -	
13	PFOMT was resolved up to the N-terminus (red) and even the	
14	His-tag (red, transparent) was partly resolved. The N-terminus	
15	fits into a cleft on the surface of the 3C3Y structure, shown as	
16	a surface model on the right. SAH (white ball-and-sticks) and	
17	Ca^{2+} (green sphere) are featured in the published structure,	
18	whereas a sulphate ion (red/yellow spheres) was bound in the	
19	newly solved structure.	58
20	5.3 Positional differences between the individual residues of the	
21	solved <i>apo</i> -PFOMT and the structure with bound SAH (pdb:	
22	3C3Y). The diffraction precision indicator [46] (DPI) of the	
23	structures was (0.137 and 0.064) Å respectively. The overall	
24	rmsd amounted to 0.9034 Å. The secondary structure of apo-	
25	PFOMT is displayed at the top. Helices are displayed as rect-	
26	angles and sheets are shown as arrows. Graphical background	
27	annotations are used to display the binding sites of SAH (green)	
28	and the metal ion (plum). The orange bars indicate regions,	
29	where much movement seems to happen upon binding or re-	
30	lease of the co-substrate. The blue bar shows the region that	
31	was annotated as "insertion loop" in previous studies [109].	59
32	5.4 The binding of different SAM analogues was measured via ITC	59
33	5.5 ITC measurements of PFOMT:effector binding. a – Binding	
34	of SAH, SAM and SAE to PFOMT. b – SAH is injected into	
35	a PFOMT solution, with (red) or without (black) addition of	
36	Mg^{2+} and caffeic acid. When Mg^{2+} and caffeic acid were already	
37	present, the binding process seems to happen quicker, but is	
38	less enthalpic. c – Upon addition of caffeic acid to the protein	
39	heat is produced, however no sensible binding curve could be	
40	obtained.	61

1	5.6 The active site of PFOMT (pdb: 3C3Y). The outline of the pro-	
2	tein backbone is displayed, with active site residues portrayed	
3	as colored sticks (cyan – F103, red – F80, turquoise – M52,	
4	yellow – Y51, white – F198, blue – W184, orange – N202, grey	
5	– as labelled). The co-substrate SAM (ball-and-stick model)	
6	was docked into the structure.	62
7	5.7 Activities of different PFOMT variants towards caffeic acid	
8	methylation. Colorations correspond to the ones used in Fig-	
9	ure 5.6.	63
10	5.8 Comparison of the active sites of a – the solved <i>apo</i> -structure	
11	(green) and b – the ligand-bound structure (steelblue; pdb:	
12	3C3Y). Waters are represented as small red spheres, calcium	
13	as a green sphere (complexing bonds are dashed) and SAH is	
14	displayed as a white ball-and-stick model. A possible hydrogen	
15	bond network (blue lines) for the ligand-bound state is displayed.	64
16	6.1 Comparison of CID and HCD MS ² spectra of eriodictyol (2). A	
17	– CID at 45 % NCE. B – HCD at 75 % NCE. C – HCD at 100 %	
18	NCE. Four different prominent peaks are annotated in each	
19	spectrum. D – The shift to smaller masses in HCD spectra	
20	and with increasing NCE is illustrated by the boxplot of the	
21	distribution of peaks with relative intensities above 1 % in each	
22	of the above spectra. E – Relationship between the activation	
23	method and the intensity of four fragments (● ^{1,3} A ⁺ , ▲ ^{1,4} B ⁺ -	
24	2H), ■ (^{1,4} B ⁺ -2H-CO), + C ₇ H ₅ ⁺) of different flavanones. . .	71
25	6.2 Comparison of CID and HCD MS ² spectra of chrysoeriol (10). A	
26	– CID at 45 % NCE. B – HCD at 75 % NCE. C – HCD at 100 %	
27	NCE. Four different prominent peaks are annotated in each	
28	spectrum. D – The shift to smaller masses in HCD spectra	
29	and with increasing NCE is illustrated by the boxplot of the	
30	distribution of peaks with relative intensities above 1 % in each	
31	of the above spectra.	75
32	6.3 Comparison of CID and HCD MS ² spectra of isorhamnetin	
33	(15). A – CID at 45 % NCE. B – HCD at 75 % NCE. C – HCD	
34	at 100 % NCE. Four different prominent peaks are annotated in	
35	each spectrum. D – The shift to smaller masses in HCD spectra	
36	and with increasing NCE is illustrated by the boxplot of the	
37	distribution of peaks with relative intensities above 1 % in each	
38	of the above spectra.	81

1	7.1 Semi-synthetic pathway to naringenin and 4'-O-methyl narin-	
2	genin in <i>N. benthamiana</i> . Enzymes not endogenous to <i>N. ben-</i>	
3	thamiana are in gray. PAL - phenylalanine ammonia lyase,	
4	C4H - cinnamic acid 4-hydroxylase, 4CL - 4-coumaric acid:CoA	
5	ligase, CHS - chalcone synthase, CHI - chalcone isomerase,	
6	SOMT2 - soy O-methyl transferase 2	88
7	7.2 Scatterplot of the first two principal components from the PCA	
8	of the HPLC data obtained from leaf material extracts. The	
9	samples are colored by leaf side (left/SOMT-2: red, right/vector	
10	control: cyan).	89
11	7.3 Biotransformation methods as described by Kim <i>et al.</i> (A) and	
12	developed in this work (B). OD – optiocal density at 600 nm,	
13	LB – LB-medium, AI – AI-medium.	90
14	7.4 The masses resulting from the fragmentation into A- and B-	
15	ring along the C-ring (dashed line, b) are evidence, that the	
16	4'-hydroxyl on the B-ring is methylated by SOMT-2	92
17	7.5 SDS-PAGE of pET28a(+) SOMT-2 expressed in <i>E. coli</i> BL21(DE3)	
18	in autoinduction medium at different temperatures (shown	
19	above). The insoluble fractions show a protein band the same	
20	height as the 40 kDa marker band, which corresponds to the	
21	SOMT-2 protein (40 425 Da). M – protein size marker, S – solu-	
22	ble fraction, I – insoluble fraction	94
23	7.6 SDS-PAGE of the insoluble and soluble fractions of the refolding	
24	reactions. Refolding reactions 2,3,8-11 seem to mainly produce	
25	misfolded insoluble protein, while the other refolding buffers	
26	(1,4-7,12) produce soluble protein.	95
27	7.7 Results of <i>in vitro</i> protein refolding trials. Measured data (left)	
28	is presented alongside the ME-plots (right). The dashed line	
29	through the ME-plots illustrates the overall mean. a – Protein	
30	concentration after refolding and rebuffering into a universal	
31	buffer. The highest yield of soluble protein was achieved in	
32	buffers 5 and 7. The ME-plots (b) illustrate the connection	
33	between a factor and the measured protein concentration, sug-	
34	gesting that high pH and arginine concentration might have	
35	been beneficial in the refolding reactions. c – Calculated con-	
36	version of naringenin to ponciretin by the refolded protein	
37	fractions. Protein refolded in buffers 1 and 7 seem to afforded	
38	the most active protein by conversion (~volume activity). The	
39	ME-plots for the conversion (d) show that the redox state (re-	
40	ducing) of the refolding environment was important to achieve	
41	active protein.	96

1	7.8 CD-spectrum of refolded SOMT-2 (black) compared to the spec-		
2	trum that was calculated (red) by the K2D3 web service (http://cbdm-01.zdv.uni-mainz.de/~andrade/k2d3//index.html) from		
3	the SOMT-2 sequence. Secondary structure estimates from the		
4	measured spectrum are 12.39 % α -helix and 32.51 % β -sheet.	99	
6	7.9 Specific activity/pH-profiles for the conversion of three different substrates (● caffeoic acid, ▲ eriodictyol, ■ iso-ferulic acid) by PFOMT. The specific activity for the non-catecholic substrate iso-ferulic acid was much lower than the specific activity for the catecholic substrates. When magnesium is omitted, the activity is increased by increasing the pH	102	
12	7.10 pH-profiles of substrate conversion along with predicted data. Predicted data from the linear regression models (blue, dashed lines) grasp the general trend of the data reasonably well to draw inferences. 95 % prediction intervals are displayed as shaded areas.	105	
17	7.11 Conversion of multiple different substrates, catecholic and non-catecholic, by PFOMT wild-type (a) and the 4'-specific variant Y51R N202W (b). Every individual box represents one substrate <i>p</i> -coumaric acid (A.1), . . . , chrysoeriol (C.4). pH/Mg ²⁺ -conditions are color coded from light to dark: ✕/✗, ✕/✓, ✗/✗, ✗/✓. — ✕(low pH), ✗(high pH), ✗(no Mg ²⁺), ✓(yes, Mg ²⁺)	108	
23	A.1 Differences in the dihedrals ψ (red) and φ (black) of the solved apo-PFOMT and the structure with bound SAH (pdb: 3C3Y). The secondary structure is displayed at the top. Helices are displayed as rectangles and sheets are shown as arrows. Graphical background annotations are used to display the binding sites of SAH (green) and the metal ion (plum). The orange bars indicate regions, where much movement seems to happen upon binding or release of the co-substrate. The blue bar shows the region that was annotated as "insertion loop" in previous studies.	119	
32	A.2 Differences in the regioselectivity of some PFOMT variants. The products observed in HPLC and LC/MS measurements switched from 3'-methylated (dark grey) to 4'-methylated (light grey) for the displayed variants. The height of the bars corresponds to the total conversion of substrate.	119	
37	C.1 Additional scatterplots of the PCA of HPLC data obtained from <i>N. benthamiana</i> leaves infiltrated by <i>A. tumefaciens</i> harbouring different constructs. A – samples colored by leaf position (top: red; bottom: cyan), B – samples colored by plant (plant 1: red; plant 2: green; plant 3: blue)	124	

1 C.2 Growth curve of <i>E. coli</i> BL21(DE3) expressing soy O-methyl 2 transferase (SOMT-2) at 37 °C. Glucose is depleted about 3 5 hours into growth, at which point the start of SOMT-2 4 expression is expected. The OD ₆₀₀ after inoculation was about 5 0.1.	125
6 C.3 SDS-PAGE gel of samples aquired during growth curve mea- 7 surements. The arrow indicates the band that could correspond 8 to the GST-tagged SOMT-2 protein.	126
9 C.4 Graphical representation of a SOMT-2 model obtained from the 10 PHYRE2 web portal (http://www.sbg.bio.ic.ac.uk/phyre2/html/ page.cgi?id=index) [98]. Cysteines are shown as sticks. The 11 distance between neighboring cysteines that could by oxidized 12 to disulfide bridges is shown in orange.	127
13 C.5 Chromatogram of the gel filtration analysis of refolded SOMT- 14 2 (blue). Gel-filtrations standards (red) were used to assess 15 the size of the SOMT-2 protein. The estimated molecular 16 weights for the eluting peaks were 165 kDa (12.47 ml) and 17 65.5 kDa (14.26 ml). Protein standard: 9.15 ml – thyroglobulin 18 (670 kDa), 12.62 ml – γ-globulin (158 kDa), 15.43 ml – ovalbu- 19 min (44 kDa), 17.63 ml – myoglobin (17 kDa), 21.11 ml – vita- 20 min B12 (1.35 kDa)	127
21 C.6 MS ² spectra of (1) and (3). (a) negative mode MS ² of (1). (b) 22 positive mode MS ² of (1). (c) positive mode MS ² of (3).	131
23 C.7 MS ² spectra of 3'4'-dimethyl eriodictyol (4). (a) positive mode 24 MS ² CID spectrum of (4). (b) positive mode MS ² HCD spectrum 25 of (4).	132
26 C.8 MS ² spectra of 3'4'-dimethyl luteolin (5). (a) positive mode MS ² 27 CID spectrum of (5). (b) positive mode MS ² HCD spectrum of 28 (5).	133
29 C.9 Product composition after conversion of flavones with PFOMT. 30 Bar chart of the the peak heights of the unidentified (black) 31 and (3' or 4')-O-methylated products (gray) in the selected ion 32 chromatograms (HCD at 100 % NCE). The conversion exper- 33 iments were conducted with the wild-type PFOMT at pH 8.6 34 with 10 mM Mg ²⁺ added.	133

List of Tables

2	3.1 Defining motifs of plant <i>O</i> -MTs as described by Joshi <i>et al.</i> [92].	18
3	4.1 Natural deep eutectic solvent (NADES)-mixtures used within	
4	this work.	26
5	4.2 Plasmids used in this work.	28
6	4.3 Primers used in this work. Recognition sites for endonucleases	
7	are underlined. Positions used for site directed mutagenesis	
8	are in lower case font.	30
9	4.4 Calculated extinction coefficients of proteins used in this work.	34
10	4.5 Factors and their high and low levels (+/-) used in the construc-	
11	tion of the fractional factorial design (FrFD).	40
12	4.6 Experimental design matrix for the FrFD.	40
13	5.1 Results of fitting a simple one-site binding model to the data	
14	obtained from ITC experiments.	60
15	7.1 Naringenin and 4'-methylated derivatives that were inquired	
16	for in the plant samples via HPLC. The core structure of the	
17	compounds is displayed on the left.	89
18	7.2 <i>In vivo</i> biotransformation of different flavonoids, phenyl-	
19	propanoids and anthraquinones by SOMT-2 in <i>E. coli</i> . Conver-	
20	sion ratios were calculated for samples taken after 30 hours.	
21	Multiple substrates containing a 4'-hydroxyl were methyl-	
22	ated. Calculation of conversion percentages are only rough	
23	estimates, because of the nature of crude medium extracts.	
24	Products were determined by LC-MS/MS.	91
25	7.3 p <i>K</i> _a -values of phenolic hydroxyl groups exemplified by <i>p</i> -	
26	cresole derivatives. Substituent positions on the aromatic ring	
27	are arbitrary and do not reflect conventions of the International	
28	Union of Pure and Applied Chemistry (IUPAC).	101

1	7.4 Maximum specific activity for the conversion of three different substrates with and without addition of magnesium. The pH at which the maximal activity was reached is indicated by the column titled “pH”.	103
5	7.5 Coefficients of the model (Equation 7.1) for activity of <i>iso</i> -ferulic acid methylation. The factor Mg is a categorical variable (addition/no addition) and can therefore only be 0 or 1.	104
8	7.6 Substrate grid that was tested for methylation with PFOMT. Four different groups of compounds were screened. The groups of flavones, flavanones and cinnamic acids each contained one representative of each motif, phenolic, catecholic, 3'-hydroxy-4'-methoxy (3O4M) and 4'-hydroxy-3'-methoxy (4O3M).	107
13	7.8 Conversion of substrates after 16 hours incubation. Only the maximum conversion is displayed, along with the conditions it was achieved under.	109
16	7.9 Products of the enzymatic methylation of the studied substrates. The products were confirmed by authentic standards or via LCMS.	110
19	A.1 Crystallographic data, phasing and refinement statistics.	118
20	B.1 Key ions in the positive mode CID and HCD ESI-MS ² spectra of flavanones.	121
22	B.2 Key ions in the positive mode CID and HCD ESI-MS ² spectra of flavones.	122
24	B.3 Key ions in the positive mode CID and HCD ESI-MS ² spectra of flavonoles.	123
26	C.1 Results for the ANOVA of the main effects model describing soluble protein obtained after refolding.	126
28	C.2 Results for the ANOVA of the main effects model describing protein activity after refolding.	126
30	C.3 Coefficients of the model (C.1) for activity of catechol methylation by PFOMT. The factor Mg is a categorical variable (addition/no addition) and can therefore only be 0 or 1.	128
33	C.4 Coefficients obtained for linear regression model using the catechols subset after shrinkage using the Lasso method and 5-fold cross validation. Only non-zero coefficients (variables actually do have an effect) are retained during the Lasso. Seed was set to 1336.	129

1	D.2 SAM analogues that have been used with MTs. Targets: <i>P</i> –	
2	peptide/protein, <i>D</i> – DNA, <i>R</i> – RNA, <i>S</i> – small molecule. . .	134
3	D.1 Overview over the constructs produced for the present thesis.	
4	Each step during the production of the construct is given in	
5	the workflow steps column. Primers (italic font) or restriction	
6	sites used during each step are displayed in parenthesis. . .	137

List of Schemes

2	6.1 Ion fragment nomenclature of flavonoid aglycones as proposed 3 by Ma <i>et al.</i> , illustrated on naringenin. Ions are labelled accord- 4 ing to the ring they contain and the positions of the C ring that 5 were broken. Thus $^{1,3}\text{A}^+$, contains the ring A and bonds 1 and 6 3 of the C ring were broken.	68
7	6.2 Major fragmentation pathways of flavanones. Activation using 8 CID conditions at 45 % NCE mainly results in neutral losses 9 of H_2O and ketene ($\text{C}_2\text{H}_2\text{O}$) from the molecular ion $[\text{M}+\text{H}]^+$ 10 (bold frame). These neutral losses are scarcely observed when 11 HCD with a NCE of 75 % or 100 % is used for activation. Here, 12 C-ring cleavages followed by neutral losses from the cleavage 13 fragments are dominant.	72
14	6.3 Proposed MS^2 fragmentation of $^{1,3}\text{A}^+$ after HCD activation. 15 In high energy MS^2 experiments, $^{1,3}\text{A}^+$ might loose two CO 16 followed by an unusual C_2H_4 . A single loss of ketene ($\text{C}_2\text{H}_2\text{O}$) 17 to afford m/z 111 is also sensible.	72
18	6.4 Major fragmentation pathways of non-methylated and methyl- 19 ated flavones. Multiple neutral losses of small molecules (e.g. 20 CO, water or ketene) and 0/4 and 1/3 C ring cleavages are 21 predominant in the MS^2 spectra of non-methylated flavones. 22 Methylated flavones loose a methyl group in CID experiments, 23 but only in HCD experiments do other fragmentation reaction 24 become obvious.	74
25	6.5 Stability of the $[\text{M}+\text{H}-\text{CH}_3]^+$ ion of flavones. The $[\text{M}+\text{H}-$ 26 $\text{CH}_3]^+$ ion of methylated flavones like diosmetin is highly 27 stabilized by resonance, explaining the high intensity of the 28 corresponding peak and limiting its fragmentation at low acti- 29 vation energies.	76

1	6.6 Proposed pathway of fragmentation of (10) after HCD acti-	
2	vation. Losses of CH ₃ [·] and CH ₄ , followed by loss of CO are	
3	the major fragmentations observed in the corresponding MS	
4	spectra. However, multiple losses of CO only occur after a loss	
5	of methane (CH ₄), possibly due to the relative stability of the	
6	benzochromenylium radical cation (iii). At 100 % NCE even	
7	higher order fragmentations were observed.	77
8	6.7 Major fragmentation pathways of flavonoles. Unlike flavones,	
9	methylated and non-methylated flavonoles share common frag-	
10	mentations, albeit signals corresponding to small molecule	
11	losses are typically small for methylated analogues. Ring frag-	
12	ments observed typically correspond to the cleavage along	
13	bonds 0/3 or 0/2. Methylated flavonols shared common frag-	
14	ments with the methylated flavones. However, loss of methanol	
15	and a couple CO was also observed. n/o – not observed (relative	
16	intensity <1 %).	79
17	6.8 Proposed pathways of fragmentation of isorhamnetin (15). Isorhamnetin might loose methyl, methane or methanol upon	
18	activation. A similar fragmentation pathway was proposed for	
19	the analogous chrysoeriol (Scheme 6.6). Some fragmentations	
20	were observed in HCD mode only (box).	82



1

2

Preface

1 Abstracts

2 1.1 English Abstract

3 The present study outlines the useability of two plant O-methyl trans-
4 ferases (O-MTs), phenylpropanoid and flavonoid O-methyl transferase
5 (PFOMT) and soy O-methyl transferase (SOMT-2), of classes I and II for
6 the biocatalytic methylation of common structural motifs encountered
7 throughout the group of plant polyphenolic compounds. Class I plant
8 O-MTs, such as PFOMT, are magnesium-dependent caffeoyl CoA depen-
9 dent O-methyltransferase (CCoAOMT)-like enzymes comprising 200 to
10 280 amino acids, generally with a limited substrate scope. Class II plant
11 O-MTs (i.e. SOMT-2) are metal-ion independent, 340 to 390 amino acids in
12 length and generally more promiscuous than class I representatives.

13 Biophysical characterization of PFOMT using Isothermal Titration
14 Calorimetry demonstrated its ability to bind the biosynthetically obtained
15 S-adenosyl-L-methionine analogue S-adenosyl-L-ethionine (SAE). How-
16 ever, although numerous variants were characterized, conversion of SAE
17 by PFOMT was not observed. Nonetheless, a novel crystal structure of the
18 *apo*-form of PFOMT obtained during the present study gives new insights
19 into the movements and domains involved in substrate binding.

20 A systematic grid of 15 flavonoids (i.e. flavanones, flavones and
21 flavonoles) with different substitutions at the B-ring was characterized by
22 tandem mass-spectrometry (MS/MS) studies in positive mode. Thereby,
23 the fragmentation patterns produced by activation via collision induced
24 dissociation (CID) and higher-energy collisional dissociation (HCD) were
25 compared. Fragmentation, especially the appearance of characteristic
26 C-ring cleavage fragments such as $^{1,3}\text{A}^+$, of methylated members of
27 flavones and flavonoles was easily achieved in HCD experiments. The
28 results obtained demonstrate the complementary nature of both activation

1 methods and the importance of HCD spectra for the identification of
2 methylated flavones and flavonols.

3 In vivo studies using SOMT-2 showed its capability to methylate
4 flavonoids and stilbenes at the 4'-position. Design of experiments and
5 fractional factorial design were used successfully to optimize *in vitro*
6 refolding conditions for SOMT-2. However, sufficiently active enzyme
7 could not be obtained. Moreover, using PFOMT it was demonstrated,
8 that the activity of this class I plant O-MT could be modulated by high
9 a pH and magnesium concentration to achieve previously unobserved
10 methylations of non-catecholic moieties such as 3'-hydroxy-4'-methoxy
11 and 4'-hydroxy-3'-methoxy. This resulted in the production of e.g. 3',4'-
12 dimethyl eriodictyol and 3',4'-dimethyl luteolin by PFOMT from hesperetin
13 and diosmetin respectively. The knowledge obtained from the MS/MS
14 studies was crucial in identifying these products.

15 1.2 Deutsche Zusammenfassung

16 Die vorliegende Arbeit umreißt die Verwertbarkeit zweier pflanzlicher
17 O-Methyltransferasen (O-MTs), PFOMT und SOMT-2, der Klassen I and
18 II für die biokatalytische Methylierung in polyphenolischen Verbindun-
19 gen verbreiteter Strukturmotive. Klasse I Planzen O-MTs, wie PFOMT,
20 sind magnesiumabhängige Kaffeoyl CoA-abhängige O-Methyltransferase
21 (CCoAOMT)-ähnliche Enzyme von 200 bis 280 Aminosäuren und einem
22 gemeinhin limitierten Substratumfang. Vertreter der Klasse II (d.h. SOMT-
23 2) sind metallionen-unabhängig, 340 bis 390 Aminosäuren lang und im
24 Allgemeinen promiskuitiver im Substratspektrum denn Vertreter der Klasse
25 I.

26 Die biophysikalische Charakterisierung der PFOMT mittels isother-
27 maler Titrationskalorimetrie zeigte die Bindung von S-Adenosyl-L-ethionin
28 (SAE), ein biosynthetisch gewonnenes S-Adenosyl-L-methionin-Derivat, an
29 das Enzym. Eine Umsetzung von SAE durch PFOMT konnte jedoch nicht
30 gezeigt werden, obgleich mehrere Enzymvarianten untersucht wurden.
31 Nichtsdestotrotz wurde eine neue Kristallstruktur des *apo*-Enzyms gelöst,
32 welche neuerliche Einblicke in die Bewegungen innerhalb des Enzyms und
33 an der Substratbindung involvierter Domänen liefert.

34 Fünfzehn Flavonoide (d.h. Flavanone, Flavone und Flavonole) mit un-
35 terschiedlichen Substitutionsmustern am B-Ring wurden mittels Tandem-

1 Massenspektrometrie (MS/MS) im positiven Modus charakterisiert. Dabei
2 wurden zwei Aktivierungsmethoden, *collision induced dissociation* (HCD)
3 und *higher-energy collisional dissociation* (CID), verglichen. HCD erle-
4 ichterte die Fragmentierung, besonders das Erscheinen durch C-Ring-
5 Spaltung entstandener Fragmente (z.B. $^{1,3}\text{A}^+$), methylierter Vertreter von
6 Flavonen und Flavonolen. Die erhaltenen Ergebnisse demonstrieren die
7 Komplementarität beider Aktivierungsmethoden und die Bedeutung von
8 HCD-Spektren für die Identifizierung methylierter Flavone und Flavonole.
9 *In vivo* Studien der SOMT-2 zeigten die Methylierung von Flavonoiden
10 und Stilbenen an der 4'-Position. Statistische Versuchplanung und ein
11 Teilstudioplan wurden erfolgreich verwendet, um die Rückfaltungsaus-
12 beuten der *in vitro* Rückfaltung der SOMT-2 zu optimieren. Jedoch konnten
13 nur ungenügende Mengen an aktivem Protein erhalten werden. Es wurde
14 weiterhin gezeigt, dass die Aktivität der PFOMT durch Variation von pH
15 und Magnesium so weit moduliert werden konnte vorher unbeschriebene
16 Methylierungen von 3'-Hydroxy-4'-methoxy und 4'-Hydroxy-3'-methoxy-
17 Motiven zu erreichen. So konnten unter anderem 3',4'-Dimethyleriodictyol
18 und 3',4'-Dimethylluteolin durch Umsetzung von Hesperetin und Dios-
19 metin mittels PFOMT produziert werden. Für die Identifizierung der
20 genannten Produkte wurde unter anderem auf das in den MS/MS-Studien
21 gewonnene Wissen zurückgegriffen.

2 List of Publications

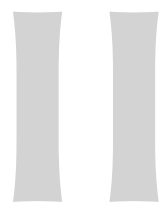
² Part of this work have been published:

- ³ 1. Wessjohann, L. A., Keim, J., Weigel, B., & Dippe, M. (2013). Alkylating enzymes. *Current Opinion in Chemical Biology*, 17(2), 229–235. <http://doi.org/10.1016/j.cbpa.2013.02.016>
- ⁶ 2. Dippe, M., Weigel, B., Heinke, R., Vogt, T., & Wessjohann, L. A. (2015). Engineering of a Mg²⁺-dependent O-methyltransferase towards novel regiospecificity. Manuscript to be submitted.

⁹ Publications that are not part of this work:

- ¹⁰ 1. Landgraf, R., Smolka, U., Altmann, S., Eschen-Lippold, L., Senning, M., Sonnewald, S., Weigel, B., ... Rosahl, S. (2014). The ABC Transporter ABCG1 Is Required for Suberin Formation in Potato Tuber Periderm. *The Plant Cell*, 13(August), 3403–3415. <http://doi.org/10.1105/tpc.114.124776>

1



2

Thesis

3 Introduction and Motivation

Secondary metabolites comprise a vast collection of organic compounds produced in nature, that do not directly parttake in the growth and development of an organism. Many functions of these natural products are unknown and remain to be elucidated, but it has been shown that they can be used for gene regulation, defense against biotic and abiotic stresses, (pollinator) attractant, communication and others. Natural compounds can be quite complex and show remarkable biological activities. The major classes of secondary compounds are terpenoids, alkaloids, phenylpropanoids including lignans/lignins, flavonoids and polyketides. This work is largely concerned about phenyl propanoids and flavonoids, as well as their modification, and will therefore mainly focus on these compounds.

3.1 Flavonoids

3.1.1 Overview

Plant phenolic compounds account for more than 40 % of the organic carbon in the biosphere and are essential for the survival of vascular plants. They are largely derived from the *phenylpropanoid* and relating pathways and take on various structural (e.g. cell walls) and non-structural roles (e.g. plant defense, flower color) [39]. The name *phenylpropanoid* describes the aromatic phenyl connected to a three-carbon chain, which biosynthetically originates from phenylalanine. Flavonoids, from the Latin *flavus* (yellow), are a diverse subclass of these phenolic compounds comprising more than 4500 different compounds described thus far and their main structural feature is the central chromane (benzodihydropyran) moiety (Figure 3.1). They consist of three rings named A, B and C. Ring A and B are of acetate and phenylpropanoid origin respectively, whereas ring C is a result of the condensation of the former. Different types of flavonoids are named

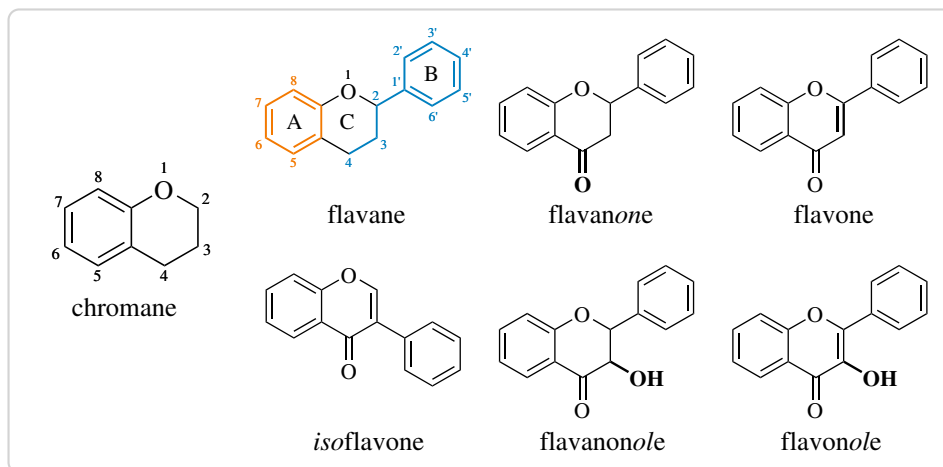


Figure 3.1: The central feature of the flavonoids is the chromane ring. The names of the different groups of flavonoids are derived from the substitution of this moiety. From a biosynthetic point of view, flavonoids are built up from phenylpropanoid (blue) and acetate derived moieties (orange).

1 depending on the substitution pattern of the chromane ring (Figure 3.1).

2 For example, a phenyl group at C-2 or C-3 gives flavonoids or isoflavonoids

3 respectively, an unsubstituted C-4 means flavane, whereas a carbonyl

4 group at C-4 indicates flavanones *et cetera*. Flavonoids are usually poly-

5 hydroxylated, but can also carry multiple other different substitutions.

6 *O*-methylations are common at all hydroxyl positions, but flavonoids can

7 also be *C*-methylated [10]. Other common derivatizations are (*O* or *C*)-

8 prenylation, (*O* or *C*)-glycosylation, methylene-dioxy bridges (C-3'/C-4'

9 or C-6/C-7) and various (*O* or *C*)-acylations (aliphatic and aromatic acids)

10 [42, 76, 183, 221].

11 In plants flavonoids are usually produced to combat biotic or abiotic

12 stresses. They can absorb highly energetic ultra violet (UV) light, suppress

13 the formation of, or scavenge reactive oxygen species (ROS) [2]. Further-

14 more, flavonoids can act as regulators during plant development [191]. A

15 growing interest in flavonoids for the use in medicinal and nutritional ap-

16 plications has been spiked by their beneficial effects on health. Flavonoids

17 possess a high antioxidant activity and also show protective effects against

18 age-related ailments, such as cardiovascular diseases and cancers. Further-

19 more, they show anti-inflammatory, hepatoprotective, antimicrobial and

20 antiviral activities [111].

21 A number of flavonoids are produced by the valorization of wastes and

22 by-products of the food industry. Citrus and olive processing byproducts

23 are especially rich in polyphenols [72, 151, 155]. However, many flavonoids

1 are scarce in nature and/or the production from by-products is not enough
2 to saturate the market demand, thus requiring different approaches for
3 production. Recent developments in the field of metabolic engineering
4 allowed for the high-level production of many flavonoids in microbial hosts,
5 such as *Escherichia coli* or *Saccharomyces cerevisiae* [198, 211]. For example,
6 eriodictyol was produced from tyrosine in metabolically engineered *E. coli*
7 at levels of up to 107 mg/ml [234], whereas naringenin was produced in
8 *S. cerevisiae* from glucose at levels of 109 mg/ml [108].

9 3.1.2 The phenyl propanoid pathway

10 Biosynthesis of flavonoids via the phenylpropanoid pathway starts
11 from phenylalanine, which is non-oxidatively deaminated by phenylala-
12 nine ammonia-lyase (PAL) to yield cinnamic acid (Figure 3.2) [74, 125].
13 Cinnamate-4-hydroxylase (C4H), a P450 monooxygenase, hydroxylates
14 the cinnamic acid at the *para*-position and 4-coumarate:CoA ligase (4CL)
15 converts the *p*-coumaric acid to its corresponding coenzyme A (CoA)-ester
16 [80, 201]. Chalcone synthase (CHS) uses 3 molecules of malonyl-CoA (pro-
17 duced from acetyl-CoA by acetyl-CoA carboxylase) to produce naringenin
18 chalcone from *p*-coumaryl-CoA [59]. Next, the linear chalcone can cyclize
19 spontaneously or catalyzed by a chalcone isomerase (CHI) via a MICHAEL-
20 type addition to afford the flavanone naringenin [88]. Naringenin can
21 serve as substrate for numerous enzymes such as flavanone-3-hydroxylase
22 (F3H), flavone synthase (FNS) or isoflavone synthase (IFS) to afford
23 dihydroflavonols, flavones or 2-hydroxyisoflavones respectively [69].
24 Dihydroflavonols are again precursors for the biosynthesis flavonols,
25 flavanols and anthocyanidines.

26 3.1.3 Biological activity

27 Flavonoids possess many properties associated with a healthy diet. They act
28 as antioxidants and can help reduce oxidative stress. Several mechanisms
29 that might be involved in the antioxidant activity of flavonoids are currently
30 discussed. They can act as scavengers for free ROS or mask metal ions by
31 chelation to suppress the production of radicals [27, 119]. The substitution
32 pattern plays an important role in the antioxidant activity. Generally, the
33 more free hydroxyls are present, the stronger the antioxidant activity of
34 the flavonoid [27]. Hydroxyls can donate an electron, or a hydrogen atom

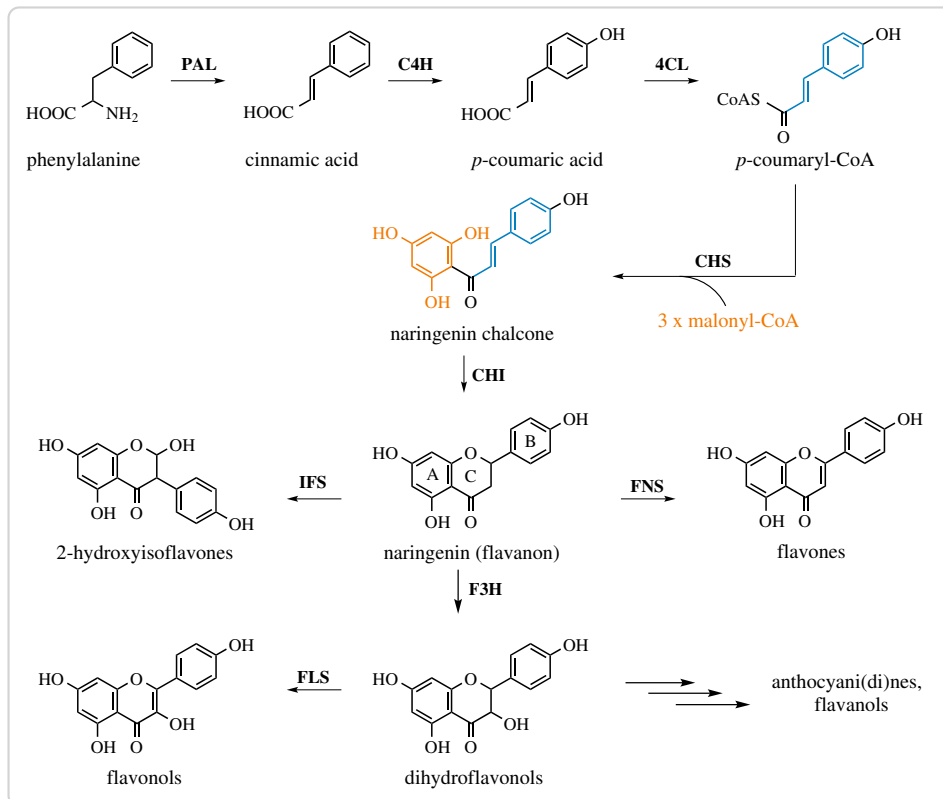


Figure 3.2.: General pathways in the biosynthesis of flavonoids. PAL – phenylalanin ammonia lyase, C4H – cinnamate-4-hydroxylase, 4CL – 4-coumarate:CoA ligase, CHS – chalcone synthase, CHI – chalcone isomerase, F3H – flavanone-3-hydroxylase, FLS – flavonol synthase, FNS – flavone synthase, IFS – isoflavone synthase.

1 to free ROS to inactive such molecules. The resulting flavonoid radicals
 2 are stabilized by resonance, however possess prooxidant properties [144].
 3 Numerous flavonoids possess antimicrobial activities [40]. For example,
 4 catechins from green and black teas have been shown to be effective against
 5 *Bacillus cereus* at nanomolar concentrations [64]. The mechanisms of action
 6 for the antimicrobial activity can be the inactivation of enzymes, binding
 7 of adhesins, membrane disruption or cell wall complexation [36].

8 3.2 Methyl transferases (MTs)

9 3.2.1 Overview

10 *S*-adenosyl-L-methionine (SAM)-dependent methyl transferases (MTs) (EC
 11 2.1.1.x) transfer the methyl group of SAM to an activated atom of an ac-
 12 ceptor molecule, via an S_N2 displacement mechanism. SAM is converted to

1 *S*-adenosyl-L-homocysteine (SAH), the co-product of the reaction, in the
2 process. There are currently over 300 manually annotated MTs, each cat-
3 alyzing a different reaction, included in the UniProtKB/Swiss-Prot database
4 (<http://www.uniprot.org>). Transfer of the methyl group to oxygen and ni-
5 trogen atoms is most common, but carbon, sulfur, selenium, arsenic atoms
6 and even halide ions can be methylated too(Figure 3.4)[171, 193]. Acceptor
7 molecules are diverse and range from relatively small natural products
8 (e.g. flavonoids) to bio-macromolecules such as nucleic acids or proteins.
9 In fact, MTs are key-tailoring enzymes for many natural products of all
10 groups (e.g. flavonoids, alkaloids or non-ribosomal peptides) [100, 109,
11 188, 211]. These small molecule methyl transferases (*sm*MTs) account for a
12 significant part of the diversity present in natural products.

13 Other MTs, such as protein methyl transferases (P-MTs), DNA methyl
14 transferases (DNA-MTs) and RNA methyl transferases (RNA-MTs) methy-
15 late proteins and nucleic acids respectively. In eukaryotes, DNA-MTs and
16 P-MTs play important roles in the epigenetic regulation of gene expression
17 and have been associated with a number of cancers and other diseases [34,
18 162, 163]. In bacteria, DNA-MTs are an essential part of the restriction
19 modification system [140].

20 According to their structure, MTs can be classified into five main groups
21 (I–V) (Figure 3.3)[174]. Class I MTs are the largest group of MTs and are
22 characterized by a central Rossmann-like $\alpha\beta\alpha$ sandwich, consisting of
23 a seven-stranded β -sheet flanked by α -helices. Most *sm*MTs, DNA-MTs
24 and some P-MTs belong to class I. Even though some of the enzymes
25 belonging to class I share as little as 10 % sequence similarity, there is a
26 pronounced structural conservation [174]. Class II MTs comprise a long
27 anti-parallel β -sheet encompassed by numerous α -helices [50]. In class III
28 MTs the SAM binding site is located between two $\alpha\beta\alpha$ domains [173]. A
29 knot structure at the C-terminus contributes to SAM binding in the *SpoU*-
30 *TrmD* (SPOUT) family of class IV RNA-MTs [145]. Protein lysine MTs
31 make up the largest part of P-MTs and structurally belong to class V MTs
32 containing a suvar3-9, enhancer-of-zeste, trithorax (SET) domain [224].
33 Interestingly, a recent study of the methyltransferome of baker's yeast (*S.*
34 *cerevisiae*) argues, that there are four more classes of MTs [218]. Opposite
35 to the studies by Schubert *et al.*, this work mainly relied on bioinformatical
36 methods for structural information. 83 out of 86 MT structures in total were
37 homology-modelled. It was shown, that two thirds of the reviewed yeast

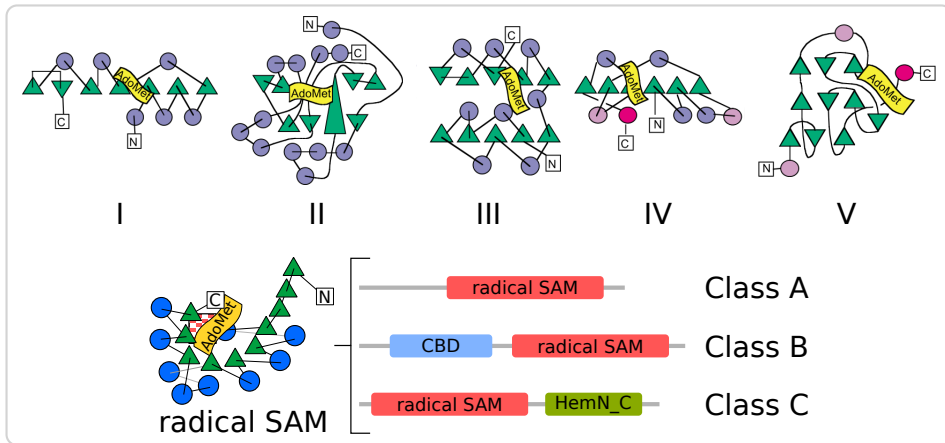


Figure 3.3: Topology plots of the five major structural classes of methyl transferases and radical SAM methyl transferases (RSMTs) (modified and extended from Schubert et al. [174]). Helices are depicted as circles and β -strands as triangles. The SAM binding site is depicted as a flag. Radical SAM methyl transferases all share a common “radical SAM”-domain, which contains the iron sulfur cluster (red checker). The individual radical SAM methyl transferase classes are differentiated according to the other domains they contain.

1 MTs belonged to class I. However, four new folding architectures, namely
 2 SSo0622-like, all- β , all- α (RNA/DNA 3-helical bundle) and transmembrane,
 3 were postulated.

4 Radical SAM methyl transferases (RSMTs) comprise another class of
 5 recently discovered MTs that contain an iron-sulfur ([4Fe-4S])-cluster coor-
 6 dinated by a three cysteine CxxxCxxC motif. RSMTs methylate unreactive
 7 centers through a radical mechanism [210]. Structural evidence suggests,
 8 that the mechanism is initiated by reductive cleavage of SAM into a re-
 9 active 5'-deoxyadenosyl (dAdo) radical by the [4Fe-4S] cluster [13, 24].
 10 Three distinct classes (A, B, C) with distinct structural and mechanistic
 11 characteristics have been recognized within the RSMTs [231]. The cen-
 12 terpiece of RSMTs is the *radical SAM* domain, whose structure was first
 13 described in the ribosomal ribonucleic acid (rRNA) methyl transferase
 14 RlmN of *E. coli* [13]. This domain consists of an α_6/β_6 partial barrel and
 15 contains the [4Fe-4S] cluster, as well as the SAM binding site (Figure 3.3).
 16 Class A only contains the radical SAM domain and mainly comprises rRNA
 17 methyl transferases. In addition to the radical SAM domain, an N-terminal
 18 cobalamin binding domain (CBD) is proposed to be contained in RSMTs
 19 of class B. Class B RSMTs methylate numerous substrates at unreactive
 20 sp³ carbon centers, heterocycles and phosphinates. Class C RSMTs most
 21 likely contain a C-terminal domain related to the coproporphyrinogen

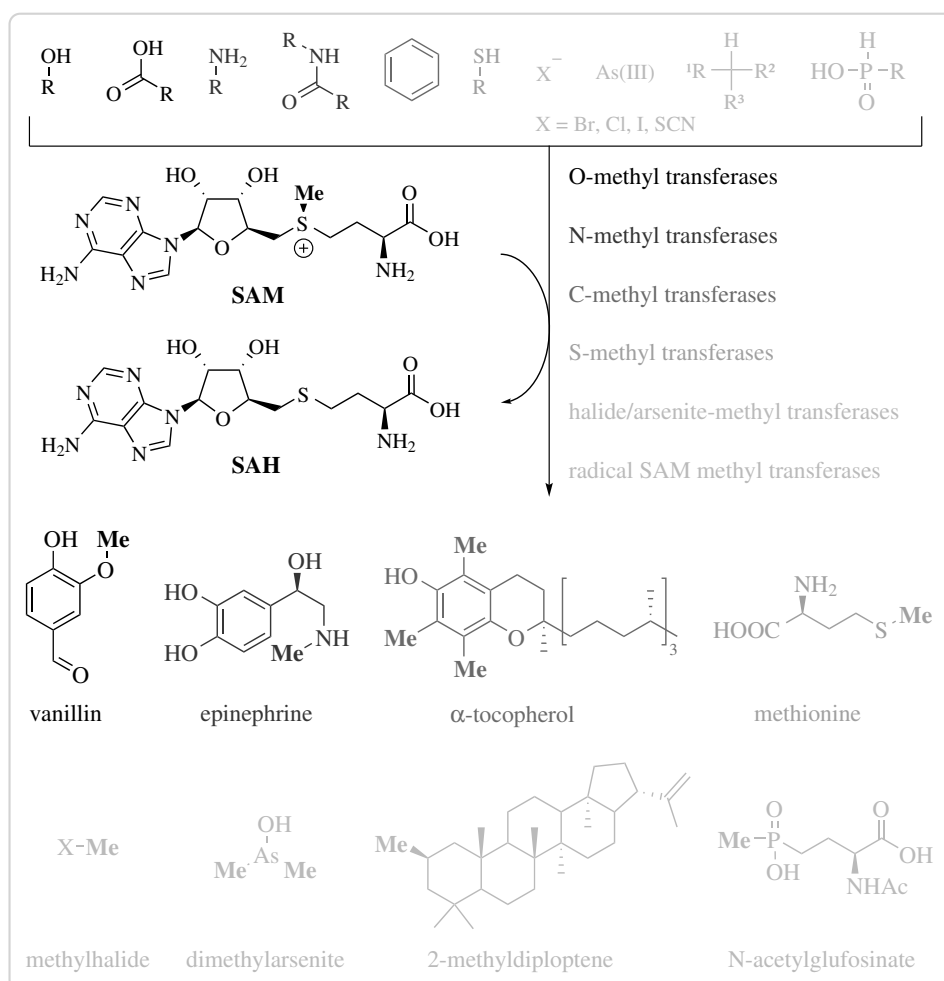


Figure 3.4: Reactions catalyzed by methyl transferases (MTs). Different shades of gray were used to differentiate between different groups of compounds and methyl transferases. In contrast to other methyl transferases, the group of radical SAM methyl transferases also requires additional co-factors to SAM.

1 III oxidase HemN in addition to the radical SAM domain [115]. Class C
2 enzymes methylate aromatic heterocycles.

3 Radical SAM chemistry within enzymes is not confined to just methyl
4 transfer. Instead, it has been shown that this type of chemistry is im-
5 portant for a number of rearrangement, cyclization, dehydrogenation,
6 bond-formation and bond-cleavage reactions in nature [24].

7 3.2.2 *S*-Adenosyl-L-methionine

8 *S*-adenosyl-L-methionine (SAM), first described in 1953 [26], is the universal
9 co-substrate for all SAM dependent methyl transferases. However, it is
10 not only involved in methyl transfer, but is essential for a myriad of other
11 reactions [24]. This makes SAM the second most ubiquitous co-substrate
12 after adenosine triphosphate (ATP).

13 The methyl group of SAM is partially positively charged due to its po-
14 sition at the sulfonium center and is in consequence highly activated.
15 The increased electrophilicity of the methyl group makes it a strong alky-
16 lation agent. Demethylated SAM is called *S*-adenosyl-L-homocysteine
17 (SAH), which is a good leaving group. Therefore, nucleophilic transfer of
18 the methyl group of SAM is thermodynamically highly favoured ($\Delta G^0 \approx$
19 -70 kJ/mol for $\text{SAM} + \text{homocysteine} \rightarrow \text{SAH} + \text{methionine}$) and allows
20 the rapid and selective methylation of a range of substrates [174]. The fact
21 that the methyl group is the least sterically hindered of all transferable
22 carbon groups makes a methyl transfer the kinetically most favourable S_N2
23 reaction (disregarding nucleophile and leaving group). Despite its apparent
24 reactivity, SAM is still quite stable at physiological conditions com-
25 pared to other sulfonium species like the trimethylsulfonium ion, which
26 quickly reacts with nucleophiles and is often used for derivatization prior
27 to GC analytics [25]. Meanwhile, SAM is readily cleaved into adenine and
28 *S*-ribosylmethionine under alkaline conditions [16] and other deteriorat-
29 ing processes such as racemization and intramolecular cleavage are to be
30 reckoned with [77].

31 SAM is produced by the enzyme SAM synthetase (EC 2.5.1.6) from me-
32 thionine and ATP in a two step reaction [190]. At first SAM is formed
33 and the triphosphate group of ATP is cleaved off. Then, the inorganic
34 triphosphate is hydrolyzed to monophosphate and diphosphate after which
35 the products are released. SAH is a common side product of all SAM de-

1 pendent MTs and can be further cleaved by SAH hydrolase (EC 3.3.1.1) to
 2 afford homocysteine and adenosine [127]. The cobalamine (vitamin B₁₂)
 3 dependent methionine synthase (EC 2.1.1.13) can remethylate homocys-
 4 teine to methionine using N⁵-methyltetrahydrofolate as a methyl donor
 5 [9]. Taken together, reactions leading from and to SAM are commonly
 6 called the activated methyl cycle.

7 3.2.3 Methyl transferase mechanisms

8 Non-radical SAM-dependent MTs catalyze the transfer of the methyl group
 9 of SAM to an activated nucleophile. The methylation reaction proceeds via
 10 a single displacement S_N2 mechanism, through an sp² hybridized transition
 state and results in the inversion of configuration (Figure 3.5). The S_N2

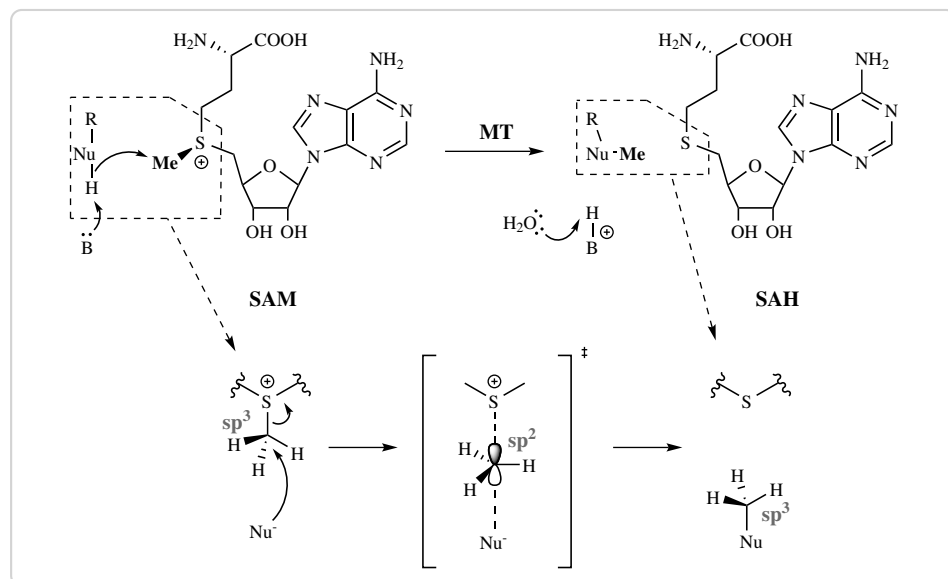


Figure 3.5: Mechanism of the methyl transfer reaction catalyzed by methyl transferases. Non-radical S-adenosyl-L-methionine dependent methyl transferases catalyze the nucleophilic transfer of a methyl group from the donor S-adenosyl-L-methionine to a nucleophile (Nu; e.g. O,N,C,S). A proton (H⁺) is usually abstracted through a general base (B), to achieve activation of the nucleophile. The proton is later transferred to the aqueous medium. The S_N2 reaction proceeds via a single transition state, during which the methyl-carbon is sp² hybridized. After transfer of the methyl to the nucleophile the carbon's configuration is inverted.

11
 12 mechanism was proposed as early as 1979 [73, 146], but only with the
 13 development of the chiral methyl group methodology (Figure 3.6) extended
 14 mechanistic studies were made possible [61, 62]. An elegant method for the
 15 synthesis of chiral acetate made use of glycolytic enzymes to convert [1-
 16 ³H]-glucose via its glycolysis intermediates to [3-²H, ³H]-lactate, which is

1 subsequently oxidized by chromiumtrioxide (Figure 3.6) [223]. The chirality
2 of the resulting acetate can be controlled by the solvents (D_2O or H_2O)
3 used during the enzymatic reactions. The chiral acetate can be used for the
synthesis of e.g. [*methyl-²H,³H*]-methionine.

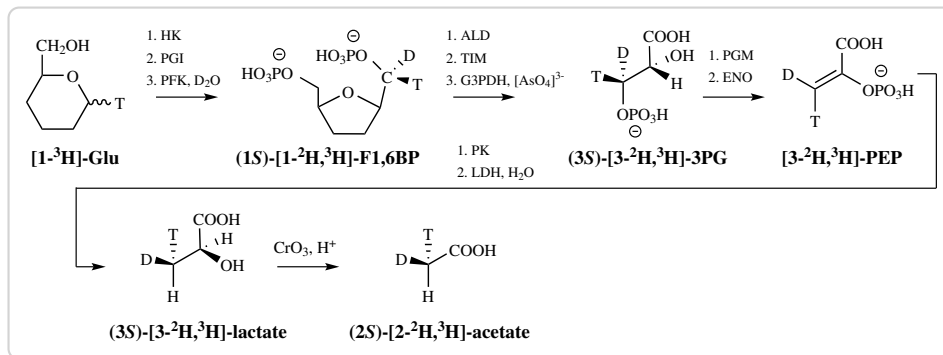


Figure 3.6.: Bioenzymatic synthesis of chiral acetate, the precursor for the synthesis of SAM carrying an assymetrical methyl, as used by Woodward et al. [223]. Ring hydroxyls of hexoses and pentoses are omitted for easier reading. HK – hexokinase, PGI – phosphoglucose isomerase, PFK – phosphofructokinase, ALD – aldolase, TIM – triose phosphate isomerase, G3PDH – glyceraldehyde-3-phosphate dehydrogenase, PGM – phosphoglycerate mutase, ENO – enolase, Glu – glucose, F1,6BP – fructose-1,6-bisphosphate, 3PG – 3-phosphoglycerate, PEP – phosphoenol pyruvate

In 1980, Woodward et al. fed *R*- and *S*-methionine containing an assymetrical methyl group to cultures of *Streptomyces griseus*. They found, that the enzymatic transfer of two methyl groups (*N* and *C*-methylation) during the indolmycin biosynthesis proceeded with inversion of the configuration, strongly implying an S_N2 mechanism [223]. This experiment also demonstrated that, *in vivo*, [*methyl-²H,³H*]-methionine is converted to [*methyl-²H,³H*]-SAM before the methyl group is transferred by a MT. *In vitro* experiments conducted using catechol O-methyl transferase (COMT) further supported the hypothesis of an S_N2 mechanism [222].

The nucleophile attacking the methyl group of SAM is usually activated by abstraction of a proton through a general base (e.g. histidine, lysine) [22, 235, 236] and/or with the help of a lewis acid such as complexed Mg^{2+} [109, 204]. In a bimolecular reaction, the rate is highly dependent on the concentration of both compounds:

$$\text{rate} = k[A][B].$$

1 Low concentrations of either result in a low rate. Thus, bimolecular reac-
2 tions are entropically disfavoured (concentration and entropy are inversely
3 correlated). MTs (and enzymes in general) strongly increase the effec-
4 tive concentration of each reactant and thereby decrease entropy, because
5 methyl donor and acceptor are bound (“immobilized”) in close proximity to
6 each other in the active site [60]. The right positioning of the substrates is
7 a major factor for efficient catalysis and enzymes go through great lengths
8 to achieve optimal alignment of substrates. One remarkable example are
9 DNA-MTs, which can flip the target nucleotide out of the DNA-helix to
10 provide the best orientation of SAM and the acceptor nucleophile [104].

11 Since the reaction catalyzed by MTs is a two substrate reaction, kinetics-
12 driven mechanistic studies have been done on a number of different MTs
13 to show the binding mode of the substrates. It turns out, that the re-
14 action mechanism varies for MTs from different organisms and classes.
15 There is no one mechanism that describes every MT. A random bi-bi bind-
16 ing mechanism is for example exhibited by rat liver COMT [37], CheR
17 protein-L-glutamate O-MT from *Salmonella typhimurium* [182] and the
18 protoporphyrin IX O-MT of *Rhodobacter capsulatus* [170]. The protopor-
19 phyrin IX MT from etiolated wheat *Triticum aestivum* on the other hand
20 shows a ping-pong bi-bi mechanism [226], whereas ordered bi-bi mecha-
21 nisms were shown for the cytosine DNA-MT MSPI and isoprenylated P-MT
22 [12, 179]. Meanwhile, the enzymes exhibiting ordered bi-bi mechanisms
23 were different in that some bound SAM first and released SAH last [179],
24 whereas the others bound the acceptor molecule first [12]. Competitive
25 product inhibition, especially by SAH, is commonly observed for MTs [8,
26 12, 179, 182].

27 The mechanisms of RSMTs are outside the scope of this work, but the
28 interested reader is referred to current reviews on the topic [24, 231].

29 3.2.4 Plant O-methyl transferases (O-MTs)

30 Plant O-methyl transferases (O-MTs) were the prime interest of this work.
31 Plant O-MTs represent a large group of plant enzymes that catalyze the
32 transfer of a methyl group to a hydroxyl or carboxyl group of phenyl-
33 propanoids, flavonoids or alkaloids. O-methylation greatly effects the
34 (bio)-chemical properties of a compound and can have profound influ-

1 ences on reactivity, solubility, bioavailability, antimicrobial or antioxidant
2 activities.

3 Plant O-MTs are subdivided into two groups according to their size
4 and the spatial relationship between three highly preserved motifs (Ta-
5 ble 3.1) [92]. Group I members, containing caffeoyl CoA dependent O-
6 methyltransferase (CCoAOMT)-like representatives, are usually between
7 110 and 140 amino acid residues shorter than group II members (\approx 340–390
amino acids). The distance between motifs A and B, and between B and C

Table 3.1: Defining motifs of plant O-MTs as described by Joshi *et al.* [92].

motif	consensus	distance to motif ...		
		...	group I	group II
A	(V,I,L)(V,L)(D,K)(V,I)GGXX(G,A)	B	19	52
B	(V,I,F)(A,P,E)X(A,P,G)DAXXXX(W,Y,F)	C	24	30
C	(A,P,G,S)(L,I,V)(A,P,G,S)XX(A,P,G,S)(K,R)(V,I)(E,I)(L,I,V)			

8
9 is also shorter in group I members, than in group II members. In contrast
10 to group II, group I plant O-MTs require Mg^{2+} for activity. Overall, they
11 are fairly similar to mammalian COMTs [92]. Group II plant O-MTs can
12 methylate a variety of substrates, whereas group I plant O-MTs are usually
13 very strict in their substrate scope utilizing only a couple of substrates.
14 However, some enzymes from group I are much more relaxed with their
15 acceptance of substrates. For example, phenylpropanoid and flavonoid
16 O-methyl transferase (PFOMT) from the ice-plant *Mesembryanthemum*
17 *crystallinum* and an O-MT from chickweed *Stellaria longipes* can utilize
18 several phenyl propanoid derived substrates [85, 232].

19 **Phenylpropanoid and flavonoid O-methyl transferase (PFOMT)**
20 is a Mg^{2+} -dependent class I plant O-MT from the ice plant *M. crystallinum*
21 and was first described in 2003 by Ibdah *et al.* [85]. PFOMT was the first
22 class I MT that provided evidence showing, that methylation of flavonoids
23 is not only restricted to class II plant O-MTs. It belongs to a subgroup
24 of class I plant O-MTs, that is distinguished from CCoAOMT by a lower
25 sequence homology and a broader substrate promiscuity and regiospeci-
26 ficity. PFOMT methylates a number of flavonoids and phenyl propanoids
27 at the *meta*-position, provided a catecholic moiety is present. Enzyme
28 purified from its native source *M. crystallinum* is truncated N-terminally
29 by 11 amino acids, although there is no known signaling sequence [206].

1 This truncation has deleterious effects on the catalytic efficiency, especially
2 towards substrates such as caffeoyl glucose and caffeoyl-CoA, but also
3 influences the regioselectivity. There is only speculation as to the purpose
4 of this N-terminal truncation *in vivo*, but metabolic regulation is plausible.

5 PFOMT is a biological dimer, as the three dimensional structure of PFOMT
6 shows (pdb: 3C3Y) [109]. Each monomer exhibits a Rossmann α/β -fold
7 consisting of 8 α -helices and 8 β -strands. The catalytically important N-
8 terminus is not resolved in the structure. SAH and Ca^{2+} were cocrystallized
9 and appear bound in the active site. Ca^{2+} is complexed by two aspartate and
10 one asparagine residues with the rest of the coordination spaces occupied
11 by waters.

12 **Soy O-methyl transferase (SOMT-2)** has been described in the litera-
13 ture to methylate multiple flavonoids at the 4'-position of the B-ring [99,
14 102, 103]. It has the highest activity towards naringenin, to produce pon-
15 ciretin (also known as isosakuranetin). No structural data of soy O-methyl
16 transferase (SOMT-2) or *in vitro* activity studies have been published to
17 date. Enzymes like SOMT-2, that methylate a *para*-monohydroxylated B
18 ring of flavonoids, either seem to be a rare occurrence or fairly inactive, since
19 descriptions of characterized representatives are scarce in the literature
20 and are only limited to a couple of enzymes [47, 172].

21 **3.3 Alkylation and biotransformations**

22 **3.3.1 Overview**

23 Alkylation reactions are a crucial factor helping nature create highly di-
24 verse natural products from a limited number of precursors and as such,
25 these reactions are becoming more and more important in biocatalysis.
26 Methylation, prenylation and glycosylation constitute the major alkylation
27 reactions in nature and can largely influence the (bio)chemical characteris-
28 tics of a compound. Intra- and intermolecular prenylation is achieved by
29 prenyl transferases, which employ mono- and oligo-prenyl diphosphates
30 and are mainly responsible for the over 70 000 terpenoids described today
31 [23]. Glycosyl transferases catalyze the formation of a glycosidic bond
32 using nucleotide- or lipid phospho-sugars (e.g. uridine diphosphate (UDP)-
33 glucose, dolichol phosphate oligosaccharides) as sugar donating substrates

1 [113]. Methylation reactions are catalyzed by MTs using SAM as methyl
2 donor and will be the focus of this section.

3 The introduction of a methyl group ($V \approx 20 \text{ \AA}^3$) for a hydrogen ($V \approx 5 \text{ \AA}^3$)
4 can have different effects, chemically and biologically. Polar groups (e.g.
5 hydroxyl, amine, carboxyl) are masked by methylation, which majorly al-
6 ters their chemistry. Possible hydrogen donors are lost and the lipophilicity
7 is increased. The methylation can act as a molecular signal, which might
8 be specifically recognized by other enzymes than the original more polar,
9 hydrogen donating group. This can in turn have dramatic physiological
10 consequences in an organism.

11 3.3.2 Methyl transferases for industrial use

12 The industrial potential of MTs has been demonstrated by several studies
13 [211]. Li and Frost [122] presented an environmentally friendly method to
14 produce vanillin from glucose by genetically modified *E. coli* cells. During
15 the fermentation, methyl transfer was achieved by recombinantly expressed
16 COMT. Recent developments mainly focus on the synthesis of structurally
17 more complex and highly valuable compounds, especially flavonoids, due to
18 their manifold biological effects (Figure 3.7). For example, ermanine (1) with
19 a claimed anti-inflammatory and antiviral activity, can be synthesized from
20 its inactive precursor kaempferol (5,7-dihydroxy-3,4'-dimethoxyflavone)
21 by whole-cell biotransformation [15]. Sequential introduction of the two
22 methyl groups was performed by OMT-9 from rice (ROMT-9) and OMT-
23 2 from soybean and resulted in almost quantitative conversion of the
24 substrate. Similarly, transformation of kaempferol and quercetin by an
25 engineered variant of the OMT-7 from *Populus deltoides* gave the 3,7-di-O-
26 methyl products in 58 % and 70 % yield, respectively [89]. The conversion
27 of naringenin (4',5,7-trihydroxyflavanone) to 3-O-methylkaempferol was
28 performed as an enzymatic two-step process involving initial oxidation by
29 flavonol synthase and methylation of the intermediate by ROMT-9 [101].

30 The most promising approach for the chemoenzymatic production of
31 flavonoids remains the *de novo* synthesis from inexpensive biosynthetic
32 precursors such as *p*-coumaric acid, which is initially processed into non-
33 methylated flavonoids and subsequently modified by O-MT reactions.
34 This way, 7-O-methyl-aromadendrin (2) and the corresponding flavone
35 genkwanin were obtained from recombinant *E. coli* in yields of 2.7 mg/l

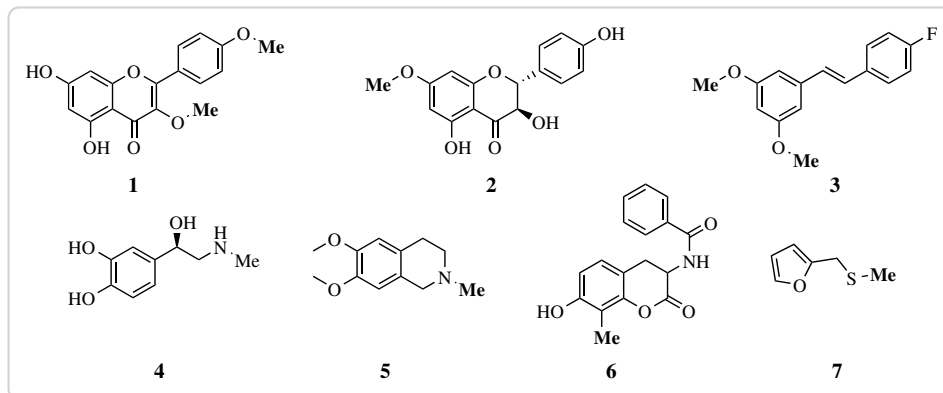


Figure 3.7.: Natural products synthesized with the help of methyl transferases. O-methyl transferases were used for the synthesis of erma-nine (**1**), 7-O-methyl-aromadendrin (**2**) and 3,5-dimethoxy-4'-fluorostilbene (**3**). N-methyl transferase (N-MT) catalyze the production of epinephrine (**4**) and N-methyltetrahydroisoquinoline (**5**), whereas 3-(benzoylamino)-8-methylumbelliferone (**6**) and furfuryl-methyl-sulfide (**7**) can be produced by C-methyl transferase (C-MT) and S-methyl transferase (S-MT)

1 and 0.2 mg/l, respectively [118, 134]. Similarly, several non-natural (e.g.
2 fluorinated) cinnamic acids can be converted to mono- and dimethylated
3 stilbenes such as 3,5-dimethoxy-4'-fluorostilbene (**3**) using a reconstructued
4 plant pathway in *E. coli*.

5 *N*-, *C*- and *S*-methyl transferases have also been successfully used
6 in biocatalytical applications. For example, epinephrine (**4**) and *N*-
7 methyltetrahydro-isoquinoline (**5**) were obtained by *in vitro* and *in vivo*
8 biotransformations of their respective precursors [138, 148]. Further-
9 more, a number of studies describe the production of several other
10 *N*-methylated alkaloid and non-alkaloid compounds [156, 161, 230].
11 *C*-methyl transferases (*C*-MTs) have been used biocatalytically to modify
12 different phenols [38] and coumarin derivatives, to obtain compounds
13 such as 3-(benzoylamino)-8-methylumbelliferone (**6**) [187]. Also, the
14 composition of the main tocopherol species in plants could be tuned by the
15 introduction of bacterial *C*-MTs [84]. *S*-methyl transferases (*S*-MTs) have
16 only seen a limited number of biocatalytic applications, but a candidate
17 from *Catharanthus roseus* shows some promiscuous activity towards
18 small aliphatic and aromatic thiols and can produce molecules such as
19 furfuryl-methyl-sulfide (**7**) [32].

20 *In vivo* biotransformations for the high-yield methylation of compounds
21 is a feasable method, especially since SAM is a rather expensive cofactor
22 (3000 to 15 000 €/g). However, SAM cannot be easily substituted for artificial

¹ analogues *in vivo*.

² 3.3.3 Artificial SAM analogues

³ SAM analogues have shown tremendous potential in *in vitro* biocatalytic
⁴ applications. The first description of novel synthetic SAM analogues with
⁵ extended carbon chains, including *S*-adenosyl-L-ethionine (SAE), allyl and
⁶ propargyl derivatives, that were also shown to be useful in modifying
⁷ DNA via the action of several DNA-MTs was provided by Dalhoff, *et al.*
⁸ [44, 45]. A whole variety of allyl derivatives was examined by different
⁹ researchers and site-specific introductions of allyl, pent-2-en-4-ynyl and
¹⁰ even 4-propargyloxy-but-2-enyl moieties into proteins (i.e. histones) was
¹¹ demonstrated using P-MTs [158, 209]. However, the larger substrate ana-
¹² logues were not necessarily accommodated by the native P-MTs making
¹³ engineering efforts for the accomodation of larger substrates inevitable
¹⁴ [209]. The specific introduction of alkine functionalized groups made it
¹⁵ then possible to use click chemistry for further functionalization and/or
¹⁶ detection of the labelled proteins, DNA or RNA (Figure 3.8) [150, 158, 175,
 209, 215].

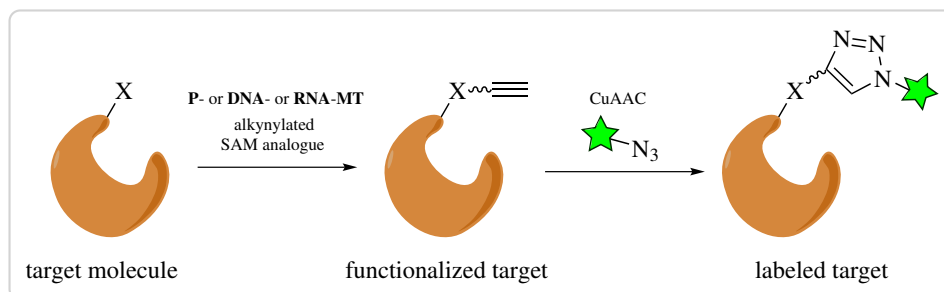


Figure 3.8: Labelling of macromolecules by using a combination of novel alkine-derivatized *S*-adenosyl-L-methionine analogues and Cu^{I} -catalyzed azide-alkyne 1,3-dipolar cycloaddition (CuAAC). Depending on the type of label used, it can be employed for detection (e.g. through fluorophores, coupled assays) or affinity purification (e.g. biotin). This technique might also be also feasable for use in activity based protein profiling (ABPP) approaches.

¹⁷
¹⁸ In 2012 Bothwell and Luo even described the exchange of the sulfonium
¹⁹ with a selenonium center, which afforded *Se*-adenosyl selenomethionine
²⁰ (SeAM) analogues that have since then been described as substrates for
²¹ several P-MTs [18, 19]. SeAM analogues have the advantage of being more
²² resistant to chemical decomposition than their sulfur counterparts, but
²³ also show enhanced transmethylation reactivity [18]. There have been

1 some reports on the use of SAM analogues by small molecule MTs. In
2 2009 Stecher *et al.* reported the use of the C-MTs NovO and CouO along
3 with synthetic SAM analogues to accomplish biocatalytic Friedel-Crafts
4 alkylations of some aminocoumarine antibiotics [187]. Lee *et al.* were the
5 first ones to describe the transfer of a keto-group from an SAM derivative by
6 means of the small molecule MTs catechol O-methyl transferase (EC 2.1.1.6)
7 and thiopurine S-methyl transferase (EC 2.1.1.67) [116]. Furthermore the
8 work done on the O-MTs RebM and RapM, which modify the antitumor
9 active natural products rebeccamycin and rapamycin respectively, shows
10 the general feasibility of using SAM analogues in combination with MTs
11 to modify small molecules [114, 184, 229]. However, no bioactivity data
12 has been reported that shows the biological activity of the newly produced
13 compounds.

14 3.4 Motivation

15 The motivation of this work was to assess the useability of plant O-methyl
16 transferases (O-MTs) for the derivatization and functionalization of phenyl
17 propanoid derived phenolics, especially flavonoids.

18 Phenylpropanoid and flavonoid O-methyl transferase (PFOMT)
19 from the ice-plant *Mesembryanthemum crystallinum* was to be used
20 as a model enzyme to study the promiscuity of class I plant O-MTs
21 towards the alkyl donor, using the hemisynthetically produced S-
22 adenosyl-L-methionine analogue S-adenosyl-L-ethionine, (2S)-2-amino-4-
23 [[(2S,3S,4R,5R)-5-(6-aminopurin-9-yl)-3,4-dihydroxyoxolan-2-yl]methyl-
24 ethylsulfonio]butanoat. Biophysical methods such as x-ray crystallography
25 and Isothermal Titration Calorimetry (ITC) should be used to study the
26 binding of the artificial analogues. The obtained knowledge could be used
27 to aid the development of novel small molecule methyl transferase with
28 desirable catalytic properties.

29 Furthermore, the enzymatic methylation of different structural motifs
30 encountered throughout the phenyl propanoids was to be studied using
31 class I and class II plant O-MTs. Soy O-methyl transferase (SOMT-2) and
32 PFOMT are examples of both classes and should thus be used in this work.
33 The results should help in understanding the specific catalytic properties
34 of both classes.

1 Furthermore, the analytical power of tandem mass-spectrometry
2 (MS/MS) to study substitutions commonly occurring in 5,7-dihydroxylated
3 flavonoids should be assessed using a distinct set of exemplary com-
4 pounds. The insights obtained should provide a reliable and fast method to
5 determine structural properties of unknown flavonoids.

4 Material And Methods

² Within this section percentages refer to volume per volume (v/v) percentages unless otherwise specified.

4.1 Materials

4.1.1 Chemicals

Enzymes and buffers used for molecular cloning were obtained from Life Technologies (Darmstadt, Germany), unless otherwise noted. Flavonoid HPLC standards were purchased from Extrasynthese (Genay, France). Deuterated solvents were acquired from Deutero GmbH (Kastellaun, Germany). Solvents, purchased from VWR (Poole, England), were distilled in-house before use.

All other chemicals were obtained from either Sigma-Aldrich (Steinheim, Germany), Applichem (Darmstadt, Germany), Carl Roth (Karlsruhe, Germany) or Merck (Darmstadt, Germany).

4.1.2 Commonly used solutions and buffers

50× 5052	25 % glycerol, 2.5 % (w/v) glucose, 10 % (w/v) α -lactose
binding buffer	50 mM Tris/HCl, 500 mM NaCl, 10 % glycerol, 2.5 mM imidazole pH 7
elution buffer	50 mM Tris/HCl, 500 mM NaCl, 10 % glycerol, 250 mM imidazole pH 7
lysis buffer	50 mM Tris/HCl, 500 mM NaCl, 10 % glycerol, 2.5 mM imidazole, 0.2 % Tween-20 pH 7
1 M MMT pH 4 (10×)	26.8 g/l L-malic acid, 78.1 g/l MES, 26.8 g/l Tris, 2.1 % 10 M HCl

1 M MMT pH 9 (10×)	26.8 g/l L-malic acid, 78.1 g/l MES, 26.8 g/l Tris, 6.7 % 10 M NaOH
20× NPS	1 M Na ₂ HPO ₄ , 1 M KH ₂ PO ₄ , 0.5 M (NH ₄) ₂ SO ₄
1 M SSG pH 4 (10×)	14.8 g/l succinic acid, 60.4 g/l NaH ₂ PO ₄ · H ₂ O, 32.8 g/l glycine, 0.4 % 10 M NaOH
1 M SSG pH 10 (10×)	14.8 g/l succinic acid, 60.4 g/l NaH ₂ PO ₄ · H ₂ O, 32.8 g/l glycine, 10.3 % 10 M NaOH
5× SDS sample buffer	10 % (w/v) SDS, 10 mM β-mercaptoethanol, 20 % glycerol, 0.2 M Tris/HCl pH 6.8, 0.05 % (w/v) bromophenolblue
1000× trace elements	50 mM FeCl ₃ , 20 mM CaCl ₂ , 10 mM MnCl ₂ , 10 mM ZnSO ₄ , 2 mM CoCl ₂ , 2 mM CuCl ₂ , 2 mM NiCl ₂ , 2 mM Na ₂ MoO ₄ , 2 mM Na ₂ SeO ₃ , 2 mM H ₃ BO ₃

1 Preparation of natural deep eutectic solvent (NADES)

2 Natural deep eutectic solvent (NADES) were prepared by adding each
 3 component in a round-bottom flask with a stirrer and stirring the mixture
 4 at 50 °C with intermittent sonication treatments until a clear solution was
 5 obtained.

Table 4.1: Natural deep eutectic solvent (NADES)-mixtures used within this work.

name	composition	mole ratio	mass fraction (w/w)
PCH	propane-1,2-diol	1:1:1	0.326
	choline chloride		0.597
	water		0.077
GCH	L-glucose	2:5:5	0.314
	choline chloride		0.608
	water		0.078

6 4.1.3 Culture media used to grow bacteria

LB-medium	10 g/l NaCl, 10 g/l tryptone, 5 g/l yeast extract, pH 7.5
LB-agar	LB + 1.5 % (w/v) agar-agar
TB-medium	12 g/l tryptone, 24 g/l yeast extract, 0.4 % glycerol, 72 mM K ₂ HPO ₄ , 17 mM KH ₂ PO ₄

ZY	10 g/l tryptone, 5 g/l yeast extract
ZYP-5052	volume fraction (v/v): 0.928 ZY, 0.05 20× NPS, 0.02 50× 5052, 0.002 1 M MgSO ₄ , 0.0002 1000× trace elements

1 4.1.4 Bacterial strains

2 *E.coli*

BL21(DE3)	F ⁻ <i>ompT hsdSB(r_B⁻,m_B⁻) gal dcm λ(DE3)</i> Invitrogen, Karlsruhe (Germany)
C41(DE3)	F ⁻ <i>ompT hsdSB(r_B⁻,m_B⁻) gal dcm λ(DE3)</i> Lucigen, Wisconsin (USA)
C43(DE3)	F ⁻ <i>ompT hsdSB(r_B⁻,m_B⁻) gal dcm λ(DE3)</i> Lucigen, Wisconsin (USA)
DH5α	F ⁻ <i>Φ80lacZΔM15 Δ(lacZYA-argF) U169 recA1 endA1 hsdR17(r_K⁻m_K⁺) phoA supE44 λ⁻ thi-1 gyrA96 relA1</i> Invitrogen, Karlsruhe (Germany)
JM110	<i>rpsL thr leu thi lacY galK galT ara tonA tsx dam dcm glnV44 Δ(lac-proAB) e14- [F' traD36 proAB⁺ lacI^q lacZΔM15] hsdR17(r_K⁻m_K⁺)</i> Martin-Luther-University Halle-Wittenberg
JW1593 (BW25113 derivative)	<i>rrnB ΔlacZ4787 HsdR514 Δ(arabAD)568 rph-1 ΔydgG (Kan^R)</i> Keio Collection, National Institute of Genetics (Japan)
MG1655	F ⁻ λ ⁻ <i>ilvG⁻ rfb-50 rph-1</i> DSMZ, Hamburg (Germany)
One Shot TOP10	F ⁻ <i>Φ80lacZΔM15 Δ(mrr-hsdRMS-mcrBC) recA1 endA1 mcrA ΔlacX74 araD139 Δ(ara-leu)7697 galU galK rpsL (Str^R) λ⁻ nupG</i> Invitrogen, Karlsruhe (Germany)
Origami(DE3)	<i>Δ(ara-leu)7697 ΔlacX74 ΔphoA Pvull phoR araD139 ahpC galE galK rpsL F'[lac + lacI q pro] (DE3)gor522::Tn10 trxB (Kan^R, Str^R, Tet^R)</i> Novagen, Wisconsin (USA)
Rosetta(DE3)	F ⁻ <i>ompT hsdSB(r_B⁻,m_B⁻) gal dcm λ(DE3) pRARE (Cam^R)</i> Novagen, Wisconsin (USA)

Rosetta(DE3) pLysS	F ⁻ <i>ompT hsdSB(r_B⁻,m_B⁻) gal dcm λ(DE3)</i> pLysSRARE (Cam ^R)
	Novagen, Wisconsin (USA)
T7 Express	<i>fhuA2 lacZ::T7 gene1 [lon] ompT gal sulA11 R(mcr-73::miniTn10-Tet^S)2 [dcm] R(zgb-210::Tn10-Tet^S) endA1 Δ(mcrC-mrr)114::IS10</i>
	NEB, Massachusetts (USA)

1 Agrobacterium tumefaciens

GV3101	chromosomal background: C58, marker gene: <i>rif</i> , Ti-plasmid: cured, opine: nopaline Sylvestre Marillonet, IPB
--------	--

2 4.1.5 Plasmids

Table 4.2.: Plasmids used in this work.

name	supplier/source
pACYCDuet-1	Merck, Darmstadt (Germany)
pCDFDuet-1	Merck, Darmstadt (Germany)
pET-20b(+)	Merck, Darmstadt (Germany)
pET-28a(+)	Merck, Darmstadt (Germany)
pET-32a(+)	Merck, Darmstadt (Germany)
pET-41a(+)	Merck, Darmstadt (Germany)
pQE30	QIAGEN, Hilden (Germany)
pUC19	Invitrogen, Karlsruhe (Germany)

3 4.1.6 Oligonucleotides and synthetic genes

4 Oligonucleotides and primers were ordered from Eurofins Genomics (Ebersberg, Germany). The purity grade was *high purity salt free* (HPSF). Synthetic genes or gene fragments were obtained from GeneArt® (Life Technologies, Darmstadt, Germany) or Eurofins Genomics (Ebersberg, Germany).

9 4.1.7 Instruments

CD-spectrometer	Jasco J-815 (Eaton, USA)
-----------------	--------------------------

electrophoresis (horizontal)	Biometra Compact XS/S (Göttingen, Germany)
electrophoresis (vertical)	Biometra Compact M (Göttingen, Germany) Biometra Minigel-Twin (Göttingen, Germany)
FPLC	ÄKTA purifier (GE Healthcare, Freiburg, Germany)
GC/MS	GC-MS-QP2010 Ultra (Shimadzu, Duisburg, Germany)
HPLC	VWR-Hitachi LaChrom Elite (VWR, Darmstadt, Germany)
ITC	MicroCal iTC200 (Malvern, Worcestershire, UK)
plate-reader	SpectraMax M5 (Molecular Devices, Biberach, Germany)
NMR-spectrometer	Varian Unity 400 (Agilent, Böblingen, Germany) Varian VNMRS 600 (Agilent, Böblingen, Germany)
photospectrometer	Eppendorf Biophotometer Plus (Hamburg, Germany) JASCO V-560 (Eaton, USA) Colibri Microvolume Spectrometer (Biozym, Hess. Oldendorf, Germany)
centrifuges	Eppendorf 5424 (Hamburg, Germany) Hettich Mikro 120 (Kirchlengern, Germany) Beckman Avanti J-E, Beckman Allegra X-30R (Krefeld, Germany)
centrifuge rotors	Beckman JA-10, JA-16.250, JS-4.3 (Krefeld, Germany)

4.1.8 Software

All mathematical and statistical computations and graphics were done with the R software (versions 3.1.X, <http://cran.r-project.org/>) [33]. Visualizations of macromolecules were arranged using the PyMol Molecular Graphics System, version 1.7.0.0 (Schrödinger, New York, USA) or UCSF Chimera version 1.9 (<http://www.cgl.ucsf.edu/chimera>) [159]. Physicochemical calculations and calculations of different molecular descriptors were performed using Marvin Beans 15.4.13.0 (ChemAxon, Budapest, Hungary) and Molecular Operating Environment 2008.10 (Chemical Computing Group, Montreal, Canada). Special software used for X-ray crystal structure solution is discussed separately in the corresponding section (4.5).

Table 4.3.: Primers used in this work. Recognition sites for endonucleases are underlined. Positions used for site directed mutagenesis are in lower case font.

name	sequence (5'→3')	cloning site
somt1	TTG <u>AAG ACA</u> AAA TGG CTT CTT CAT TAA ACA ATG GCC G	BpiI
somt2	TT <u>G AAG ACA</u> AGG ACA CCC CAA ATA CTG TGA GAT CTT CC	BpiI
somt3	TTG <u>AAG ACA</u> AGT CCT TAG GAA CAC CTT TCT GGG AC	BpiI
somt4	TT <u>G AAG ACA</u> AAA GCT CAA GGA TAG ATC TCA ATA AGA GAC	BpiI
pfromt1.fw	CAG AGA GGC cTA TGA GAT TGG CTT GC	
pfromt1.rv	GCA AGC CAA TCT CAT AgG CCT CTC TG	
pfromt2.fw	<u>CAT ATG</u> GAT TTT GCT GTG ATG AAG CAG GTC	NdeI
pfromt2.rv	<u>GAA TTC</u> AAT AAA GAC GCC TGC AGA AAG TG	EcoRI
pRha1.fw	CTC TAG <u>CAG ATC</u> TCG GTG AGC ATC ACA TCA CCA CAA TTC	BglII
pRha1.rv	CAA TTG AGG ATC <u>CCC ATT</u> TTA ACC TCC TTA GTG	BamHI
pUC1.fw	GCG TAT TGG Gag aTC TTC CGC TTC CTC	
pUC1.rv	GAG GAA GCG GAA GAt ctC CCA ATA CGC	

4.2 Molecular Biology

2 Basic molecular biology methods like polymerase chain reaction (PCR),
 3 DNA restriction/ligation, DNA gel electrophoresis, preparation of com-
 4 petent cells and transformation were performed based on the protocols
 5 summarized by Sambrook and Russell [167]. Plasmid DNA was isolated
 6 using the QIAprep® Spin Miniprep Kit (QIAGEN, Hilden, Germany) accord-
 7 ing to the manufacturer's instructions. In vitro site-directed mutatgenesis
 8 was set-up according to the protocol of the *QuikChange™ Site-Directed*
 9 *Mutagenesis* kit [3] offered by Agilent Technologies (Santa Clara, USA).
 10 Nucleotide fragments obtained by PCR, restriction/ligation procedures or
 11 excision from electrophoresis gels were purified and concentrated using the
 12 *Nucleospin Gel and PCR Clean-up* kit provided by Machery-Nagel (Düren,
 13 Germany) according to the instructions provided by the manufacturer.

4.2.1 Golden Gate Cloning

15 The Golden Gate cloning procedure is a one-pot method, meaning the re-
 16 striction digestion and ligation are carried out in the same reaction vessel at
 17 the same time [55, 106]. Consequently PCR-fragments, destination vector,
 18 restriction endonuclease and ligase are added together in this reaction.
 19 The methodology employs type II restriction enzymes, which together
 20 with proper design of the fragments allow for a ligation product lacking
 21 the original restriction sites. For digestion/ligation reactions of fragments

1 containing BpiI sites, 20 fmol of each fragment or vector, together with 5 U
 2 of BpiI and 5 U of T4 ligase were combined in a total volume of 15 µl 1×
 3 ligase buffer. For fragments to be cloned via BsaI sites, BpiI in the above
 4 reaction was substituted by 5 U BsaI. The reaction mixture was placed in a
 5 thermocycler and incubated at 37 °C for 2 min and 16 °C for 5 min. These
 6 two first steps were repeated 50 times over. Finally, the temperature was
 7 raised to 50 °C (5 min) and 80 °C (10 min) to inactivate the enzymes.

8 The *SOMT2* gene was amplified from pET28a-SOMT using primers
 9 *somt1–somt4* (Table 4.3), cloned into vector pICH41308 (level 0) using BpiI
 10 and consequently subcloned into the level 1 module pICH75044, alongside
 11 35S promoter and nopaline synthase (nos)-terminator, using BsaI (Fig-
 12 ure 4.1). The resulting construct was denoted as pBEW107.

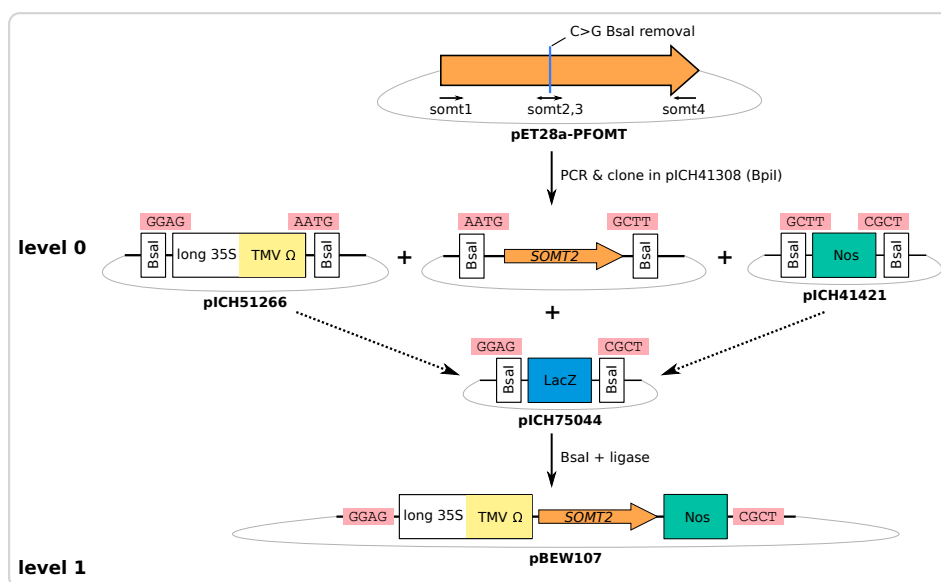


Figure 4.1.: Golden Gate cloning scheme for soy O-methyl transferase (*SOMT-2*)

13 4.2.2 Subcloning of genes

14 All subcloning procedures were performed according to section 4.2 and
 15 specifically subsection 4.2.1. Specific steps for the subcloning of any genes
 16 discussed can be found in the appendix (p.137). The *pfomt* gene was sub-
 17 cloned from the pQE-30 vector kindly provided by Thomas Vogt (Leibniz-
 18 Institute of Plant Biochemistry (IPB), Halle, Germany) into the pET-28a(+)
 19 vector. The *somt-2* gene was subcloned from the pQE-30 vector kindly
 20 provided by Martin Dippe (IPB, Halle, Germany) into the pET-28-MC vector.

1 4.2.3 Transformation of electrocompetent *Agrobacterium tumefaciens* cells

3 A 50 µl aliquot of electrocompetent *A. tumefaciens* cells was thawed on
4 ice. (50 to 100) ng of plasmid were added, the solution was mixed gently
5 and transferred to a pre-cooled electroporation cuvette. After pulsing
6 (2.5 kV, 200 Ω) 1 ml of lysogeny broth (LB)-medium was added, the mixture
7 transferred to a 1.5 ml tube and incubated for (3 to 4) hours at 28 °C. The
8 culture was centrifuged (10 000 × g, 1 min) and 900 µl supernatant were
9 discarded. The pellet was resuspended in the remaining liquid, plated
10 onto LB-agar plates supplemented with 40 µg/ml rifampicin and 50 µg/ml
11 carbencillin and incubated at 28 °C for (2 to 3) days.

12 4.3 Treatment of plant material

13 4.3.1 Infiltration of *Nicotiana benthamiana*

14 Before infiltration *N. benthamiana* plants were pruned, such that only
15 leaves to be infiltrated remained with the plant (Figure 4.2). 5 ml cultures
16 of transformed *A. tumefaciens* in LB-medium (with 40 µg/ml rifampicin
17 and 50 µg/ml carbencillin) were grown over night at 28 °C and 220 rpm.
18 OD₆₀₀ of the culture was measured and adjusted to 0.2 by dilution with
19 infiltration buffer (10 mM MES/NaOH, 10 mM MgSO₄ pH 5.5). When mul-
20 tiple *A. tumefaciens* transformed with different constructs/plasmids were
21 used for infiltration, the cultures were mixed and diluted using infiltration
22 buffer, such that OD₆₀₀ of each culture in the mix was 0.2. The solution was
23 infiltrated into the abaxial side of *N. benthamiana* leaves using a plastic
24 syringe. The leaf material was harvested after 7 days.

25 Infiltration of *N. benthamiana* for *in vivo* biotransformation using 26 SOMT-2

27 Both sides of *N. benthamiana* leaves were infiltrated with different sam-
28 ples (Figure 4.2). The left side was infiltrated with *A. tumefaciens* cul-
29 tures transformed with pAGM10733 (phenylalanine ammonia-lyase (PAL)),
30 pAGM10406 (chalcone synthase (CHS)) and pBEW107 (SOMT-2). For the
31 right side the *A. tumefaciens* culture containing pBEW107 was replaced by
32 a control: *A. tumefaciens* transformed with the empty vector pICH75044.

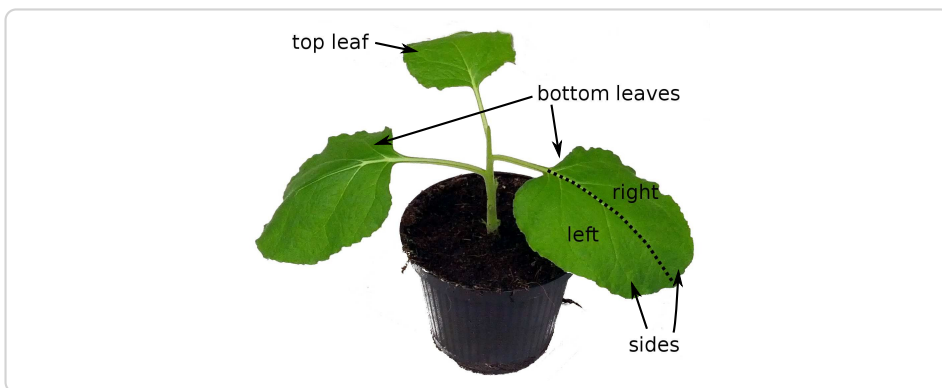


Figure 4.2: Pruned *N. benthamiana* plant, with two bottom and one top leaf, ready to be infiltrated.

1 4.3.2 Plant material harvest

2 Infiltrated/Infected areas of *N. benthamiana* leaf material were cut out
3 and grouped by plant number, leaf position (top/bottom) and leaf side
4 (right/left). The grouped clippings were weighed, frozen in liquid nitrogen,
5 ground to a powder, freeze-dried and stored at -80 °C.

6 4.3.3 Extraction of flavonoids from *N. benthamiana* 7 leaves

8 Two tips of a small spatula of freeze-dried material (\approx 6 mg), were weighed
9 exactly and extracted with 500 μ l 75 % aqueous methanol containing 1 mM
10 ascorbic acid, 0.2 % formic acid and 0.1 mM flavone (internal standard).
11 Therefore the suspension was vortexed for 30 s, rotated on an orbital shaker
12 for 10 min and vortexed again for 30 s. The suspension was centrifuged
13 (20 000 $\times g$, 4 °C, 10 min) and the supernatant transferred to a new tube, to
14 remove the insoluble plant material. The supernatant was centrifuged again
15 (20 000 $\times g$, 4 °C, 10 min) and the resulting supernatant was transferred to
16 a HPLC-vial and stored at -20 °C until analysis.

17 4.4 Protein biochemistry

18 Stock solutions of antibiotics, IPTG or sugars were prepared according to
19 the pET System Manual by Novagen [154], unless otherwise noted.

Table 4.4.: Calculated extinction coefficients of proteins used in this work.

protein/enzyme	$\epsilon_{280\text{nm}}^{1\text{ g/l}}$ in $\text{ml mg}^{-1} \text{cm}^{-1}$
PFOMT (reduced)	0.714
PFOMT Y51K N202W (reduced)	0.852
SOMT-2 (oxidized)	1.263
SOMT-2 (reduced)	1.247

1 4.4.1 Determination of protein concentration

2 Protein concentrations were estimated using the absorption of protein
 3 solutions at 280 nm, which is mainly dependent on the amino acid com-
 4 position of the protein studied [70]. Extinction coefficients of proteins
 5 were calculated from the amino acid sequence using the ExpPASy servers's
 6 ProtParam tool [66].

7 4.4.2 Protein production test (expression test)

8 The heterologous production of proteins in *E. coli* was assessed in a small
 9 scale protein production test, henceforth called expression test. Single
 10 colonies of *E. coli* transformed with the constructs to be studied were used
 11 to inoculate a 2 ml starter culture in LB-medium containing the appro-
 12 priate antibiotics. The working concentrations of antibiotics used was
 13 as follows: 200 µg/ml ampicillin, 150 µg/ml kanamycin, 50 µg/ml chloram-
 14 phenicol, 20 µg/ml tetracycline. The starter culture was allowed to grow
 15 at 37 °C and 200 rpm over night. A 5 ml sampling culture of the medium
 16 to be studied containing the appropriate antibiotics was prepared. The
 17 media tested included LB, terrific broth (TB) and auto-induction media like
 18 ZYP-5052. The sampling culture was inoculated to an OD₆₀₀ of 0.075 using
 19 the starter culture and incubated at different temperatures and 200 rpm in
 20 a shaking incubator. 1 mM isopropyl-D-thiogalactopyranosid (IPTG) was
 21 added when the OD₆₀₀ reached 0.6-0.8, if appropriate for the studied con-
 22 struct. 1 ml samples were removed after different times of incubation (e.g.
 23 4, 8, 12 hours), subfractionated (4.4.3) and analyzed via SDS-polyacrylamide
 24 gel electrophoresis (PAGE) (4.4.6).

1 4.4.3 Protein subfractionation

2 The protein subfractionation procedure described herein was adapted from
3 the protocol described in the pET Manual [154]. Overall 5 protein sub-
4 fractions can be obtained, including *total cell protein*, *culture supernatant*
5 (*medium*) *protein*, *periplasmic protein*, *solute cytoplasmic protein* and *in-*
6 *soluble protein*. The OD₆₀₀ of the culture sample was measured and the
7 cells harvested by centrifugation at 10 000 × g, 4 °C for 5 minutes. The pro-
8 tein in the supernatant medium was concentrated by precipitation with
9 trichloro acetic acid (TCA) (4.4.4) for SDS-PAGE analysis. The periplasmic
10 protein was prepared (4.4.5) and also concentrated by TCA precipitation
11 for SDS-PAGE. Cells were lysed by resuspending the cell pellet in (OD₆₀₀
12 × V × 50) µl of bacterial protein extraction reagent (B-PER) and vortexing
13 vigorously for 30 s. The suspension was incubated at room temperature
14 (RT) for 30 min to assure complete lysis. To separate insoluble protein
15 and cell debris from the soluble cytosolic protein, the suspension was
16 centrifuged at 10 000 × g and 4 °C for 10 min. Soluble cytoplasmic protein
17 was contained in the supernatant, whereas insoluble protein remained
18 in the pellet. For SDS-PAGE analysis of the insoluble protein, the pellet
19 was resuspended in the same volume of B-PER. To obtain only the total
20 cell protein fraction, the preparation of periplasmic and soluble cytosolic
21 protein was omitted. Sample volumes of 10 µl of each fraction were used
22 for SDS-PAGE analysis.

23 4.4.4 Protein sample concentration by TCA precipita- 24 tion

25 Diluted protein samples were concentrated by TCA precipitation in micro-
26 centrifuge tubes. Therefore 0.1 volume (V) of 100 % (w/v) TCA in water
27 was added to the clarified sample, which was then vortexed for 15 s and
28 placed on ice for a minimum of 15 min. The sample was centrifuged at
29 14 000 × g, 4 °C for 15 min. The supernatant was discarded and the pellet
30 was washed twice with 0.2 V ice-cold acetone. The acetone was removed
31 and the pellet set to air-dry in an open tube. After drying, the protein
32 pellet was resuspended in 0.1 V phosphate buffered saline (PBS) contain-
33 ing 1 × SDS-sample buffer by heating to 85 °C and vigorous vortexing, to
34 achieve a 10 × concentration. After resuspension the sample was analyzed
35 by SDS-PAGE or stored at -20 °C until use.

1 4.4.5 Preparation of periplasmic protein

2 Target proteins may be directed to the periplasmic space by N-terminal
3 signal sequences like *pelB* or *DsbA/C* [133]. The periplasma is, other than
4 the cytosol, an oxidizing environment and often used for the production
5 of proteins containing disulfide linkages. The preparation of periplasmic
6 protein was accomplished by an osmotic shock protocol modified from
7 Current Protocols in Molecular Biology [7]. The cell pellet was resus-
8 pended in the same volume as the culture sample of 30 mM tris-HCl, 20 %
9 (w/v) sucrose, pH 8 and 1 mM ethylenediaminetetraacetic acid (EDTA) was
10 added. The suspension was stirred for 10 min at RT and the cells were
11 collected by centrifugation at $10\,000 \times g$, 4 °C for 10 min. The supernatant
12 was discarded and the cell pellet was resuspended in the same volume of
13 ice-cold 5 mM MgSO₄. The suspension was stirred for 10 min on ice, while
14 the periplasmic proteins were released into the solution. The cells were
15 collected by centrifugation as before. Periplasmic proteins were contained
16 in the supernatant.

17 4.4.6 Discontinuous SDS-polyacrylamide gel electrophore- 18 sis (SDS-PAGE)

19 The analysis of samples via SDS-PAGE was realized via the discontinuous
20 system first described by Laemmli, which allows separation of proteins
21 based on their electrophoretic mobility, which in turn depends on their
22 size [112]. The SDS-PAGE procedure was carried out according to standard
23 protocols described by Sambrook and Russell [167]. Very dilute and/or
24 samples with high ionic strength were concentrated and/or desalted by
25 the TCA precipitation procedure described in subsection 4.4.4. Generally a
26 10 % (acrylamide/bisacrylamide) running gel combined with a 4 % stacking
27 gel was used. Reducing SDS-PAGE sample buffer was added to the protein
28 sample to be analyzed, whereafter the sample was heated to 95 °C for
29 5 min, to allow for total unfolding of the protein. After cooling to RT the
30 samples were transferred into the gel pockets for analysis. The *PageRuler™*
31 *Prestained Protein Ladder* (Life Technologies GmbH, Darmstadt, Germany)
32 was used as a molecular weight (MW) marker and run alongside every
33 analysis as a reference. Gels were stained using a staining solution of 0.25 %
34 Coomassie Brilliant Blue G-250 (w/v) in water:methanol:acetic acid (4:5:1)
35 and destained by treatment with water:methanol:acetic acid (6:3:1).

1 4.4.7 Buffer change of protein samples

2 The buffer in protein samples was exchanged either by dialysis, or by
3 centrifugal filter concentrators (Amicon® Ultra Centrifugal Filter; Merck,
4 Darmstadt, Germany). Large volumes of highly concentrated protein so-
5 lutions were preferably dialyzed. Respectively, very dilute samples were
6 concentrated and rebuffered using centrifugal concentrators. Dialysis was
7 carried out at least twice against a minimum of 100 times the sample vol-
8 ume. Dialysis steps were carried out at RT for 2 hours, or over-night at
9 4 °C. Centrifugal concentrators were used according to the manufacturers
10 instructions.

11 4.4.8 Production of recombinant protein

12 Heterologous production of PFOMT

13 Phenylpropanoid and flavonoid O-methyl transferase (PFOMT) was pro-
14 duced as a N-terminally (His)₆-tagged fusion protein. A 2 ml starter cul-
15 ture of LB containing 100 µg/ml kanamycin was inoculated with a single
16 colony of *E. coli* BL21(DE3) transformed with pET28-pfomt and incubated
17 at 37 °C, 220 rpm for 6 hours. The main culture (N-Z-amino, yeast extract,
18 phosphate (ZYP-5052) containing 200 µg/ml kanamycin) was inoculated
19 with the starter culture such that OD₆₀₀ was 0.05. The culture was incu-
20 bated in a shaking incubator at 37 °C, 220 rpm over night (≈16 h). Due to
21 the autoinducing nature of the ZYP-5052 medium, addition of IPTG was
22 not neccesary. Cells were harvested by centrifugation at 10 000 × g, 4 °C
23 for 10 min and the supernatant discarded. The pellet was resuspended
24 in 50 mM Tris/HCl, 500 mM NaCl, 2.5 mM imidazole, 10 % glycerol pH 7
25 using a volume of ≈10 ml/g of cell pellet. The cells were lysed by sonica-
26 tion (70 % amplitude, 1 s on-off-cycle) for 30 seconds, which was repeated
27 twice. The crude lysate was clarified by centrifugation at 15 000 × g, 4 °C
28 for 15 minutes followed by filtration through a 0.45 µm filter. Consequently,
29 the His-tagged PFOMT was purified by immobilized metal affinity chro-
30 matography (IMAC) (4.4.10). The eluted PFOMT protein was dialyzed
31 (4.4.7) against 25 mM HEPES, 100 mM NaCl, 5 % glycerol pH 7 and stored
32 at -20 °C until use.

1 Heterologous production of SOMT-2

2 SOMT-2 was produced as a fusion protein with an N-terminal His-tag. A
3 starter LB-culture (\approx 2 ml) containing 100 μ g/ml kanamycin was inoculated
4 with a single colony of *E. coli* BL21(DE3) transformed with pET28MC-somt
5 and incubated at 37 °C, 220 rpm for 6 hours. The starter culture was used to
6 inoculate the main culture (LB-medium containing 100 μ g/ml kanamycin),
7 such that OD₆₀₀ \approx 0.05. The culture was incubated at 37 °C, 220 rpm in a
8 shaking incubator until OD₆₀₀ \approx 0.6. Expression was induced by addition of
9 1 mM IPTG. Incubation continued at 37 °C, 220 rpm for 6 hours. Cells were
10 harvested by centrifugation (10 000 $\times g$, 4 °C, 10 min) and used, or stored at
11 –20 °C until use. SOMT-2 was produced in inclusion bodies (IBs), which
12 were prepared as laid out in subsection 4.4.9.

13 4.4.9 Preparation of inclusion bodies (IBs)

14 Often, when recombinant protein is produced in high levels in *E. coli* it is
15 accumulated in so-called inclusion bodies (IBs) [166]. The accumulating IBs
16 consist mainly of the overproduced target protein, which is inherently quite
17 pure already. IBs can be selectively recovered from *E. coli* cell lysates and
18 can consequently be refolded. IBs were prepared according to a modified
19 protocol by Palmer [157]. The cells were resuspended in 5 ml/g_{cells} IB
20 lysis buffer (100 mM Tris/HCl, 1 mM EDTA pH 7), 0.5 mM phenylmethyl-
21 sulfonylfluoride (PMSF) was added as protease inhibitor. The solution was
22 homogenized using a tissue grinder homogenizer (Ultra Turrax®; IKA® -
23 Werke GmbH & Co. KG, Staufen, Germany). 200 μ g/ml lysozyme was added
24 to aid in the breakage of cells and the cells were lysed by sonicating thrice
25 at 70 % amplitude (1 s on-off-cycle) for 30 seconds. DNase I (10 μ g/ml) was
26 added and the solution was incubated on ice for 10 min. The lysate was
27 clarified by centrifuging for 1 h at 20 000 $\times g$, 4 °C. The supernatant was
28 discarded and the pellet was resuspended in 5 ml/g_{cells} IB wash buffer I
29 (20 mM EDTA, 500 mM NaCl, 2 % (w/v) Triton X-100 pH), followed by thor-
30 ough homogenization. The solution was centrifuged (30 min at 20 000 $\times g$,
31 4 °C), the supernatant discarded and the pellet was washed twice more.
32 To remove detergent, the pellet was washed twice again with IB washing
33 buffer II (20 mM EDTA, 100 mM Tris/HCl pH 7). The IBs were resuspended
34 in IB solubilization buffer (100 mM Tris/HCl, 5 mM DTT, 6 M GdmCl pH 7),

1 such that the protein concentration was about 25 mg/ml and stored at
2 –20 °C until use.

3 4.4.10 Purification of His-tagged proteins using immo- 4 bilized metal affinity chromatography (IMAC)

5 N- or C-terminal oligo-histidine tags (His-tags) are a common tool to ease
6 purification of recombinantly produced proteins. The free electron pairs
7 of the imidazol nitrogens of histidines can complex divalent cations such
8 as Mg²⁺ or Ni²⁺, which are usually immobilized on a matrix of nitrilo
9 triacetic acid (NTA)-derivatives. The affinity of the His-tag is correlated
10 with its length and tagged proteins can simply be eluted by increasing
11 the concentration of competing molecules (e.g. imidazole). His-tagged
12 protein was purified by fast protein liquid chromatography (FPLC) via Ni²⁺-
13 (HisTrap FF crude) or Co²⁺-NTA (HiTrap Talon FF crude) columns, obtained
14 from GE Healthcare (Freiburg, Germany), following modified suppliers
15 instructions. First the column was equilibrated with 5 column volumes (CV)
16 of binding buffer (50 mM Tris/HCl, 500 mM NaCl, 10 % glycerol, 2.5 mM
17 imidazole pH 7). The sample (generally clarified lysate) was applied to
18 the column using a flow of 0.75 ml/min. Unbound protein was removed by
19 washing with 3 CV binding buffer. Unspecifically bound proteins were
20 washed away by increasing the amount of elution buffer (50 mM Tris/HCl,
21 500 mM NaCl, 10 % glycerol, 250 mM imidazole pH 7) to 10 % (constant for
22 3 to 5 CV). Highly enriched and purified target protein was eluted with 6
23 to 10 CV of 100 % elution buffer.

24 4.4.11 Refolding of SOMT-2 on a micro scale using de- 25 sign of experiments (DoE)

26 Design of experiments (DoE) and fractional factorial design (FrFD) have
27 been successfully used to optimize the refolding conditions of several
28 proteins [4, 11, 214]. Thus, an approach using fractional factorial design
29 (FrFD) was used to find optimal refolding conditions for SOMT-2. Factors
30 studied were pH (buffer), arginine, glycerol, divalent cations, ionic strength,
31 redox system, cyclodextrin and co-factor addition. The experimental matrix
32 was constructed using the FrF2 package (<http://cran.r-project.org/web/packages/FrF2/index.html>) in the R software.
33

Table 4.5.: Factors and their high and low levels (+/-) used in the construction of the fractional factorial design (FrFD).

factor	symbol	setting (level)		unit
		-	+	
pH	A	5.5	9.5	-
arginine	B	0	0.5	M
glycerol	C	0	10	% (v/v)
divalent cations [†]	D	no	yes	-
ionic strength [‡]	E	low	high	-
redox state [*]	F	reducing	redox-shuffling	-
α -cyclodextrin	G	0	30	mM
SAH	H	0	0.5	mM

[†]no: 1 mM EDTA; yes: 2 mM CaCl₂, MgCl₂[‡]low: 10 mM NaCl, 0.5 mM KCl; high: 250 mM NaCl, 10 mM KCl^{*}reducing: 5 mM DTT; redox-shuffling: 1 mM glutathione (GSH), 0.2 mM glutathione disulfide (GSSG)**Table 4.6.**: Experimental design matrix for the FrFD.

Experiment	A	B	C	D	E	F	G	H
1	+	+	+	-	-	-	-	+
2	-	-	-	-	-	-	-	-
3	+	-	+	+	-	+	+	-
4	-	+	+	-	+	+	+	-
5	+	+	-	-	+	+	-	-
6	-	+	-	+	+	-	+	+
7	+	+	-	+	-	-	+	-
8	-	-	+	-	+	-	+	+
9	+	-	+	+	+	-	-	-
10	-	-	-	-	-	+	+	+
11	+	-	-	+	+	+	-	+
12	-	+	+	+	-	+	-	+

- 1 The buffers were mixed from stock solutions and prepared in 1.5 ml
 2 microcentrifuge tubes immediately prior to the experiment. 50 μ l of solu-
 3 bilized SOMT-2 (1 mg/ml) in IB solubilization buffer was added to 1 ml of
 4 each buffer followed by a short vortex boost for rapid mixing. The final
 5 protein concentration in the refolding reaction was 50 μ g/ml, whereas the
 6 remaining GdmCl concentration was \approx 286 mM. The refolding reactions
 7 were incubated at RT for 1 hour, followed by an over night incubation at
 8 4 °C. After incubation the refolding reactions were centrifuged (10 000 \times g,
 9 4 °C, 10 min) to separate insoluble and soluble protein fractions. The su-
 10 pernatant was transferred to a new tube, whereas the pellet was washed
 11 twice with 200 μ l acetone and once with 400 μ l methanol/acetone (1:1).
 12 The pellet was resuspended in 100 μ l PBS with 20 μ l SDS-PAGE sample

1 buffer and 10 µl were used for SDS-PAGE analysis. 100 µl of the super-
2 natant were concentrated using TCA precipitation (4.4.4) and analyzed by
3 SDS-PAGE. The remaining supernatant was rebuffered into 50 mM 2-[Bis(2-
4 hydroxyethyl)amino]-2-(hydroxymethyl)propane-1,3-diol (BisTris) pH 7.5
5 using Amicon® Ultra 0.5 ml centrifugal filters (Merck, Darmstadt, Germany)
6 according to the manufacturers instructions. The pre-weighed collection
7 tubes were re-weighed after recovery and the volume of recovered liquid
8 calculated ($\rho \approx 1 \text{ g/cm}^3$). The sample was filled up to 100 µl using 50 mM
9 BisTris pH 7.5 and the protein concentration was assessed using the Roti®-
10 Quant protein quantification solution (Carl Roth, Karlsruhe, Germany)
11 according to the manufacturers description. 50 µl of each refolded sample
12 was used for an activity test using naringenin as substrate (4.6.3). The
13 reactions were incubated over night and stopped by the extraction method.
14 However, before the actual extraction 1 µl of anthracene-9-carboxylic acid
15 (AC-9) was added as internal standard. The samples were analyzed by
16 high-performance liquid chromatography (HPLC).

17 Assessment of refolding performance

18 The performance of each buffer on the refolding of SOMT-2 was examined
19 by comparing the SDS-PAGE results, as well as the amount of soluble
20 protein and the conversion of naringenin over night (see subsection 4.6.3).
21 Main effects were analyzed qualitatively using main effects plots [20].

22 Upscaling of refolding reactions

23 Refolding reactions were scaled up to 50 ml. Therefore 2.5 ml solubilized
24 SOMT-2 (1 mg/ml) were added over 10 minutes to 50 ml of refolding buffer
25 while stirring at RT. The refolding reaction was allowed to complete over
26 night at 4 °C.

27 4.4.12 Enzymatic production of SAM and SAE

28 S-adenosyl-L-methionine (SAM) and S-adenosyl-L-ethionine (SAE) were
29 prepared according to the method described by Dippe, et. al [49].

30 Preparative reactions (20 ml) were performed in 0.1 M Tris/HCl, 20 mM
31 MgCl₂, 200 mM KCl pH 8.0 and contained 7.5 mM adenosine triphosphate
32 (ATP), 10 mM D,L-methionine or D,L-ethionine, for the production of SAM

1 or SAE respectively, and 0.2 U S-adenosylmethionine synthase (SAMS) vari-
2 ant I317V. The reaction was stopped by lowering the pH to 4 using 10 M
3 acetic acid after 18 h of incubation at 30 °C, 60 rpm. After 10 min incubation
4 on ice the solution was centrifuged ($15\ 000 \times g$, 10 min) to remove insoluble
5 matter. The supernatant was transferred to a round bottom flask, frozen in
6 liquid nitrogen and lyophilized. Crude products were extracted from the
7 pellet using 73 % ethanol and purified using ion exchange chromatography
8 (IEX). IEX was performed on a sulfopropyl sepharose matrix (25 ml) via
9 isocratic elution (500 mM HCl). Before injection, the crude extract was
10 acidified to 0.5 M HCl using concentrated hydrochloric acid. After elu-
11 tion, the product containing fractions were dried via lyophilization. The
12 amount of product was determined by UV/VIS-spectroscopy at 260 nm
13 using the published extinction coefficient of SAM ($\varepsilon_0 = 15\ 400\ M^{-1}\ cm^{-1}$)
14 after resuspension in water [178].

15 4.5 Crystallographic Procedures

16 4.5.1 Crystallization of proteins

17 Commercially available crystallization screens were used to find initial
18 crystallization conditions. The tested screens included kits available from
19 Hampton Research (Aliso Viejo, USA) and Jena Bioscience (Jena, Ger-
20 many). Crystallization screens were processed in 96-well micro-titer plate
21 (MTP)s, where each well possessed 4 subwells aligned in a 2×2 matrix.
22 The subwells were divided into 3 shallow wells for sitting drop vapour
23 diffusion experimental setups and a fourth subwell, which was deep enough
24 to act as buffer reservoir. This way the performance of each crystallization
25 buffer could be assessed using three different protein solutions with vary-
26 ing concentrations, effectors etc. A pipetting robot (Cartesian Microsys,
27 Zinsser-Analystik; Frankfurt, Germany) was used to mix 200 nl of each,
28 protein and buffer solution, for a final volume of 400 nl. The crystallization
29 preparations were incubated at 16 °C and the progress of the experiment
30 was documented by an automated imaging-system (Desktop Minstrel UV,
31 Rigaku Europe, Kent, UK). Furthermore, fine screens (e.g. for refinement of
32 crystallization conditions) were set up by hand in 24-well MTPs using the
33 hanging drop vapour diffusion method.

1 PFOMT

2 PFOMT protein was concentrated to (6 to 8) mg/ml and rebuffered to 10 mM
3 Tris/HCl pH 7.5 using Amicon® Ultracel centrifugal concentrators (10 kDa
4 MWCO). The concentrated protein solution was centrifuged at 14 000 × g,
5 4 °C for 10 min to remove any insoluble material or aggregates. Flavonoids
6 and phenylpropanoid substrates were added to the protein solution from
7 10 mM stock solution in dimethyl sulfoxide (DMSO). Crystallization screens
8 were set up as described above.

9 *apo*-PFOMT was crystallized using the following conditions – 2 M
10 (NH₄)₂SO₄, 20 %glycerol. The protein solution contained 0.25 mM SAE,
11 0.25 mM MgCl₂, 0.25 mM eriodictyol and 7.53 mg/ml (0.262 mM) PFOMT .

12 Crystallization of proteins using NADES

13 NADES have the potential to be excellent solvents for hydrophobic com-
14 pounds such as flavonoids or cinnamic acids [43] and in addition they are
15 able to stabilize and activate enzymes [81].

16 Four different model proteins (bovine trypsin, hen-egg white lysozyme,
17 proteinase K and *Candida cylindrica* lipase B) were used to assess the
18 capability of NADES for protein crystallization. PCH was tested in a
19 full factorial grid layout using PCH concentrations of (20, 30, 40 and
20 50) % combined with buffers of different pH. The buffers included 0.1 M
21 sodium acetate pH (4.5 and 5.5), 0.1 M sodium citrate pH 6.5, 0.1 M 2-[4-
22 (2-hydroxyethyl)piperazin-1-yl]ethanesulfonic acid (HEPES)/NaOH pH (7
23 and 7.5) and 0.1 M Tris/HCl pH 8.5. Thus, the full factorial design had a
24 size of 4 × 6 = 24 different conditions. Protein solutions were prepared
25 from lyophilized protein and were as follows: 90 mg/ml trypsin in 10 mg/ml
26 benzamidine, 3 mM CaCl₂; 75 mg/ml lysozyme in 0.1 M sodium acetate pH
27 4.6; 24 mg/ml proteinase K in 25 mM Tris/HCl pH 7.5 and 6 mg/ml lipase B
28 in water. For crystallization 2 µl enzyme solution and 1 µl reservoir buffer
29 were mixed and set up in a hanging drop experiment on a 24-well MTP.
30 The experiments were set up at 4 °C.

31 4.5.2 Data collection and processing

32 Crystallographic data were collected at the beamline of the group of Profes-
33 sor Stubbs (MLU, Halle, Germany). The beamline was equipped with a ro-
34 tating anode X-ray source MicroMax007 (Rigaku/MSC, Tokio, Japan), which

1 had a maximum power of 0.8 kW (40 kV, 20 mA) and supplied monochro-
2 matic Cu-K α -radiation with a wavelength of 1.5418 Å. Diffraction patterns
3 were detected with a Saturn 944+ detector (CCD++, Rigaku/MSC, Tokio,
4 Japan).

5 Indexing and integration of the reflexes via Fourier transformation (FT)
6 was accomplished using *XDS* [93, 94, 95] or *MOSFLM* [160]. *Scala* [57],
7 which is integrated in the Collaborative Computational Project No. 4
8 (CCP4)-Suite, was used for scaling of the intensities.

9 4.5.3 Structure solution

10 For the determination of the electron density $\rho(\mathbf{r})$, where \mathbf{r} is the positional
11 vector, from the diffraction images by FT two terms are necessary as
12 coefficients; the *structure factor amplitudes*, $F_{\text{obs}}(\mathbf{h})$ and the *phase angles* or
13 *phases*, $\alpha(\mathbf{h})$, where \mathbf{h} is the reciprocal index vector. The structure factor
14 amplitudes can be directly determined from the measured and corrected
15 diffraction intensities of each spot. However, the phase information is lost
16 during the detection of the diffracted photons and there is no direct way to
17 determine the phases. This constitutes the so-called *phase problem*. Thus,
18 additional phasing experiments are necessary in order to obtain the phases.
19 A variety of phasing experiments are available, which include *marker*
20 *atom substructure methods*, *density modification* and *molecular replacement*
21 (*MR*) techniques [197]. Phases of the structures herein were exclusively
22 determined by *MR* [164, 165]. *MR* was performed using the software
23 *Phaser* [141, 142], which is included in the CCP4-Suite [216]. A previously
24 published PFOMT structure (PDB-code: 3C3Y [109]) was used as a template
25 during *MR* procedure for the PFOMT structure solution.

26 4.5.4 Model building, refinement and validation

27 Macromolecular model building and manipulation, as well as real space
28 refinement and Ramachandran idealization were performed using the Crys-
29 tallographic Object-Oriented Toolkit (*Coot*) software [54]. Structure re-
30 finement was done using the software REFMAC5 [152, 202] as part of the
31 CCP4-suite or the Phyton-based Hierachial Environment for Integrated
32 Xtallography (PHENIX) [1]. Validation of the structures was carried out
33 using the web service MolProbity (<http://molprobity.biochem.duke.edu/>)
34 [30]. Structure visualization and the preparation of figures was performed

1 using PyMOL (Schrödinger, New York, USA) and UCSF Chimera (<http://www.cgl.ucsf.edu/chimera>) [159].

3 4.5.5 ***In silico* substrate docking**

4 *In silico* molecular docking studies were performed using the AutoDock
5 Vina 1.1.2 or AutoDock 4.2.6 software in combination with the AutoDockTools-
6 Suite (<http://autodock.scripps.edu/>) [82, 149, 199]. Substrates were docked
7 into the PFOMT structure with the PDB-code 3C3Y. The grid box, which
8 determines the search space, was manually assigned to center at 1.581,
9 5.196 and 25.718 (x, y, z) and had size of (22, 20 and 25) Å (x, y, z). The
10 exhaustiveness of the global search for AutoDock Vina was set to 25,
11 whereas the rest of the input parameters were kept at their defaults.

12 4.6 Analytics

13 4.6.1 Recording of growth curves

14 Starter cultures (\approx 2 ml) of the transformed *E. coli* cells were prepared in the
15 medium to be studied, containing the appropriate antibiotics. The cultures
16 were incubated at 37 °C, 200 rpm over night and harvested by centrifuga-
17 tion ($5000 \times g$, 4 °C, 5 min). The pellet was resuspended in 15 ml PBS and
18 the suspension centrifuged ($5000 \times g$, 4 °C, 5 min). The supernatant was
19 discarded and the washing step repeated once more. The washed pellet
20 was resuspended in 2 ml of the medium to be studied with the appropriate
21 antibiotics and the OD₆₀₀ was measured. Three independent 50 ml cultures
22 of the medium containing the appropriate antibiotics were inoculated such
23 that OD⁶⁰⁰ \approx 0.05 using the washed cell suspension. The cultures were
24 incubated at the conditions to be studied and sampled at appropriate inter-
25 vals of time (\approx 1 h). One ml samples were kept on ice until all samples were
26 aquired. 100 µl aliquots of the samples were transferred into a clear MTP
27 and the OD₆₀₀ was measured.

28 Green fluorescent protein (GFP) fluorescence was measured accordingly,
29 but the MTP used was opaque. Exitation (λ^{ex}) and emission (λ^{em}) wave-
30 lengths were (470 and 510) nm respectively.

1 4.6.2 *In vitro* determination of glucose

2 The glucose concentration in clarified, aqueous samples was determined by
3 a modified version of the glucose assay kit procedure provided by Sigma-
4 Aldrich [181]. Glucose oxidase (GOD) oxidizes D-glucose to gluconic acid,
5 whereby hydrogen peroxide is produced. The hydrogen peroxide can be
6 detected and quantified by horseradish peroxidase (HRP), which reduces
7 the produced H₂O₂ and thereby oxidizes its chromogenic substrate o-
8 dianisidine via consecutive one-electron transfers. The oxidized diimine
9 form of o-dianisidine can then be measured photospectrometrically [31].

10 The methodology employs a coupled photospectrometric assay using
11 GOD and HRP with o-dianisidine as reporter substrate. The assay was
12 prepared in MTP-format. A reaction solution containing 12.5 U/ml GOD,
13 2.5 U/ml HRP and 0.125 mg/ml o-dianisidine dihydrochloride in 50 mM
14 sodium acetate pH 5.1 was prepared. Sample solutions from culture su-
15 pernatants were typically diluted in 9 volumes of water. The reaction
16 was started, by adding 50 µl reaction solution to 25 µl of sample and was
17 incubated at 37 °C and 200 rpm for 30 min in a shaking incubator. 50 µl
18 6 M sulfuric acid was added to stop the reaction and achieve maximum
19 color development (full oxidation of any o-dianisidine charge transfer com-
20 plexes) (Figure 4.3). The developed pink color was measured at 540 nm in
21 a MTP-reader. A calibration curve of a standard D-glucose solutions (0 to
22 100 µg/ml), that was always part of the experiments, was used to quantify
23 the sample measurements.

24 4.6.3 *In vitro* O-methyl transferase (O-MT) assay

25 O-methyl transferase (O-MT) assays were conducted in a total volume of
26 (50 to 100) µl. The standard assay buffer was 100 mM Tris/HCl, 2.5 µM
27 GSH pH 7.5. 1 mM MgCl₂, which was otherwise omitted, was added for
28 reactions using cation dependent O-MTs (e.g. PFOMT). Reactions contained
29 0.5 mM alkyl donor (e.g. (S,S)-SAM) and 0.4 mM flavonoid or cinnamic
30 acid substrate. Enzymatic reactions were started by addition of enzyme
31 (usually 0.2 mg/ml) and incubated at 30 °C. Reactions were stopped by
32 addition of 500 µl ethyl acetate containing 2 % formic acid and vortexed for
33 15 s to extract the hydrophobic phenylpropanoids and flavonoids. After
34 centrifugation (10 000 × g, 4 °C, 10 min) the organic phase was transferred
35 into a new tube. The reaction was extracted once more with 500 µl ethyl

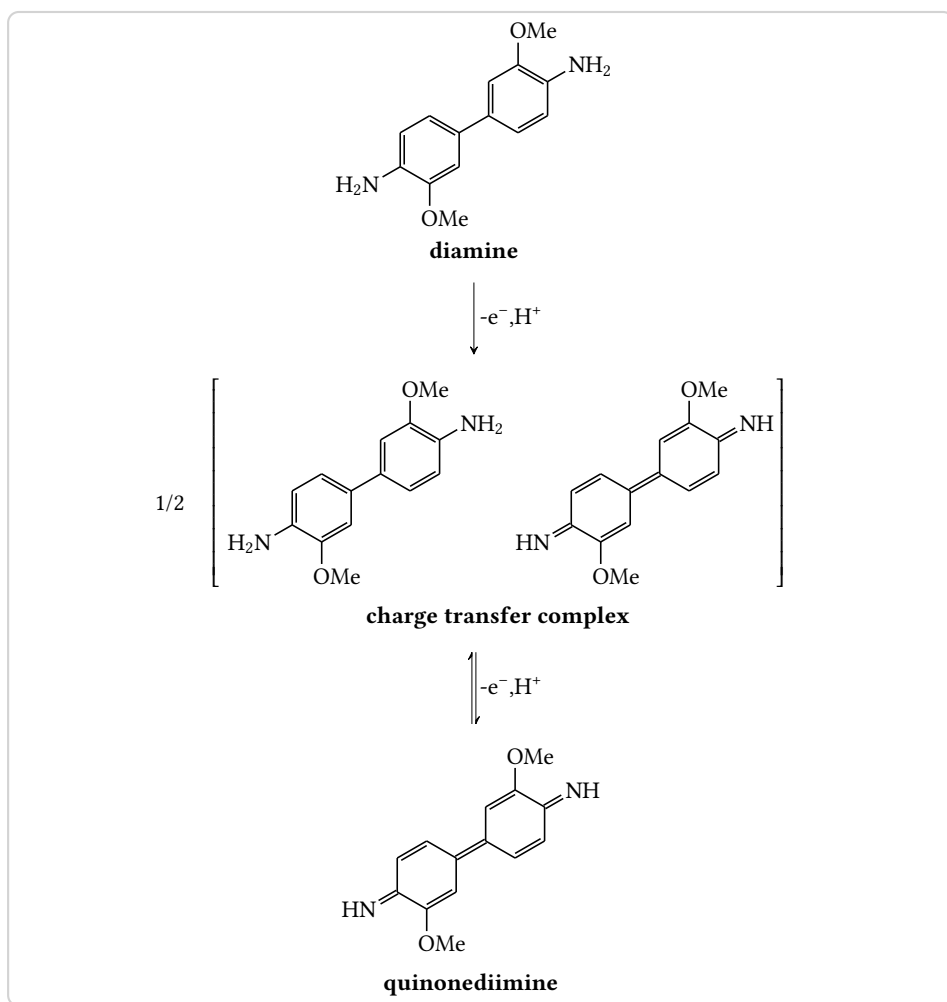


Figure 4.3: Oxidation of the reporter substrate *o*-dianisidine. Consecutive one-electron transfers lead to the fully oxidized diimine form of *o*-dianisidine. The first electron transfer is believed to produce a charge transfer complex intermediate. [31, 91]

1 acetate, 0.2 % formic acid and the pooled organic phases were evaporated
2 using a vacuum concentrator (Concentrator 5301; eppendorf, Hamburg,
3 Germany). The residue was dissolved in methanol and centrifuged at
4 $10\,000 \times g$ for 10 min to remove unsoluble matter. The supernatant was
5 transferred into a HPLC vial and analyzed by HPLC (4.6.8). When detection
6 of hydrophobic (e.g. flavonoids) and hydrophilic compounds (e.g. SAM, S-
7 adenosyl-L-homocysteine (SAH)) was performed simultaneously reactions
8 were stopped by addition of 0.3 volumes 10 % (w/v) TCA in 50 % acetonitrile.
9 The mixture was vortexed for complete mixing and incubated on ice for at
10 least 30 min. After centrifugation ($10\,000 \times g$, 4 °C, 10 min) the supernatant
11 was transferred into HPLC-sample vials and analyzed (see 4.6.8).

12 Measurement of activity/pH profiles

13 Assays to measure activity over larger pH ranges were set up in 50 mM L-
14 malic acid/MES/Tris (MMT)- (pH 4 to 9) or succinate/sodium phosphate/g-
15 lycine (SSG)-buffer (pH 4 to 10) to keep the concentrations of buffer salts
16 constant for each pH [153]. The protein of interest was first extensively
17 dialyzed against the reaction buffer (e.g. MMT, SSG) at pH 7 with added
18 EDTA (5 mM) and then against the same buffer without EDTA. Standard
19 reaction conditions were 50 mM buffer, 0.4 mM alkyl acceptor (e.g. caffeic
20 acid), 0.5 mM SAM, 2.5 µM GSH and 0.2 mg/ml enyzme. MgCl₂ was either
21 omitted or added at 10 mM to assess influences of divalent cations. Assays
22 were stopped as described in 4.6.3 and analyzed accordingly.

23 Estimation of product concentration and enzymatic activities

Product concentrations were estimated from HPLC runs. The automatically integrated peaks of SAM and SAH provided the area under the curve (AUC). From the AUC of both peaks the concentrations were estimated as follows.

Under the assumption, that

$$AUC^{\text{SAH}} + AUC^{\text{SAM}} = 1 \sim c_0^{\text{SAM}},$$

the fraction and concentration of one (e.g. SAH) can be estimated by

$$x^{\text{SAH}} = \frac{AUC^{\text{SAH}}}{AUC^{\text{SAH}} + AUC^{\text{SAM}}}$$

and

$$c^{\text{SAH}} = x^{\text{SAH}} \times c_0^{\text{SAM}}.$$

1 The amount n is obtained by multiplying the concentration c by the in-
2 jection volume V . Enzymatic activities (i.e. initial rates) can be calculated
3 from the concentrations by standard procedures.

4 4.6.4 Photospectrometric assay for the methylation of 5 catecholic moieties

6 Catecholic moieties can form stable complexes in the presence of heavy
7 metals such as copper or iron [143, 176]. Hence, caffeic acid can complex
8 ferric (Fe^{3+}) ions and form a colored complex with $\lambda_{\text{max}} = 595 \text{ nm}$ [48]. Since
9 the complex formation is specific for caffeic acid and methylated derivatives
10 (i.e. ferulic and iso-ferulic acid) cannot complex Fe^{3+} , this can be used as a
11 measure for methylation reactions. O -MT assays were prepared as before
12 (subsection 4.6.3). However, the reactions were stopped by addition of 0.1
13 volumes 1 M Tris/HCl pH 8, immediately followed by 0.5 volumes catechol
14 reagent (2 mM FeCl_3 in 10 mM HCl). The complex formation reaction was
15 allowed to equilibrate for 5 min at RT and the absorbance at 595 nm was
16 measured.

17 4.6.5 Concentration of SOMT-2 using hydrophobic in- 18 teraction chromatography (HIC)

19 After refolding using rapid dilution protein samples are very dilute and a
20 concentration step is required. Refolded SOMT-2 was concentrated directly
21 from the refolding buffer using hydrophobic interaction chromatography
22 (HIC). The ammonium sulfate concentration of the protein sample was
23 brought to 1 M using a 2 M $(\text{NH}_4)_2\text{SO}_4$ solution and the pH was adjusted to
24 7 using 5 M NaOH. The sample was centrifuged ($20\,000 \times g$, 4 °C, 30 min)
25 to remove insoluble material and the clarified supernatant was applied to
26 a 1 ml HiTrap Phenyl FF (Low Sub) (GE Healthcare, Freiburg, Germany),
27 which had been equilibrated with high salt buffer (1 M $(\text{NH}_4)_2\text{SO}_4$, 50 mM
28 HEPES pH 7). The target protein was eluted using a stepwise gradient
29 ((1, 0.8, 0.6, 0.4, 0.2 and 0) M $(\text{NH}_4)_2\text{SO}_4$, 50 mM HEPES pH 7; 5 CV each)
30 to remove the ammonium sulfate. The column was washed using 20 %

1 ethanol. Before SDS-PAGE analysis the eluted high salt fractions were
2 desalted using TCA precipitation (4.4.4).

3 4.6.6 Analytical gel filtration

4 Analytical gel filtration was done using a Superdex 200 10/300 GL column
5 (GE Healthcare, Freiburg, Germany) in combination with a FPLC system
6 according to the manufacturers instructions. The column was equilibrated
7 using an appropriate buffer (e.g. 0.1 M Tris/HCl pH 7.5) and 100 µl of
8 sufficiently concentrated (≥ 1 mg/ml) protein sample were injected. The
9 Gel Filtration Standard by Bio-Rad (München, Germany) was run separately
10 to assess the size of the proteins in the analyzed sample.

11 4.6.7 Binding experiments using Isothermal Titration 12 Calorimetry (ITC)

13 Isothermal Titration Calorimetry (ITC) can be used to directly characterize
14 the thermodynamics of an observed process, be this a binding interaction
15 or an enzymatic reaction [63]. ITC measurements to describe the interac-
16 tion between PFOMT and its substrates/effectors were performed using a
17 MicroCal iTC200 device (Malvern, Worcestershire, UK). PFOMT protein
18 was extensively dialyzed against 50 mM MMT-buffer pH 7 prior to ITC
19 experiments. The solution was subsequently centrifuged ($14\,000 \times g$, 4 °C,
20 10 min), to remove insoluble matter and aggregates. The dialysate was
21 stored at 4 °C and used to prepare substrate and effector solutions. Gener-
22 ally 50 µM protein was provided in the ITC cell and the effectors/substrates
23 to be titrated were loaded into the syringe. The substance concentration in
24 the syringe was ten times higher than the protein solution. Experiments
25 were carried out at 20 °C unless otherwise stated. The stirring speed was
26 set to 500 rpm. The injection volume was set to (2 to 4) µl, amounting to a
27 total of 10 to 19 injections.

28 4.6.8 High-performance liquid chromatography (HPLC) 29 analytics

30 Due to their aromaticity, methanolic extracts of flavonoids exhibit two
31 major absorption peaks in the UV/VIS region of the light spectrum in the
32 range of (240 to 400) nm [132]. However, even the more simple phenyl

1 propanoids (e.g. cinnamic acids) show absorption of light in the UV/VIS-
2 region. Methanolic extracts of flavonoids and phenyl propanoids were
3 analyzed by HPLC using a photo diode array (PDA)-detector, which was
4 set to record in the range of (200 to 400) nm. HPLC runs were performed
5 on a reverse-phase C-18 end-capped column (YMC-Pack ODS-A; YMC
6 Europe, Dinslaken, Germany) with a pore size of 120 Å. The mobile phase
7 was aqueous acetonitrile supplemented with 0.2 % formic acid. The flow
8 was kept constant at 0.8 ml/min. 10 µl O-MT enzyme assay extract (4.6.3)
9 were injected and analyzed using an acetonitrile gradient starting with
10 5 % acetonitrile (4 min). The acetonitrile content was increased to 100 %
11 in 21 min and was kept at 100 % for 5 min. Peaks were integrated from
12 the 280 nm trace using the software provided by the manufacturer of the
13 device.

14 **4.6.9 Liquid chromatography-tandem mass spectrome- 15 try (LC-MS/MS) measurements**

16 The positive and negative ion high resolution electrospray ionization (ESI)
17 and collision induced dissociation (CID) MS_n spectra as well as higher-
18 energy collisional dissociation (HCD) MS/MS spectra were obtained from an
19 Orbitrap Elite mass spectrometer (Thermo Fisher Scientific, Bremen, Ger-
20 many) equipped with an heated-electrospray ionization (H-ESI) ion source
21 (positive spray voltage 4.5 kV, negative spray voltage 3.5 kV, capillary tem-
22 perature 275 °C, source heater temperature 250 °C, Fourier transform mass
23 spectrometry (FTMS) resolving power (RP) 30 000). Nitrogen was used as
24 sheath and auxiliary gas. The MS system was coupled with an ultra-high
25 performance liquid chromatography (UHPLC) system (Dionex UltiMate
26 3000, Thermo Fisher Scientific), equipped with a RP-C18 column (particle
27 size 1.9 µm, pore size 175 Å, 50 x 2.1 mm inner diameter, Hypersil GOLD,
28 Thermo Fisher Scientific, column temperature 30 °C) and a photodiode
29 array detector ((190 to 400) nm, ThermoFisher Scientific). For the UHPLC a
30 gradient system was used starting from H₂O:CH₃CN 95:5 (each containing
31 0.2 % formic acid) raised to 0:100 within 10 min and held at 0:100 for further
32 3 min. The flow rate was 150 µl/min.

33 The mass spectra (buffer gas: helium) were recorded using normalized
34 collision energies (NCE) of (30 to 45) % and (75 to 100) % for CID and HCD
35 mass spectra respectively (see Appendix). The instrument was externally

1 calibrated using the Pierce® LTQ Velos ESI positive ion calibration solution
2 (product number 88323, ThermoFisher Scientific, Rockford, IL, 61105 USA)
3 and the Pierce® LTQ Velos ESI negative ion calibration solution (prod-
4 uct number 88324, ThermoFisher Scientific, Rockford, IL, 61105 USA) for
5 positive and negative ionization mode respectively.

¹ 5 Engineering of phenylpropanoid
² and flavonoid O-methyl trans-
³ ferase (PFOMT)

1

Evaluation of PFOMT towards the acceptance of long-chain SAM analogues

² Benjamin Weigel^{1,a}, Martin Dippe, Ludger A. Wessjohann^{1,c}

Contact: bweigel@ipb-halle.de^a, law@ipb-halle.de^c

Affiliation: Leibniz-Institute of Plant Biochemistry, Department of Bioorganic Chemistry¹

Keywords: methyl transferase, pfomt, SAM

3 Abstract

4 The cation dependent phenylpropanoid and flavonoid O-methyl trans-
5 ferase (PFOMT) from the ice plant, *Mesembryanthemum crystallinum*,
6 methylates a number of flavonoids and phenyl propanoids. A newly
7 solved crystal structure of the protein without any bound ligand shows
8 the fully resolved N-terminus, which acts as a lid to close off the
9 active site. Binding of co-substrates (analogues) (e.g. S-adenosyl-L-
10 homocysteine (SAH), S-adenosyl-L-methionine (SAM), S-adenosyl-L-
11 ethionine (SAE)) is more entropically driven as the chain length increases.
12 However, even though the ethyl-analogue of SAM – SAE – was shown
13 to bind to the enzyme, no conversion of the model substrate caffeic
14 acid was observed for the wild-type and several engineered variants.

15

¹⁶ 5.1 Introduction

17 Small changes to molecules can have profound influences on their chemical,
18 physical and biological properties. For example, butyric acid esters differing
19 only by a few methylene groups already exhibit quite divergent smells.
20 However, not only the macroscopically qualitative properties can differ. The
21 quantifiable psychotomimetic effect of methylated and ethylated lysergic
22 acid amids differ by at least an order of magnitude [78, 180]. There are
23 many more of these so-called structure activity relationship (SAR) and
24 quantitative structure activity relationship (QSAR) studies on any number
25 of compounds [5, 135, 168].

26 Methylation reactions are one of the key tailoring steps during natural
27 product biosynthesis and can in consequence greatly affect a molecules
28 bio- and physicochemical behavoir [120, 188]. Methyl transferases (MTs)

1 catalyze the transfer of a methyl group from the co-substrate SAM to an
2 activated atom of the acceptor molecule [188].

3 Between the highly complex core structures of natural products, which
4 are produced by a plethora of enzymes (e.g. poly ketide synthases (PKSs),
5 non-ribosomal peptide synthases (NRPSs), terpene cyclases), and the rather
6 simple alkyl-modification introduced by methylation, nature is missing
7 some medium-sized modification options that proceed as elegantly as the
8 methylation by MTs. Thus, natural products containing longer chain alkyl
9 modifications like ethyl or propyl moieties on O, N or S-centers have rarely,
10 if ever been observed.¹

11 It has recently been shown however, that a wide array of SAM analogues
12 are used as co-substrates by a variety of MTs [188]. The majority of the
13 work so far has been done on protein methyl transferases (P-MTs) and DNA
14 methyl transferases (DNA-MTs), since epi-genetics and finding regions of
15 gene-regulation is of great interest. However, small molecule methyl trans-
16 ferases (*sm*MTs) have also been shown to accept different SAM analogues
17 [114, 116, 184, 187, 229]. There have been a great many of SAM analogues
18 synthesized, both chemically and enzymatically, that were consequently
19 studied with the help of MTs [44, 184, 188].

20 The O-methyl transferase (O-MT) PFOMT is a highly promiscuous en-
21 zyme with regards to its flavonoid substrates and has extensively been
22 characterized [22, 85, 109, 206]. However, the promiscuity towards different
23 SAM analogues has not yet been described. Combination of both, substrate
24 and co-substrate promiscuity in the small molecule MT PFOMT could pro-
25 vide a powerful tool towards the biosynthetic production of novel small
26 molecules with potentially new and promising biological activities. Func-
27 tionalization/Detection of substrates could furthermore provide a means
28 of finding new compounds/substrates in complex (e.g. biological) samples
29 analogous to activity based protein profiling (ABPP) approaches.

30 In this work we show, that PFOMT binds the co-substrate analogues SAH,
31 SAM and SAE with similar affinities. A newly developed crystal structure
32 of the *apo*-enzyme shows the fully resolved N-terminus is lodged in a
33 cleft atop the active site, closing it off. Although semi-rationally designed

¹Reaxys searches for natural product isolates with a molecular mass between (150 and 1500) containing the substructures methyl, ethyl or propyl connected to a heteroatom return 66759, 2797 and 52 results respectively. However, it stands to note that 70 % of the propyl results were either esters or otherwise activated moieties. [53]

1 enzyme variants could not afford enzymatic ethylation of substrates, the
2 regio-selectivity of the methylation reaction was altered.

3 5.2 Crystallization of PFOMT

4 The crystal structure of PFOMT was published in 2008, however binding of
5 substrates could not be accomplished [109]. Nonetheless, the demethylated
6 co-substrate SAH was cocrystallized. The first goal of this study was to
7 crystallize the *apo*-form of the enzyme, to obtain a system that allows for
8 the soaking of substrates. At the same time, PFOMT was to be cocrystallized
9 along with an acceptor substrate and the co-substrate analogs SAE and
10 SAH.

11 At first the already available crystallization procedures were evaluated
12 [109]. However, reproduction of these results could not be accomplished
13 and new crystallization conditions had to be found.

14 Several commercially available buffer solutions (see section 4.5) were
15 screened in combination with different protein solutions (e.g. solutions
16 containing co-substrates and acceptor substrates or not) to obtain protein
17 crystals co-crystallized with substrates or of the *apo*-form. Crystals were
18 obtained in various wells after a few days. The crystal shape varied from
19 very smooth and almost cubic (high ammonium sulfate) over spherulites
20 and intergrown crystals (CaCl_2 , PEG-4000) to brittle and ragged needles
21 (LiCl , PEG-6000) (Figure 5.1).

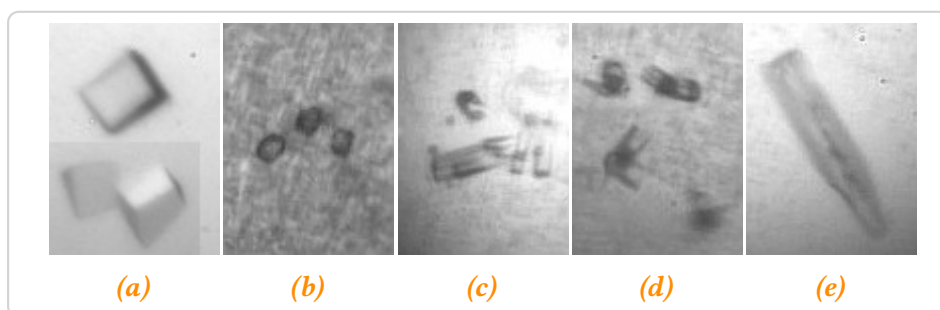


Figure 5.1: Some crystal and pseudo-crystal shapes that were observed during the crystallization screen. a – high $(\text{NH}_4)_2\text{SO}_4$, b-c – CaCl_2 , PEG-4000, e – LiCl , PEG-6000

22 Crystals that were large enough ($\geq 50 \mu\text{m}$), were screened for diffrac-
23 tion at the home-source after cryoprotection. A rough estimate of the
24 resolution, cell parameters and the space group was acquired, if the diffrac-
25 tion images could be indexed. The screened crystals all had similar cell

1 parameters and belonged to the same space group, $P2_12_12_1$, as the pre-
2 viously published structure (pdb: 3C3Y)[109]. However, the unit cell of
3 crystals that grew out of high ammonium sulfate concentrations ($\geq 1.8\text{ M}$)
4 was approximately four times as large as that of the published structure.
5 Several datasets were collected of crystals from high $(\text{NH}_4)_2\text{SO}_4$, since
6 these seemed to be promising candidates to find differences in the bound
7 substrates. Datasets of crystals that grew from other conditions were
8 insufficient for structure solution.

9 The crystal structure of *apo*-PFOMT

10 PFOMT crystallized without any bound substrates under conditions of high
11 $(\text{NH}_4)_2\text{SO}_4$. One dataset was solved to completion to obtain a complete
12 structure of this novel *apo*-PFOMT at a resolution of 1.95 Å (Table A.1). The
13 assymetric unit of *apo*-PFOMT contained two homodimers (4 monomers)
14 (Figure 5.2a), rather than just one homodimer (3C3Y). The active site of each
15 monomer was found to be empty except for a sole sulfate ion, which was
16 positioned where the amino- and carboxylate groups of the SAH residue in
17 the 3C3Y structure (Figure 5.2b). Shifts in the structure of some loops were
18 observed and contrary to the previously published structure the entire
19 N-terminus was resolved up to and including the His-tag.

20 The resolved N-terminus contained another N-terminal α -helix, which
21 was positioned in a cleft on the surface, where substrates may be bound
22 [109]. This interaction extends up to the His-tag. Considerable movement
23 was observed in different parts of the protein, when no substrate was bound,
24 some of which can be attributed to SAM and metal ion binding residues
25 (Figure 5.3 and Figure A.1) as is obvious for the loop region between β -
26 sheet 1 and α -helix 4. Nonetheless, most of the movement seemed to be
27 restricted to areas, which are not directly involved in the binding of either
28 SAM or metal ions. However, all of the regions that moved are located at
29 or near the active site.

30 Unfortunately soaking of these “*apo*”-crystals did not afford binding of
31 substrates.

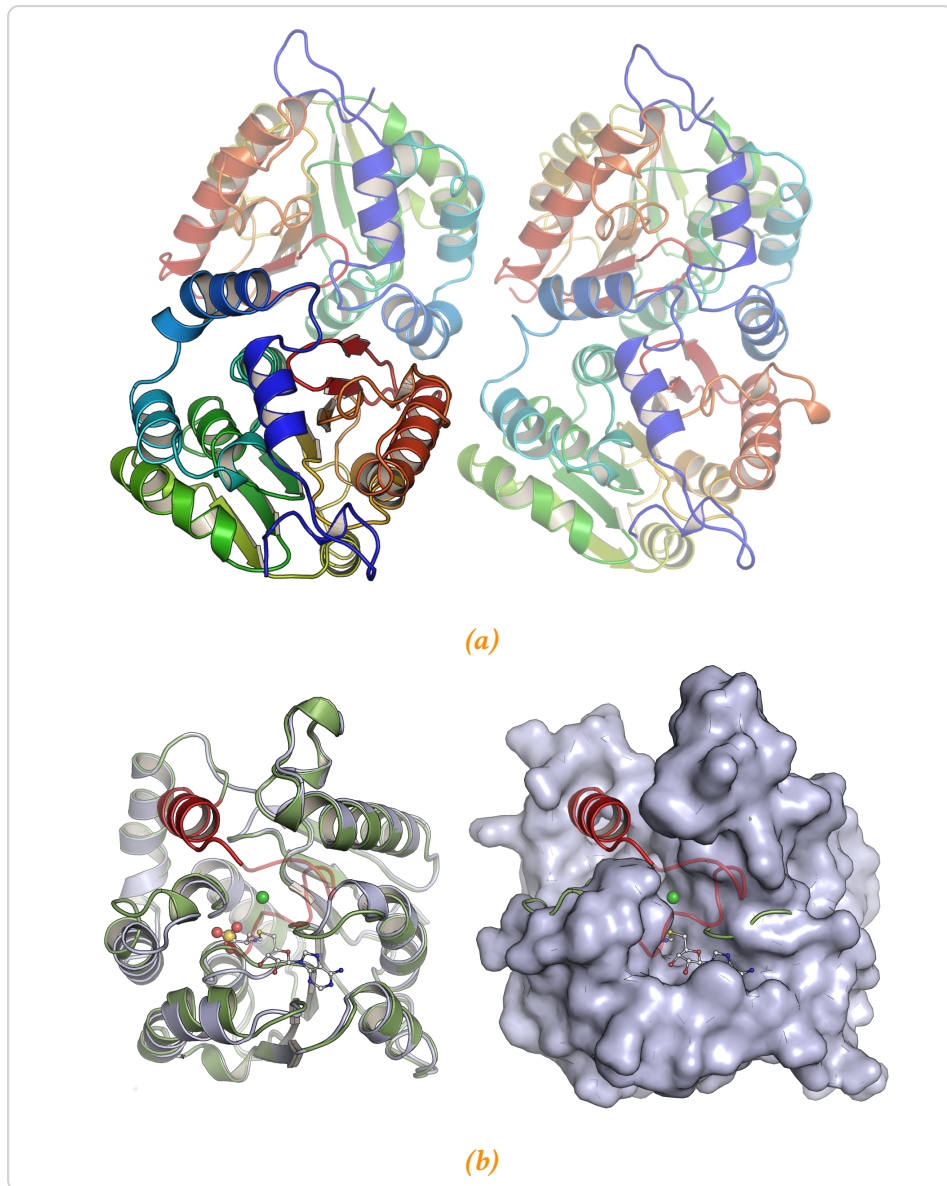


Figure 5.2.: An overview of the features in the apo-PFOMT structure. **a** – The assymmetric unit of apo-PFOMT consists of two homodimers (4 monomers). Individual monomers are rainbow colored from N- (blue) to C-terminus (red). **b** – Comparison of 3C3Y (steelblue) and apo-PFOMT (green). The N-terminus of apo-PFOMT was resolved up to the N-terminus (red) and even the His-tag (red, transparent) was partly resolved. The N-terminus fits into a cleft on the surface of the 3C3Y structure, shown as a surface model on the right. SAH (white ball-and-sticks) and Ca^{2+} (green sphere) are featured in the published structure, whereas a sulphate ion (red/yellow spheres) was bound in the newly solved structure.

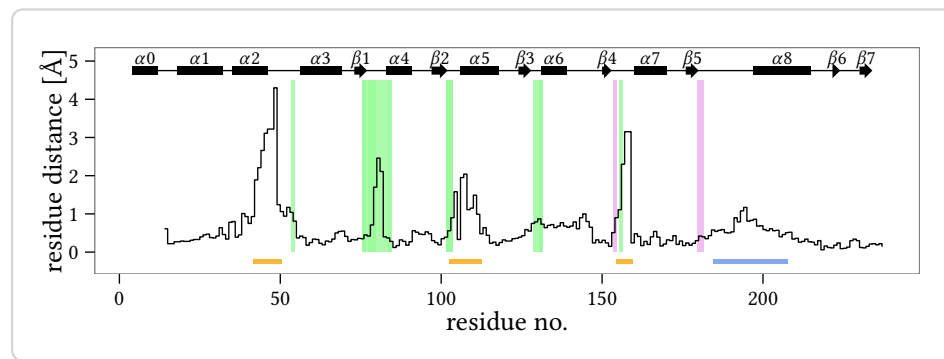


Figure 5.3.: Positional differences between the individual residues of the solved apo-PFOMT and the structure with bound SAH (pdb: 3C3Y). The diffraction precision indicator [46] (DPI) of the structures was (0.137 and 0.064) Å respectively. The overall rmsd amounted to 0.9034 Å. The secondary structure of apo-PFOMT is displayed at the top. Helices are displayed as rectangles and sheets are shown as arrows. Graphical background annotations are used to display the binding sites of SAH (green) and the metal ion (plum). The orange bars indicate regions, where much movement seems to happen upon binding or release of the co-substrate. The blue bar shows the region that was annotated as "insertion loop" in previous studies [109].

5.3 Substrate binding studies using ITC

The binding of different substrates to PFOMT was examined by Isothermal Titration Calorimetry (ITC), to determine whether the enzyme can bind non-natural SAM analogues. The homologues SAH, SAM and SAE were selected to also study the influence of the alkyl chain length on binding (Figure 5.4). Furthermore the binding of the substrate caffeic acid and the influence of Mg²⁺ addition on substrate binding was investigated.

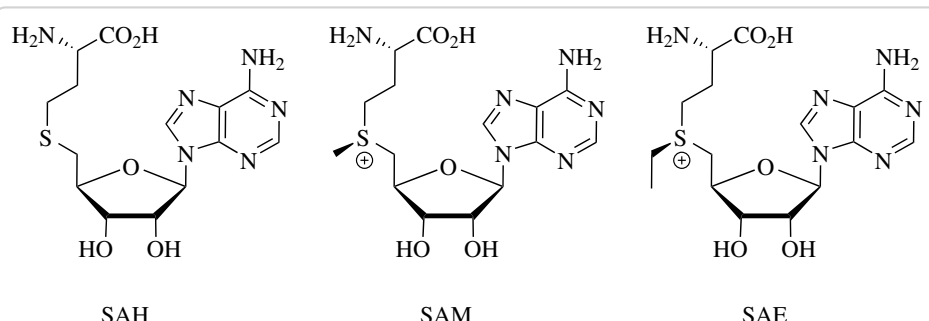


Figure 5.4.: The binding of different SAM analogues was measured via ITC

The K_D values of SAH, SAM and SAE were all in the low micromolar range, around 2 μM. However, the binding enthalpy clearly decreased with the length of the aliphatic chain connected to the sulfur atom (Figure 5.5a).

1 The binding of SAH, gave off more heat than the binding of SAM, which
 2 in turn gave off more heat than the binding of SAE (Table 5.1). Thus, the
 3 entropic influence must get larger with increasing chain length in order
 4 for equations (5.1) and (5.2) to still hold true.

$$\Delta G = \Delta H - T\Delta S \quad (5.1)$$

5

$$\Delta G = \Delta G^0 - RT \ln K \quad (5.2)$$

6 Indeed, the value for ΔS was negative for binding of SAH, but positive
 7 for the binding of SAM and SAE (Table 5.1). This relationship between the
 8 change of entropy and the change of enthalpy has been found for many
 9 biological systems and is called enthalpy-entropy compensation (EEC)
 10 [52, 71, 177]. The stoichiometry for the binding process is given by the
 11 parameter N . For all the ligands SAH, SAM and SAE this value was found
 12 to be about 0.5, which corresponds to one bound molecule ligand per dimer
 13 of PFOMT (Table 5.1).

14 Upon titration of caffeic acid to PFOMT small amounts of released heat
 15 were detected for the system (Figure 5.5c). When the enzyme was incubated
 16 with SAH prior to addition of caffeic acid the released heat was slightly
 17 increased. The slope of the ITC profile also got steeper. However, the data
 18 obtained could not be fitted to afford a sensible solution. When caffeic acid
 19 and Mg^{2+} were incubated with PFOMT prior to addition of SAH, the process
 20 of heat production as observed by ITC had a steeper slope (Figure 5.5b).
 21 Nonetheless, the thermodynamic parameters did not differ significantly.
 22 Mg^{2+} , in the form of an $MgCl_2$ solution, titrated to the enzyme solution did
 23 not cause signals during the ITC experiments.

Table 5.1: Results of fitting a simple one-site binding model to the data obtained from ITC experiments.

	K_D [μM]	ΔH [cal mol $^{-1}$]	ΔS [cal mol $^{-1}$ K $^{-1}$]	N
SAH	2.06 ± 4.27	$-10\,380 \pm 1025$	-9.41	0.505 ± 0.038
SAM	1.08 ± 3.50	-4606 ± 242	11.6	0.492 ± 0.018
SAE	2.22 ± 3.79	-1338 ± 190	21.3	0.513 ± 0.050

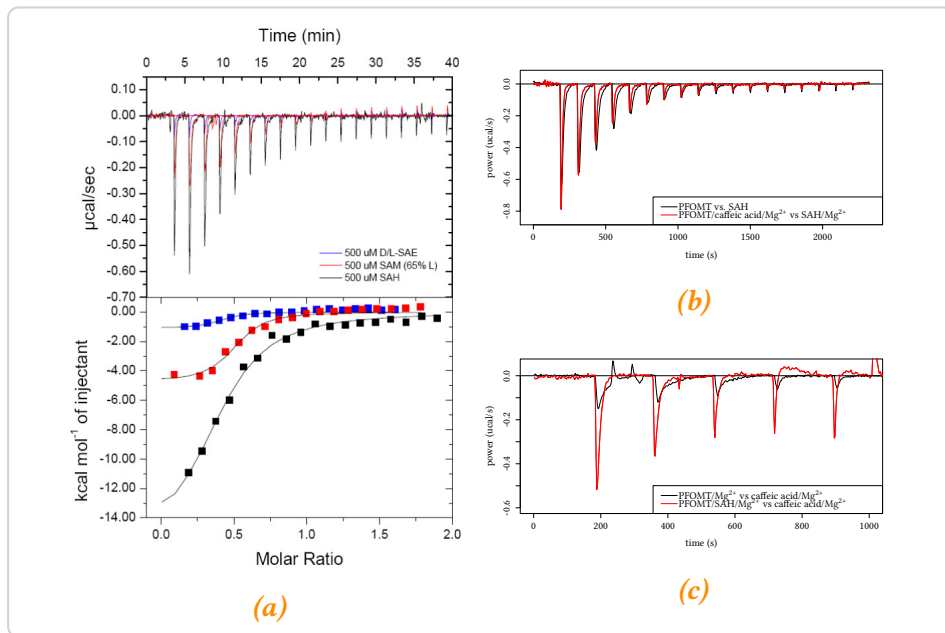


Figure 5.5.: ITC measurements of PFOMT:effector binding. **a** – Binding of SAH, SAM and SAE to PFOMT. **b** – SAH is injected into a PFOMT solution, with (red) or without (black) addition of Mg^{2+} and caffeinic acid. When Mg^{2+} and caffeinic acid were already present, the binding process seems to happen quicker, but is less enthalpic. **c** – Upon addition of caffeinic acid to the protein heat is produced, however no sensible binding curve could be obtained.

1 5.4 Study of variants for long-chain alkyla- 2 tions

3 Since the ability to bind the elongated analogue SAE was present in
4 wild-type PFOMT, the activity of the PFOMT protein towards SAE was
5 tested. Activity tests were performed with caffeinic acid as substrate under
6 standard reaction conditions. Unfortunately no ethylation of the substrate
7 by PFOMT was observed, even after extended incubation times.

8 Consequently enzyme variants were prepared to achieve a PFOMT vari-
9 ant with an ethylation activity, since a number of groups were able to
10 accomplish transalkylation with larger substrates by expanding the avail-
11 able space in the active site [209]. The available crystal structures of PFOMT
12 were consulted to select suitable residues. Residues that were exchanged
13 were selected based upon their position in the active site and in relation
14 to the substrate(s) (Figure 5.6). The residues were exchanged to the non-
15 spaceous alanine, as well as amino acids frequently observed at homologous
16 positions in other class I O-MTs.

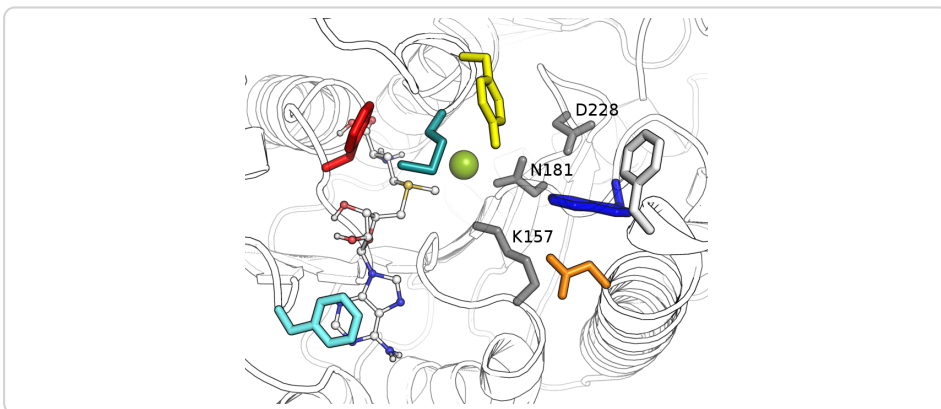


Figure 5.6.: The active site of PFOMT (pdb: 3C3Y). The outline of the protein backbone is displayed, with active site residues portrayed as colored sticks (cyan – F103, red – F80, turquoise – M52, yellow – Y51, white – F198, blue – W184, orange – N202, grey – as labelled). The co-substrate SAM (ball-and-stick model) was docked into the structure.

1 Over 20 enzyme variants were prepared to assess, whether PFOMT ethylation activity would improve over the wild-type. However, no ethylation
2 activity was observed for either variant. Some of the new variants however
3 displayed an increased methylation activity with the substrates caffeic acid
4 and SAM (Figure 5.7). The methylation activity of some of the variants in-
5 creased by over 4-fold. Interestingly most amino acid substitutions proved
6 as beneficial.
7

8 Methylation activity benifited greatly from the replacement of bulky
9 hydrophobic residues by smaller and/or charged residues in the vicinity of
10 the acceptor substrates (Tyr51, Trp184 and Phe198). However, this was not
11 a general trend since the substitutions N202W and Y51W also improved
12 methylation activity. Looking more closely at residue Tyr51, the activity
13 enhancing effect was greatest, when the tyrosine was substituted by the
14 basic amino acids lysine or arginine. In addition to an enhanced activity
15 the selectivity for the hydroxyl position to be methylated was also altered
16 in these variants. This was not apparent, when caffeic acid was used as a
17 substrate. However when a flavonoid, especially eriodictyol, was used not
18 only the 3' hydroxyl, but to some extent the 4' hydroxyl was methylated
19 (Figure A.2). This effect was improved in some double variants, where also
20 position 202 was altered. For example the variant Y51R N202W almost
21 exclusively methylated flavonoid substrates at the 4' position. A detailed
22 discussion of the results was published in a peer reviewed journal.

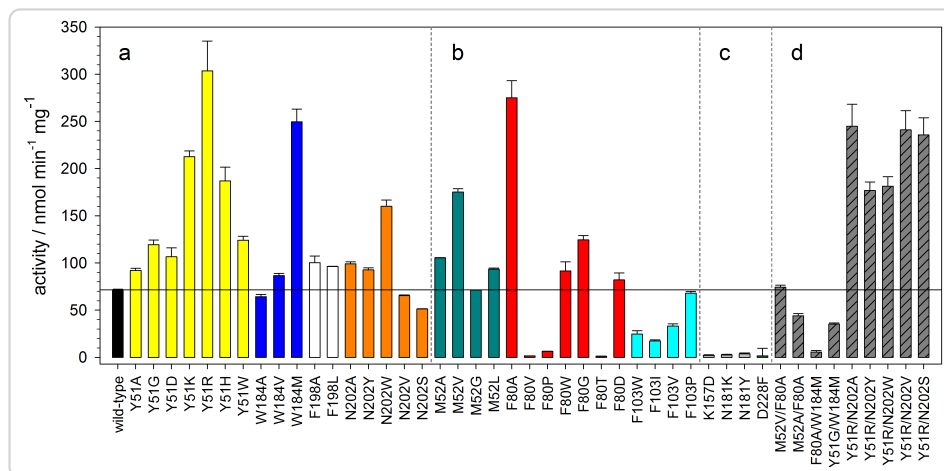


Figure 5.7: Activities of different PFOMT variants towards caffeic acid methylation. Colorations correspond to the ones used in Figure 5.6.

1 5.5 Conclusion/Discussion

2 Whereas the binding of SAH was solely dependent on the large negative
 3 enthalpy, the binding of SAE was almost entirely driven by entropy, since
 4 ΔH was close to 0 (Table 5.1). Entropy gain can be a major driving force
 5 for ligand-protein interactions and in some cases ligand binding can be en-
 6 tirely attributed this gain in entropy [123]. Displacement of protein-bound
 7 water molecules contributes strongly to the entropic gain. There were
 8 some waters present in the active site of PFOMT in the crystal structure
 9 developed herein. However, no metal ion was present in the active site
 10 in the *apo*-PFOMT structure. Furthermore Mg²⁺ titration via ITC did not
 11 afford significant signals, suggesting the notion, that the metal is only
 12 bound along with the co-substrate (Figure 5.8). It has been suggested, that
 13 the entropy cost to transfer one water molecule from bulk to the protein-
 14 bound state can be up to 7 cal mol⁻¹ K⁻¹ [51]. The replacement of ordered
 15 waters from the active site or from a hydrated metal ion by a growing
 16 aliphatic chain could therefore explain the gain in entropy, and SAH is
 17 positioned in a way to warrant exactly that (Figure 5.8). Also, the hydro-
 18 gen and metal complexing bonds consequently lost could explain the less
 19 negative enthalpy. However, this is purely hypothetical since more evident
 20 data is missing. Additional insight might be gained by expanding the ITC
 21 experiments to even longer SAM analogues. The limited space in the active
 22 site, which forces the growing side chain to expel water and possibly the
 23 metal ion might also be the reason for the inactivity of PFOMT towards

1 SAE. If the metal ion is blocked from its complexing moieties, activation of
2 the substrate hydroxyl would be hindered.

3 Comparison of the novel *apo*-PFOMT and the published structure (pdb:
4 3C3Y) suggests that the movement (upon ligand binding) along multiple
5 parts of the backbone proximal to the active site pocket is a main contributor
6 to the overall rmsd of 0.9 Å (Figure 5.3).

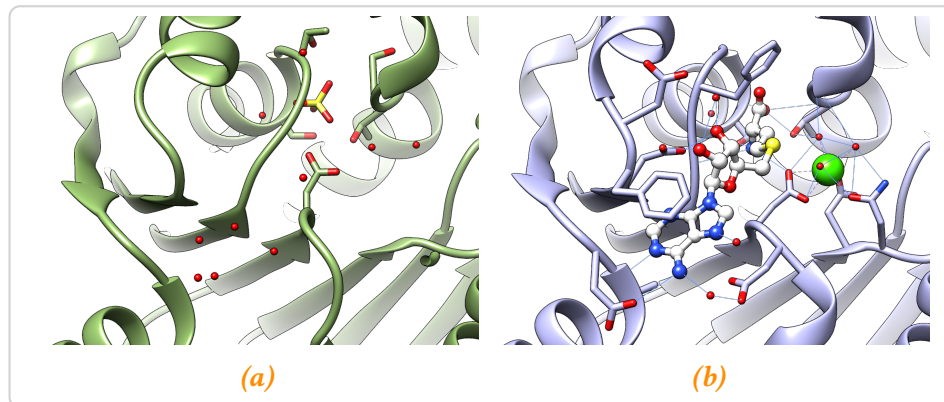


Figure 5.8.: Comparison of the active sites of **a** – the solved apo-structure (green) and **b** – the ligand-bound structure (steelblue; pdb: 3C3Y). Waters are represented as small red spheres, calcium as a green sphere (complexing bonds are dashed) and SAH is displayed as a white ball-and-stick model. A possible hydrogen bond network (blue lines) for the ligand-bound state is displayed.

7 The N-terminus of PFOMT seems to act as a lid, which is closed in the
8 *apo*-form, but highly flexible and therefore unresolved in the ligand bound
9 form. Furthermore, the native enzyme has been shown to be truncated,
10 starting only at residue 12 and being less catalytically efficient than the full
11 length protein [109, 206]. The work presented here consequently supports
12 the notion that the N-terminus plays an important role on the regulation
13 of the enzymatic activity.

14 During our studies, transethylation activities could not be observed
15 for any of the prepared PFOMT variants. However, some of the variants
16 showed higher methylation activities towards caffeic acid and even different
17 regioselectivities (3'→4') than the wild-type.

18 Given the fact that only residues in the active site and therefore in direct
19 contact with the substrates were prepared, the laid out findings provide
20 novel hints for indirect proximal regions in the PFOMT structure that
21 might be studied using site-directed mutagenesis, gene-shuffling or similar
22 approaches in order to work towards a variant that can in fact employ
23 SAE for transalkylation reactions. Furthermore variation of these regions

1 might provide variants with altered substrate specificities which are of
2 high interest.

3 **5.6 Contributions**

4 Benjamin Weigel wrote the manuscript, prepared figures, sub-cloned, pro-
5 duced and crystallized PFOMT, solved the *apo*-structure and conducted the
6 ITC experiments. Dr. Martin Dippe prepared most of the PFOMT variants
7 and ethylation activity tests. Dr. Christoph Partier (group of Prof. Dr.
8 Milton T. Stubbs, MLU Halle-Wittenberg) helped collect X-ray datasets.

¹ 6 Tandem mass-spectrometry ² studies of flavonoids

1

Comparative CID and HCD MS/MS studies for the characterization of flavonoid aglycones

Benjamin Weigel^{1,a}, Annegret Laub^{1,b}, Jürgen Schmidt^{1,c}, Ludger A.

² Wessjohann^{1,d}

Contact: bweigel@ipb-halle.de^a, alaub@ipb-halle.de^b, jschmidt@ipb-halle.de^c, law@ipb-halle.de^d

Affiliation: Leibniz-Institute of Plant Biochemistry, Department of Bioorganic Chemistry¹

Keywords: tandem mass spectrometry, LCMS, flavonoids

3 Abstract

4 Flavonoids are an important class of natural compounds and make
5 up a large part of the world's biomass. Due to their anti-inflammatory
6 and anti-oxidant properties, many health benefits are associated with
7 flavonoids and there is a growing interest to use flavonoids in medici-
8 nal and dietary contexts. The availability of methods that provide for
9 a quick and reliable identification of flavonoids from different sources
10 is therefore essential. In this work a range of flavonoids was stud-
11 ied using liquid chromatography coupled mass-spectrometry (LC/MS).
12 Two modes of activation, namely CID and HCD, were evaluated to
13 study fragmentation of flavonoids from their [M+H]⁺ molecular ions. It
14 was found, that HCD outperformed CID in the ring-fragmentations of
15 methylated flavonoids. Together, both methods provide complementary
16 information that can be used to distinguish different types of flavonoids.

17

18 6.1 Introduction

19 Liquid chromatography-tandem mass spectrometry (LC-MS/MS) has been
20 widely used for the identification of compounds from complex samples,
21 such as crude mixtures from plant or bacterial extracts and is an unexpend-
22 able method in the field of metabolomics [56, 124, 128, 169].

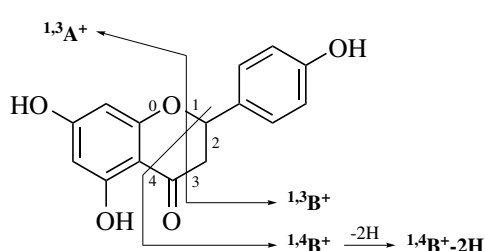
23 Ionization of samples in LC-MS/MS instruments is usually achieved
24 by soft methods operating at atmospheric pressure, such as electrospray
25 ionization (ESI) [212] or atmospheric pressure chemical ionisation (APCI)

1 [79]. However, small molecules rarely produce fragment ions under these
 2 conditions and usually only the $M+H]^+$ or $M-H]^-$ of the molecular ion is
 3 observed. A range of different approaches has been used to circumvent
 4 this draw-back. The most direct approach is to use electron ionization
 5 (EI), where the analytes are bombarded with electrons, for ionization.
 6 However, EI is operating under high-vacuum and the coupling with liquid
 7 chromatography (LC)-systems is not trivial [203]. In order to still generate
 8 fragments in liquid chromatography coupled mass-spectrometry (LC/MS)
 9 MS/MS methods such as collision induced dissociation (CID) or surface-
 10 induced dissociation (SID) were developed [185].

11 Flavonoids comprise a huge chemical space, with millions of theoretical
 12 structures [213]. Due to their biological activities and associated health
 13 benefits, applications to quickly identify and characterize these compounds
 14 are of special interest. Already, a number of studies have been published
 15 that show how MS/MS-approaches using CID can aid in the structural
 16 characterization of flavonoids [28, 41, 58, 67, 83, 117, 121, 131, 136, 137].
 17 Researchers have reported that specific patterns of fragmentation along
 18 the C-ring can be observed for different classes of flavonoids and can
 19 help differentiate between them [41, 131]. However, it was found that the
 20 cleavage of the C-ring is less commonly observed for flavonoids methylated
 21 at the B-ring, while the loss of small molecules becomes predominant [41,
 22 131].

23 Fragments of flavonoid aglycones can be represented by a systematic
 24 nomenclature first proposed by Ma *et al.* [131]. The labels $^{i,j}A^+$ and $^{i,j}B^+$
 25 refer to fragments containing an intact A or B ring, with the superscripts
 26 i and j denoting the bonds of the C-ring that were broken (Scheme 6.1).

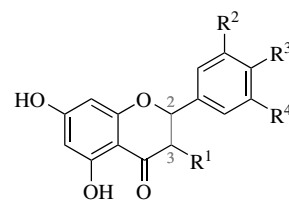
Our group currently works with methyl transferases that act on flavonoids.



Scheme 6.1: Ion fragment nomenclature of flavonoid aglycones as proposed by Ma *et al.*, illustrated on naringenin. Ions are labelled according to the ring they contain and the positions of the C ring that were broken. Thus $^{1,3}A^+$, contains the ring A and bonds 1 and 3 of the C ring were broken.

1 Identifying the site of methylation is a crucial step in identifying the product
 2 of an enzymatic methylation. MS/MS has been shown to be a rather quick
 3 and reliable method to identify characteristic key ions of flavonoids, that
 4 can help identify the localization of different functional groups [41, 58, 110,
 5 130, 131]. In this work the complementarity of two activation methods,
 6 CID and higher-energy collisional dissociation (HCD), for the structural
 7 characterization of flavonoids (Table 6.1), especially those methylated at
 8 the B-ring, in positive ionization mode was evaluated. An specific array of
 9 different flavonoids (Table 6.1) was studied, to get a holistic impression of
 10 the fragmentations of these compounds.

Table 6.1.: Substrates studied in this work. Three classes of flavonoids were tested: flavanones (1-5), flavones (6-10) and flavonols (11-15). The topology of the bond between C2 and C3 in the C-ring specifying flavanones or flavones/flavonols is denoted with - (single) or = (double), respectively.



	name	[M+H] ⁺	C2-C3	R ¹	R ²	R ³	R ⁴
1	naringenin	273	-	H	H	OH	H
2	eriodictyol	289	-	H	OH	OH	H
3	ponciretin	287	-	H	H	OCH ₃	H
4	hesperetin	303	-	H	OH	OCH ₃	H
5	homoeriodictyol	303	-	H	OCH ₃	OH	H
6	apigenin	271	=	H	H	OH	H
7	luteolin	287	=	H	OH	OH	H
8	acacetin	285	=	H	H	OCH ₃	H
9	diosmetin	301	=	H	OH	OCH ₃	H
10	chrysoeriol	301	=	H	OCH ₃	OH	H
11	kaempferol	287	=	OH	H	OH	H
12	quercetin	303	=	OH	OH	OH	H
13	myricetin	317	=	OH	OH	OH	OH
14	kaempferide	301	=	OH	H	OCH ₃	H
15	isorhamnetin	317	=	OH	OCH ₃	OH	H

11 6.2 Fragmentation of flavanones

12 Positive ionization MS² spectra of flavanones (Table B.1) are mostly charac-
 13 terized by a base peak at *m/z* 153, which corresponds to the A-ring fragment
 14 ^{1,3}A⁺ of the flavonoid skeleton (Scheme 6.2). In contrast, negative mode
 15 MS² spectra of 3,7-dihydroxy flavanones show an *m/z* 151, which corre-
 16 spond to the negatively charged ^{1,3}A⁻ ion [58]. Even when *m/z* 153 was

1 not the base peak, it was still dominant in the spectrum with intensities
2 ranging between 20 % and 77 %. Peaks corresponding to the molecular ions
3 $[M+H]^+$ were not observed for any of the flavanones. The structure of the
4 ion $^{1,3}A^+$ corresponding to m/z 153 is the same for all compounds (1) to (5)
5 (Scheme 6.2). Peaks corresponding to mass-to-charge ratio (m/z) values of
6 the respective $(^{1,4}B^+-2H)$ ions are also present in the mass spectra of each
7 flavanone. Apart from the ions $^{1,3}A^+$ and $(^{1,4}B^+-2H)$, the CID- and HCD-
8 mass spectra of the flavanones differ significantly. CID mainly triggers
9 neutral losses directly from the molecular ion. Losses of water (18 Da) and
10 one or two ketene units (C_2H_2O , 42 Da) are predominant and afford ions
11 of relatively high masses (Scheme 6.2) [96].

12 Fragment ions from cleavage of the C-ring ($^{1,3}A^+$ and $(^{1,4}B^+-2H)$) are fur-
13 ther decomposed under the higher energy conditions in HCD experiments.
14 Thus, the resulting HCD spectra generally display smaller m/z than the CID
15 spectrum (Figure 6.1). Increasing the normalized collision energy (NCE)
16 from 75 to 100 % in HCD experiments further increased fragmentation.
17 This is made clear by the increasing intensities of smaller fragments upon
18 raising the NCE (Figure 6.1).

19 Further fragmentation of ion $(^{1,4}B^+-2H)$ seems to depend on the sub-
20 stituents of the B-ring. Only $(^{1,4}B^+-2H)$ from eriodictyol (2) loses a water,
21 as suggested by a peak at m/z 145. However, the loss of CO is the most
22 prominent decomposition of $(^{1,4}B^+-2H)$. The intensities of the peaks cor-
23 responding to the $(^{1,4}B^+-2H-CO)$ fragment were as high as 36 % in HCD
24 experiments (Figure 6.1). Naringenin (1) seems to sequentially lose two
25 CO in HCD mode to afford m/z 91 (intensities at 75 and 100 % NCE at 24
26 and 100 %, respectively). This m/z is a strong indicator of a benzylum
27 or tropylium cation (Scheme 6.2). Decay of $(^{1,4}B^+-2H)$ of the other fla-
28 vanones likely leads to a stable bicyclo[4.1.0]heptatrienyl cation as the high
29 intensity of peak m/z 89 in HCD mode suggests. Methylated flavanones
30 (3), (4) and (5) show a loss of CO followed by a loss of a methyl radical
31 ($^{1,4}B^+-2H-CO-CH_3\cdot$), as suggested by the respective m/z values of 118 and
32 134. Another CO loss from this fragment is possible for ponciretin (3) to
33 produce an ion m/z 90, which is at 49 % intensity in the HCD spectrum
34 recorded with NCE of 75 %. The evidence suggests, that this ion's structure
35 is best described by a benzylum/tropylium radical cation (Scheme 6.2).
36 It is proposed, that ion $^{1,3}A^+$ can decompose via two different pathways
37 under HCD conditions (Scheme 6.3). A loss of ketene from $^{1,3}A^+$ results in

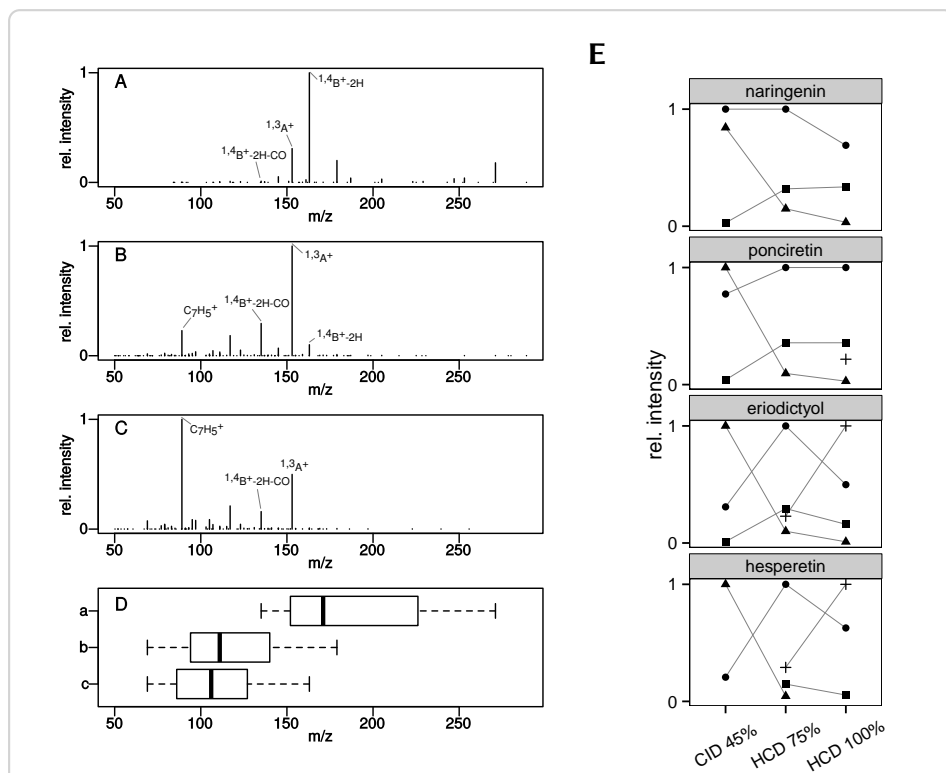
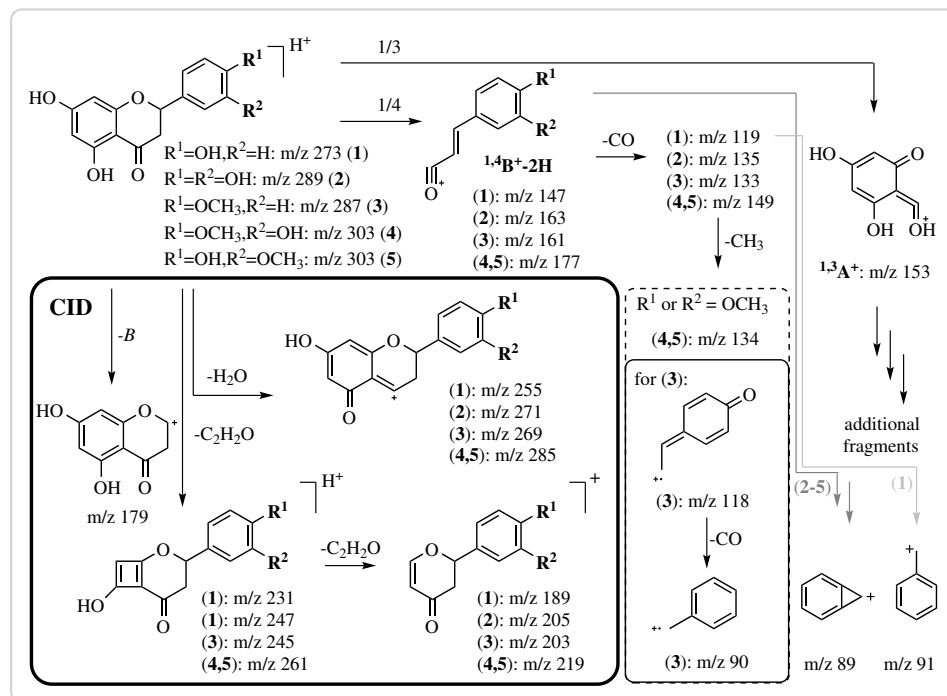
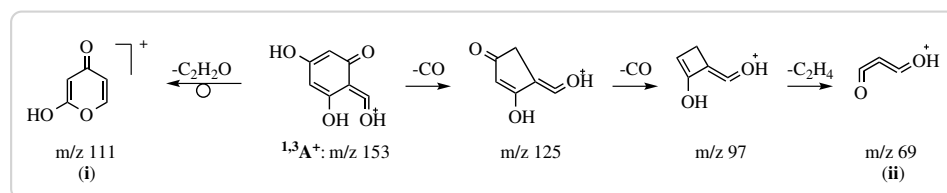


Figure 6.1: Comparison of CID and HCD MS^2 spectra of eriodictyol (2). **A** – CID at 45 % NCE. **B** – HCD at 75 % NCE. **C** – HCD at 100 % NCE. Four different prominent peaks are annotated in each spectrum. **D** – The shift to smaller masses in HCD spectra and with increasing NCE is illustrated by the boxplot of the distribution of peaks with relative intensities above 1 % in each of the above spectra. **E** – Relationship between the activation method and the intensity of four fragments (● $^{1,3}A^+$, ▲ $^{1,4}B^+-2H$, ■ $^{1,4}B^+-2H-CO$, + $C_7H_5^+$) of different flavanones.



Scheme 6.2: Major fragmentation pathways of flavanones. Activation using CID conditions at 45 % NCE mainly results in neutral losses of H_2O and ketene (C_2H_2O) from the molecular ion $[M+H]^+$ (bold frame). These neutral losses are scarcely observed when HCD with a NCE of 75 % or 100 % is used for activation. Here, C-ring cleavages followed by neutral losses from the cleavage fragments are dominant.



Scheme 6.3: Proposed MS^2 fragmentation of $^{1,3}A^+$ after HCD activation. In high energy MS^2 experiments, $^{1,3}A^+$ might lose two CO followed by an unusual C_2H_4 . A single loss of ketene (C_2H_2O) to afford m/z 111 is also sensible.

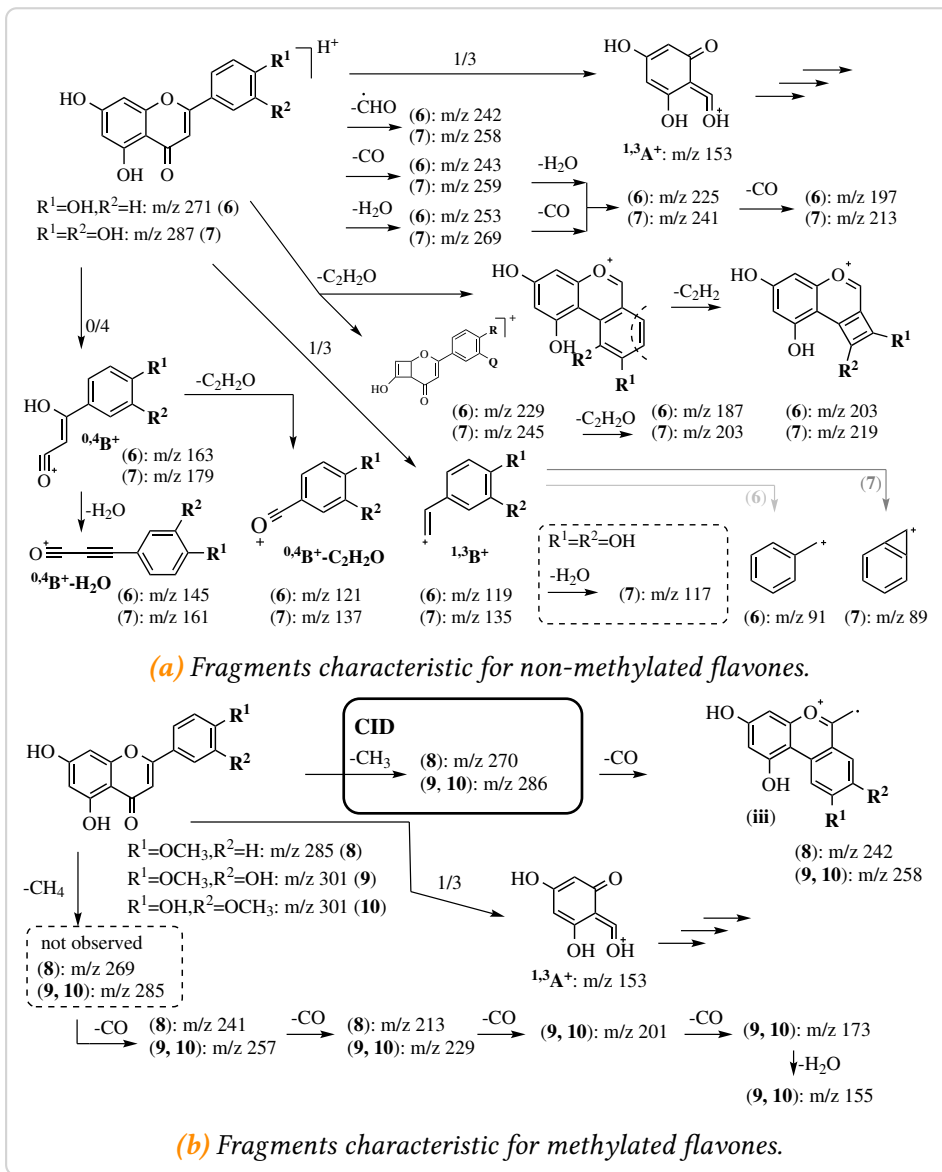
1 $m/z 111$. Pyranone (i) is suggested as a structure for this ion. Sequential 2 losses of two CO and a C_2H_4 could afford ion (ii). However, further MS^n 3 experiments are necessary to confirm these proposals.

6.3 Fragmentation of flavones

5 The principle fragmentation of flavone aglycones apigenin (6), luteolin 6 (7), acacetin (8) and chrysoeriol (10) in positive mode CID tandem mass 7 spectrometry was discussed previously [110, 131]. Non-methylated (6, 7)

1 and methylated flavones (**8 – 10**) show significantly different MS² spectra
2 (Table B.2). Apigenin (**6**) and luteolin (**7**) MS² spectra show a characteristic
3 *m/z* 153, corresponding to the ^{1,3}A⁺ ion, as a base peak in CID mode and at
4 low activation energies in HCD mode (Scheme 6.4). Contrary to the fla-
5 vanones, the MS² of non-methylated flavones show the peak corresponding
6 to the molecular ion [M+H]⁺, which is strongest in HCD at NCE of 75 %.
7 Characteristic neutral losses of water, CO and ketene (C₂H₂O) were also
8 observed for (**6**) and (**7**) (Scheme 6.4, Table B.2). MS-peaks corresponding
9 to a loss of a formyl radical, resulting in [M+H-CHO]^{•+} were also observed
10 for (**6**) and (**7**). Loss of ketene is proposed to proceed via two different path-
11 ways, such that further neutral losses of another ketene, or C₂H₂ might be
12 explained (Scheme 6.4). Besides the characteristic ^{1,3}A⁺ fragment, apigenin
13 (**6**) and luteolin (**7**) MS² spectra also present peaks corresponding to the
14 B-ring fragments ^{1,3}B⁺ (*m/z* 119 and 135) and ^{0,4}B⁺ (*m/z* 163 and 179). From
15 the mass differences of these fragments, the substitution on the B-ring
16 can be deduced. The ^{0,4}B⁺ ion might further degrade by neutral losses of
17 ketene (32 Da) or water (18 Da). The base peaks at a NCE of 100 % in HCD,
18 *m/z* 91 (**6**) and *m/z* 89 (**7**), are most likely due to a further decomposition
19 of ^{1,3}B⁺ in a fashion similar to the flavanones to afford a benzylum or
20 bicycloheptatrienyl cation respectively (Scheme 6.4).

21 The most noteable difference between the methylated and non-
22 methylated representatives is the almost complete lack of any frag-
23 mentation of the methylated flavones other than a methyl loss, in CID
24 experiments (Table B.2, Figure 6.2). A relatively stable radical cation is
25 formed after the loss of a methyl group, due to the fact that the whole
26 system is essentially conjugated (Scheme 6.5). Any other loss would
27 break this conjugation and therefore requires a higher activation energy.
28 HCD experiments at NCE of (75 to 100) % were suitable to fragment the
29 methylated flavones (**8–10**). The base peak in the HCD spectra of (**8**)
30 (*m/z* 242) and (**9, 10**) (*m/z* 257) at 75 % NCE was attributed to another loss
31 of CO from the [M+H-CH₃]^{•+} ion, while the base peak *m/z* 153 at 100 %
32 NCE likely corresponds to the ^{1,3}A⁺ ion (Figure 6.2). Further losses from
33 [M+H-CH₃-CO]^{•+}, with the proposed structure of a benzochromenylium
34 radical cation (**iii**), were not observed (Scheme 6.4, Table B.2). Mass-to-
35 charge ratios of 241 (**8**) and 257 (**9, 10**) were attributed to a neutral loss
36 of methane (CH₄), followed by a loss of CO (Scheme 6.4, Scheme 6.6).
37 Interestingly, the abundance of a peak corresponding to a [M+H-CH₄]⁺



Scheme 6.4: Major fragmentation pathways of non-methylated and methylated flavones. Multiple neutral losses of small molecules (e.g. CO, water or ketene) and 0/4 and 1/3 C ring cleavages are predominant in the MS^2 spectra of non-methylated flavones. Methylated flavones loose a methyl group in CID experiments, but only in HCD experiments do other fragmentation reaction become obvious.

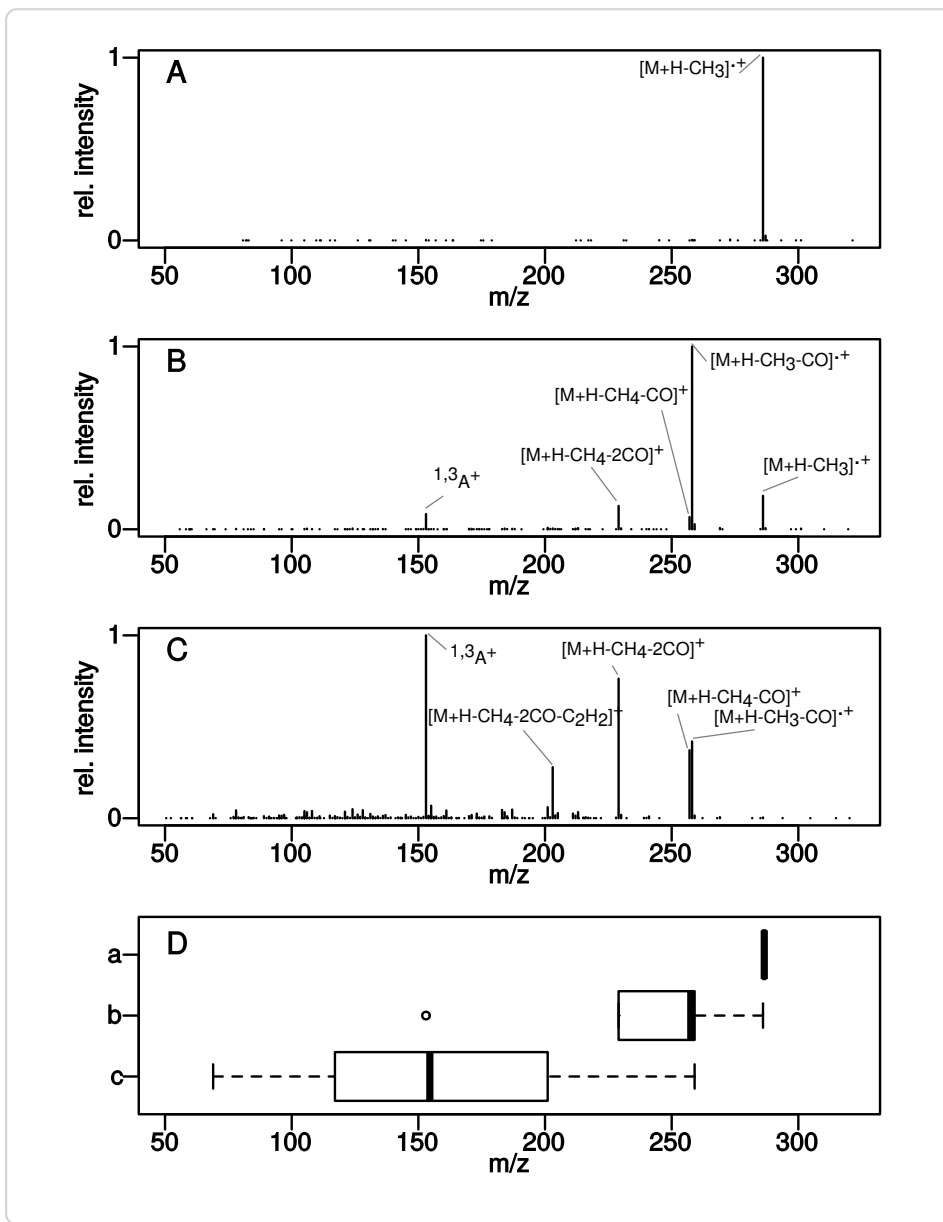
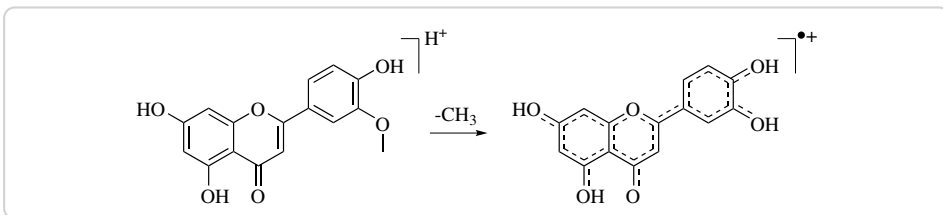


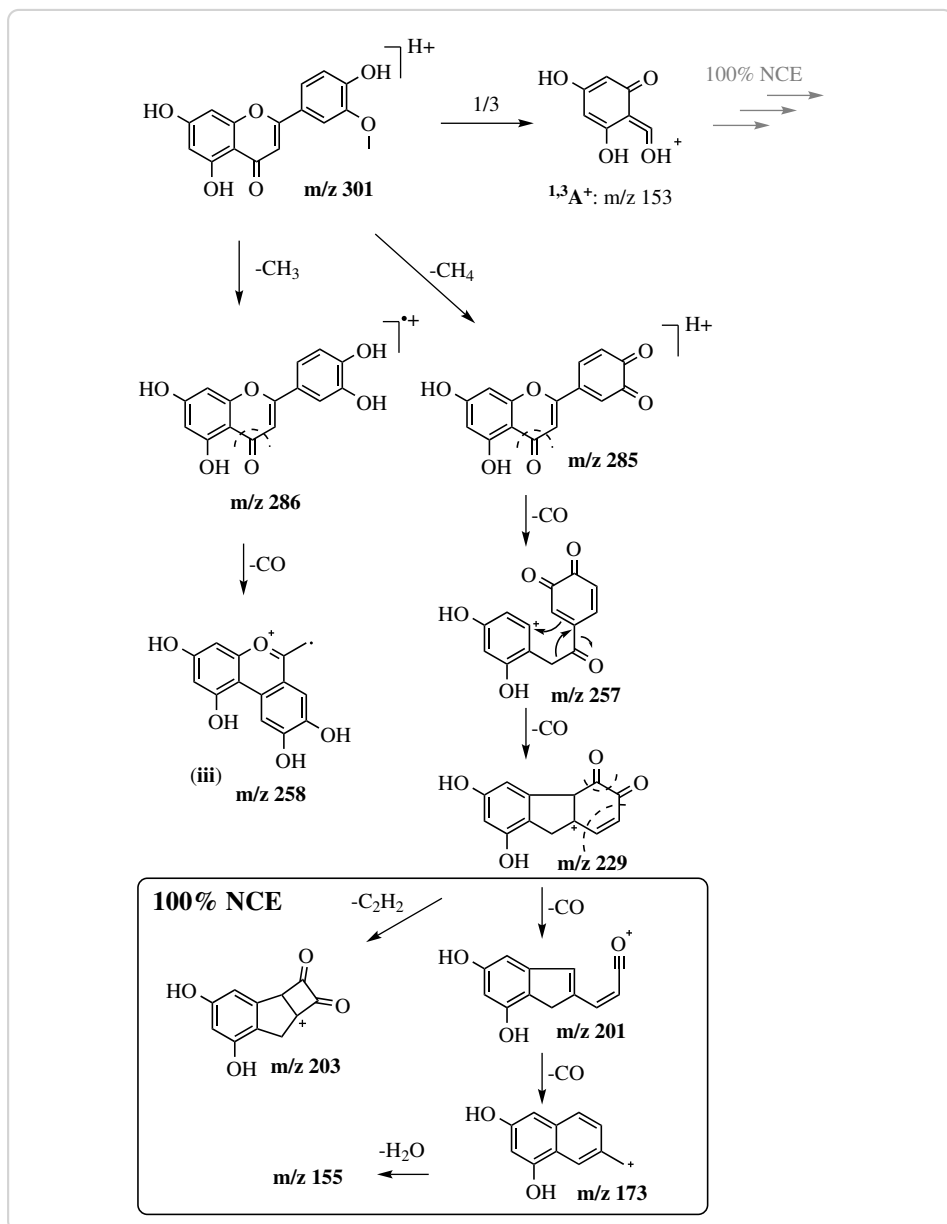
Figure 6.2.: Comparison of CID and HCD MS^2 spectra of chrysoeriol (**10**). **A** – CID at 45 % NCE. **B** – HCD at 75 % NCE. **C** – HCD at 100 % NCE. Four different prominent peaks are annotated in each spectrum. **D** – The shift to smaller masses in HCD spectra and with increasing NCE is illustrated by the boxplot of the distribution of peaks with relative intensities above 1 % in each of the above spectra.



Scheme 6.5: Stability of the $[M+H-CH_3]^{*+}$ ion of flavones. The $[M+H-CH_3]^{*+}$ ion of methylated flavones like diosmetin is highly stabilized by resonance, explaining the high intensity of the corresponding peak and limiting its fragmentation at low activation energies.

1 ion was below 1 % in all spectra, illustrating its susceptibility for additional
 2 losses. The fragment $[M+H-CH_4-CO]^{*+}$ on the other hand might undergo
 3 further neutral losses of up to three CO (compounds **10** and **9**) as is
 4 illustrated for chrysoeriol in Scheme 6.6. However, instead of additional
 5 CO losses, fragment $[M+H-CH_3-2CO]^{*+}$ of (**10**) or (**9**) might as well loose
 6 a C_2H_2 (Scheme 6.6), as suggested by the MS^2 spectra (Table B.2). The
 7 only C-ring fragmentation of the methylated flavones (**8–10**) occurs at
 8 positions 1/3, as the observed m/z 153 ($^{1,3}A^+$) suggests. The higher energy
 9 MS^2 spectra suggest, that the $^{1,3}A^+$ fragment might deteriorate further in
 10 the same manner as described for the flavanones (Scheme 6.3). Numerous
 11 minor peaks in the MS^2 HCD spectra of compounds (**8–10**) could not be
 12 assigned a fragment or structure, but many even numbered m/z values
 13 suggest quite complex rearrangements.

14 The general trend of smaller sized fragments at higher activation energies
 15 is also true for flavones (Figure 6.2).

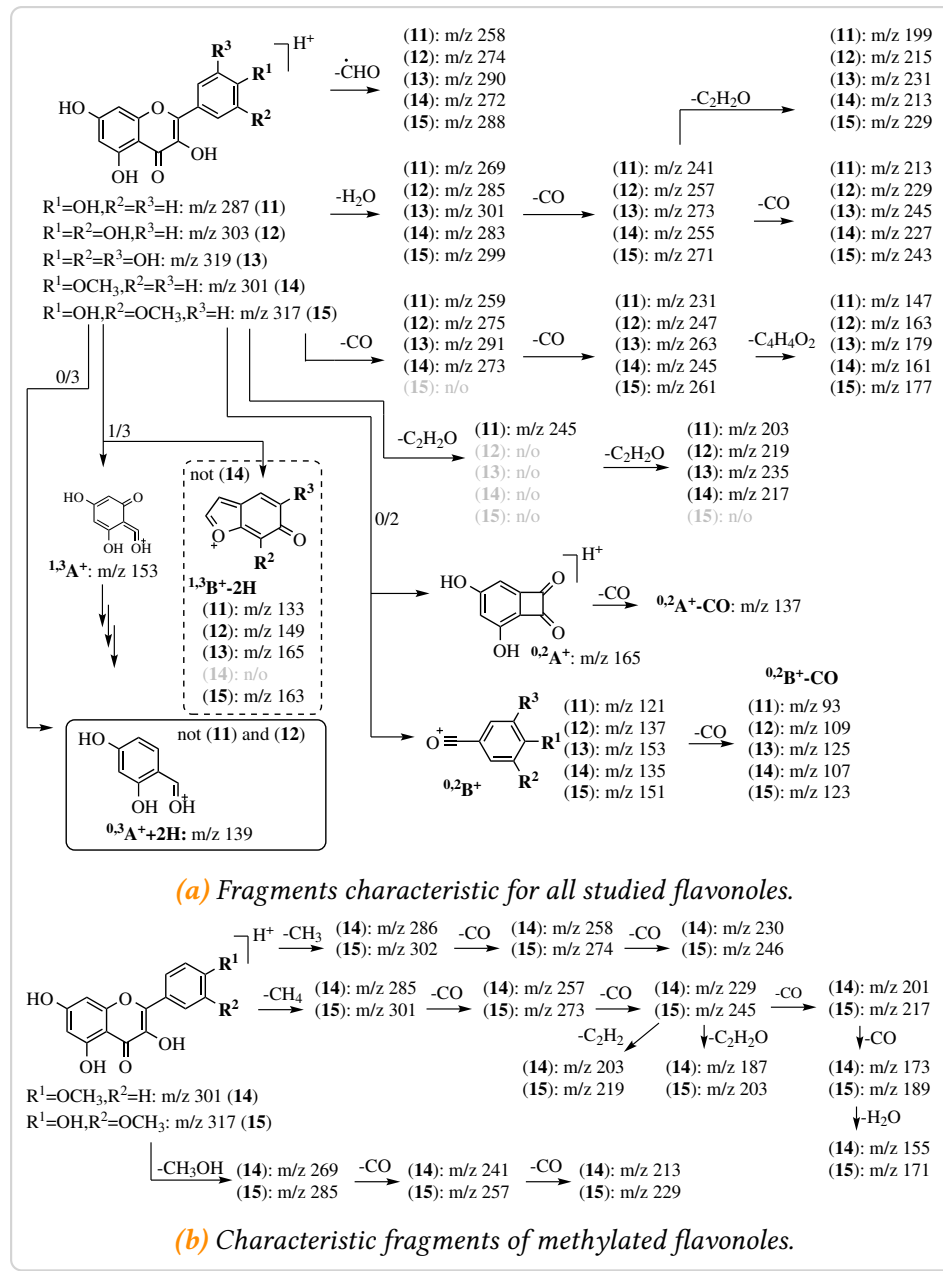


Scheme 6.6: Proposed pathway of fragmentation of (10) after HCD activation. Losses of CH_3^+ and CH_4 , followed by loss of CO are the major fragmentations observed in the corresponding MS spectra. However, multiple losses of CO only occur after a loss of methane (CH_4), possibly due to the relative stability of the benzochromenylium radical cation (iii). At 100 % NCE even higher order fragmentations were observed.

1 6.4 Fragmentation of flavonols

2 The principle fragmentation pathways of kaempferol (**11**), quercetin (**12**),
3 myricetin (**13**) and isorhamnetin (**15**) in CID tandem mass spectrome-
4 try have been previously reported [131, 136, 220]. Other than flavones,
5 methylated and non-methylated flavonols share similar fragment(ation)s.
6 Whereas in CID methylated flavones hardly showed any fragmentation
7 beyond a methyl loss, methylated flavonoles kaempferide (**14**) and isorham-
8 netin (**15**) exhibited the same losses as their non-methylated counterparts,
9 albeit at a much lower level (Table B.3, Scheme 6.7 and 6.3). These observa-
10 tions are in full agreement with previous reports [131] and hold true in CID
11 as well as HCD measurements. The observed losses from the molecular
12 ion $[M+H]^+$ are essentially the same as those that were described for the
13 flavones (**6**, **7**) (compare Scheme 6.7 and 6.4). Lots of high intensity peaks
14 presented in the MS^2 spectra of flavonoles and the base peaks changed be-
15 tween compounds. The base peak of (**11**) in the CID spectra was at m/z 165,
16 which corresponds to the $^{0,2}A^+$ fragment (Scheme 6.7). The signals m/z 257
17 and 273 corresponding to the $[M+H-H_2O]^+$ ions were the base peak in the
18 CID- MS^2 spectra of (**12**) and (**13**) respectively. The $[M+H-CH_3]^{•+}$ ions were
19 highly abundant in the CID experiments of (**14**) and (**15**). The base peak of
20 (**15**) m/z 302 corresponds to this fragment. Fragment $(^{0,3}A^+ + 2H)$ fits the
21 m/z 139, which was the base peak in the CID spectrum of (**14**). The MS
22 signal m/z 153 corresponding to fragment $^{1,3}A^+$ was at low abundance in
23 CID spectra, especially for the methylated falvonols (Figure 6.3). However,
24 in HCD experiments m/z 153 was the base peak of all flavonols, except
25 kaempferide (**14**) where m/z 229 was at 100 % relative intensity.

26 Neutral losses of CO, water or a formyl radical are suggested by the col-
27 lected spectra (Scheme 6.7, Table B.3). Only for kaempferol (**11**), a neutral
28 loss of 42 Da corresponding ketene was observed. However, MS^2 spectra
29 of all flavonols, except (**15**), contained signals that could be assigned to the
30 ion $[M+H-2C_2H_2O]^+$, suggesting a loss of two ketene units. This advocates
31 the notion that the $[M+H-C_2H_2O]^+$ ion of flavonols might be highly unsta-
32 ble. Other than the flavones, flavonoles can loose two sequential CO and
33 another $C_4H_4O_2$, confirming previously published data [131]. The spectra
34 furthermore suggest, that the $[M+H-H_2O-CO]^+$ fragment of flavonols can
35 loose another 42 Da (C_2H_2O), which was not spotted previously. The data
36 also clearly show, that neutral losses off of the molecular ion are most



Scheme 6.7: Major fragmentation pathways of flavonoles. Unlike flavones, methylated and non-methylated flavonoles share common fragmentations, albeit signals corresponding to small molecule losses are typically small for methylated analogues. Ring fragments observed typically correspond to the cleavage along bonds 0/3 or 0/2. Methylated flavonols shared common fragments with the methylated flavones. However, loss of methanol and a couple CO was also observed. n/o – not observed (relative intensity <1 %).

1 abundant in CID experiments, whereas the shift to smaller masses in HCD
2 experiments is obvious (Table B.3, Figure 6.3).

3 The studied flavonoles all displayed an MS signal at m/z 153 corresponding
4 to the $^{1,3}\text{A}^+$ fragment, just as the flavanones and flavones with a 5,7-
5 dihydroxy-substitution of the A-ring did. This further highlights the di-
6 agnostic nature of the $^{1,3}\text{A}^+$ fragment of flavonoids in MS/MS spectra. At
7 higher energies, $^{1,3}\text{A}^+$ can further decompose in a manner discussed in the
8 previous sections (Scheme 6.3). Characteristic ring cleavage fragments of
9 flavonols include $^{0,2}\text{A}^+$, $^{0,2}\text{B}^+$ and $^{1,3}\text{B}^+-2\text{H}$ [131, 136], all of which were
10 confirmed in the present study. Overall, the intensity of the $^{0,2}\text{A}^+$ and
11 $^{1,3}\text{B}^+-2\text{H}$ fragments decreased in HCD over CID experiments, whereas the
12 intensity of ions $^{0,2}\text{A}^+-\text{CO}$, $^{0,2}\text{B}^+$ and $^{1,3}\text{A}^+$ increased (Figure 6.3).

13 Apart from the discussed fragmentations, MS^2 spectra of the methylated
14 flavonols (**14**) and (**15**) also showed fragmentations typical of methyl esters,
15 namely methyl, methane and methanol loss. Methyl and methane loss
16 followed by sequential losses of carbon monoxide were already shown
17 for flavones (**8–10**) and are postulated to proceed in a similar manner in
18 flavonols (**14**) and (**15**) (Scheme 6.8). Because of the extra hydroxyl at
19 the C-ring, methylated flavonols such as isorhamnetin can lose two CO
20 instead of just one after loss of a methyl radical (compare Scheme 6.8 and
21 (Scheme 6.6)). Other than flavones, spectra of methylated flavonols (**14**)
22 and (**15**) also showed signals (m/z 269 and m/z 285) corresponding to a loss
23 of methanol. The data suggests, that these $[\text{M}+\text{H}-\text{CH}_3\text{OH}]^+$ fragments can
24 loose up to two CO, similar to the loss of water and CO (Scheme 6.8 and
25 6.7). The peaks with m/z 301, 273, 245, 217 and 189 in the HCD spectra of
26 isorhamnetin (**15**), suggest a loss of up to four CO after the initial loss of
27 methane (Scheme 6.8). As mentioned before, the smaller mass fragments
28 corresponding to multiple neutral losses are more pronounced at higher
29 activation energies and were thus limited to HCD experiments at a NCE of
30 100 % (Figure 6.3, Scheme 6.8).

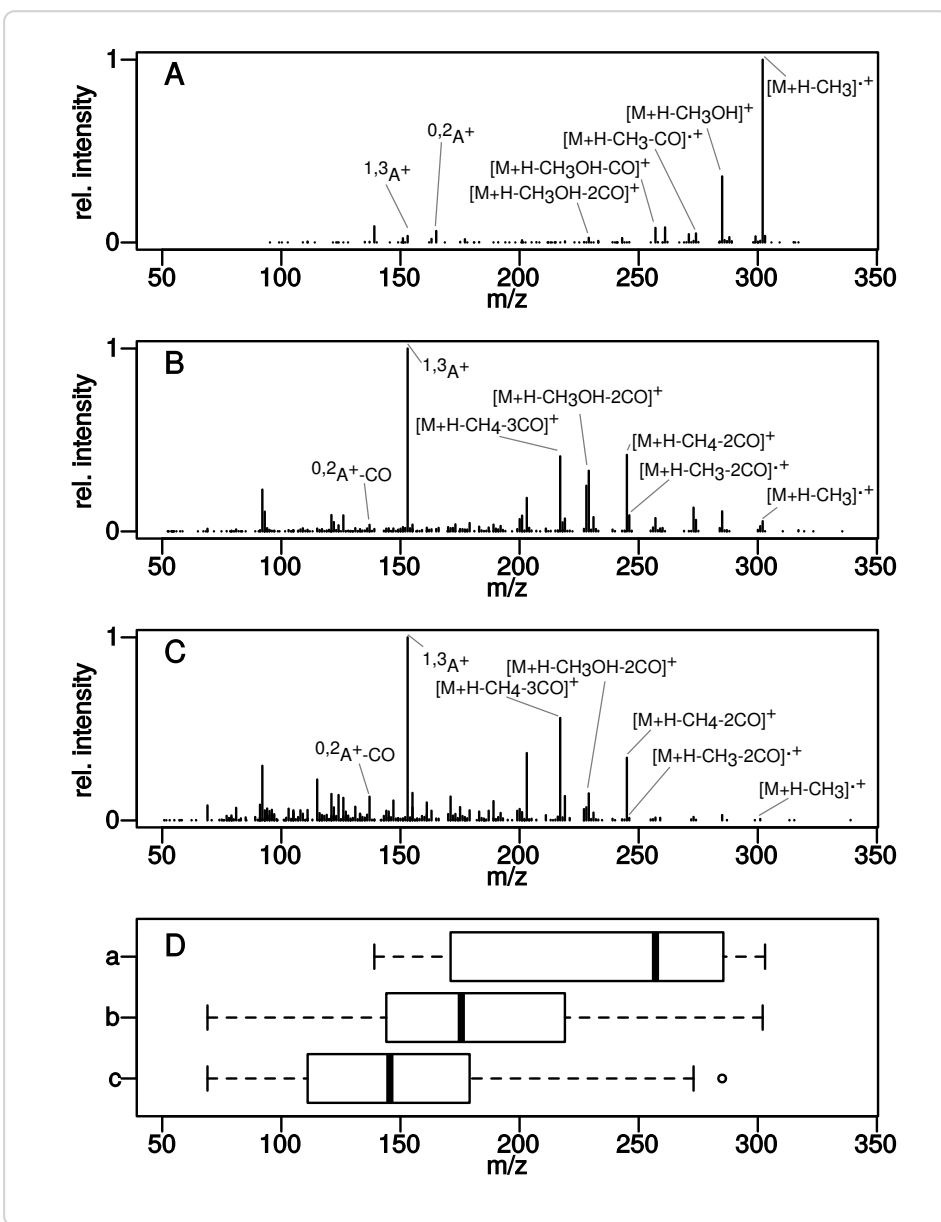
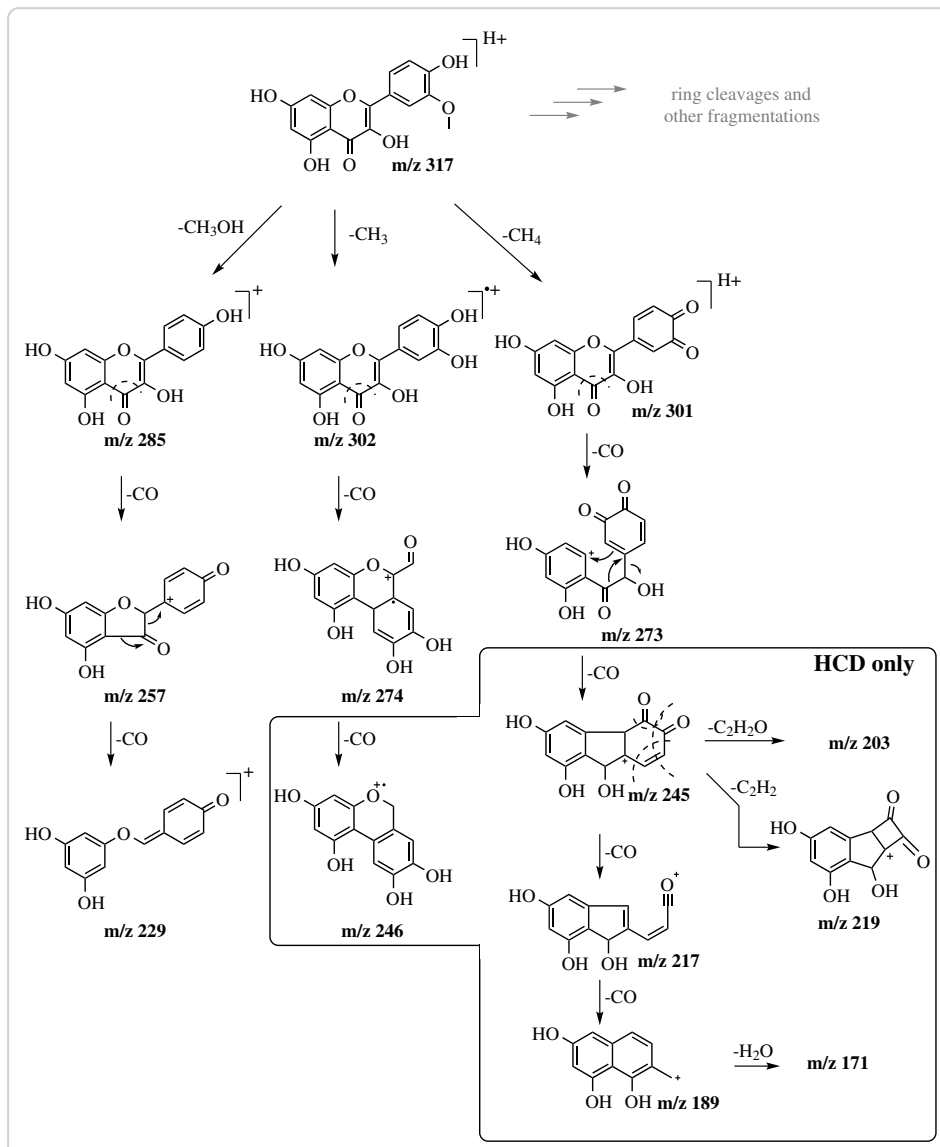


Figure 6.3: Comparison of CID and HCD MS² spectra of isorhamnetin (**15**). **A** – CID at 45 % NCE. **B** – HCD at 75 % NCE. **C** – HCD at 100 % NCE. Four different prominent peaks are annotated in each spectrum. **D** – The shift to smaller masses in HCD spectra and with increasing NCE is illustrated by the boxplot of the distribution of peaks with relative intensities above 1 % in each of the above spectra.



Scheme 6.8: Proposed pathways of fragmentation of isorhamnetin (**15**). Isorhamnetin might lose methyl, methane or methanol upon activation. A similar fragmentation pathway was proposed for the analogous chrysoeriol (Scheme 6.6). Some fragmentations were observed in HCD mode only (box).

1 6.5 Conclusions

2 This comprehensive study shows that, taken together, data from CID and
3 HCD experiments can be complementary to give a much deeper under-
4 standing of structural features of flavonoids. Mass errors were calculated
5 for each postulated fragment and ranged from (0.4 to 10) ppm, highlight-
6 ing the accuracy of the instrument which also allowed for the accurate
7 determination of molecular formulas from MS signals.

8 The complementary nature of CID and HCD is especially striking,
9 when comparing spectra of (9) and (10). CID fragmentation of these B-ring
10 methylated flavones afforded MS spectra, where a methyl loss was by far
11 the dominant fragmentation. HCD on the other hand provided higher
12 order fragmentations combined with a higher signal-to-noise ratio, for a
13 deeper insight into structural features. These higher order fragmentations
14 were accelerated by increasing the activation energy, but interpretability
15 of the corresponding spectra was limited. However, with the help of *in*
16 *silico* methods for the interpretation of MS/MS spectra [14, 219] and the
17 computing power available today, the information contained in highly
18 complex spectra might become more easily accessible. Nonetheless, fine-
19 tuning of the activation energy is an option to optimize fragmentation
20 intensities, especially of the C-ring fragmentations.

21 Flavones and flavonols share similar patterns of fragmentation and dis-
22 play a loss of a CHO radical, which distinguishes their MS² spectra from
23 those of the flavanones. Distinguishing characteristics between MS²
24 spectra of flavones and flavonols are the C-ring fragmentations, where the ^{0,4}B⁺
25 fragment was typically limited to flavones, whereas a (strong) ^{0,2}A⁺ frag-
26 ment was only observed for (non-methylated) flavonols. While methylated
27 flavanones did not differ in their fragmentations from their non-methylated
28 analogues, MS spectra of methylated and non-methylated flavones and
29 flavonols showed significant differences. Noticable loss of CH₃• or CH₄,
30 followed by losses of CO were typical signs of methylated flavones or
31 flavonols. Loss of methanol was observed in methylated flavonols and in
32 small amounts at 100 % NCE in flavones, not however in the MS² spectra
33 of flavanones. Under the right conditions, all of the studied 5,7-dihydroxy
34 substituted flavonoids presented a ^{1,3}A⁺ ion, with a characteristic *m/z* 153.
35 This information might be of value for studies that want to determine the
36 position of a derivatization of the flavonoid core. To the authors knowledge,

1 a pathway for the decomposition of $^{1,3}\text{A}^+$ at high activation energies was
2 proposed for the first time in this work and is universal for all studied
3 compounds. A signal m/z 91, stemming from the decay of the $^{1,4}\text{B}^+$ or $^{1,3}\text{B}^+$
4 ion, might be a hint for a *para*-monohydroxylated B-ring on flavanones and
5 flavones respectively. Conversely, a peak m/z 89 can point in the direction
6 of multiple substitutions on the B-ring.

7 In summary, the complementary nature of the studied activation methods
8 CID and HCD provides more thorough data for the study of flavonoids.
9 Key ions might only present themselves in the spectra of either method,
10 and together with differences and similarities in the MS/MS spectra, can
11 be used to gain additional insights into the structural characteristics of a
12 studied compound.

13 6.6 Contributions

14 Benjamin Weigel prepared substances, analyzed mass spectral data and
15 prepared manuscript. Annegret Laub and Jürgen Schmidt conducted LC/MS
16 measurement runs. Through helpful discussions, Jürgen Schmidt helped
17 tremendously with the preparation of the manuscript.

¹ 7 Enzymatic methylation of non- ² catechols

1

Enzymatic methylation of non-catecholic aromatic hydroxyls using class I and class II methyl transferases

Benjamin Weigel^{1,a}, Martin Dippe^{2,b}, Annegret Laub^{1,b}, Ludger A.

² Wessjohann^{1,d}

Contact: bweigel@ipb-halle.de^a, mdippe@ipb-halle.de^b, alaub@ipb-halle.de^c, law@ipb-halle.de^d

Affiliation: Leibniz-Institute of Plant Biochemistry, Department of Bioorganic Chemistry¹

Keywords: methyl transferase, SAM, biocatalysis

3 Abstract

4 Phenylpropanoid and flavonoid O-methyl transferase (PFOMT) and
5 soy O-methyl transferase (SOMT-2) are S-adenosyl-L-methionine (SAM)-
6 dependent methyl transferases (MTs), belonging to classes I (23–27 kDa,
7 cation-dependent) and II (38–43 kDa, cation-independent) respectively.
8 Methylation of non-catecholic aromatic hydroxyls (phenolic, 3'-hydroxy-
9 4'-methoxy (3O4M), 4'-hydroxy-3'-methoxy (4O3M)) exemplified by dif-
10 ferent compound classes was achieved by both enzymes. This is the first
11 time this behavior is described for PFOMT. It is shown, that the activity
12 of PFOMT towards non-catechols is increased at high pH. Adjusting the
13 pH to more basic conditions can also partly remedy the deleterious effect of
14 missing Mg²⁺ for class I enzyme PFOMT. Soluble SOMT-2 enzyme was ob-
15 tained by optimizing *in vitro* refolding conditions using fractional factorial
16 design (FrFD) and design of experiments (DoE). However, the activity of
17 the refolded SOMT-2 was insufficient for *in vitro* experiments.

18

19 7.1 Introduction

20 Phenyl propanoid derived polyphenols are one of the most abundant plant
21 secondary product in nature. Representatives such as flavonoids and an-
22 thocyanidins play important roles in plant development, flower color or in
23 the defense systems combating biotic and abiotic stresses. Lignin, the main
24 component of wood, is mostly comprised of phenyl propanoid alcohols and
25 is responsible for the structure and rigidity in (lignified) vascular plants.

1 The properties of flavonoids, lignins and other is largely influenced
2 by their derivatization pattern, and thus so-called tailoring enzymes
3 are widespread in nature. Tailoring enzymes such as methyl-, prenyl-
4 and glycosyl-transferases are responsible for hydroxylations, (*C* and
5 *O*)-methylations, -prenylations and -glycosylations, which are common
6 derivatizations of polyphenols, respectively [42, 76, 183, 188, 211, 221].

7 The biosynthetic or biocatalytic production of tailor made natural mate-
8 rials (e.g. lignins) with desireable properties is an important step towards a
9 more ecological and economical industry and has the potential to greatly
10 impact many areas of modern life [235]. Flavonoids and polyphenols such as
11 resveratrol, that exhibit health-beneficial effects (e.g. antioxidative, antimi-
12 crobial), are often used in functional foods or to improve the “properties”
13 of food products [36, 120, 227].

14 It is therefore of great importance to evaluate and develop new methods
15 to biocatalytically produce known and new polyphenols with interest-
16 ing properties. The aim of this study was to assess two plant *O*-methyl
17 transferases (*O*-MTs), PFOMT and SOMT-2, of classes I and II towards
18 their potential for the methylation of structural motifs commonly found
19 in polyphenols. The main interest was to study methylation of so-called
20 non-catecholic moieties, such as phenolic, 3'-hydroxy-4'-methoxy (3O4M)
21 and 4'-hydroxy-3'-methoxy (4O3M) structural motifs and to see whether
22 permethoxylated compounds could be produced by these enzymes.

23 7.2 SOMT-2

24 SOMT-2 is already well characterized in the literature and acts on flavonoids
25 as well as isoflavonoids[99, 102, 103]. However, *in vitro* data of this enzyme
26 has not been published. It was selected as a model candidate as a class
27 II plant *O*-MT, that can already methylate 4'-hydroxyls of non-catecholic
28 flavonoids.

29 7.2.1 *In vivo* biotransformation in *Nicotiana benthami-* 30 *ana*

31 The group of Sylvestre Marillonet (IPB) established an efficient system
32 to clone and assemble multi enzyme pathways in *Nicotiana benthamiana*,
33 using a modular cloning toolbox, which has already been used to produce

1 flavonoids [107]. All the genes required to establish the pathway up to
 2 naringenin in *N. benthamiana* in theory had been cloned previously (Figure
 3 7.1). Only the *SOMT2* gene needed to be cloned into a suitable vector
 4 to be transiently expressed in *N. benthamiana*. Infiltrated plants were har-

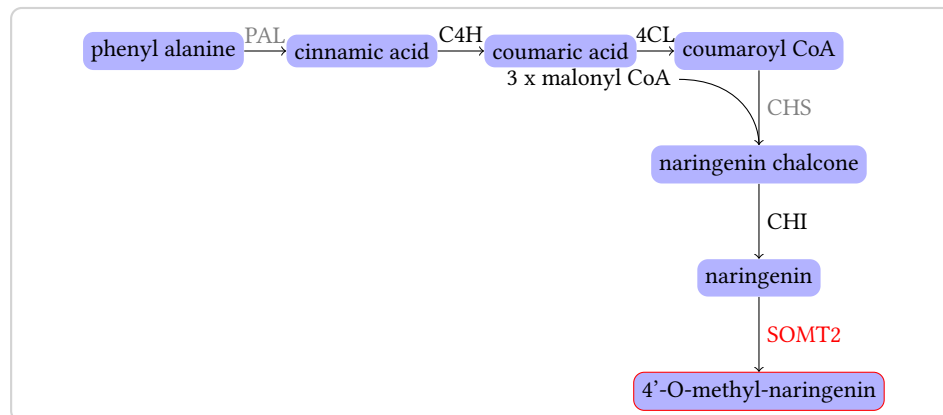


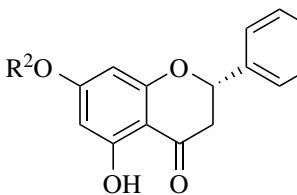
Figure 7.1. Semi-synthetic pathway to naringenin and 4'-O-methyl naringenin in *N. benthamiana*. Enzymes not endogenous to *N. benthamiana* are in gray. PAL - phenylalanine ammonia lyase, C4H - cinnamic acid 4-hydroxylase, 4CL - 4-coumaric acid:CoA ligase, CHS - chalcone synthase, CHI - chalcone isomerase, SOMT2 - soy O-methyl transferase 2

4
 5 vested after 7 days (see section 4.3). The average weight loss after freeze
 6 drying was 87.5 %.

7 The dried material was extracted and analyzed via high-performance
 8 liquid chromatography (HPLC) to determine whether ponciretin or the
 9 “down-stream” glycosylated products (poncirin, didymine) were produced
 10 (Table 7.1). However, through comparison with authentic standards it
 11 was apparent, that none of the expected compounds were detected. This
 12 finding suggest, that neither naringenin, nor any “down-stream” flavonoids
 13 (ponciretin, poncirin, didymin) were present in detectable amounts in the
 14 plant tissue at the time of harvest. Although unlikely, it cannot be exluded
 15 that higher amounts of the compounds of interest were present at some
 16 point in the tissue.

17 The HPLC chromatograms were analyzed by principal component analy-
 18 sis (PCA) after the data were aligned, centered and scaled, to assess whether
 19 the collected plant material samples were different from one another (Figure
 20 7.2 and C.1). The PCA-plot shows that the samples of the different
 21 leaf sides do not separate, indicating no difference between infiltration
 22 with the *SOMT* gene and vector control between the first two principal
 23 components, which account for 80 % of the variance. However, there is a

Table 7.1.: Naringenin and 4'-methylated derivatives that were inquired for in the plant samples via HPLC. The core structure of the compounds is displayed on the left.

	R ¹	R ²	name
	H	H	naringenin
	CH ₃	H	ponciretin
	CH ₃	rutinose ¹	poncirin
	CH ₃	neohesperidose ²	didymine

¹ slight separation between top and bottom leaves in the second principal

² component and between plant 3 and plants (1 and 2) in the first principal component (appendix, Figure C.1). This suggest, that the chemical com-

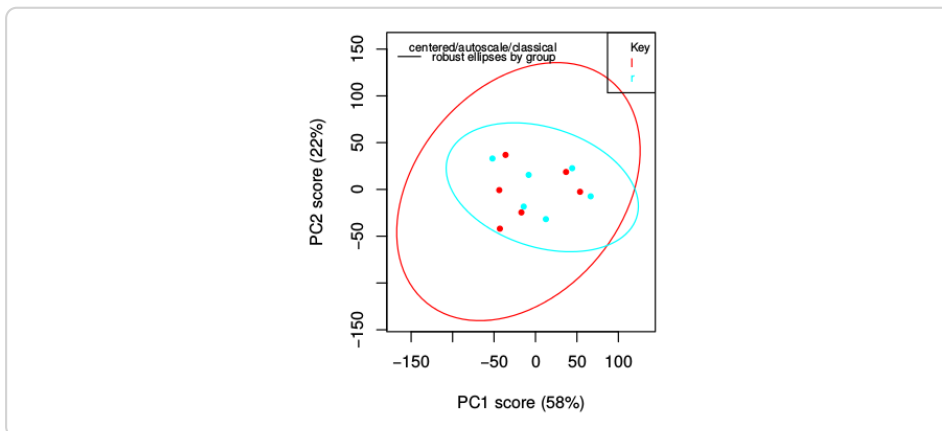


Figure 7.2.: Scatterplot of the first two principal components from the PCA of the HPLC data obtained from leaf material extracts. The samples are colored by leaf side (left/SOMT-2: red, right/vector control: cyan).

³

⁴ position as detected by HPLC is slightly different in the top and bottom
⁵ leaves, as well as between the different plants.

7.2.2 In vivo biotransformation in *E. coli*

⁷ Kim *et al.* [99, 102, 103] showed, that SOMT-2 could be used for the biotrans-
⁸ formation of different flavonoids in *E. coli* live cultures. The *SOMT-2* gene
⁹ was cloned into the pET28a(+) and pET41a(+) vectors, to obtain constructs
¹⁰ for the production of SOMT-2 without and with a N-terminal Glutathion
¹¹ S-transferase (GST)-tag, respectively since both have been used success-
¹² fully [99, 102, 103]. However, methylated flavonoids were not detected
¹³ when biotransformations were prepared according to the methods of the
¹⁴ aforementioned authors (Figure 7.3a). Thus, the biotransformation medium

1 was changed to auto-induction (AI)-medium with 0.05 % glucose [189].
 Measured growth curves showed, that the glucose present in the medium

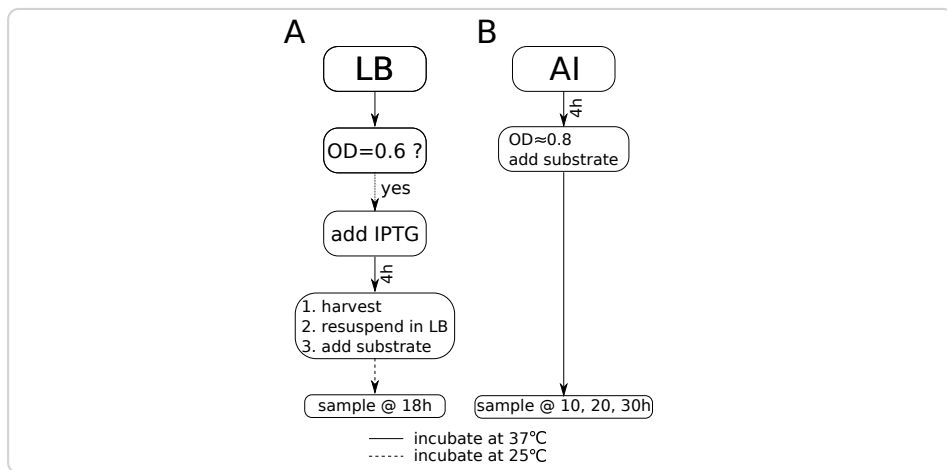


Figure 7.3.: Biotransformation methods as described by Kim et al. (A) and developed in this work (B). OD – optiocal density at 600 nm, LB – LB-medium, AI – AI-medium.

2
 3 was depleted after about 5 hours into growth (appendix, Figure C.2). Ex-
 4 pression of the *SOMT-2* gene is expected to begin at this time, because the
 5 catabolite repression on the *lac* promoter would be relieved and the pro-
 6 moter would be activated by the lactose present in the AI-medium. Thus,
 7 0.1 mM of flavonoid substrate were added at 4 hours to minimize its influ-
 8 ence on growth and possible degradation. Although sodium dodecylsulfate
 9 (SDS)-polyacrylamide gel electrophoresis (PAGE) samples were prepared
 10 throughout the course of the experiment, accumulating SOMT-2 could not
 11 be clearly distinguished from endogenous *E. coli* protein in the SDS-PAGE
 12 gels (appendix, Figure C.3). Nonetheless, methylation of some of the tested
 13 substrates was observed over a course of 30 hours (Table 7.2). Therefore,
 14 the sampled medium was extracted using acidified ethyl acetate. Liquid
 15 chromatography coupled mass-spectrometry (LC/MS) was employed to
 16 determine the site of methylation, since this method is highly sensitive
 17 and numerous structural studies on flavonoids using tandem-mass spec-
 18 trometry experiments have highlighted the feasibility of this approach (see
 19 chapter 6) [58, 117]. Collision induced dissociation (CID) was used to obtain
 20 structural information about the target molecules, since soft ionization
 21 techniques (e.g. electrospray ionization (ESI)) used in LC/MS instruments
 22 primarily produce protonated and deprotonated molecular ions, but rarely
 23 yield fragments [185]. The CID method collides the precursor ions with

Table 7.2.: In vivo biotransformation of different flavonoids, phenylpropanoids and anthraquinones by SOMT-2 in *E. coli*. Conversion ratios were calculated for samples taken after 30 hours. Multiple substrates containing a 4'-hydroxyl were methylated. Calculation of conversion percentages are only rough estimates, because of the nature of crude medium extracts. Products were determined by liquid chromatography-tandem mass spectrometry (LC-MS/MS).

substrate	class	4'-OH conversion product	
alizarin	anthraquinone	✗	✗
purpurin	anthraquinone	✗	✗
apigenin	flavone	✓	✓(≥54 %) 4'-O-methyl apigenin
chrysin	flavone	✗	✗
genistein	isoflavone	✓	✓(<1 %) Biochanin A
galangin	flavonol	✗	✗
kaempferol	flavonol	✓	✓(≥6 %) kaempferide
naringenin	flavanone	✓	✓(≥55 %) ponciretin
eriodictyol	flavanone	✓	✓(≥40 %) hesperetin
homoeriodictyol	flavanone	✓	✓(>6 %) 3',4'-(<i>O,O</i>)-dimethyl eriodictyol
hesperetin	flavanone	✗	✗
phloretin	chalcone	✓	✗
resveratrol	stilbene	✓	✓(≥86 %) 4'-O-methyl resveratrol
<i>p</i> -coumaric acid	cinnamic acid	✓	✗
caffeic acid	cinnamic acid	✓	✗
reosmin	cinnamic acid [†]	✓	✗

[†] dihydro cinnamic ketone

1 a neutral target gas while increasing the energy to induce fragmentation.

2 The produced fragments vary depending on the energy chosen for frag-

3 mentation. Flavonoids follow certain different fragmentation pathways

4 [58, 117]. The fragmentation of interest in this work, was the one along the

5 C-ring, which produces two fragments (A- and B-ring) (Figure 7.4b). The

6 mass of the A- and B-ring fragments gives strong evidence for the position

7 (ring) at which methylation occurred. Using the CID technique, an energy of

8 30 eV proved sufficient to fragment most flavonoids along the C-ring as is

9 shown here for the methylated naringenin (Figure 7.4). The molecular ion

10 [M+H]⁺ of the methylated naringenin has a mass-to-charge ratio (*m/z*) of

11 287.092. The fragments helping to derive structural information are *m/z* 133

12 and *m/z* 153, which can only be explained if the B-ring was methylated

13 (Figure 7.4b). If the A-ring was methylated, the expected fragment ions of A

14 and B-ring would have *m/z*-values of 167 and 119 respectively. The LC/MS

15 results suggest, that methylation occurred exclusively at the 4'-hydroxyl,

16 as there was no conversion detected, when the 4'-hydroxyl was absent

17 (Table 7.2). A free 4'-hydroxyl seems therefore necessary for a substance

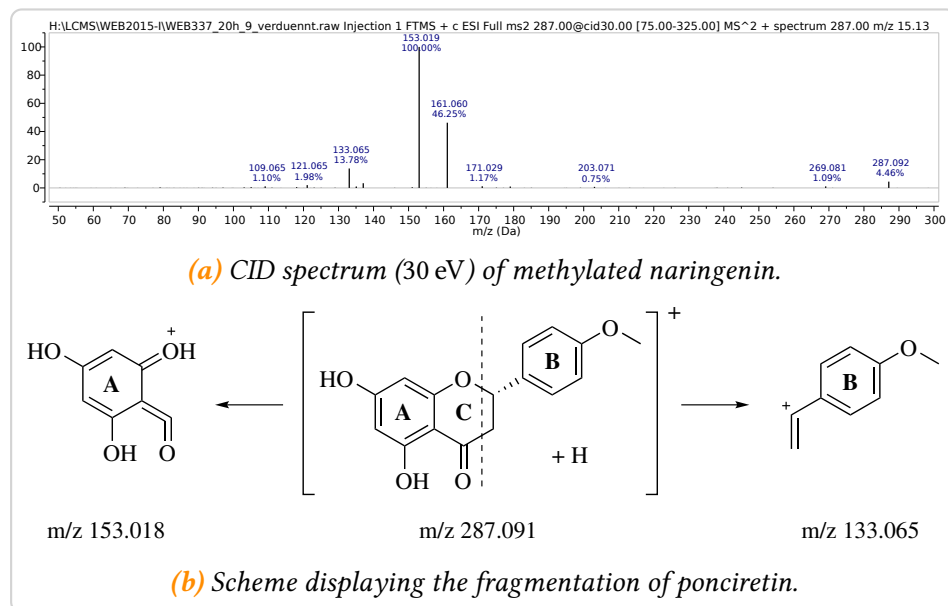


Figure 7.4: The masses resulting from the fragmentation into A- and B-ring along the C-ring (dashed line, b) are evidence, that the 4'-hydroxyl on the B-ring is methylated by SOMT-2

1 to be a substrate for SOMT-2, which confirms the previous results [99,
 2 102]. Conversion was observed for 4'-hydroxylated (iso)flavonoids and the
 3 stilbene resveratrol, however conversion rates of the isoflavone genistein
 4 were very low. No conversion of anthraquinones, cinnamic acid derivates
 5 or chalcones was detected, which is also in accordance with previously
 6 published data [99, 102]. SOMT-2 acts on phenolic, catecholic as well as (4-
 7 hydroxy-3-methoxy-phenyl)-moeities, as is suggested by the assay results
 8 that showed methylation of naringenin, eriodictyol and homoeriodictyol
 9 respectively. The methylation of (4-hydroxy-3-methoxy-phenyl)-moieties
 10 and of stilbenes are properties of SOMT-2 that have not been described
 11 before.

12 The conversion ratios were assessed, but are beset with large errors due
 13 to the nature of *E. coli* rich medium extracts. The highest conversions were
 14 observed for flavanones and flavones (up to $\geq 55\%$). The tested isoflavones
 15 and flavonols showed much lesser conversion ratios (less than 10%). The
 16 conversion ratios of apigenin ($\geq 54\%$) and naringenin ($\geq 55\%$) are com-
 17 parable to the ones published previously [99, 102]. However, genistein
 18 only showed minute conversions, which is in disagreement with the data
 19 previously published [99, 102]. Conversion of eriodictyol, homoeriodictyol
 20 and kaempferol were not reported before.

1 The biotransformation of resveratrol to 3,5-dihydroxy-4'-methoxy-
2 stilbene showed a conversion ratio of $\geq 86\%$ in 30 hours. This is roughly
3 double the conversion which was recently reported for *in vivo* biotransfor-
4 mations using the specific resveratrol O-MT sbCOM1, which only achieved
5 42 % conversion in 36 hours [97].

6 7.2.3 *In vitro* studies using recombinantly produced 7 SOMT-2

8 *In vivo* biotransformations are an important tool for the primary charac-
9 terization of enzymes. However, because live organisms are used and lots
10 of variables are unknown, these systems can cause large errors and are
11 not fit to thoroughly characterize an enzyme. Initially, SOMT-2 was to be
12 purified to homogeneity to be later thoroughly characterized *in vitro*, since
13 the recombinant production of SOMT-2 in *E. coli* as a fusion protein with
14 an N-terminal T7-tag was previously shown. However, the recombinant
15 enzyme had not been characterized [99].

16 Protein production test

17 Initial protein production tests were carried out using *SOMT-2* cloned
18 into pET28a(+) with an N-terminal His₆-tag. However, SOMT-2 was not
19 produced in soluble form (Figure 7.5). Numerous systems were tested
20 for the expression of *SOMT-2*. *E. coli* strains used for the trials included
21 BL21(DE3), Rosetta(DE3), Origami(DE3), C41(DE3), C43(DE3), C41(DE3)
22 pLys, C43(DE3) pLys and DH5 α . The *SOMT-2* gene was cloned into mul-
23 tiple other vectors, including pET20b for periplasmic protein production,
24 pET32 for expression with an Trx-tag and vectors that carry promoters
25 for induction by rhamnose. Multiple media, including terrific broth (TB),
26 lysogeny broth (LB) and autoinduction media were used along with dif-
27 ferent inducers (e.g. lactose, rhamnose, isopropyl-D-thiogalactopyranosid
28 (IPTG)) at different temperatures. Nonetheless SOMT-2 could not be pro-
29 duced in a soluble form and expression only resulted in inclusion bodies
30 (IBs).

31 *In vitro* protein refolding

32 Since the SOMT-2 protein could not be obtained in soluble formen, when
33 recombinantly expressed in *E. coli*, the IBs were prepared [166] and used for

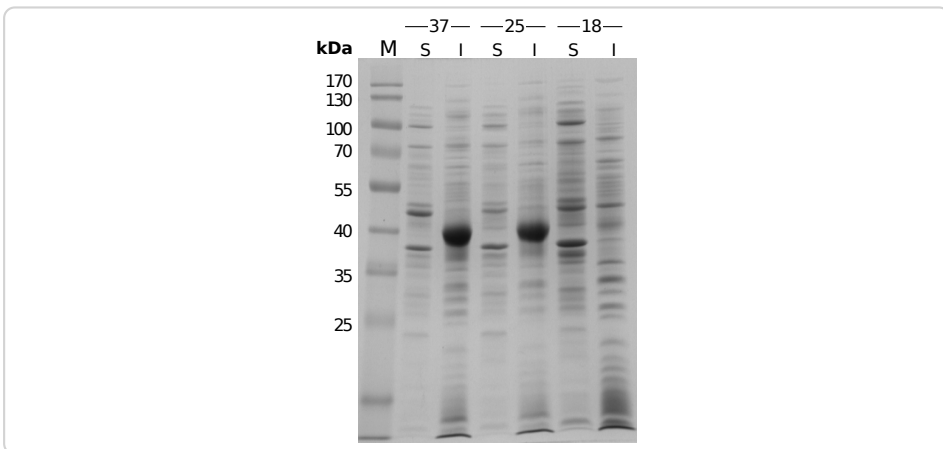


Figure 7.5.: SDS-PAGE of *pET28a(+)* SOMT-2 expressed in *E. coli* BL21(DE3) in autoinduction medium at different temperatures (shown above). The insoluble fractions show a protein band the same height as the 40 kDa marker band, which corresponds to the SOMT-2 protein (40 425 Da). M – protein size marker, S – soluble fraction, I – insoluble fraction

1 *in vitro* refolding studies. For *in vitro* protein refolding, IBs are solubilized
 2 using denaturants such as GdmCl or urea. The native tertiary structure of
 3 the protein is then restored by removal of the denaturant under the “right”
 4 conditions (e.g. pH, salt, additives, etc.). However, this is no trivial task
 5 since initially the “right” conditions have to be found by trial and error.
 6 The refolding process competes with misfolding and aggregation processes
 7 and refolding buffers have to be optimized in order to obtain an efficient
 8 refolding system with the best possible results [166, 214, 225]. Refolding
 9 efficiency is best measured via biological activity, but even with adequate
 10 assays refolding studies are a time-consuming process. The number of
 11 experiments required to even test only four variables, for example pH, salt,
 12 temperature and protein concentration with 3 states each (e.g. low, medium,
 13 high) in all possible combinations results in $3^4 = 81$. An experimental setup,
 14 which accounts for all possible variable (factor) combinations is also called
 15 a *full factorial design*. These setups capture main effects, as well as higher
 16 level interaction effects [20, 147]. However, for screening purposes only a
 17 fraction of the experiments can be run. The objective of these fractional
 18 factorial design (FrFD) experiments is to identify the variables, which have
 19 large effects and are worth expanding the experimental investigation upon.
 20 FrFDs have been successfully used for a number of protein refolding trials
 21 [196, 205, 214].

22 The following factors were studied for the *in vitro* refolding of SOMT-2:

1 pH, arginine addition, glycerol addition, addition of divalent cations, ionic
 2 strength, redox system, cyclodextrin addition and effector (*S*-adenosyl-L-
 3 homocysteine (SAH)) addition. These factors were used, because all have
 4 been shown to influence refolding success [4, 6, 11, 29, 65, 200, 205, 214,
 5 225]. Two factor levels were used in a twelve-run design. This is sufficient
 6 to find some main effects, however no statement about interaction effects
 7 can be made. For a complete listing of the buffers and conditions the reader
 8 is referred to the materials and methods chapter (Tables 4.5 and 4.6).

9 Big differences between soluble and insoluble fractions of different re-
 10 folding buffers could already be noticed from the SDS-PAGE gels (Figure 7.6,
 11 see subsection 4.4.11). Refolding buffers 2,3 and 8–11 mainly produced
 12 insoluble protein, whereas the majority of the protein in refolding buffers 1,
 13 4–7 and 12 was in soluble form after an overnight refolding reaction (Tables
 14 4.5 and 4.6, Figure 7.6). After rebuffering the cleared refolding reactions
 15 into a unified buffer the protein concentrations were estimated by BRAD-
 16 FORD-assays [21]. The protein concentrations measured by BRADFORD's
 17 method were consistent with the observations from the SDS-PAGE gels
 18 (compare Figure 7.7a and 7.6). Soluble protein was obtained for buffers 1,
 19 4–7 and 12. The highest amount of soluble protein was present, when the
 refolding reaction took place in buffers 5 or 7. The common denominator

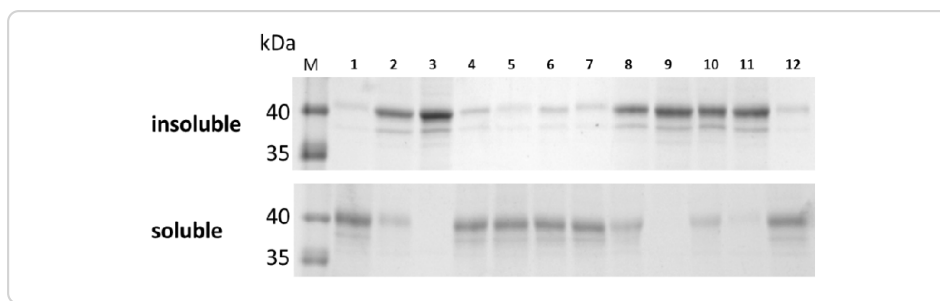


Figure 7.6.: SDS-PAGE of the insoluble and soluble fractions of the refolding reactions. Refolding reactions 2,3,8–11 seem to mainly produce misfolded insoluble protein, while the other refolding buffers (1,4–7,12) produce soluble protein.

20
 21 of those buffers is that all of them contained arginine, whose addition has
 22 proven beneficial for many refolding applications [29, 65, 200].

23 **Main effects plots (ME-plots)** illustrate the difference between level
 24 means for each factor. Therefore, the mean of the measured property (i.e.
 25 protein concentration) for each level of every factor, described by + or -, of
 26 the used refolding buffers is plotted in relation to the overall mean. For
 27 example, the levels of the factor pH are “low” (-) and “high” (+). When x_i^-

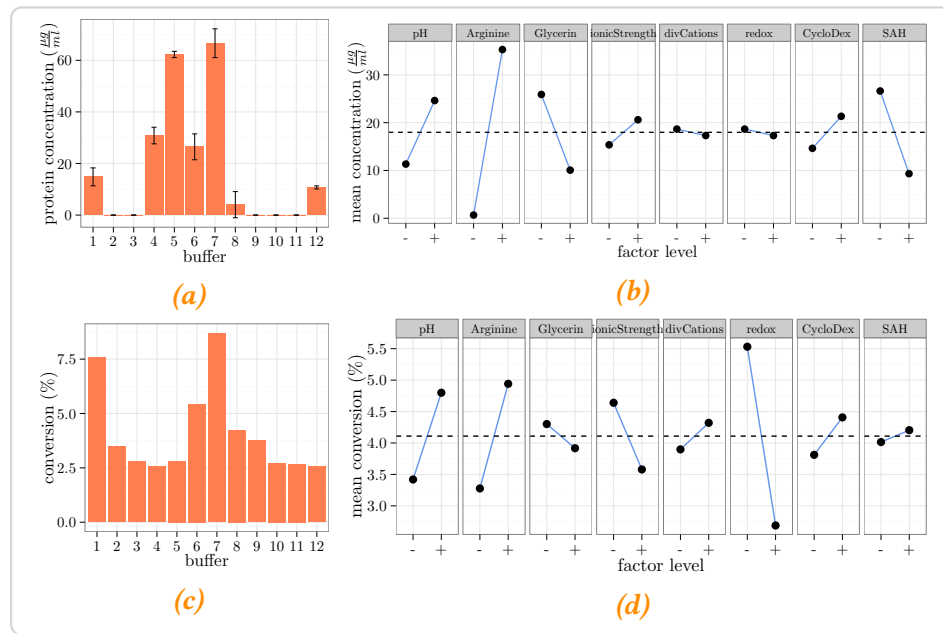


Figure 7.7: Results of *in vitro* protein refolding trials. Measured data (left) is presented alongside the main effects plots (ME-plots) (right). The dashed line through the ME-plots illustrates the overall mean. **a** – Protein concentration after refolding and rebuffering into a universal buffer. The highest yield of soluble protein was achieved in buffers 5 and 7. The ME-plots (**b**) illustrate the connection between a factor and the measured protein concentration, suggesting that high pH and arginine concentration might have been beneficial in the refolding reactions. **c** – Calculated conversion of naringenin to ponciretin by the refolded protein fractions. Protein refolded in buffers 1 and 7 seem to afforded the most active protein by conversion (~volume activity). The ME-plots for the conversion (**d**) show that the redox state (reducing) of the refolding environment was important to achieve active protein.

1 is the measured concentration from a refolding reaction in buffer i with
2 “low” pH and x_j^+ is the measured concentration from a refolding reaction
3 in buffer j with “high” pH, then the level means \bar{x}^- and \bar{x}^+ are calculated
4 as follows:

$$\bar{x}^- = \frac{1}{n} \cdot \sum_{i=1}^n x_i^-$$

$$\bar{x}^+ = \frac{1}{n} \cdot \sum_{j=1}^n x_j^+$$

5 In the presented experiment “low” pH buffers were buffers 2, 4, 6, 8, 10 and
6 12, whereas “high” pH buffers were buffers 1, 3, 5, 7, 9 and 11, thus the

1 level means were calculated as such:

$$\bar{x}^+ = \frac{x_1^+ + x_3^+ + x_5^+ + x_7^+ + x_9^+ + x_{11}^+}{6} = 24.63$$

$$\bar{x}^- = \frac{x_2^- + x_4^- + x_6^- + x_8^- + x_{10}^- + x_{12}^-}{6} = 11.34$$

2 The ME-plots for protein concentration suggest, that arginine was likely
 3 an important factor for the refolding of SOMT-2 (Figure 7.7b). Furthermore,
 4 the addition of SAH or glycerin and the pH seemed to have an influence,
 5 whereas the other factors seemed to play only minor roles to achieve high
 6 concentrations of soluble protein after refolding. However, the Analysis of
 7 Variance (ANOVA) test, which gave a *p*-value of 0.0158 for factor *arginine*,
 8 suggests that only arginine addition had a significant influence on refolding,
 9 when the significance level is set to 5 % (appendix, Table C.1). The other
 10 *p*-values are all higher than 0.05, which suggests the other factors had no
 11 influence on the yield of soluble protein. Only the *p*-value for factor *SAH*
 12 (0.0897) would suggest significance, if the significance level was raised to
 13 10 %.

However, soluble protein is not necessarily active. Therefore activity tests were conducted with the refolded protein samples to check for naringenin conversion (Figure 7.7c). The conversion of naringenin to ponciretin was calculated from the area under the curve (AUC) of the substrate and product peaks as follows:

$$conversion = \frac{AUC_{ponciretin}}{AUC_{naringenin} + AUC_{ponciretin}}$$

14 Although the substrate naringenin was already contaminated with about
 15 2.5 % ponciretin, this value was not subtracted from the measured con-
 16 versions to avoid introduction of unnecessary errors. The protein activity
 17 in the refolded samples was generally very low, as suggested by the low
 18 conversions after an overnight activity assay. The maximum conversion of
 19 about 8.7 % (6.2 %) was observed for the protein sample refolded in buffer 7.
 20 The activity of the protein samples did not correlate well with the amount
 21 of soluble protein (Figure 7.7). This becomes clear from the samples re-
 22 folded in buffers 4 and 5, where the amount of soluble protein was high
 23 but the observed activity was at a baseline level.

24 The ME-plot suggests that the main effects for obtaining high amounts
 25 of soluble protein and obtaining active protein after refolding are differ-

1 ent (Figure 7.7d). Most notably, the redox state of the refolding reaction
2 seemed to have a big influence on the protein sample's activity. The redox
3 state however had almost no influence on the yield of soluble protein (Fig-
4 ure 7.7b). Indeed, the ANOVA test suggests that using reducing refolding
5 conditions (DTT) over a redox-shuffling system (GSH:GSSG, oxidizing) has
6 a significant influence on methylation activity judged by the *p*-value 0.0218
7 of the factor *redox* (appendix, Table C.2). However, there is the possibil-
8 ity for SOMT-2 to form intramolecular disulfide bridges, as the modelled
9 structure suggests (Figure C.4). There are also reports, which showed that
10 intermolecular disulfide bridges can contribute to the stability of, mainly
11 archeal, MTs and have no influence on the enzymatic activity [68, 75, 90].
12 Nevertheless most MTs are only active under reducing conditions and
13 literature suggests, that sometimes assays of MTs are explicitly conducted
14 under reducing conditions [85, 236]. Reducing environments reduce the
15 chance of disulfide cross-linked protein mono- and oligomers and allow
16 the enzyme to be more flexible, which might be important for catalysis.
17 When using a significance level of 10 %, the *p*-value for *arginine* is 0.0824,
18 which also suggests a significant influence of this factor on the chance to
19 obtain active protein after refolding. This is plausible, since there cannot
20 be any activity when no soluble protein is present, and refolding reactions
21 without added arginine did not afford any soluble protein. Judging from the
22 ANOVA test, the remaining factors like *glycerin*, *ionic strength* or *divalent*
23 *cations* had no significant impact on the protein activity after refolding.

24 Due to the promising results obtained from the refolding trials, which
25 implicated that the best overall refolding performance (i.e. soluble pro-
26 tein and activity) was achieved in buffer 7 (50 mM borate/NaOH, 0.5 M
27 arginine, 2 mM CaCl₂, 2 mM MgCl₂, 10 mM NaCl, 0.5 mM KCl, 30 mM α -
28 cyclodextrin, 5 mM DTT pH 8.5), this buffer was used to scale up the
29 refolding reaction from a total volume of 1.05 ml to a volume of 50 ml.
30 After concentration of soluble protein from the scaled-up refolding reac-
31 tion, activity tests were conducted. Unfortunately, the refolded SOMT-2
32 showed no activity for naringenin methylation, which was evidence that
33 the scaled-up refolding was unsuccessful. Nonetheless, gel filtration chro-
34 matography and circular dichroism (CD) spectroscopy were used as a
35 tool to study the three-dimensional structure of the refolded SOMT-2. The
36 retention volume for the major peak eluted during the gel filtration run was
37 12.47 ml, but in the chromatogram a shoulder at 14.26 ml was clearly dis-

1 tinguishable (Figure C.5). Molecular masses of the proteins corresponding
 2 to the peaks were estimated from commercial gel filtration protein stan-
 3 dards. The first peak corresponds to a molecular weight of approximately
 4 165 kDa, whereas the shoulder at 14.26 ml corresponds to a globular protein
 5 of approximately 65.5 kDa. 65.5 kDa is roughly the weight of one SOMT-2
 6 monomer (40 kDa) or a dimer, whereas a mass of 165 kDa would indicate a
 7 tetramer. These results were further indication, that the majority of the
 8 refolded protein was not in the expected native dimeric state. However, the
 9 refolded SOMT-2 had adopted some kind of fold that allowed for it to be in
 soluble form. Furthermore, the CD spectrum (Figure 7.8) suggested, that

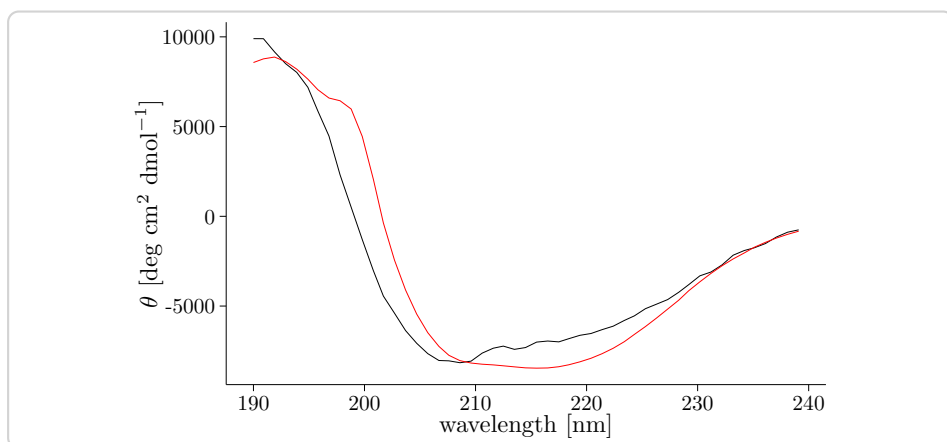


Figure 7.8: CD-spectrum of refolded SOMT-2 (black) compared to the spectrum that was calculated (red) by the K2D3 web service (<http://cbdm-01.zdv.uni-mainz.de/~andrade/k2d3//index.html>) from the SOMT-2 sequence. Secondary structure estimates from the measured spectrum are 12.39 % α -helix and 32.51 % β -sheet.

10
 11 the refolded SOMT-2 possessed a secondary structure and was not present
 12 as an unfolded random coil. The secondary structure was estimated from
 13 the measured CD-spectrum by the K2D3 web service [126]. According
 14 to the K2D3 calculations, the secondary structure elements consisted of
 15 12.39 % α -helix and 32.51 % β -sheet. However, the calculated protein model
 16 (Figure C.4) suggests the α -helix content might be much higher (52.3 %),
 17 whereas the β -sheet content might accordingly be lower (15.4 %). These
 18 findings further indicate, that the refolded protein was not in a native state,
 19 which might be the cause of the lack of enzymatic activity. Even over the
 20 course of many trials a successful large scale refolding of SOMT-2 yielding
 21 active protein could not be achieved.

1 These results display that DoE combined with FrFD can be a valuable tool
2 for the identification of main factors during protein refolding. However,
3 there still exists a discrepancy between small scale refolding reactions and
4 the process of upscaling, which might not be trivial.

5 **7.3 PFOMT**

6 PFOMT is a class I plant *O*-MT, that was throuroughly characterized in
7 previous studies [22, 48, 85, 109, 206]. It is easily obtained by heterologous
8 expression in *E. coli* after which it is fairly active and stable, which is
9 importantz for *in vitro* experiments. The activity of PFOMT in relation to
10 the pH of the buffer and magnesium addition was the main aim of this part
11 of the study.

12 **7.3.1 Phenolic hydroxyls**

13 Phenolic hydroxyl groups have pK_a -values of around 10 as demonstrated
14 by four *p*-cresole derivatives (Table 7.3). Catecholic systems have two pK_a -
15 values, one for each hydroxyl group. The 3-hydroxyl (R^2) of the displayed
16 example has a much smaller pK_a than the 4-hydroxyl (R^1). This is in part
17 due to the mesomeric (+M) and inductive (+I/-I) properties the substituents
18 exhibit. The M and I-effects let the 3-OH be deprotonated first, which in
19 turn significantly lowers the acidity and thus increases the pK_a of the 4-OH.
20 (4-hydroxy-3-methoxy)- and (3-hydroxy-4-methoxy)-derivatives have a
21 similar pK_a , with the *meta*-position slightly more acidic due to the +I-effect
22 of the methyl substituent. The nucleophilicity of these phenolic groups
23 happens to coincide with their BRØNSTED acidity. Chemically speaking the
24 hydroxyl group with the lower pK_a always reacts first with an electrophile.
25 However, different enzymes are able to regioselectivly methylate the
26 3- or the 4-OH of such catecholic systems. Enzyme's active sites cre-
27 ate a "microclimate", which can selectively raise or lower the effective
28 pK_a of functional groups and allows for the efficient manipulation of the
29 macroscopically observed regioselectivity.

30 Previous studies have established that PFOMT is a 3'-*O*-methyl trans-
31 ferase, which is not able to methylate substrates that bear either phenolic
32 (e.g. naringenin), (3'-hydroxy-4-methoxy)- (e.g. hesperetin) or (4'-hydroxy-
33 3-methoxy)-moieties (e.g. homoeriodictyol) [85]. In these previous studies,
34 the reactions were all run under the same "standard" conditions. However,

Table 7.3.: pK_a -values of phenolic hydroxyl groups exemplified by *p*-cresole derivatives. Substituent positions on the aromatic ring are arbitrary and do not reflect conventions of the International Union of Pure and Applied Chemistry (IUPAC).

	R ¹	R ²	$pK_a^{-R^1}$	$pK_a^{-R^2}$
	OH	H	10.36	–
	OH	OH	13.1	9.55
	OH	O-Me	10.34	–
	O-Me	OH	–	10.08

1 the reaction buffer can have a tremendous impact on enzymes and their
 2 reactions. Therefore reaction conditions require optimization, just as the
 3 enzymes themselves, to augment an enzymatic process [17, 105].

4 Using PFOMT reaction conditions were screened, to assess if any would
 5 promote the methylation of non-catecholic substrates. Although enzymes
 6 create a specific environment for catalysis, changes in the pH of the medium
 7 can still affect said environment and therefore enzymatic activity, especially
 8 if charged groups are part of the catalytic mechanism. In the catalytic
 9 mechanism of PFOMT a catalytic triad of Lys-Asn-Asp, two of which are
 10 charged, is proposed to play a major role [22]. Furthermore, PFOMT is a
 11 magnesium dependent enzyme and the activity is affected by altering the
 12 concentration of Mg²⁺ or substitution of Mg²⁺ by other divalent cations
 13 [85]. Thus, the pH was chosen to be varied along with Mg²⁺ concentration
 14 in order to study the influence of those two factors on the methylation
 15 reaction.

16 7.3.2 PFOMT pH-profiles are influenced by Mg²⁺

17 PFOMT was dialyzed against 50 mM succinate/sodium phosphate/glycine
 18 (SSG)-buffer pH 7.5 containing 5 mM ethylenediaminetetraacetic acid
 19 (EDTA) and again against the same buffer with the EDTA omitted, to ob-
 20 tain enzyme that was virtually free of bound divalent cations. pH-profiles
 21 (pH 5.5 – 9.5) of three different substrates (caffeic acid, iso-ferulic acid, erio-
 22 dictyol) were obtained in the same unified buffer system (succinate/sodium
 23 phosphate/glycine, 2:7:7 molar ratio). The pH-profiles were measured
 24 without and with the addition of 10 mM MgCl₂. Maximum methylation
 25 activity (\approx 1500 pkat/mg) towards the catecholic substrates (i.e. caffeic acid,
 26 eriodictyol) was observed when magnesium was added and the pH was

1 about 6.5 (Figure 7.9 and Table 7.4). However, the observed maximum
 2 activity shifted towards basic pH values (pH 9.45), when magnesium was
 3 omitted from the reaction. The maximum activity for methylation of
 4 iso-ferulic acid was measured at pH 9.45, regardless of whether magnesium
 was added. The catecholic substrates caffeic acid and eriodictyol were

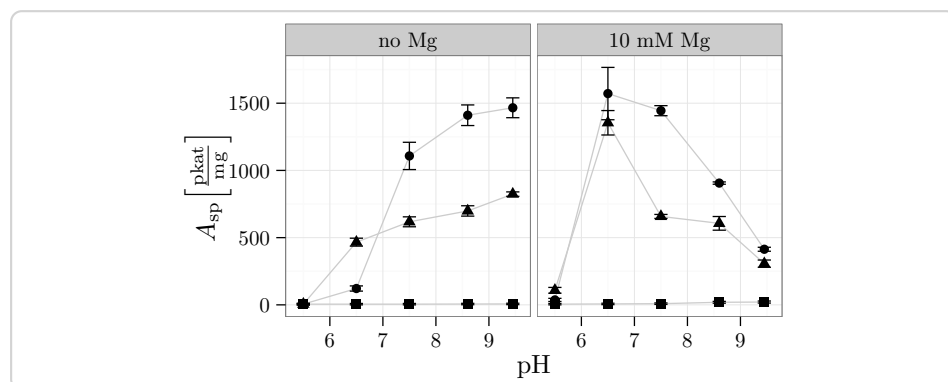


Figure 7.9: Specific activity/pH-profiles for the conversion of three different substrates (● *caffeic acid*, ▲ *eriodictyol*, ■ *iso-ferulic acid*) by PFOMT. The specific activity for the non-catecholic substrate *iso-ferulic acid* was much lower than the specific activity for the catecholic substrates. When magnesium is omitted, the activity is increased by increasing the pH

5 converted by PFOMT much more quickly than *iso-ferulic acid*, which is a
 6 (3-hydroxy-4-methoxy)-substituted cinnamic acid (Figure 7.9).

7 The highest specific activity A_{sp} for *iso-ferulic acid* conversion was two
 8 orders of magnitude lower than the highest activity for the conversion
 9 of the other two substrates. Nonetheless, conversion was observed for
 10 *iso-ferulic acid* with increasing pH and even an influence of magnesium
 11 was observed (Figure 7.9 and Table 7.4). *Iso-ferulic acid* was converted
 12 rather slowly without the addition of Mg^{2+} ($A_{sp} = 7 \text{ pkat/mg}$). However,
 13 addition of 10 mM Mg^{2+} increased the rate of *iso-ferulic acid* conversion
 14 by 3-fold, from 7 pkat/mg to 21 pkat/mg at pH 9.45 (Table 7.4).

15 The specific activities observed for the conversion of *caffeic acid* are
 16 comparable to published data [49]. For the two catecholic substrates, the
 17 pH-optimum shifted from neutral to alkaline pHs, when Mg^{2+} was omitted.
 18 However, the maximum activity remained roughly the same, even though
 19 magnesium addition seemed to have a slight rate increasing effect. Rate
 20 enhancements of up to 3-fold were observed at pH 9.45, when Mg^{2+} was
 21 omitted compared to when it was present. The maximum activities without
 22 magnesium were observed at pH 9.45 with 1466 pkat/mg and 824 pkat/mg
 23 for *caffeic acid* and *eriodictyol* respectively, while with 10 mM Mg^{2+} the

1 maximum activities were recorded at pH 6.5 and increased to 1572 pkat/mg
and 1354 pkat/mg respectively.

Table 7.4: Maximum specific activity for the conversion of three different substrates with and without addition of magnesium. The pH at which the maximal activity was reached is indicated by the column titled “pH”.

substrate	Mg ²⁺	pH	$A_{sp} \left[\frac{mU}{mg} \right]$	$A_{sp} \left[\frac{\text{pkat}}{mg} \right]$
caffeic acid	FALSE	9.45	88	1466
caffeic acid	TRUE	6.50	94	1572
eriodictyol	FALSE	9.45	49	824
eriodictyol	TRUE	6.50	81	1354
iso-ferulic acid	FALSE	9.45	0.4	7
iso-ferulic acid	TRUE	9.45	1.2	21

2

3 During the catalysis of a methyl transferase reaction, the acceptor moiety
4 of the substrate is activated by abstraction of a proton. At high pH-values,
5 the substrates might already be deprotonated, thus increasing the rates
6 of reaction, while the enzyme just acts as a scaffold. High pH-values
7 would also mean that the mainly the 4'-hydroxyl of the catechols would be
8 deprotonated (Table 7.3). However, an increasing amount of 4'-methylation
9 was not observed contradicting the notion, that an already deprotonated
10 substrate entered the active site. It is more likely, that the external milieu
11 influences the enzymes active site and makes the active side chains more
12 basic. However, why the addition of magnesium would shift the pH-
13 optimum back to neutral pH-values is not clear.

To statistically support the presented findings, the collected data were also studied from a statisticians point of view, which is described in the following paragraph in a bit more detail. The shown results are solely included for purposes of making statistics based inferences in the context of domain knowledge. Relationships between independent variables X_1, \dots, p influencing a system and the outcome Y of such a system can be mathematically described. The simplest relationship between one independent variable X_1 and the dependent variable Y is a linear one and is defined mathematically by a linear equation $Y = \beta_1 X_1 + \beta_0$. The coefficient β_1 describes how much Y is altered by one unit X , while β_0 is the offset. Even seemingly non-linear outcomes of Y might be sufficiently described by multi-term linear equations such as

$$Y = \beta_0 + \beta_1 X_1 + \beta_2 X_2 + \dots + \beta_p X_p + \epsilon,$$

1 when the independent variables X_1, \dots, p are known. Linear regression models
 2 of this form can be used to make statistically sound inferences about a
 3 studied system and were thus used to assess the relationship between
 4 PFOMT's methylation activity and pH-modulation as well as Mg^{2+} addition.
 5 Two subsets of the activity data were prepared first. The subsets split
 6 the data into substrates with catecholic (i.e. caffeic acid, eriodictyol) and
 7 substrates without catecholic (i.e. iso-ferulic acid) motifs. This was done
 8 to simplify the interpretability of the results, since the activities of the
 9 catecholic and non-catecholic substrates differed greatly. The iso-ferulic
 10 acid data was fit to the linear model

$$\text{activity} = \beta_0 + \beta_1 \times \text{Mg} + \beta_2 \times \text{pH} + \beta_3 \times (\text{Mg} \times \text{pH}), \quad (7.1)$$

11 which contains one term, $\beta_3 \times \text{pH} \times \text{Mg}$, to account for an interaction effect
 12 between magnesium and pH besides the main effects terms. This model
 13 explains about 93.6 % of the variance ($R^2 = 0.9355$) of the measured data
 14 (Table 7.5). Fitting the data in the R software using the `stats::lm()` function
 15 also calculates *p*-values associated with each parameter estimate. The

Table 7.5. Coefficients of the model (Equation 7.1) for activity of iso-ferulic acid methylation. The factor Mg is a categorical variable (addition/no addition) and can therefore only be 0 or 1.

	Estimate	Std. Error	t value	p-value
(Intercept)	-241.4238	420.1485	-0.57	0.5864
pH	38.4239	54.9778	0.70	0.5108
Mg	-2201.3084	594.1797	-3.70	0.0100 *
pH×Mg	373.8131	77.7503	4.81	0.0030 **

significance codes: '*' 5 % level; '***' 1 % level

15
 16 smallest *p*-value 0.0030 was calculated for the interaction factor pH×Mg,
 17 and strongly suggests that there is a significant interaction between methylation
 18 activity on iso-ferulic acid and Mg^{2+} addition combined with pH-
 19 modulation. The parameter estimate β_3 for this term is almost 374. Since
 20 in this case Mg is categorical and can only be 0 (no magnesium added)
 21 or 1 (magnesium added) the interaction term $\beta_3 \times \text{pH} \times \text{Mg}$ resolves to 0,
 22 if no magnesium was added. This means that when Mg^{2+} is added, the
 23 activity (in AU min⁻¹) is increased by 374 for each unit the pH is raised.
 24 The *p*-value for pH as a main effect is rather high, suggesting pH alone
 25 has no significant impact on the activity. The parameter estimate β_1 for

1 factor Mg however has a low *p*-value of 0.010, which suggest that its im-
 2 pact on activity is significant. Due to the categorical nature of Mg, this
 3 means, that the activity is decreased by 2201 AU min^{-1} when magnesium
 4 is added. However, this information is only of importance when predicting
 5 the activity outside of the measured pH range, which was not the aim here.
 6 Together, these results illustrate, that neither magnesium addition, nor the
 7 pH alone would have such a strong effect on the activity as both factors
 8 combined had.

9 The data of the second subset containing of the catecholic substrates
 10 was also modelled in a similar fashion (see Appendix C.2.1). It was found,
 11 that the pH has a much stronger influence on the methylation activity
 12 of PFOMT towards catechols than iso-ferulic acid. Interaction between
 13 magnesium addition and pH-modulation were also suggested for the cat-
 14 echolic substrates from this data. For a more thourough discussion see
 15 Appendix C.2.1. In addition to pure inference based modelling, models can
 16 also be used to make predictions based on (new) independent variables
 17 (Figure 7.10). However, it cannot be stressed enough that models do not
 reflect the truth, but are rather another tool to gain insight into a system.

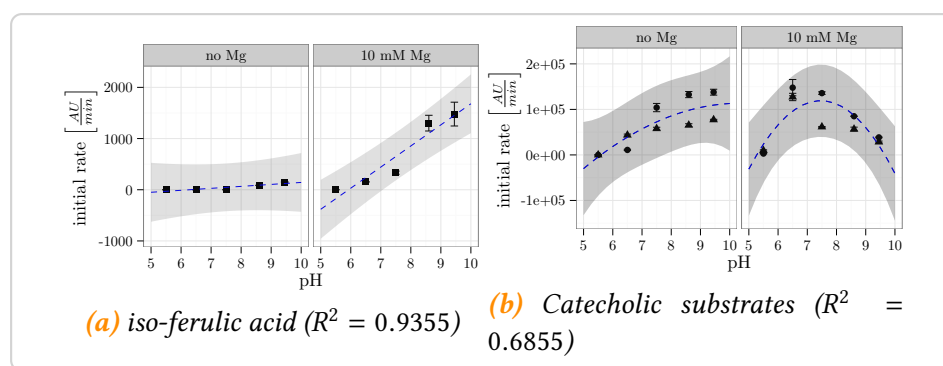


Figure 7.10: pH-profiles of substrate conversion along with predicted data. Predicted data from the linear regression models (blue, dashed lines) grasp the general trend of the data reasonably well to draw inferences. 95 % prediction intervals are displayed as shaded areas.

18
 19 To the knowledge of the author, this is the first time the effects of Mg^{2+}
 20 and pH on methyl transferase activity were systematically analyzed. It was
 21 shown, that catecholic and non-catecholic substrates could be activated
 22 sufficiently by PFOMT at high pHs without the addition of Mg^{2+} . It is
 23 improbable that, if the active site retained the same miromilieu under every
 24 reaction condition, an influence on the rate of reaction would be observed.
 25 This could be a hint, that the enzyme relays the chemical information of

1 the environment directly to the substrate to aid in activation. Furthermore,
2 omission of Mg²⁺ shifts the pH-optimum of the reaction catalyzed by
3 PFOMT to higher pH-values. It would be of interest to analyze this behavior
4 with further systematic studies and multiple levels of Mg²⁺ concentrations.

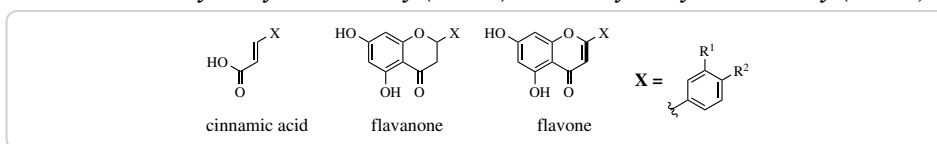
5 7.3.3 Methylation of different chemical motifs

6 The previous section showed the conversion of non-catecholic *iso*-ferulic
7 acid by PFOMT and prompted additional experiments with other different
8 non-catechols from multiple flavonoid subgroups (Table 7.6). The tested
9 substrates were selected from three different compound groups (cinnamic
10 acids, flavones, flavanones) and each group contained each of four structural
11 motifs – phenol, catechol, 3'-hydroxy-4'-methoxy (3O4M) and 4'-hydroxy-
12 3'-methoxy (4O3M). Each substrate was assessed for conversion with two
13 enzymes (PFOMT wild-type and 4'-specific variant Y51R N202W) at four
14 different conditions. Magnesium addition and pH were varied for the
15 different conditions (pH/Mg²⁺: low/no, low/yes, high/no, high/yes). The
16 “low” and “high” pH-values were 7.5 and 8.6, respectively. When Mg²⁺
17 was added the concentration was 10 mM. The reactions were incubated at
18 30 °C for 16 h (see section 4.6.3).

19 Conversion of all substrates, catecholic and non-catecholic, by the wild-
20 type could be demonstrated. The highest conversion of non-catecholic
21 substrates was shown for 3'-hydroxy-4'-methoxy substituted compounds,
22 especially cinnamic acids and flavanones where conversions of up to 25 %
23 were observed. Conversions of substances with free 4'-hydroxyl groups did
24 not extend beyond 7 % (chrysoeriol). This was to be expected, due to the
25 fact that PFOMT is a 3'-specific MT at physiological conditions. However,
26 unexpectedly the 4'-specific variant hardly showed any conversion of non-
27 catecholic substrates. High pH favoured the conversion of non-catechols.

28 There was almost complete conversion of the catecholic substrates (eri-
29 odictyol, luteolin and caffeic acid) after 16 h of incubation regardless the
30 reaction conditions, at least when the wild-type enzyme was used (Fig-
31 ure 7.11 and Table 7.8). This suggests, that the reaction period was chosen
32 too long for this group of substrates and effects of pH or magnesium ad-
33 dition on this group cannot be distinguished. Conversion was observed
34 for all tested substrates at least under high pH-conditions, when the wild-
35 type was employed (Figure 7.11). The 4'-variant however hardly showed

Table 7.6.: Substrate grid that was tested for methylation with PFOMT. Four different groups of compounds were screened. The groups of flavones, flavanones and cinnamic acids each contained one representative of each motif, phenolic, catecholic, 3'-hydroxy-4'-methoxy (3O4M) and 4'-hydroxy-3'-methoxy (4O3M).



substrate	group	motif	R ¹	R ²
A.1 <i>p</i> -coumaric acid	cinnamic acid	phenolic	H	OH
A.2 caffeic acid	cinnamic acid	catecholic	OH	OH
A.3 iso-ferulic acid	cinnamic acid	3O4M	OH	OMe
A.4 ferulic acid	cinnamic acid	4O3M	OMe	OH
B.1 naringenin	flavanon	phenolic	H	OH
B.2 eriodictyol	flavanon	catecholic	OH	OH
B.3 hesperetin	flavanon	3O4M	OH	OMe
B.4 homoeriodictyol	flavanon	4O3M	OMe	OH
C.1 apigenin	flavone	phenolic	H	OH
C.2 luteolin	flavone	catecholic	OH	OH
C.2 diosmetin	flavone	3O4M	OH	OMe
C.4 chrysoeriol	flavone	4O3M	OMe	OH

1 any conversion of non-catecholic substrates (Figure 7.11b). Generally, the
 2 highest conversions of non-catecholic substrates were observed at high
 3 pH and high Mg²⁺ conditions (Figure 7.11). For example, conversion of
 4 iso-ferulic acid was up to 25 % at pH 8.6 with 10 mM Mg²⁺ in the reac-
 5 tion. This is a 10-fold increase over the conversion of 2.5 %, which was
 6 observed at pH 7.5 with no magnesium added. These findings support
 7 the claims from the previous subsection 7.3.2, that PFOMT activity might
 8 be modulated enough by pH and magnesium to achieve methylation of
 9 non-catecholic phenyl propanoid substrates. Again, the trend in the data
 10 suggests, that methylation efficiency of non-catecholic moieties increases
 11 with pH, but especially in combination with the addition of magnesium .
 12 Overall, methylation of 3O4M motifs was highest apart from the catecholic
 13 substrates. Observed conversions of close to 25 % for the cinnamic acid
 14 and flavanone substrates (iso-ferulic acid and hesperetin) were observed.
 15 For these substrates the conversion increased by almost 5-fold upon Mg²⁺
 16 addition, which is close to the observed increase of the initial rate of iso-
 17 ferulic acid methylation (subsection 7.3.2). Similar results have been shown
 18 for SaOMT5, an O-MT from *Streptomyces avermitilis*, where the enzymatic

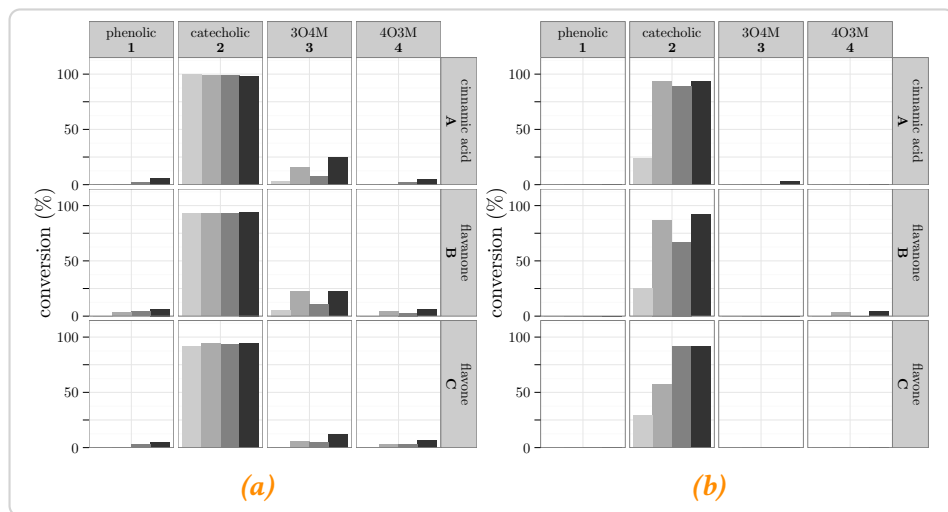


Figure 7.11: Conversion of multiple different substrates, catecholic and non-catecholic, by PFOMT wild-type (a) and the 4'-specific variant Y51R N202W (b). Every individual box represents one substrate *p*-coumaric acid (A.1), . . . , chrysophenol (C.4). pH/Mg²⁺-conditions are color coded from light to dark: —/X, —/✓, ↗/X, ↗/✓. — (low pH), ↗ (high pH), X (no Mg²⁺), ✓ (yes, Mg²⁺)

1 activity towards quercetin increased by about 5-fold from metal-free con-
 2 ditions to magnesium addition [228]. Conversion of the somewhat more
 3 rigid flavone diosmetin (max. conversion 12 %) was lower by at least factor
 4 two compared to hesperetin and *iso*-ferulic acid (Table 7.8, Figure 7.11).
 5 At low pH-values and without addition of Mg²⁺ barely any conversion of
 6 the non-catecholic substrates was observed. The fact, that conversion of
 7 3O4M-moiety bearing substrates is greater than that of the *para*-phenolic
 8 and 4O3M substrates could be due to the fact that the wild-type of PFOMT
 9 by and large methylates 3'-hydroxyls at physiological conditions.

10 The 4'-specific variant for the most part only showed conversion of the
 11 catecholic substrates. Only some conversion of homoeriodictyol (\approx 4 %)
 12 and *iso*-ferulic acid (\approx 3 %) was observed under high pH/Mg²⁺ conditions
 13 (Table 7.8, Figure 7.11). However, for the catecholic substrates the same
 14 trend – increasing pH/Mg²⁺ increases activity – as before holds true. Con-
 15 trol experiments without enzyme at high pH and 10 mM Mg²⁺ revealed,
 16 that no substrate conversion took place under these conditions, meaning
 17 the enzyme must be involved in the conversion.

18 Products and methylation sites were identified by comparison to au-
 19 thentic standards, or by LC-MS/MS (Table 7.9). As previous studies demon-
 20 strated, the products for the conversion of the catecholic substrates by the
 21 wild-type and variant were the 3'-methylated and 4'-methylated substrates

Table 7.8.: Conversion of substrates after 16 hours incubation. Only the maximum conversion is displayed, along with the conditions it was achieved under.

substrate	wild-type			4'-specific variant Y51R N202W		
	conversion %	pH	Mg ²⁺	conversion %	pH	Mg ²⁺
A.1 <i>p</i> -coumaric acid	6	↗	✓			
A.2 caffeic acid [†]	100 [‡]		(all)	93		(all)
A.3 iso-ferulic acid	25	↗	✓	3	↗	✓
A.4 ferulic acid	5	↗	✓			
B.1 naringenin	6	↗	✓			
B.2 eriodictyol [†]	94		(all)	92	↗	✓
B.2 hesperetin	22	↘	✓			
B.4 homoeriodictyol	6	↗	✓	4	↗	✓
C.1 apigenin	5	↗	✓			
C.2 luteolin [†]	95		(all)	92	↗	
C.3 diosmetin	12	↗	✓			
C.4 chrysoeriol	7	↗	✓			

[†]wild-type: substrate conversion was maximal for all pH/Mg²⁺ combinations.

[‡]conversion of caffeic acid by the wild-type was set to 100 %.

1 respectively [48, 85, 109, 206]. As expected, methylation took place on the
2 B-ring of the flavonoids. Ponciretin and acacetin were produced, when
3 naringenin and apigenin were converted by PFOMT respectively. However,
4 conversion of the 3O4M and 4O3M flavonoids (hesperetin/chrysoeriol and
5 homoeriodictyol/diosmetin respectively), afforded the 3',4'-dimethylated
6 compounds. This demonstrates, that even the PFOMT wild-type is able to
7 methylate the 4'-position of flavonoids, given the right conditions (pro-
8 longed incubation, high pH, no free 3'-hydroxyl). Furthermore, another
9 type of product, eluting earlier than the corresponding substrates, was ob-
10 served for the flavones apigenin, chrysoeriol and diosmetin after conversion
11 with the wild-type in the LC/MS runs. Unfortunately, these products could
12 not be identified. Nonetheless the production of these products seemed
13 favoured over the 3' or 4'-O-methylated ones, when a free 3'-hydroxyl was
14 absent (Appendix, Figure C.9).

15 Enzymatic methylation of the non-catecholic cinnamic acids also af-
16 forded two different types of product, methyl esters and methyl ethers.
17 Methylation of *p*-coumaric acid only gave rise to the corresponding *methyl*
18 *ester* (Appendix C.3). Two different products were observed for the en-

1 zymatic methylation of ferulic acid and *iso*-ferulic acid. One product was
 2 the methyl ester of the corresponding cinnamic acid, whereas the other
 3 product was the di-ether, 3,4-dimethyl caffeic acid.

Table 7.9.: Products of the enzymatic methylation of the studied substrates. The products were confirmed by authentic standards or via LCMS.

substrate	product	
	wild-type	4'variant
<i>p</i> -coumaric acid	<i>p</i> -hydroxy methylcinnamate [†] [87]	
caffeic acid	ferulic acid	ferulic acid
<i>iso</i> -ferulic acid	caffeic acid dimethyl ether, <i>iso</i> -ferulic acid methyl ester [†]	n/d
ferulic acid	caffeic acid dimethyl ether, ferulic acid methyl ester [†]	
naringenin	ponciretin	
eriodictyol	homoeriodictyol	hesperetin
hesperetin	3',4'-dimethyl eriodictyol [†]	
homoeriodictyol	3',4'-dimethyl eriodictyol [†]	3',4'-dimethyl eriodictyol [†]
apigenin	acacetin	
luteolin	chrysoeriol	n/d
diosmetin	3',4'-dimethyl luteolin [†]	
chrysoeriol	3',4'-dimethyl luteolin [†]	

[†]determined via LCMS; n/d – not determined

3
 4 To the authors knowledge, this is the first time that methylation of
 5 a diverse set of non-catecholic substrates was described for a class I
 6 magnesium-dependent methyl transferase. A flavonoid-specific *O*-MT
 7 from *Catharanthus roseus* was described to methylate the 4'-position,
 8 when the substrates B-ring possessed a 4O3M substitution [172]. However,
 9 said enzyme only showed marginal activities towards catechols and 3O4M
 10 derivatives. A class II *O*-MT from wheat, named TaOMT2, is able to
 11 sequentially methylate the three hydroxyl-groups on the B-ring of tricetin,
 12 in the proposed order 3'-methyl → 3',5'-dimethyl → 3',4',5'-trimethyl
 13 [233]. However, methylation of dihydroxy-derivatives such as luteolin and
 14 eriodictyol by TaOMT2 only afforded 3'-mono-methylated products, which
 15 is similar to PFOMT. Nonetheless, TaOMT2 can methylate tamarixetin, the
 16 4O3M derivative of quercetin, albeit at low activities.

17 Of the two PFOMT enzymes, 4'-specific variant and wild-type, only
 18 the wild-type showed significant methylation of non-catecholic moieties.

1 These findings support the previous results, that could show a pH and
2 magnesium-dependent rate of methylation of *iso*-ferulic acid (subsection 7.3.2). Although methylation of 3'-hydroxyl groups was preferred
3 by the wild-type, a tendency to methylate 4'-hydroxyls, when these were
4 the only ones present, could be demonstrated. Furthermore, methylation of
5 the acid functionalities of cinnamic acids was demonstrated using PFOMT.

6
7 The N-terminus of PFOMT is important for the function of the enzyme,
8 as was demonstrated in previous studies, however the role of it *in vivo* is
9 still not fully understood [85, 109, 207]. It cannot be ruled out that it acts as a
10 signal sequence that can direct the enzyme to different compartments. The
11 findings presented here might give some implications as to the regulation of
12 O-MTs, such as PFOMT, since the milieu can be quite different in different
13 cell compartments in plants [139].

14 7.4 Conclusion

15 Enzymatic methylation of non-catecholic moieties, was studied using
16 the two methyl transferases PFOMT and SOMT-2, of classes I and II re-
17 spectively. Therefore multiple different flavonoid and phenylproanoid
18 substrates, displaying either single phenolic, catecholic, 3'-hydroxy-4'-
19 methoxy or 4'-hydroxy-3'-methoxy moieties, were tested. Furthermore,
20 the influence of pH and magnesium addition on PFOMT was systematically
21 studied.

22 In *in vivo* biotransformation experiments it could be shown, that the
23 class II O-methyl transferase SOMT-2 is able to methylate flavonoids and
24 stilbenes at the 4'-OH of the B-ring, regardless the exact moiety (phenolic,
25 catecholic, 4'-hydroxy-3'-methoxy). Although overall the conversions were
26 very low, the conversion of the stilbene resveratrol was superior over all
27 other tested substrates ($\geq 86\%$ vs. $\geq 55\%$). SOMT-2 showed methylating ac-
28 tivity exclusively when a free 4'-OH was present, suggesting it only acts on
29 4'-hydroxyl groups. Unfortunately, these results are purely based on *in vivo*
30 biotransformations carried out in *E. coli*. SOMT-2 could not be obtained in
31 pure, soluble form for *in vitro* characterization. Nonetheless, using SOMT-2
32 it was shown that design of experiments (DoE) and fractional factorial
33 design (FrFD) can be valuable tools for the systematic determination of
34 factors that influence refolding of O-MTs.

1 *In vitro* experiments using the class I *O*-methyl transferase PFOMT,
2 showed that non-catecholic substrates could be methylated. These findings
3 are contrary to the belief, that PFOMT only acted on vicinal aromatic
4 dihydroxyls that are present in compounds such as eriodictyol or caffeic
5 acid. The best conversion of non-catechols was achieved for substrates
6 with 3'-hydroxy-4'-methoxy-moieties (e.g. hesperetin, *iso*-ferulic acid),
7 even though conversion was observed for phenolic (e.g. naringenin) and 4'-
8 hydroxy-3'-methoxy-substrates (e.g. homoeriodictyol), thus demonstrating
9 the ability of PFOMT to methylate both 3'- and 4'-hydroxyls. The best
10 conversions were obtained using the PFOMT wild-type at elevated pH and
11 after Mg²⁺ addition. Magnesium addition and pH displayed synergistic
12 effects, meaning the effects of both are not just additive. pH optimum of
13 PFOMT shifted from around pH 7 to more basic conditions (pH >8), when
14 Mg²⁺ was omitted. Although no magnesium was present under these high
15 pH conditions, it seemed as though the chemical environment surrounding
16 the enzyme was relayed into the active site. Thus, non-catecholic substrates
17 were methylated at high pH without magnesium, whereas they were hardly
18 methylated at low pH without the addition of magnesium. These findings
19 also show, that the linear stepwise optimization of reaction conditions might
20 not always yield the best overall results, when it comes to such complex
21 systems as enzymes and that synergistic effects need to be considered when
22 looking for the best working conditions.

8 Summary

2 Plant secondary metabolites comprise a vast collection of compounds with
3 a myriad of biological activities and functions, that include defense against
4 biotic and abiotic stresses, communication as well as gene regulation. These
5 biological activities are largely determined by the compounds substitution
6 patterns Phenyl propanoid derived phenolic compounds such as flavonoids
7 make up a major part of the secondary metabolites in plants and tailoring
8 enzymes such as methyl-, prenyl- and glycosyl-transferases are responsible
9 of putting a finish on their molecular structure. This work aimed to study
10 the ability of two plant *O*-methyl transferases (*O*-MTs), phenylpropanoid
11 and flavonoid *O*-methyl transferase (PFOMT) and soy *O*-methyl transferase
12 (SOMT-2), for the alkylation of common structural motifs in polyphenols.

13 In the first part PFOMT was characterized by biophysical methods,
14 which showed that the enzyme is able to bind the non-natural ethylated
15 *S*-adenosyl-L-methionine (SAM) analogue *S*-adenosyl-L-ethionine (SAE).
16 Conversion of SAE was however not observed. In addition a novel crystal
17 structure of the *apo*-form of PFOMT was solved that gave insights into the
18 movements associated with substrate binding.

19 The second part comprised of a tandem mass-spectrometry (MS/MS)-
20 study of 15 flavonoids of different classes (i.e. flavanones, flavones and
21 flavonoles). Two activation methods, collision induced dissociation (CID)
22 and higher-energy collisional dissociation (HCD), were shown to produce
23 complementary information that enables a fast and reliable structural
24 characterization of the studied substances.

25 Finally, a comprehensive study showed the methylation of several non-
26 catecholic flavonoids, stilbenes and cinnamic acids by the enzymes SOMT-2
27 and PFOMT *in vivo* and *in vitro*. For the first time methylation of phenolic,
28 3'-hydroxy-4'-methoxy and 4'-hydroxy-3'-methoxy, which was achieved
29 through the modulation of the reaction conditions (e.g. pH, magnesium
30 concentration), by PFOMT could be demonstrated.

1 Together, the results presented herein show that both class I and II plant
2 O-MTs can be used to methylate non-catecholic moieties of polyphenolic
3 compounds. Modulation of the reaction conditions is a worthwhile study
4 and might bring to light new activities, that were not to be expected. This is
5 of specific interest for biocatalytic reactions, where the naturally observed
6 reaction might not be the desired behavior of an enzyme. Furthermore
7 these results might spark new discussions about the regulation and function
8 of enzymes in different compartments (i.e. reaction milieus).

9 Acknowledgements

10 Affidavit

2 I hereby declare that this document has been written only by the un-
3 dersigned and without any assistance from third parties. Furthermore, I
4 confirm that no sources have been used in the preparation of this document
5 other than those indicated in the thesis itself.

6 Date: , Location: , Signature:

1



2

Appendix

¹A Engineering of PFOMT

Table A.1.: Crystallographic data, phasing and refinement statistics.

140519_PFOMT	
<i>data collection</i>	
resolution (Å)	1.95
total reflections	392 368
unique reflections	125 822
completeness (%)	99.12
$I/\sigma(I)$	9.9
space group	$P2_12_12_1$
cell dimensions (Å)	
<i>a</i>	86.16
<i>b</i>	128
<i>c</i>	129.3
<i>refinement</i>	
$R_{\text{work}}/R_{\text{free}}$	0.21369 / 0.24700
rmsd bond lengths (Å)	0.0199
rmsd bond angles (°)	2.0568
B-values (Å ²)	21.593
<i>Ramachandran plot (%)</i>	
favoured	96.82
allowed	2.38
outliers	0.8

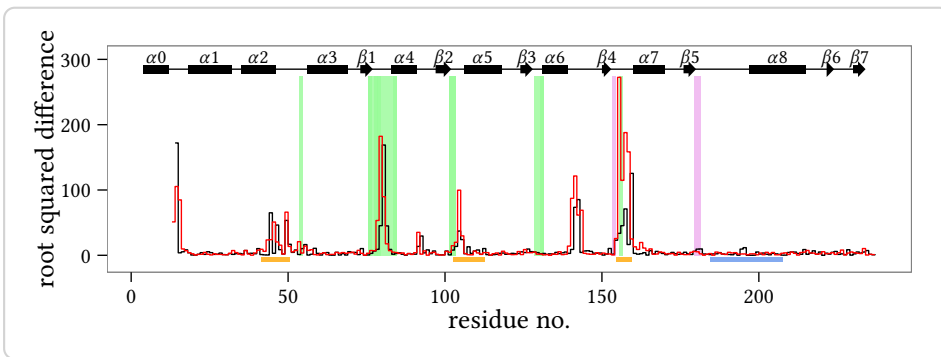


Figure A.1.: Differences in the dihedrals ψ (red) and φ (black) of the solved apo-PFOMT and the structure with bound S-adenosyl-L-homocysteine (SAH) (pdb: 3C3Y). The secondary structure is displayed at the top. Helices are displayed as rectangles and sheets are shown as arrows. Graphical background annotations are used to display the binding sites of SAH (green) and the metal ion (plum). The orange bars indicate regions, where much movement seems to happen upon binding or release of the co-substrate. The blue bar shows the region that was annotated as "insertion loop" in previous studies.

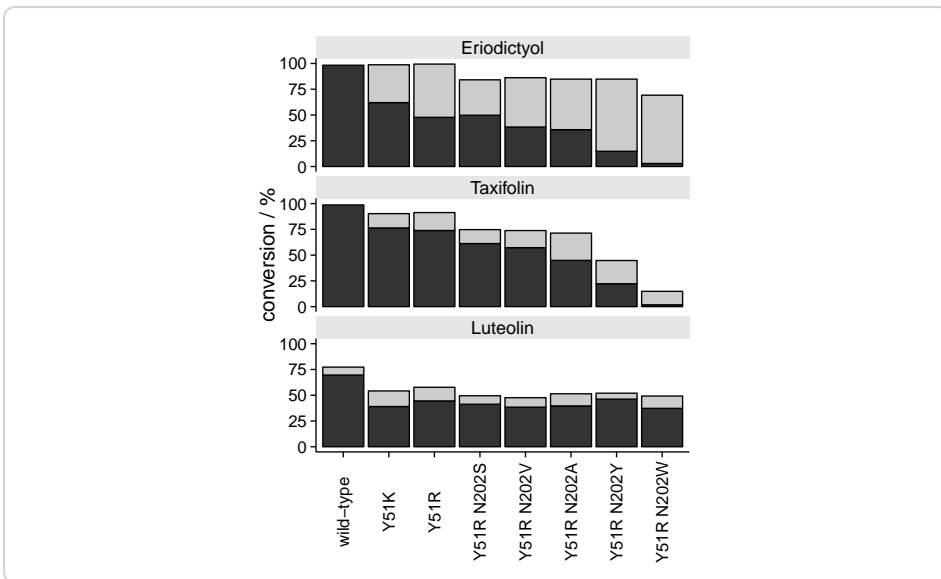


Figure A.2.: Differences in the regioselectivity of some phenylpropanoid and flavonoid O-methyl transferase (PFOMT) variants. The products observed in high-performance liquid chromatography (HPLC) and liquid chromatography coupled mass-spectrometry (LC/MS) measurements switched from 3'-methylated (dark grey) to 4'-methylated (light grey) for the displayed variants. The height of the bars corresponds to the total conversion of substrate.

¹ B Tandem mass-spectrometry
² studies of flavonoids

Table B.1: Key ions in the positive mode CID and HCD ESI-MS² spectra of flavanones.

fragment	CID, 45% NCE					HCD, 75% NCE					HCD, 100% NCE				
	(1)	(2)	(3)	(4)	(5)	(1)	(2)	(3)	(4)	(5)	(1)	(2)	(3)	(4)	(5)
2 [M+H-H ₂ O] ⁺	255(1)	271(18)	269(1)	285(10)	285(4)										
4 [M+H-C ₂ H ₂ O] ⁺	231(4)	247(3)	245(3)	261(2)	261(2)										
5 [M+H-2C ₂ H ₂ O] ⁺	189(5)	205(3)	203(4)	219(2)	219(1)										
8 AC ⁺	179(4)	179(20)	179(5)	179(28)	179(30)	179(1)	179(1)	179(2)	179(2)	179(2)	179(2)	179(2)	179(2)	179(1)	179(1)
11 1,3A ⁺	153(100)	153(31)	153(77)	153(21)	153(57)	153(100)	153(100)	153(100)	153(100)	153(100)	153(69)	153(50)	153(100)	153(63)	153(58)
12 1,3A ⁺ -CO						97(3)	111(2)	111(1)	111(1)	111(1)	111(2)	111(2)	111(1)	125(1)	125(1)
13 1,3A ⁺ -C ₂ H ₂ O						97(4)	97(3)	97(4)	97(4)	97(4)	97(10)	97(8)	97(15)	97(9)	97(9)
14 1,3A ⁺ -2CO						69(2)	69(2)	69(2)	69(2)	69(2)	69(9)	69(8)	69(13)	69(9)	69(8)
15 1,3A ⁺ -2CO-C ₂ H ₄						147(84)	163(100)	161(100)	177(100)	147(15)	163(10)	161(10)	177(4)	177(2)	147(3)
17 1,4B ⁺ -2H						119(32)	135(29)	133(36)	149(15)	149(11)	119(34)	135(16)	133(36)	149(5)	149(3)
18 1,4B ⁺ -2H-H ₂ O						91(24)	90(3)	118(11)	134(11)	134(7)	91(100)	90(49)	90(49)	117(13)	117(26)
19 1,4B ⁺ -2H-CO						91(24)	90(3)	117(15)	117(32)						
20 1,4B ⁺ -2H-CO-CH ₃						91(24)	90(3)	91(1)	91(2)	91(100)	117(21)				
22 1,4B ⁺ -2H-2CO						91(24)	90(3)	89(23)	89(29)	89(24)	91(100)	89(100)	89(100)	89(100)	89(100)
23 1,4B ⁺ -2H-2CO-CH ₃															
24 1,4B ⁺ -2H-C ₂ H ₂ O-H ₂ O															
25 1,4B ⁺ -2H-H ₂ O-CO															
26 C ₇ H ₇ ⁺															
27 C ₇ H ₅ ⁺															

Table B.2: Key ions in the positive mode CID and HCD ESI-MS² spectra of flavones.

fragment	CID, 45 % NCE					HCD, 75 % NCE					HCD, 100 % NCE			
	(6)	(7)	(8)	(9)	(10)	(6)	(7)	(8)	(9)	(10)	(6)	(7)	(9)	(10)
1 [M+H] ⁺	271 (2)					271 (84)	287 (66)	285 (4)			271 (2)	287 (2)		
2 [M+H-CH ₃] ^{•+}	253 (1)	269 (9)	270 (100)	286 (100)		253 (3)	269 (6)	270 (9)	286 (20)	286 (18)				
3 [M+H-H ₂ O] ⁺	243 (7)	259 (9)				243 (7)					243 (2)			
4 [M+H-CO] ⁺	242 (14)	258 (47)				242 (1)	258 (3)				242 (2)	258 (2)		
5 [M+H-CHO] ^{•+}	229 (21)	245 (13)	243 (1)			229 (4)								
6 [M+H-C ₂ H ₂ O] ⁺			242 (7)											
7 [M+H-CH ₃ -CO] ^{•+}														
8 [M+H-CH ₄ -CO] ⁺														
9 [M+H-H ₂ O-CO] ⁺														
14 [M+H-CH ₄ -2CO] ⁺														
15 [M+H-H ₂ O-2CO] ⁺														
16 [M+H-2C ₂ H ₂ O] ⁺														
17 [M+H-CH ₃ OH-2CO] ^{•+}														
18 [M+H-CH ₄ -2CO-C ₂ H ₂] ⁺														
20 [M+H-CH ₄ -3CO] ⁺														
23 [M+H-CH ₄ -4CO] ⁺														
24 [M+H-2CO-2C ₂ H ₂ O] ⁺														
27 0.4B ⁺														
28 0.4B ⁺ -H ₂ O	163 (6)	179 (7)				131 (2)	147 (1)				143 (1)	187 (2)	185 (1)	203 (31)
25 0.4B ⁺ -C ₂ H ₂ O	145 (13)	161 (12)				163 (8)	179 (3)				131 (5)	147 (3)	173 (3)	201 (6)
29 1,3A ⁺	121 (6)	137 (7)				145 (17)	161 (16)				163 (2)			173 (2)
30 1,3A ⁺ -CO	153 (100)	153 (100)	153 (5)			121 (16)	137 (12)				145 (41)	161 (29)		
31 1,3A ⁺ -C ₂ H ₂ O						153 (100)	153 (100)	153 (11)	153 (8)		121 (25)	137 (16)		
32 1,3A ⁺ -2CO						125 (1)	125 (2)				153 (84)	153 (87)	153 (100)	153 (100)
33 1,3A ⁺ -2CO-C ₂ H ₄						111 (2)	111 (2)				125 (3)	125 (2)		
34 1,3B ⁺						97 (2)					111 (4)	111 (3)		
35 1,4A ⁺ +2H						69 (4)	69 (5)				97 (9)	97 (1)		
39 C ₇ H ₇ ⁺	119 (12)	135 (11)	133 (2)			119 (49)	135 (40)	133 (3)			69 (24)	69 (22)	69 (1)	97 (2)
40 C ₇ H ₅ ⁺	91 (1)					91 (26)	127 (1)				69 (35)			69 (2)
						89 (17)					91 (100)	127 (2)		
											89 (7)	89 (100)	89 (3)	89 (1)

Table B.3: Key ions in the positive mode CID and HCD ESI-MS² spectra of flavonoids.

fragment	CID, 45 % NCE					HCD, 75 % NCE					HCD, 100 % NCE				
	(11)	(12)	(13)	(14)	(15)	(11)	(12)	(13)	(14)	(15)	(11)	(12)	(13)	(14)	(15)
1 [M+H] ⁺						287(25)	303(8)	319(1)	301(9)	286(12)	302(6)				
2 [M+H-CH ₃] ^{•+}						286(62)	302(100)			285(5)	301(3)				285(1)
3 [M+H-CH ₄] ⁺						285(2)	283(2)	299(3)	269(2)	285(6)	301(1)				
4 [M+H-H ₂ O] ⁺						299(3)		259(3)				269(2)	285(3)		
5 [M+H-CO] ⁺						291(6)	273(3)								
6 [M+H-CHO] ^{•+}						272(20)	288(3)	258(10)	274(4)		272(2)				269(3) 285(3)
7 [M+H-CH ₃ OH] ^{•+}						269(11)	285(36)			269(11)	285(11)				
8 [M+H-C ₂ H ₂ O] ⁺															
9 [M+H-CH ₃ OH-CO] ^{•+}															
10 [M+H-CH ₃ -CO] ^{•+}															
12 [M+H-CH ₄ -CO] ⁺															
13 [M+H-H ₂ O-CO] ⁺															
14 [M+H-2CO] ⁺															
15 [M+H-CH ₃ OH-CO] ^{•+}															
17 [M+H-CH ₃ -2CO] ^{•+}															
19 [M+H-CH ₄ -2CO] ⁺															
20 [M+H-H ₂ O-2CO] ⁺															
21 [M+H-3CO] ⁺															257(2)
22 [M+H-2C ₂ H ₂ O] ⁺															
23 [M+H-H ₂ O-CO-C ₂ H ₂ O] ^{•+}															
23 [M+H-CH ₃ OH-2CO] ^{•+}															
24 [M+H-CH ₄ -2CO-2C ₂ H ₂] ⁺															
25 [M+H-H ₂ O-2CO-C ₂ H ₂] ⁺															
26 [M+H-CH ₄ -3CO] ⁺															
27 [M+H-CH ₄ -2CO-C ₂ H ₂ O] ⁺															
28 [M+H-CH ₄ -4CO] ⁺															
29 [M+H-2CO-2C ₂ H ₂ O] ⁺															
31 0,2A ⁺															
32 0,2A ⁺ -CO															
33 0,2B ⁺															
35 0,3A ⁺ +2H															
37 1,3A ⁺															
38 1,3A ⁺ -CO															
39 1,3A ⁺ -C ₂ H ₂ O															
40 1,3A ⁺ -2CO															
41 1,3A ⁺ -2CO-C ₂ H ₄															
42 1,3B ⁺ -2H															
49 C ₇ H ₇ ⁺															
50 C ₇ H ₅ ⁺															

¹ C Enzymatic methylation of non- ² catechols

³ C.1 SOMT expression studies

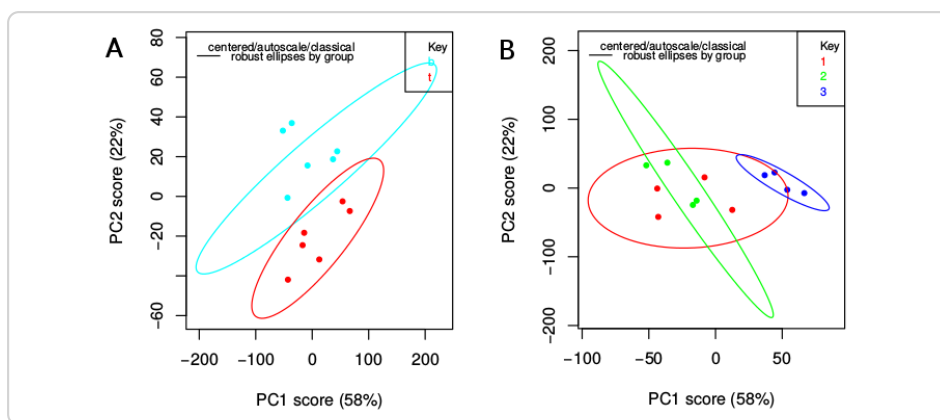


Figure C.1: Additional scatterplots of the principal component analysis (PCA) of high-performance liquid chromatography (HPLC) data obtained from *N. benthamiana* leaves infiltrated by *A. tumefaciens* harbouring different constructs. **A** – samples colored by leaf position (top: red; bottom: cyan), **B** – samples colored by plant (plant 1: red; plant 2: green; plant 3: blue)

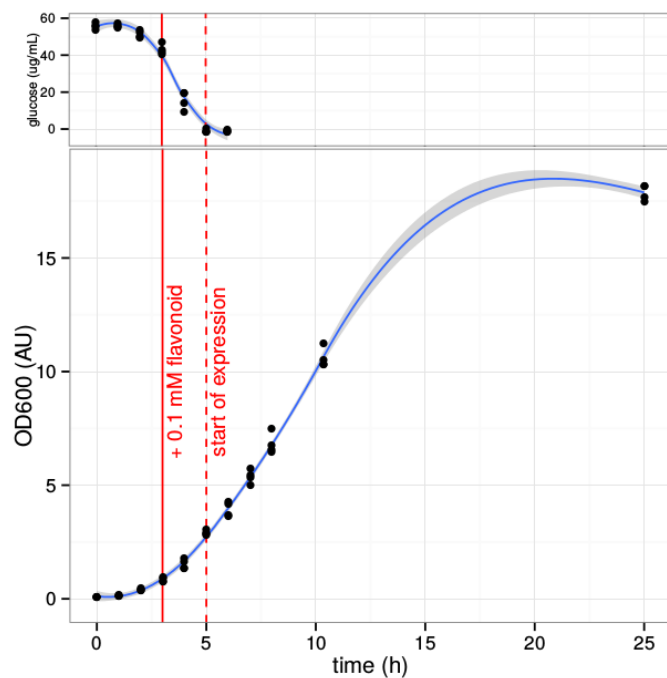


Figure C.2.: Growth curve of *E. coli* BL21(DE3) expressing soy O-methyl transferase (SOMT-2) at 37 °C. Glucose is depleted about 5 hours into growth, at which point the start of SOMT-2 expression is expected. The OD₆₀₀ after inoculation was about 0.1.

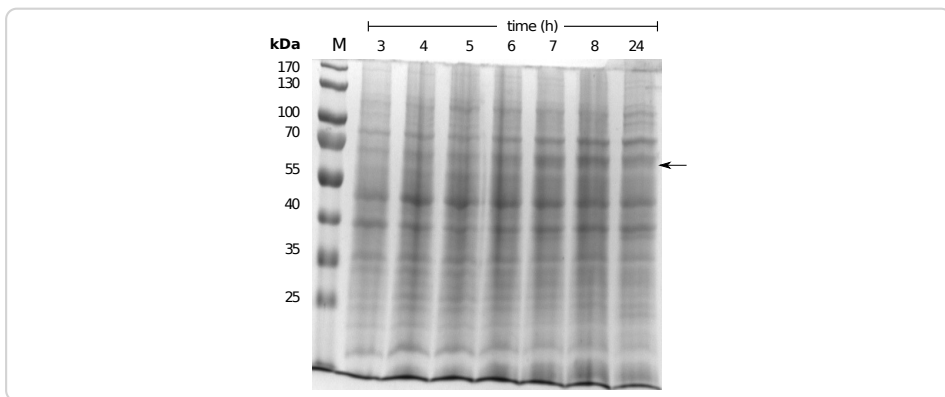


Figure C.3.: sodium dodecylsulfate (SDS)-polyacrylamide gel electrophoresis (PAGE) gel of samples acquired during growth curve measurements. The arrow indicates the band that could correspond to the GST-tagged SOMT-2 protein.

Table C.1.: Results for the Analysis of Variance (ANOVA) of the main effects model describing soluble protein obtained after refolding.

	df	Sum Sq	Mean Sq	F value	Pr(>F)	
Arginine	1	3595.63	3595.63	24.56	0.0158	*
pH	1	529.87	529.87	3.62	0.1533	
Glycerin	1	752.08	752.08	5.14	0.1083	
ionicStrength	1	82.37	82.37	0.56	0.5077	
divCations	1	5.49	5.49	0.04	0.8588	
redox	1	5.52	5.52	0.04	0.8584	
CycloDex	1	134.67	134.67	0.92	0.4083	
SAH	1	896.83	896.83	6.13	0.0897	•
Residuals	3	439.26	146.42			

significance codes: '•' 10 % level; '** 5 % level

Table C.2.: Results for the ANOVA of the main effects model describing protein activity after refolding.

	df	Sum Sq	Mean Sq	F value	Pr(>F)	
Arginine	1	8.31	8.31	6.62	0.0824	•
pH	1	5.71	5.71	4.55	0.1227	
Glycerin	1	0.44	0.44	0.35	0.5945	
ionicStrength	1	3.38	3.38	2.69	0.1997	
divCations	1	0.54	0.54	0.43	0.5605	
redox	1	24.26	24.26	19.31	0.0218	*
CycloDex	1	1.07	1.07	0.85	0.4250	
SAH	1	0.11	0.11	0.09	0.7893	
Residuals	3	3.77	1.26			

significance codes: '•' 10 % level; '** 5 % level

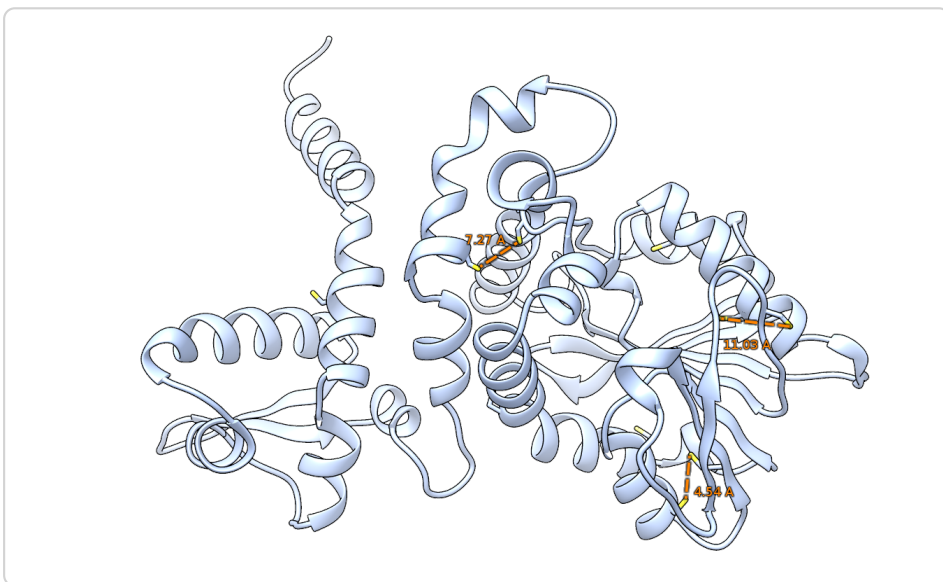


Figure C.4.: Graphical representation of a soy O-methyl transferase (SOMT-2) model obtained from the PHYRE2 web portal (<http://www.sbg.bio.ic.ac.uk/phyre2/html/page.cgi?id=index>) [98]. Cysteines are shown as sticks. The distance between neighboring cysteines that could by oxidized to disulfide bridges is shown in orange.

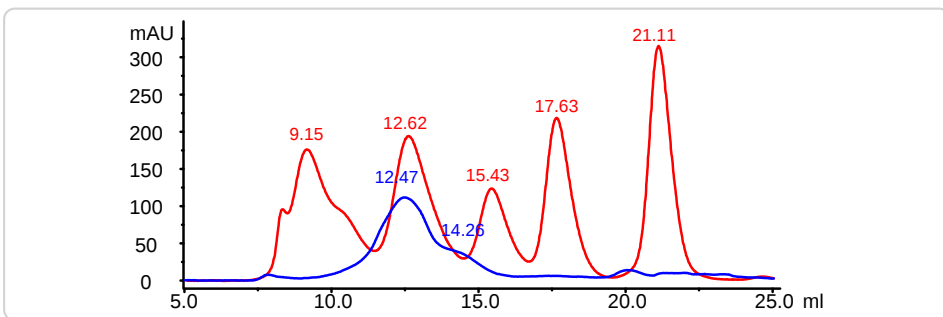


Figure C.5.: Chromatogram of the gel filtration analysis of refolded SOMT-2 (blue). Gel-filtrations standards (red) were used to assess the size of the SOMT-2 protein. The estimated molecular weights for the eluting peaks were 165 kDa (12.47 ml) and 65.5 kDa (14.26 ml). Protein standard: 9.15 ml – thyroglobulin (670 kDa), 12.62 ml – γ -globulin (158 kDa), 15.43 ml – ovalbumin (44 kDa), 17.63 ml – myoglobin (17 kDa), 21.11 ml – vitamin B12 (1.35 kDa)

¹ C.2 Conversion of non-catechols by PFOMT

² C.2.1 Modelling and shrinkage of catechols subset (pH ³ profile)

⁴ The bell-shaped pH profile for the catecholic substrates showed, that there
⁵ might be a quadratic relationship between pH and activity. A bell-shaped
⁶ pH profile is common for most enzymatic reactions, where ionizable groups
⁷ are involved in the reaction [35]. A quadratic term was thus included into the
⁸ linear model to capture this relationship:

$$\text{activity} = \beta_0 + \beta_1 \times \text{Mg} + \beta_2 \times \text{pH} + \beta_3 \times (\text{Mg} \times \text{pH}) + \beta_4 \times \text{pH}^2 + \beta_5 \times (\text{pH}^2 \times \text{Mg}). \quad (\text{C.1})$$

The model describes the actual data reasonable well, with about 68.6 % of

Table C.3.: Coefficients of the model (C.1) for activity of catechol methylation by PFOMT. The factor Mg is a categorical variable (addition/no addition) and can therefore only be 0 or 1.

	Estimate	Std. Error	t value	p-value
(Intercept)	-421929.9946	356063.7085	-1.18	0.2557
Mg	-839999.8874	503550.1257	-1.67	0.1175
pH	103271.3345	97739.1728	1.06	0.3086
pH ²	-4977.7406	6512.6996	-0.76	0.4574
Mg × pH	266920.7964	138224.0638	1.93	0.0740 •
Mg × pH ²	-19830.2264	9210.3481	-2.15	0.0492 *

significance codes: • 10 % level; ** 5 % level

the variance explained ($R^2 = 0.6855$) (Figure 7.10). Also here the p-values for the coefficients β_3 (0.074) and β_4 (0.0492) suggest an interaction between Mg^{2+} and pH (Table C.3), at significant levels of 10 and 5 % respectively. The coefficient estimate of 266920 for β_3 illustrates, that for the catecholic substrates the effect of the pH is much larger than for the methylation of iso-ferulic acid. In addition to the simplified linear model (Equation C.1) a more complex linear model,

$$\text{activity} = \beta_0 + \beta_1 \times \text{Mg} + \beta_2 \times \text{pH} + \beta_3 \times \text{pH}^2 + \beta_4 \times (\text{Mg} \times \text{pH}) + \beta_5 \times (\text{pH}^2 \times \text{Mg}) + \beta_6 \times (\text{pH} \times \text{pH}^2) + \beta_7 \times (\text{Mg} \times \text{pH} \times \text{pH}^2), \quad (\text{C.2})$$

⁹ was prepared and shrunken via the LASSO method and 5-fold cross validation (Table C.4) [195]. The LASSO is a shrinkage method that can shrink

1 coefficients to exactly zero and thus make a complex model less complex
 2 and therefore more interpretable [195]. The shrunken model only contained
 3 the factors **pH**, **pH×Mg**, **pH×pH²** and **pH×Mg×pH²**. The large coefficient
 4 estimate for parameter β_2 (**pH**) suggests, that in fact the pH has a large in-
 5 fluence on the activity. This is contrary to the linear model (Equation C.1),
 6 which, judged by the *p*-value for this coefficient, suggested otherwise.
 7 However, the shrunken model also shows that the activity is dependent on
 8 the interaction of pH and magnesium, which supports the implications of
 9 the linear model (Equation C.1). The results of the the shrunken model and
 10 the results obtained by linear modelling are further statistical evidence that
 11 pH and Mg²⁺ show main effects and also interaction effects which seem
 12 to be associated with the enzyme's activity towards catecholic substrates
 13 (i.e eriodictyol, caffeic acid). Nonetheless, all of these rather simple models
 14 can not reflect the reality of such complex systems as enzymes where lots
 of factors play important roles.

Table C.4.: Coefficients obtained for linear regression model using the catechols subset after shrinkage using the Lasso method and 5-fold cross validation. Only non-zero coefficients (variables actually do have an effect) are retained during the Lasso. Seed was set to 1336.

variable	coefficient
(Intercept)	-467632.3821
pH	94469.8366
pH×Mg	19068.9540
pH×pH²	-381.5863
pH×Mg×pH²	-292.3608

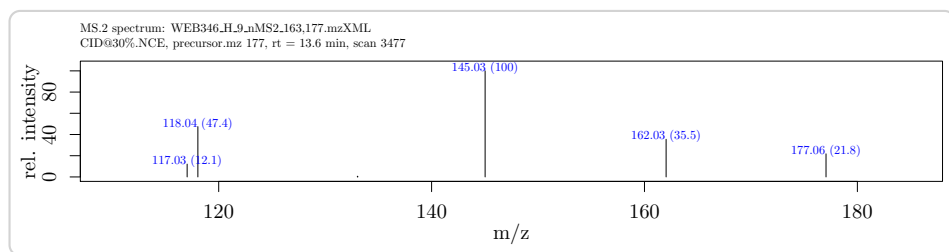
15

16 **C.3 Identification of products from conver- 17 sion of non-catechols by PFOMT**

18 **C.3.1 *p*-Coumaric acid methylester**

19 The product obtained by conversion of *p*-coumaric acid by phenylpropanoid
 20 and flavonoid O-methyl transferase (PFOMT) was determined as 4-hydroxy
 21 cinnamic acid methyl ester. The negative mode MS² spectrum showed four
 22 prominent peaks *m/z* 177 (21) [M-H]⁻, 162(35), 145(100) and 118(47). If
 23 the enzymatic product was the methyl ether, one would expect a strong
 24 *m/z* 133, corresponding to [M-H-CO₂]⁻ [186]. However *m/z* 133 was not

1 observed, strongly suggesting the methyl ester. Comparison of the obtained
2 data with literature data confirmed the methyl ester as sole product [87].



3 C.3.2 *iso*-Ferulic acid esters and caffeic acid dimethylether

4 Methylation of *iso*-ferulic acid and ferulic acid afforded two methylated
5 products with retention times of 12.9 and 13.7 min. The compound eluting
6 at 12.9 min was identified as caffeic acid dimethylether (**1**) through compar-
7 ison to an authentic standard, whereas the compounds eluting about one
8 minute later were identified as the ferulic (**2**) and *iso*-ferulic acid methyl
9 esters (**3**). Since the the retention time is an indicator for the polarity of
10 an eluting compound and the methyl ester is much more unpolar than
11 the dimethyl ether, it comes as no surprise that the latter elutes earlier
12 on a reversed-phase column. Ionization of the enzymatic products was
13 difficult in negative mode, but easily achieved in positive mode. The only
14 peaks in the positive mode MS² spectra of (**1**) and (**2,3**) were *m/z* 191 and
15 *m/z* 177 respectively. This indicates a loss of water and methanol from the
16 dimethylether and methyl ester respectively.

17 C.3.3 3',4'-dimethyl eriodictyol

18 Conversion of homoeriodictyol or hesperetin by PFOMT afforded
19 3',4'-dimethyl eriodictyol (**4**). The product was identified by liquid
20 chromatography-tandem mass spectrometry (LC-MS/MS). Products from
21 both conversions possessed the same retention times of 14.54 min. The
22 collision induced dissociation (CID) spectra of these products showed
23 five distinct signals at *m/z* 299 (14), 191(100), 179(62), 165(17) and 153(67)
24 (Figure C.7). The *m/z* 299 corresponds to the ion $[M+H-H_2O]^+$, showing
25 that both, homoeriodictyol as well as hesperetin were methylated. The
26 *m/z* 153 corresponds to the $^{1,3}A^+$ fragment, which is characteristic for
27 3,7-dihydroxy substituted flavonoids. This indicates a methylation of the

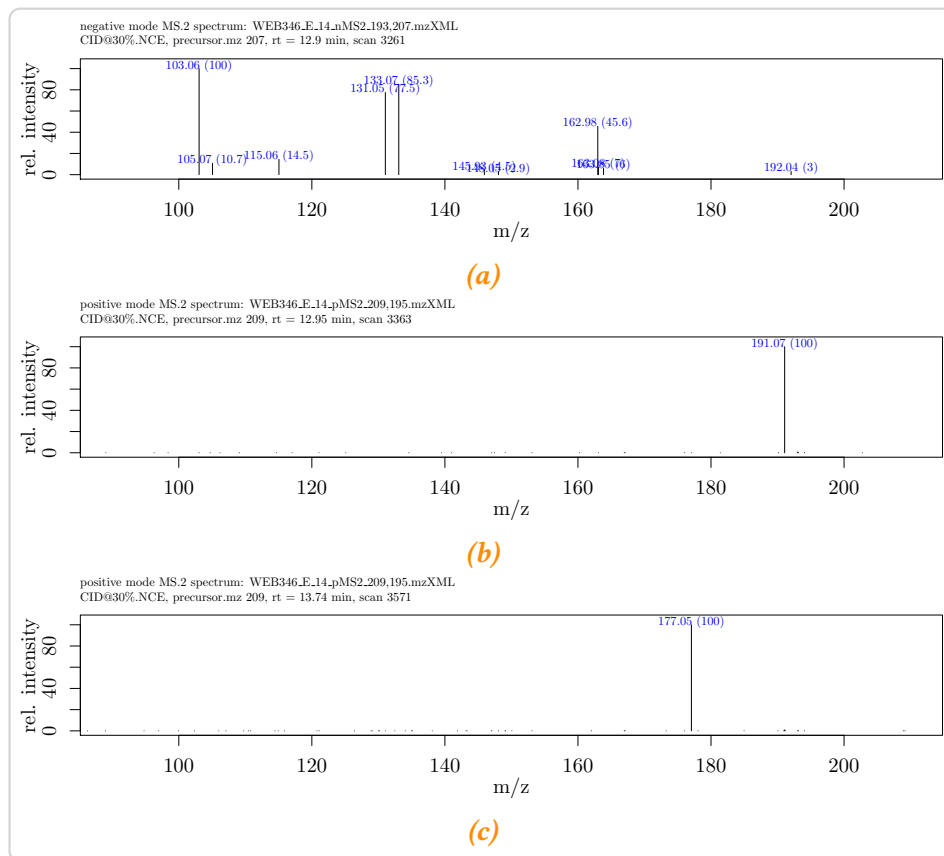


Figure C.6.: MS^2 spectra of (1) and (3). (a) negative mode MS^2 of (1). (b) positive mode MS^2 of (1). (c) positive mode MS^2 of (3).

1 B-ring. Further evidence of a dimethoxylated B-ring is the fragment $^{1,4}\text{B}^+$ -
 2 H with m/z 191. The fragmentation pattern of 3',4'-dimethyl eriodictyol
 3 agrees with the general fragmentation of flavanones described in chapter 6.

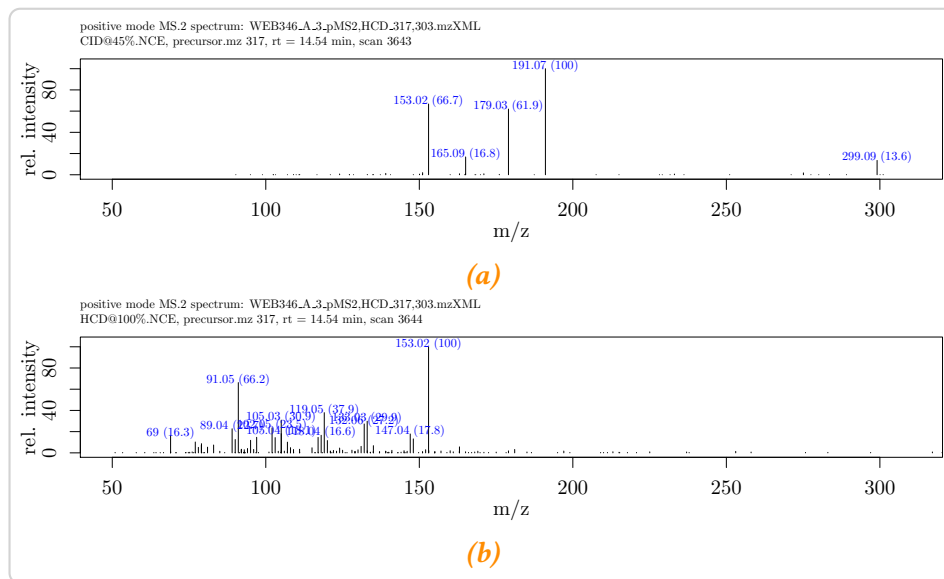


Figure C.7: MS^2 spectra of 3',4'-dimethyl eriodictyol (**4**). **(a)** positive mode MS^2 CID spectrum of (**4**). **(b)** positive mode MS^2 HCD spectrum of (**4**).

4 C.3.4 3',4'-dimethyl luteolin

5 Conversion of diosmetin and chrysoeriol by PFOMT afforded 3',4'-dimethyl
 6 luteolin (**5**) and an unidentified product. (**5**) eluted after 14.53 min. The
 7 CID spectrum of (**5**) shows three signals, m/z 300 (100), 299(87) and 271(17)
 8 (Figure C.8). These signals correspond to the $[\text{M}+\text{H}-\text{CH}_3]^+$, $[\text{M}+\text{H}-\text{CH}_4]^+$
 9 and $[\text{M}+\text{H}-\text{CH}_4-\text{CO}]^+$ ions respectively. The higher-energy collisional dis-
 10 sociation (HCD) spectrum of (**5**) clearly shows a peak with m/z 153 amongst
 11 other masses. Again, this is spectrometric evidence of a 3,7-dihydroxylated
 12 flavonoid (fragment $^{1,3}\text{A}^+$) demonstrating a 3',4'-dimethylation. The
 13 unidentified products of the conversions of apigenin, diosmetin and
 14 chrysoeriol eluted after 12.59, 12.77 and 12.69 min respectively.

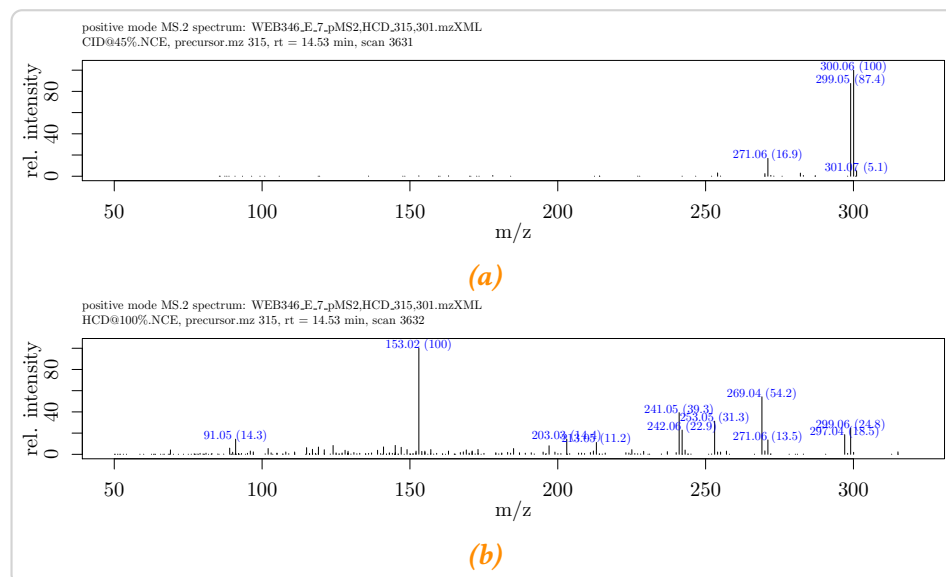


Figure C.8.: MS^2 spectra of 3',4'-dimethyl luteolin (**5**). (a) positive mode MS^2 CID spectrum of (**5**). (b) positive mode MS^2 HCD spectrum of (**5**).

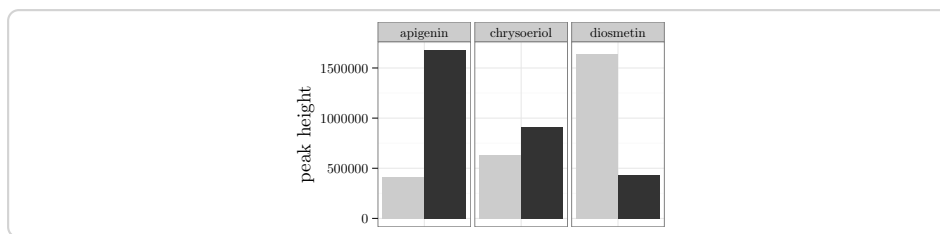


Figure C.9.: Product composition after conversion of flavones with PFOMT. Bar chart of the peak heights of the unidentified (black) and (3' or 4')-O-methylated products (gray) in the selected ion chromatograms (HCD at 100 % NCE). The conversion experiments were conducted with the wild-type PFOMT at pH 8.6 with 10 mM Mg²⁺ added.

¹D Additional information

Table D.2.: SAM analogues that have been used with MTs. Targets: P – peptide/protein, D – DNA, R – RNA, S – small molecule.

analogue	enzyme	target	references
<i>SAM</i>			
-CH ₂ -CH ₃	PRMT1, M.TaqI, M.HhaI, M.BcnIB, RebM, RapM	S,P,D	[44, 114, 184, 194] ¹
-CH ₂ -CH ₂ -CH ₃	PRMT1, M.TaqI, M.HhaI, M.BcnIB	P,D	[44, 194]
-CH ₂ -CH ₂ -CH ₂ -CH ₃	PRMT1	P	[194]
-CH ₂ -C ₆ H ₅	NovO, CouO, PRMT1	S,P	[187, 194]
-CH ₂ -C(=O)-CH ₃	COMT, TPMT, CazF	S	[116, 217]

¹Singh *et al.* (2014) published a series of 44 biocatalytically synthesized SAM and *Se*-adenosyl selenomethionine (SeAM) derivatives, most of which were not tested towards their alkyl donation potential in MT reactions.

analogue	enzyme	target	references
$-\text{CH}_2-\text{CH}=\text{CH}_2$	NovO, CouO, RapM, PRMT1, M.TaqI, M.HhaI, M.BcnIB, RebM, Tgs	P,S,D	[44, 114, 175, 184, 187, 192, 194, 208, 209]
$-\text{CH}_2-\text{CH}=\text{CH}-\text{CH}_3$	NovO, CouO	S	[187]
$-\text{CH}_2-\text{C}\equiv\text{CH}$	Dim-5, <i>HsMLL</i> , TRM1, NovO, CouO, PRMT1	P,R,S	[86, 187, 208, 209, 215]
$-\text{CH}_2-\text{C}\equiv\text{N}$	RebM	S	[184]
$-\text{CH}_2-\text{CH}_2-\text{C}\equiv\text{CH}$	PKMT	P	[86]
$-\text{CH}_2-\text{CH}_2-\text{CH}_2-\text{C}\equiv\text{CH}$	PKMT	P	[86]
$-\text{CH}_2-\text{C}\equiv\text{C}-\text{CH}_3$	NovO, CouO, M.HhaI, M.TaqI, M.BcnIB	S,D	[44, 129, 187]
$-\text{CH}_2-\text{C}\equiv\text{C}-\text{CH}_2-\text{CH}_3$	M.HhaI	D	[129]
$-\text{CH}_2-\text{C}\equiv\text{C}-\text{CH}_2-\text{NH}_2$	M.HhaI	D	[129]
$-\text{CH}_2-\text{C}\equiv\text{C}-\text{CH}_2-\text{NH}-\text{C}(=\text{O})(-\text{CH}_2-)_3-\text{NH}_2$	M.HhaI	D	[129]
$-\text{CH}_2-\text{C}\equiv\text{C}(-\text{CH}_2-)_3-\text{NH}_2$	M.HhaI	D	[129]
$-\text{CH}_2-\text{C}\equiv\text{C}(-\text{CH}_2-)_3-\text{NH}-\text{C}(=\text{O})(-\text{CH}_2-)_3-\text{NH}_2$	M.HhaI	D	[129]
$-\text{CH}_2-\text{C}\equiv\text{C}(-\text{CH}_2-)_3-\text{C}\equiv\text{CH}$	M.HhaI	D	[129]
$-\text{CH}_2-\text{C}\equiv\text{C}(-\text{CH}_2-)_3-\text{N}_3$	M.HhaI	D	[129]
$-\text{CH}_2-\text{CH}=\text{CH}-\text{C}\equiv\text{CH}$	Dim-5, <i>HsMLL</i> , TRM1, PRMT1, Tgs	P,R	[86, 150, 158, 175, 208, 209, 215]
$-\text{CH}_2-\text{CH}=\text{CH}-\text{CH}_2-\text{C}\equiv\text{CH}$			[86, 208]
$-\text{CH}_2-\text{CH}=\text{CH}-\text{CH}_2-\text{O}-\text{CH}_2-\text{C}\equiv\text{CH}$	PRMT1	P	[208, 209]

Appendix D. Additional information

analogue	enzyme	target	references
<i>SeAM</i>			
-CH ₃			
-CH ₂ -C≡CH	Dim-5, <i>HsMLL</i> ,	P,R,S TRM1, RebM, CazF	[19, 184, 215, 217]
<i>N</i> -mustard derivatives			
-CH ₂ -CH ₂ -I	RebM	S	[229]

Table D.1: Overview over the constructs produced for the present thesis. Each step during the production of the construct is given in the workflow steps column. Primers (*italic font*) or restriction sites used during each step are displayed in parenthesis.

construct name	description	entry structures	con-	destination	workflow steps (primers/cloning sites)
pBEW103	pBEW102 with BamHI cloning site	pBEW102			
pBEW104	rhaP _{BAD} promoter	pBEW4b			amplification (<i>pRha1.fw/rv</i>), cloning (BglII, BamHI)
pBEW106	pICH413038-somt	pET28MC-somt			amplification (<i>somt1/2/3/4</i>), golden gate cloning (BpuI)
pBEW107		pICH5126e, pBEW106, pICH41421			golden gate cloning (BsaI)
pET28-pfomt	<i>pfomt</i> gene in pET-28a(+), endogenous NdeI site removed N-terminal pfB-tag fusion for periplasmic expression	pQE30-pfomt	pET-28a(+)		mutagenesis (<i>pfomt1.fw/rv</i>), amplification (<i>pfomt2.fw/rv</i>), cloning (NdeI, EcoRI)
pET20-somt			pET20-b(+)		
pET28-somt	N-terminal TrX-tag fusion		pET28-a(+)		
pET32-somt	N-terminal GST-tag fusion		pET-32a(+)		
pET41-somt	added BglII site		pET-41a(+)		
pUC19*	pUC19 derivative with <i>lsrA</i> promoter	pUC19	-		mutagenesis (<i>pLIC1.fw/rv</i>)
pUCB1		lsr-XX-DAS	pUC19*		cloning (NdeI, BglIII)

¹Bibliography

- 2 [1] Paul D. Adams et al. “PHENIX: A comprehensive Python-based
3 system for macromolecular structure solution”. en. In: *Acta Crystallographica Section D: Biological Crystallography* 66.2 (Feb. 2010),
4 pp. 213–221.
- 6 [2] Giovanni Agati et al. “Flavonoids as antioxidants in plants: location
7 and functional significance.” In: *Plant science : an international
8 journal of experimental plant biology* 196 (Nov. 2012), pp. 67–76.
- 9 [3] Agilent Technologies. *QuikChange II Site-Directed Mutagenesis Kit:
10 Instruction Manual*. 2011.
- 11 [4] Neda Akbari et al. “Efficient refolding of recombinant lipase from
12 Escherichia coli inclusion bodies by response surface methodology”.
13 In: *Protein Expression and Purification* 70.2 (Apr. 2010), pp. 254–259.
- 14 [5] Martin Alexander and B. K. Lustigman. “Effect of Chemical Struc-
15 ture on Microbial Degradation of Substituted Benzenes”. In: *Journal
16 of Agricultural and Food Chemistry* 14.4 (July 1966), pp. 410–413.
- 17 [6] Bernd Anselment et al. “Experimental optimization of protein re-
18 folding with a genetic algorithm”. In: *Protein Science* 19.11 (2010),
19 pp. 2085–2095.
- 20 [7] F Ausubel et al. “Current Protocols in Molecular Biology”. In: (2008),
21 p. 23.
- 22 [8] Peter Ball et al. “Kinetic Properties of a Soluble Catechol 0-
23 Methyltransferase of Human Liver”. In: *Eur J Biochem* 26 (1972),
24 pp. 560–569.
- 25 [9] R V Banerjee and R G Matthews. “Cobalamin-dependent methio-
26 nine synthase.” In: *The FASEB journal : official publication of the
27 Federation of American Societies for Experimental Biology* 4.5 (1990),
28 pp. 1450–1459.
- 29 [10] G.M. Barton. “New C-methylflavanones from Douglas-fir”. In: *Phy-
30 tochemistry* 11.1 (Jan. 1972), pp. 426–429.
- 31 [11] Isabelle Benoit et al. “Expression in Escherichia coli, refolding and
32 crystallization of Aspergillus niger feruloyl esterase A using a se-
33 rial factorial approach”. In: *Protein Expression and Purification* 55.1
34 (Sept. 2007), pp. 166–174.

Bibliography

- 1 [12] Sanjoy K. Bhattacharya and Ashok K. Dubey. “Kinetic mechanism
2 of cytosine DNA methyltransferase MspI”. In: *Journal of Biological
3 Chemistry* 274.21 (1999), pp. 14743–14749.
- 4 [13] Amie K Boal et al. “Structural basis for methyl transfer by a radical
5 SAM enzyme.” In: *Science (New York, N.Y.)* 332.6033 (2011), pp. 1089–
6 1092.
- 7 [14] S. Bocker and F. Rasche. “Towards de novo identification of metabo-
8 lites by analyzing tandem mass spectra”. In: *Bioinformatics* 24.16
9 (2008), pp. i49–i55.
- 10 [15] Gyu Kim Bong et al. “Synthesis of ermanin, 5,7-dihydroxy-3,4'-
11 dimethoxyflavone from kaempferol, 3,5,7,4'-tetrahydroxyflavone
12 with two O-methyltransferases expressed in *E. coli*”. In: *Bulletin of
13 the Korean Chemical Society* 27.3 (2006), pp. 357–358.
- 14 [16] Ronald T. Borchardt. “Mechanism of alkaline hydrolysis of S-
15 adenosyl-L-methionine and related sulfonium nucleosides”. In:
16 *Journal of the American Chemical Society* 101.2 (1979), pp. 458–463.
- 17 [17] U. T. Bornscheuer et al. “Engineering the third wave of biocatalysis”.
18 In: *Nature* 485.7397 (May 2012), pp. 185–194.
- 19 [18] Ian R. Bothwell and Minkui Luo. “Large-scale, protection-free syn-
20 thesis of Se-adenosyl-l-selenomethionine analogues and their ap-
21 plication as cofactor surrogates of methyltransferases”. In: *Organic
22 Letters* 16.11 (2014), pp. 3056–3059.
- 23 [19] Ian R. Bothwell et al. “Se-adenosyl-L-selenomethionine cofactor
24 analogue as a reporter of protein methylation”. In: *Journal of the
25 American Chemical Society* 134.36 (2012), pp. 14905–14912.
- 26 [20] George E. P. Box, J. Stuart Hunter, and William G. Hunter. *Statistics
27 for Experimenters: Design, Innovation, and Discovery*. 2nd ed. New
28 York: Wiley-Interscience, 2005.
- 29 [21] M M Bradford. “A rapid and sensitive method for the quantita-
30 tion of microgram quantities of protein utilizing the principle of
31 protein-dye binding.” In: *Analytical biochemistry* 72.1-2 (May 1976),
32 pp. 248–254.
- 33 [22] Wolfgang Brandt, Kerstin Manke, and Thomas Vogt. “A catalytic
34 triad – Lys-Asn-Asp – Is essential for the catalysis of the methyl
35 transfer in plant cation-dependent O-methyltransferases”. In: *Phy-
36 tochemistry* 113 (May 2015), pp. 130–139.
- 37 [23] W Brandt et al. “Molecular and structural basis of metabolic di-
38 versity mediated by prenyldiphosphate converting enzymes”. In:
39 *Phytochemistry* 70.15-16 (Oct. 2009), pp. 1758–1775.
- 40 [24] Joan B Broderick et al. “Radical S - Adenosylmethionine Enzymes”.
41 In: (2014).

- 1 [25] W. Butte. "Rapid method for the determination of fatty acid pro-
2 files from fats and oils using trimethylsulphonium hydroxide for
3 transesterification". In: *Journal of Chromatography A* 261 (1983),
4 pp. 142–145.
- 5 [26] G. L. Cantoni. "S-Adenosylmethionine; Anew intermediate formed
6 enzymatically from L-methionine and adenosinetriphosphate". In:
7 *The Journal of Biological Chemistry* 204 (1953), pp. 403–416.
- 8 [27] Guohua Cao, Emin Sofic, and Ronald L. Prior. "Antioxidant and
9 Prooxidant Behavior of Flavonoids: Structure-Activity Relation-
10 ships". In: *Free Radical Biology and Medicine* 22.5 (Jan. 1997),
11 pp. 749–760.
- 12 [28] Hung Ju Chen, Baskaran Stephen Inbaraj, and Bing Huei Chen.
13 "Determination of phenolic acids and flavonoids in Taraxacum
14 formosanum kitam by liquid chromatography-tandem mass spec-
15 trometry coupled with a post-column derivatization technique". In:
16 *International Journal of Molecular Sciences* 13.1 (2012), pp. 260–285.
- 17 [29] Jing Chen et al. "Different Effects of L -Arginine on Protein Re-
18 folding : Suppressing Aggregates of Hydrophobic Interaction, Not
19 Covalent Binding". In: (2008), pp. 1365–1372.
- 20 [30] Vincent B. Chen et al. "MolProbity: All-atom structure validation
21 for macromolecular crystallography". In: *Acta Crystallographica*
22 *Section D: Biological Crystallography* 66.1 (Jan. 2010), pp. 12–21.
- 23 [31] a Claiborne and Irwin Fridovich. "of of of". In: *Society* 18 (1979),
24 pp. 2324–2329.
- 25 [32] Heather Coiner et al. "Methylation of sulphhydryl groups: a new
26 function for a family of small molecule plant O-methyltransferases." In:
27 *The Plant journal : for cell and molecular biology* 46.2 (Apr. 2006),
28 pp. 193–205.
- 29 [33] Austria Computing, R Foundation for Statistical Vienna. *R: A lan-*
30 *guage and environment for statistical computing*. Vienna, Austria,
31 2008.
- 32 [34] Robert a. Copeland. "Molecular pathways: Protein methyltrans-
33 ferases in cancer". In: *Clinical Cancer Research* 19.23 (2013),
34 pp. 6344–6350.
- 35 [35] Athel Cornish-Bowden. *Fundamentals of Enzyme Kinetics*. 3rd ed.
36 London: Portland Press Ltd, 2004.
- 37 [36] Marjorie Murphy Cowan. "Plant Products as Antimicrobial Agents".
38 In: *Clin. Microbiol. Rev.* 12.4 (1999), pp. 564–582.
- 39 [37] J K Coward, E P Slixz, and F Y Wu. "Kinetic studies on catechol O-
40 methyltransferase. Product inhibition and the nature of the catechol
41 binding site." In: *Biochemistry* 12.12 (1973), pp. 2291–2297.

- 1 [38] Ivana Crnović, Roderich Süssmuth, and Ullrich Keller. “Aromatic
2 C-Methyltransferases with Antipodal Stereoselectivity for Struc-
3 turally Diverse Phenolic Amino Acids Catalyze the Methylation
4 Step in the Biosynthesis of the Actinomycin Chromophore”. In:
5 *Biochemistry* 49.45 (Nov. 2010), pp. 9698–9705.
- 6 [39] Rodney Croteau, Toni M Kutchan, and Norman G Lewis. “Secondary
7 Metabolites”. In: *Biochemistry Molecular Biology of Plants*. Ed. by B.
8 Buchanan, W. Grussem, and R. Jones. Vol. 7. 7. 2000, pp. 1250–1318.
- 9 [40] T.P. Tim Cushnie and Andrew J. Lamb. “Antimicrobial activity of
10 flavonoids”. In: *International Journal of Antimicrobial Agents* 26.5
11 (Nov. 2005), pp. 343–356.
- 12 [41] Filip Cuyckens and Magda Claeys. “Mass spectrometry in the struc-
13 tural analysis of flavonoids”. In: *Journal of Mass Spectrometry* 39.1
14 (2004), pp. 1–15.
- 15 [42] Ermias Dagne et al. “O-Geranylated and O-prenylated flavonoids
16 from Millettia ferruginea”. In: *Phytochemistry* 29.8 (1990), pp. 2671–
17 2673.
- 18 [43] Yuntao Dai et al. “Natural deep eutectic solvents as new potential
19 media for green technology”. In: *Analytica Chimica Acta* 766 (Mar.
20 2013), pp. 61–68.
- 21 [44] Christian Dalhoff et al. “Direct transfer of extended groups from
22 synthetic cofactors by DNA methyltransferases.” In: *Nature chemi-*
23 *cal biology* 2.1 (2006), pp. 31–32.
- 24 [45] Christian Dalhoff et al. “Synthesis of S-adenosyl-L-methionine
25 analogs and their use for sequence-specific transalkylation of DNA
26 by methyltransferases.” In: *Nature protocols* 1.4 (2006), pp. 1879–
27 1886.
- 28 [46] Daresbury Laboratory. “No Title”. In: *Newsletter on protein crystal-*
29 *lography* 33 (1997), pp. 25–30.
- 30 [47] Bettina E. Deavours et al. “Functional analysis of members of the
31 isoflavone and isoflavanone O-methyltransferase enzyme families
32 from the model legume *Medicago truncatula*”. In: *Plant Molecular*
33 *Biology* 62.4-5 (2006), pp. 715–733.
- 34 [48] Martin Dippe et al. “Engineering of a Mg²⁺-dependent O-
35 methyltransferase towards novel regiospecificity”. In: *manuscript*
36 *submitted* (2015).
- 37 [49] M. Dippe et al. “Rationally engineered variants of S-adenosylmethionine
38 (SAM) synthase: reduced product inhibition and synthesis of ar-
39 tificial cofactor homologues”. en. In: *Chem. Commun.* 51.17 (Feb.
40 2015), pp. 3637–3640.

- 1 [50] M M Dixon et al. “The structure of the C-terminal domain of me-
2 thionine synthase: presenting S-adenosylmethionine for reductive
3 methylation of B12.” In: *Structure (London, England : 1993)* 4.11
4 (1996), pp. 1263–1275.
- 5 [51] J D Dunitz. “The entropic cost of bound water in crystals and
6 biomolecules.” In: *Science (New York, N.Y.)* 264.5159 (Apr. 1994),
7 p. 670.
- 8 [52] J D Dunitz. “Win some, lose some: enthalpy-entropy compensation
9 in weak intermolecular interactions.” In: *Chemistry & biology* 2.11
10 (Nov. 1995), pp. 709–712.
- 11 [53] Elsevier. *Reaxys, version 2.19790.2*.
- 12 [54] P. Emsley et al. “Features and development of Coot”. In: *Acta*
13 *Crystallographica Section D: Biological Crystallography* 66.4 (2010),
14 pp. 486–501.
- 15 [55] Carola Engler, Romy Kandzia, and Sylvestre Marillonnet. “A one
16 pot, one step, precision cloning method with high throughput ca-
17 pability”. In: *PLoS ONE* 3.11 (Jan. 2008), e3647.
- 18 [56] Madeleine Ernst et al. “Mass spectrometry in plant metabolomics
19 strategies: from analytical platforms to data acquisition and pro-
20 cessing.” en. In: *Natural product reports* 31.6 (June 2014), pp. 784–
21 806.
- 22 [57] Philip Evans. “Scaling and assessment of data quality”. In: *Acta*
23 *Crystallographica Section D: Biological Crystallography* 62.1 (Jan.
24 2006), pp. 72–82. arXiv: S0907444905036693 [doi:10.1107].
- 25 [58] Nicolas Fabre et al. “Determination of flavone, flavonol, and fla-
26 vanone aglycones by negative ion liquid chromatography elec-
27 trospray ion trap mass spectrometry”. In: *Journal of the American*
28 *Society for Mass Spectrometry* 12.6 (2001), pp. 707–715.
- 29 [59] J L Ferrer et al. “Structure of chalcone synthase and the molecular
30 basis of plant polyketide biosynthesis.” In: *Nature structural biology*
31 6.8 (1999), pp. 775–784.
- 32 [60] Alan Fersht. *Structure and mechanism in protein science*. Ed. by
33 Michelle R. Julet and Georgia L. Hadler. New York: W.H. Freeman
34 and Company, 1999.
- 35 [61] H G Floss and M D Tsai. “Chiral methyl groups.” In: *Advances in*
36 *enzymology and related areas of molecular biology* 50 (Jan. 1979),
37 pp. 243–302.
- 38 [62] Heinz G. Floss and Sungsook Lee. “Chiral Methyl Groups: Small is
39 Beautiful”. In: *Acc. Chem. Res.* 26.3 (1993), pp. 116–122.

- 1 [63] Matthew W. Freyer and Edwin a. Lewis. “Isothermal Titration
2 Calorimetry: Experimental Design, Data Analysis, and Probing
3 Macromolecule/Ligand Binding and Kinetic Interactions”. In: *Methods in Cell Biology* 84.07 (Jan. 2008), pp. 79–113.
- 5 [64] Mendel Friedman et al. “Antimicrobial activities of tea catechins
6 and theaflavins and tea extracts against *Bacillus cereus*.” In: *Journal*
7 of food protection 69.2 (2006), pp. 354–361.
- 8 [65] Akiko Fujimoto, Atsushi Hirano, and Kentaro Shiraki. “Ternary
9 system of solution additives with Arginine and salt for refolding of
10 beta-galactosidase”. In: *Protein Journal* 29.3 (2010), pp. 161–166.
- 11 [66] Gasteiger E. et al. “Protein Identification and Analysis Tools on the
12 ExPASy Server”. In: *The Proteomics Protocols Handbook*, Humana
13 Press. Ed. by John M. Walker. Humana Press, 2005, pp. 571–607.
- 14 [67] Paul J. Gates and Norberto P. Lopes. “Characterisation of Flavonoid
15 Aglycones by Negative Ion Chip-Based Nanospray Tandem Mass
16 Spectrometry”. In: *International Journal of Analytical Chemistry*
17 2012 (2012), pp. 1–7.
- 18 [68] Christine L. Gee et al. “Disulfide-linked dimers of human adrenaline
19 synthesizing enzyme PNMT are catalytically active”. In: *Biochimica et Biophysica Acta - Proteins and Proteomics* 1750.1 (June 2005),
21 pp. 82–92.
- 22 [69] Azra Gholami et al. “Natural product biosynthesis in *Medicago*
23 species.” In: *Natural product reports* 31.3 (2014), pp. 356–80.
- 24 [70] S C Gill and P H von Hippel. “Calculation of protein extinction coefficients
25 from amino acid sequence data.” In: *Analytical biochemistry*
26 182.2 (Nov. 1989), pp. 319–326.
- 27 [71] Paola Gilli et al. “Enthalpy-Entropy Compensation in Drug-
28 Receptor Binding”. In: *Journal of Physical Chemistry* 98.5 (Feb.
29 1994), pp. 1515–1518.
- 30 [72] R M Goodrich and R J Braddock. “Major By-Products of the Florida
31 Citrus Processing”. In: *Processing* (2006), pp. 1–4.
- 32 [73] Carmen H. Gray et al. “.alpha.-Deuterium and carbon-13 isotope
33 effects for a simple, intermolecular sulfur-to-oxygen methyl-
34 transfer reaction. Transition-state structures and isotope effects in
35 transmethylation and transalkylation”. In: *Journal of the American
36 Chemical Society* 101.15 (1979), pp. 4351–4358.
- 37 [74] Erich Grotewold. *The Science of Flavonoids The Science of Flavonoids*.
38 Ed. by Erich Grotewold. 1st ed. New York: Springer, 2006, pp. 1–274.
- 39 [75] Amandine Guelorget et al. “Insights into the hyperthermostability
40 and unusual region-specificity of archaeal *Pyrococcus abyssi* tRNA
41 m1A57/58 methyltransferase”. In: *Nucleic Acids Research* 38.18
42 (2010), pp. 6206–6218.

Bibliography

- 1 [76] R. Hegnauer. *The Flavonoids*. Ed. by J. B. Harborne. 1st ed. Vol. 15.
2 Chapman and Hall, 1976, p. 357.
- 3 [77] J L Hoffman. "Chromatographic analysis of the chiral and cova-
4 lent instability of S-adenosyl-L-methionine." In: *Biochemistry* 25.15
5 (1986), pp. 4444–4449.
- 6 [78] Albert Hofmann. *Die Mutterkornalkaloide*. Solothurn: Nachtschat-
7 ten Verlag, 2000.
- 8 [79] E.C. Horning et al. "Liquid chromatograph–mass spectrometer–
9 computer analytical systems". In: *Journal of Chromatography A* 99
10 (Jan. 1974), pp. 13–21.
- 11 [80] Yonglin Hu et al. "Crystal structures of a *Populus tomentosa* 4-
12 coumarate:CoA ligase shed light on its enzymatic mechanisms." In:
13 *The Plant cell* 22.9 (2010), pp. 3093–3104.
- 14 [81] Ze Lin Huang et al. "Deep eutectic solvents can be viable enzyme
15 activators and stabilizers". In: *Journal of Chemical Technology and*
16 *Biotechnology* October 2013 (2014).
- 17 [82] Ruth Huey et al. "Software news and update a semiempirical free
18 energy force field with charge-based desolvation". In: *Journal of*
19 *Computational Chemistry* 28.6 (Apr. 2007), pp. 1145–1152.
- 20 [83] Richard J. Hughes et al. "A tandem mass spectrometric study of
21 selected characteristic flavonoids". In: *International Journal of Mass*
22 *Spectrometry* 210-211 (2001), pp. 371–385.
- 23 [84] Sarah C Hunter and Edgar B Cahoon. "Enhancing vitamin E in
24 oilseeds: unraveling tocopherol and tocotrienol biosynthesis." In:
25 *Lipids* 42.2 (Mar. 2007), pp. 97–108.
- 26 [85] Mwafaq Ibdah et al. "A Novel Mg²⁺-dependent O-Methyltransferase
27 in the Phenylpropanoid Metabolism of *Mesembryanthemum* crys-
28 tallinum". In: *Journal of Biological Chemistry* 278.45 (Nov. 2003),
29 pp. 43961–43972.
- 30 [86] Kabirul Islam et al. "Expanding cofactor repertoire of protein lysine
31 methyltransferase for substrate labeling". In: *ACS Chemical Biology*
32 6.7 (2011), pp. 679–684.
- 33 [87] Tiffany M. Jarrell et al. "Characterization of organosolv switchgrass
34 lignin by using high performance liquid chromatography/high reso-
35 lution tandem mass spectrometry using hydroxide-doped negative-
36 ion mode electrospray ionization". In: *Green Chemistry* 16.5 (2014),
37 p. 2713.
- 38 [88] J M Jez et al. "Structure and mechanism of the evolutionarily unique
39 plant enzyme chalcone isomerase." In: *Nature structural biology* 7.9
40 (2000), pp. 786–791.

- 1 [89] Eun Ji Joe et al. “Engineering of flavonoid O-methyltransferase for
2 a novel regioselectivity.” In: *Molecules and cells* 30.2 (Aug. 2010),
3 pp. 137–41.
- 4 [90] Julien Jorda and Todd O. Yeates. “Widespread disulfide bonding in
5 proteins from thermophilic archaea”. In: *Archaea* 2011 (2011).
- 6 [91] P.D. Josephy, Thomas Eling, and R.P. Mason. “The horseradish
7 peroxidase-catalyzed oxidation of 3, 5, 3’, 5’-tetramethylbenzidine.
8 Free radical and charge-transfer complex intermediates.” In: *Journal
9 of Biological Chemistry* 257.7 (1982), pp. 3669–3675.
- 10 [92] Chandrashekhar P. Joshi and Vincent L. Chiang. “Conserved
11 sequence motifs in plant S-adenosyl-L-methionine-dependent
12 methyltransferases”. In: *Plant Molecular Biology* 37.4 (1998),
13 pp. 663–674.
- 14 [93] Wolfgang Kabsch. “Automatic processing of rotation diffraction
15 data from crystals of initially unknown symmetry land cell con-
16 stants”. In: *Journal of Applied Crystallography* 26.pt 6 (Dec. 1993),
17 pp. 795–800.
- 18 [94] Wolfgang Kabsch. “Integration, scaling, space-group assignment
19 and post-refinement”. In: *Acta Crystallographica Section D: Bio-
20 logical Crystallography* 66.2 (Feb. 2010), pp. 133–144.
- 21 [95] Wolfgang Kabsch. “Xds”. In: *Acta Crystallographica Section D: Bio-
22 logical Crystallography* 66.2 (Feb. 2010), pp. 125–132.
- 23 [96] Jinguo Kang, Larry a Hick, and William E Price. “A fragmentation
24 study of isoflavones in negative electrospray ionization by MS n
25 ion trap mass spectrometry and triple quadrupole mass spectrom-
26 etry”. In: *Rapid Communications in Mass Spectrometry* 21.6 (2007),
27 pp. 857–868.
- 28 [97] Sun-Young Kang et al. “Biosynthesis of methylated resveratrol
29 analogs through the construction of an artificial biosynthetic path-
30 way in *E. coli*.” In: *BMC biotechnology* 14.1 (2014), p. 67.
- 31 [98] Lawrence a Kelley et al. “The Phyre2 web portal for protein model-
32 ing, prediction and analysis.” In: *Nature protocols* 10.6 (June 2015),
33 pp. 845–858.
- 34 [99] Bong Gyu Kim et al. “Multiple regiospecific methylations of a
35 flavonoid by plant O-methyltransferases expressed in *E. coli*”. In:
36 *Biotechnology Letters* 27.23–24 (Dec. 2005), pp. 1861–1864.
- 37 [100] Bong Gyu Kim et al. “Plant Flavonoid O-Methyltransferases: Sub-
38 strate Specificity and Application”. In: *Journal of Plant Biology* 53.5
39 (Sept. 2010), pp. 321–329.
- 40 [101] Bong-Gyu Kim, Eun Ji Joe, and Joong-Hoon Ahn. “Molecular char-
41 acterization of flavonol synthase from poplar and its application to
42 the synthesis of 3-O-methylkaempferol.” In: *Biotechnology letters*
43 32.4 (Apr. 2010), pp. 579–84.

- 1 [102] Dae Hwan Kim et al. “Regiospecific methylation of naringenin
2 to ponciretin by soybean O-methyltransferase expressed in Es-
3 cherichia coli”. In: *Journal of Biotechnology* 119.2 (Sept. 2005),
4 pp. 155–162.
- 5 [103] Min Ji Kim, Bong Gyu Kim, and Joong Hoon Ahn. “Biosynthesis of
6 bioactive O-methylated flavonoids in Escherichia coli”. In: *Applied*
7 *Microbiology and Biotechnology* 97.16 (2013), pp. 7195–7204.
- 8 [104] Saulius Klimasauskas et al. “Hhal methyltransferase flips its target
9 base out of the DNA helix”. In: *Cell* 76.2 (1994), pp. 357–369.
- 10 [105] K M Koeller and C H Wong. “Enzymes for chemical synthesis.” In:
11 *Nature* 409.6817 (Jan. 2001), pp. 232–240.
- 12 [106] Youichi Kondou et al. “cDNA Libraries”. In: *Methods* 729 (2011),
13 pp. 183–197.
- 14 [107] Kristin König. “Engineering of the Anthocyanin Biosynthetic Path-
15 way in Nicotiana benthamiana”. Master. Martin-Luther-Universität
16 Halle-Wittenberg, 2014.
- 17 [108] Frank Koopman et al. “De novo production of the flavonoid narin-
18 genin in engineered *Saccharomyces cerevisiae*.” In: *Microbial cell*
19 *factories* 11 (2012), p. 155.
- 20 [109] Jakub G. Kopycki et al. “Biochemical and Structural Anal-
21 ysis of Substrate Promiscuity in Plant Mg²⁺-Dependent O-
22 Methyltransferases”. In: *Journal of Molecular Biology* 378.1 (Apr.
23 2008), pp. 154–164.
- 24 [110] Fabian Kuhn et al. “Differentiation of isomeric flavone/isoflavone
25 aglycones by MS2 ion trap mass spectrometry and a double neutral
26 loss of CO”. In: *Rapid Communications in Mass Spectrometry* 17.17
27 (2003), pp. 1941–1949.
- 28 [111] Shashank Kumar and Abhay K. Pandey. “Chemistry and Biological
29 Activities of Flavonoids: An Overview”. In: *The Scientific World*
30 *Journal* 2013.7 (2013), pp. 1–16.
- 31 [112] U K Laemmli. “Cleavage of structural proteins during the assem-
32 bly of the head of bacteriophage T4.” In: *Nature* 227.5259 (1970),
33 pp. 680–685.
- 34 [113] L L Lairson et al. “Glycosyltransferases: structures, functions, and
35 mechanisms.” In: *Annual review of biochemistry* 77 (2008), pp. 521–
36 555.
- 37 [114] Brian J. C. Law et al. “Site-specific bioalkylation of rapamycin by
38 the RapM 16-O-methyltransferase”. In: *Chem. Sci.* (2015), pp. 2885–
39 2892.
- 40 [115] Gunhild Layer et al. “Crystal structure of coproporphyrinogen III
41 oxidase reveals cofactor geometry of Radical SAM enzymes”. In:
42 *EMBO Journal* 22.23 (2003), pp. 6214–6224.

Bibliography

- 1 [116] Bobby W K Lee et al. “Enzyme-catalyzed transfer of a ketone group
2 from an S-adenosylmethionine analogue: A tool for the functional
3 analysis of methyltransferases”. In: *Journal of the American Chemical Society* 132.11 (2010), pp. 3642–3643.
- 5 [117] Jong Suk Lee et al. “Identification of flavonoids using liquid chro-
6 matography with electrospray ionization and ion trap tandem mass
7 spectrometry with an MS/MS library”. In: *Rapid Communications in Mass Spectrometry* 19.23 (2005), pp. 3539–3548.
- 9 [118] Effendi Leonard et al. “Expression of a soluble flavone synthase
10 allows the biosynthesis of phytoestrogen derivatives in *Escherichia coli*.” In: *Applied microbiology and biotechnology* 70.1 (Mar. 2006),
12 pp. 85–91.
- 13 [119] Monica Leopoldini et al. “Iron chelation by the powerful antioxidant
14 flavonoid quercetin”. In: *Journal of Agricultural and Food Chemistry*
15 54.17 (2006), pp. 6343–6351.
- 16 [120] Jakob P. Ley et al. “Evaluation of bitter masking flavanones from
17 Herba Santa (*Eriodictyon californicum* (H. & A.) Torr., Hydrophyl-
18 laceae)”. In: *Journal of Agricultural and Food Chemistry* 53.15 (2005),
19 pp. 6061–6066.
- 20 [121] Chen Li et al. “Tandem mass spectrometric fragmentation be-
21 havior of lignans, flavonoids and triterpenoids in *< i>Streblus asper</i>*”. In: *Rapid Communications in Mass Spectrometry* 28.21
23 (2014), pp. 2363–2370.
- 24 [122] Kai Li and J W Frost. “Synthesis of Vanillin from Glucose”. In:
25 7863.Table 1 (1998), pp. 10545–10546.
- 26 [123] Liwei Li et al. “PDBcal: A comprehensive dataset for receptor-ligand
27 interactions with three-dimensional structures and binding ther-
28 modynamics from isothermal titration calorimetry”. In: *Chemical
29 Biology and Drug Design* 71.6 (June 2008), pp. 529–532.
- 30 [124] Manuel Liebeke et al. “Metabolome Analysis of Gram-Positive Bac-
31 teria such as *Staphylococcus aureus* by GC-MS and LC-MS”. In:
32 *Methods in Molecular Biology* 815 (Jan. 2012), pp. 377–398.
- 33 [125] Gordon V. Louie et al. “Structural Determinants and Modulation of
34 Substrate Specificity in Phenylalanine-Tyrosine Ammonia-Lyases”.
35 In: *Chemistry and Biology* 13.12 (2006), pp. 1327–1338.
- 36 [126] Caroline Louis-Jeune, Miguel a. Andrade-Navarro, and Carol Perez-
37 Iratxeta. “Prediction of protein secondary structure from circular
38 dichroism using theoretically derived spectra”. In: *Proteins: Struc-
39 ture, Function and Bioinformatics* 80.2 (Feb. 2012), pp. 374–381.
- 40 [127] J D Lozada-Ramírez et al. “Cloning, overexpression, purification,
41 and characterization of S-adenosylhomocysteine hydrolase from
42 *Corynebacterium efficiens* YS-314.” In: *Biotechnology progress* 24.1
43 (2008), pp. 120–7.

- 1 [128] Liang Lu et al. “A High-Resolution LC-MS-Based Secondary
2 Metabolite Fingerprint Database of Marine Bacteria”. en. In:
3 *Scientific Reports* 4 (Jan. 2014), p. 6537.
- 4 [129] Gražvydas Lukinavičius et al. “Enhanced chemical stability of
5 AdoMet analogues for improved methyltransferase-directed la-
6 beling of DNA”. In: *ACS Chemical Biology* 8.6 (2013), pp. 1134–
7 1139.
- 8 [130] Y L Ma, H V Heuvel, and M Claeys. “Characterization of 3-
9 methoxyflavones using fast-atom bombardment and collision-
10 induced dissociation tandem mass spectrometry.” In: *Rapid com-
11 munications in mass spectrometry : RCM* 13.19 (1999), pp. 1932–
12 42.
- 13 [131] Y. L. Ma et al. “Characterization of flavone and flavonol aglycones
14 by collision-induced dissociation tandem mass spectrometry”. In:
15 *Rapid Communications in Mass Spectrometry* 11.12 (1997), pp. 1357–
16 1364.
- 17 [132] Tom J. Mabry, K. R. Markham, and M. B. Thomas. *The System-
18 atic Identification of Flavonoids*. Berlin, Heidelberg: Springer Berlin
19 Heidelberg, 1970.
- 20 [133] Savvas C Makrides and Savvas C Makrides. “Strategies for Achiev-
21 ing High-Level Expression of Genes in *Escherichia coli*”. In: *Micro-
22 biological reviews* 60.3 (1996), pp. 512–538.
- 23 [134] Sailesh Malla et al. “Production of 7-O-methyl aromadendrin, a
24 medicinally valuable flavonoid, in *Escherichia coli*.” In: *Applied and
25 environmental microbiology* 78.3 (Feb. 2012), pp. 684–94.
- 26 [135] S. V. Mani, D. W. Connell, and R. D. Braddock. “Structure activity re-
27 lationships for the prediction of biodegradability of environmental
28 pollutants”. en. In: *Critical Reviews in Environmental Control* 21.3-4
29 (Jan. 1991), pp. 217–236.
- 30 [136] Raymond E. March and Xiu Sheng Miao. “A fragmentation study
31 of kaempferol using electrospray quadrupole time-of-flight mass
32 spectrometry at high mass resolution”. In: *International Journal of
33 Mass Spectrometry* 231.2-3 (2004), pp. 157–167.
- 34 [137] Raymond March and Jennifer Brodbelt. “Analysis of flavonoids:
35 Tandem mass spectrometry, computational methods, and NMR”.
36 In: *Journal of Mass Spectrometry* 43.12 (Dec. 2008), pp. 1581–1617.
- 37 [138] Nektaria Markoglou and Irving W Wainer. “Biosynthesis in an on-
38 line immobilized-enzyme reactor containing phenylethanolamine
39 N-methyltransferase in single-enzyme and coupled-enzyme for-
40 mats.” In: *Journal of chromatography. A* 948.1-2 (Mar. 2002), pp. 249–
41 56.

Bibliography

- 1 [139] Alexandre Martinière et al. “Development and properties of genet-
2 ically encoded pH sensors in plants.” In: *Frontiers in plant science*
3 4. December (2013), p. 523.
- 4 [140] M McClelland, M Nelson, and E Raschke. “Effect of site-specific
5 modification on restriction endonucleases and DNA modifica-
6 tion methyltransferases.” In: *Nucleic acids research* 22.17 (1994),
7 pp. 3640–3659.
- 8 [141] Airlie J. McCoy. “Solving structures of protein complexes by molec-
9 ular replacement with Phaser”. In: *Acta Crystallographica Section*
10 *D: Biological Crystallography* 63.1 (Jan. 2006), pp. 32–41.
- 11 [142] Airlie J. McCoy et al. “Phaser crystallographic software”. In: *Journal*
12 *of Applied Crystallography* 40.4 (Aug. 2007), pp. 658–674.
- 13 [143] Edoardo Mentasti, Ezio Pelizzetti, and Guido Saini. “Reactions be-
14 tween iron(III) and catechol (o-dihydroxybenzene). Part II. Equi-
15 libria and kinetics of the redox reaction in aqueous acid solution”.
16 en. In: *Journal of the Chemical Society, Dalton Transactions* 23 (Jan.
17 1973), p. 2609.
- 18 [144] Diana Metodiewa et al. “Quercetin may act as a cytotoxic prooxi-
19 dant after its metabolic activation to semiquinone and quinoidal
20 product”. In: *Free Radical Biology and Medicine* 26.1-2 (Jan. 1999),
21 pp. 107–116.
- 22 [145] Gurvan Michel et al. “The structure of the RlmB 23S rRNA methyl-
23 transferase reveals a new methyltransferase fold with a unique
24 knot”. In: *Structure* 10.10 (2002), pp. 1303–1315.
- 25 [146] Ivan Mihel et al. “.alpha.-Deuterium isotope effects and transition-
26 state structure in an intramolecular model system for methyl-
27 transfer enzymes”. In: *Journal of the American Chemical Society*
28 101.15 (July 1979), pp. 4349–4351.
- 29 [147] Douglas Montgomery. *Design and Analysis of Experiments*. 5th ed.
30 New York: John Wiley & Sons, 2008, p. 680.
- 31 [148] Takashi MORISHIGE, Kum-Boo CHOI, and Fumihiko SATO. “In
32 Vivo Bioconversion of Tetrahydroisoquinoline by Recombinant
33 Coclaurine N -Methyltransferase”. In: *Bioscience, Biotechnology and*
34 *Biochemistry* 68.4 (May 2014), pp. 939–941.
- 35 [149] Garrett M. Morris et al. “Software news and updates AutoDock4
36 and AutoDockTools4: Automated docking with selective recep-
37 tor flexibility”. In: *Journal of Computational Chemistry* 30.16 (Dec.
38 2009), pp. 2785–2791.
- 39 [150] Yuri Motorin et al. “Expanding the chemical scope of RNA:methyltransferases
40 to site-specific alkynylation of RNA for click labeling”. In: *Nucleic*
41 *Acids Research* 39.5 (2011), pp. 1943–1952.

Bibliography

- 1 [151] N. Mulinacci et al. "Polyphenolic content in olive oil waste waters
2 and related olive samples". In: *Journal of Agricultural and Food
3 Chemistry* 49.8 (2001), pp. 3509–3514.
- 4 [152] Garib N. Murshudov, Alexei a. Vagin, and Eleanor J. Dodson. "Re-
5 finement of macromolecular structures by the maximum-likelihood
6 method". In: *Acta Crystallographica Section D: Biological Crystal-
7 lography* 53.3 (May 1997), pp. 240–255.
- 8 [153] Janet Newman. "Novel buffer systems for macromolecular crystal-
9 lization". In: *Acta Crystallographica Section D: Biological Crystal-
10 lography* 60.3 (2004), pp. 610–612.
- 11 [154] Novagen. *pET System Manual*. 11th ed. Vol. 123. 2 Pt 1. Darmstadt:
12 EMD Chemicals, 2014, p. 369. arXiv: 1007.2303v3.
- 13 [155] Zouhaier B Ouallagui et al. "Valorization of Olive Processing By-
14 Products : Characterization , Investigation of Chemico-Biological
15 Activities and Identification of Active Compounds". In: 64 (2012),
16 pp. 61–64.
- 17 [156] Javier Palazón et al. "Application of metabolic engineering to the
18 production of scopolamine." In: *Molecules (Basel, Switzerland)* 13.8
19 (Jan. 2008), pp. 1722–42.
- 20 [157] Ira Palmer and Paul T. Wingfield. "Preparation and extraction of in-
21 soluble (Inclusion-body) proteins from Escherichia coli". In: *Current
22 Protocols in Protein Science* 1.SUPPL.70 (Nov. 2012), Unit6.3.
- 23 [158] Wibke Peters et al. "Enzymatic site-specific functionalization of
24 protein methyltransferase substrates with alkynes for click label-
25 ing". In: *Angewandte Chemie - International Edition* 49.30 (2010),
26 pp. 5170–5173.
- 27 [159] Eric F. Pettersen et al. "UCSF Chimera - A visualization system for
28 exploratory research and analysis". In: *Journal of Computational
29 Chemistry* 25.13 (2004), pp. 1605–1612.
- 30 [160] Harold R. Powell. "The Rossmann Fourier autoindexing algorithm
31 in MOSFLM". In: *Acta Crystallographica Section D: Biological Crys-
32 tallography* 55.10 (1999), pp. 1690–1695.
- 33 [161] O. Rigbers and S.-M. Li. "Ergot Alkaloid Biosynthesis in As-
34 pergillus fumigatus: OVERPRODUCTION AND BIOCHEMICAL
35 CHARACTERIZATION OF A 4-DIMETHYLALLYLTRYPTOPHAN
36 N-METHYLTRANSFERASE". In: *Journal of Biological Chemistry*
37 283.40 (Aug. 2008), pp. 26859–26868.
- 38 [162] K D Robertson. "DNA methylation, methyltransferases, and cancer."
39 In: *Oncogene* 20.24 (2001), pp. 3139–3155.
- 40 [163] Keith D Robertson. "DNA methylation and human disease." In:
41 *Nature reviews. Genetics* 6.8 (2005), pp. 597–610.

- 1 [164] M. G. Rossmann and D. M. Blow. "The detection of sub-units within
2 the crystallographic asymmetric unit". In: *Acta Crystallographica*
3 15.1 (Jan. 1962), pp. 24–31.
- 4 [165] Michael G. Rossmann. "Molecular replacement - Historical back-
5 ground". In: *Acta Crystallographica - Section D Biological Crystal-*
6 *lography* 57.10 (Sept. 2001), pp. 1360–1366.
- 7 [166] Rainer Rudolph and Hauke Lilie. "In vitro folding of inclusion body
8 proteins". In: *The FASEB Journal* 10.1 (1996), pp. 49–56.
- 9 [167] J Sambrook and D W Russell. *Molecular Cloning: A Laboratory Man-*
10 *ual*. 3rd ed. Cold Spring Harbor (NY, USA): Cold Spring Harbor
11 Laboratory Press, 2001.
- 12 [168] Cleydson Breno R Santos et al. "A SAR and QSAR study of new
13 artemisinin compounds with antimalarial activity". In: *Molecules*
14 19.1 (2014), pp. 367–399.
- 15 [169] Yuji Sawada and Masami Yokota Hirai. *Integrated LC-MS / MS sys-*
16 *tem for plant metabolomics*. en. May 2013.
- 17 [170] Artur Sawicki and Robert D Willows. "S-adenosyl-L-methionine:magnesium-
18 protoporphyrin IX O-methyltransferase from Rhodobacter capsu-
19 latus: mechanistic insights and stimulation with phospholipids."
20 In: *The Biochemical journal* 406.3 (2007), pp. 469–478.
- 21 [171] Jason W. Schmidberger et al. "Halomethane biosynthesis: Struc-
22 ture of a SAM-dependent halide methyltransferase from arabidop-
23 sis thaliana". In: *Angewandte Chemie - International Edition* 49.21
24 (2010), pp. 3646–3648.
- 25 [172] Gudrun Schröder et al. "Flavonoid methylation: A novel 4'-O-
26 methyltransferase from Catharanthus roseus, and evidence that
27 partially methylated flavanones are substrates of four different
28 flavonoid dioxygenases". In: *Phytochemistry* 65.8 (2004), pp. 1085–
1094.
- 30 [173] H L Schubert et al. "The X-ray structure of a cobalamin biosyn-
31 thetic enzyme, cobalt-precorrin-4 methyltransferase." In: *Nature*
32 *structural biology* 5.7 (1998), pp. 585–592.
- 33 [174] Heidi L. Schubert, Robert M. Blumenthal, and Xiaodong Cheng.
34 "Many paths to methyltransfer: A chronicle of convergence". In:
35 *Trends in Biochemical Sciences* 28.6 (2003), pp. 329–335.
- 36 [175] Daniela Schulz, Josephin Marie Holstein, and Andrea Rentmeister.
37 "A chemo-enzymatic approach for site-specific modification of
38 the RNA cap". In: *Angewandte Chemie - International Edition* 52.30
39 (2013), pp. 7874–7878.
- 40 [176] N. Schweigert, a. JB Zehnder, and R. I L Eggen. "Chemical properties
41 of catechols and their molecular modes of toxic action in cells, from
42 microorganisms to mammals". In: *Environmental Microbiology* 3.2
43 (2001), pp. 81–91.

- 1 [177] Mark S. Searle, Martin S. Westwell, and Dudley H. Williams. “Application of a generalised enthalpy-entropy relationship to binding co-operativity and weak associations in solution”. en. In: *Journal of the Chemical Society, Perkin Transactions 2* 1 (Jan. 1995), p. 141.
- 5 [178] S K Shapiro and D J Ehninger. “Methods for the analysis and preparation of adenosylmethionine and adenosylhomocysteine.” In: *Analytical biochemistry* 15.2 (May 1966), pp. 323–333.
- 8 [179] Y. Q. Shi and R. R. Rando. “Kinetic mechanism of isoprenylated protein methyltransferase”. In: *Journal of Biological Chemistry* 267.14 (1992), pp. 9547–9551.
- 11 [180] Alexander Ann Shulgin. *Tihkal: The Continuation*. Ed. by Dan Joy. 1st ed. Berkeley: Transform Press, 1997, p. 804.
- 13 [181] Sigma-Aldrich. *Technical Bulletin no. 2003-03: freezing of microbial samples prior to testing*. Parenteral Drug Association. 2003.
- 15 [182] Simon A. Simms and Kotha Subbaramaiah. “Kinetic Mechanism of the CheR Methyltransferase”. In: *Journal of Biological Chemistry* 266.19 (1991), pp. 12741–12746.
- 18 [183] Henrik T. Simonsen et al. “Methylenedioxy- and methoxyflavones from Melicope coodeana syn. Euodia simplex”. In: *Phytochemistry* 60.8 (Aug. 2002), pp. 817–820.
- 21 [184] Shanteri Singh et al. “Facile chemoenzymatic strategies for the synthesis and utilization of S-adenosyl-L-methionine analogues”. In: *Angewandte Chemie - International Edition* 53.15 (2014), pp. 3965–3969.
- 25 [185] Lekha Sleno and Dietrich a. Volmer. “Ion activation methods for tandem mass spectrometry”. In: *Journal of Mass Spectrometry* 39.10 (2004), pp. 1091–1112.
- 28 [186] Qingqing Song et al. “Potential of hyphenated ultra-high performance liquid chromatography-scheduled multiple reaction monitoring algorithm for large-scale quantitative analysis of traditional Chinese medicines”. In: *RSC Adv.* 5.71 (2015), pp. 57372–57382.
- 32 [187] Harald Stecher et al. “Biocatalytic Friedel-Crafts alkylation using non-natural cofactors”. In: *Angewandte Chemie - International Edition* 48.50 (Jan. 2009), pp. 9546–9548.
- 35 [188] Anna Winona Struck et al. “S-Adenosyl-Methionine-Dependent Methyltransferases: Highly Versatile Enzymes in Biocatalysis, Biosynthesis and Other Biotechnological Applications”. In: *Chem-BioChem* 13.18 (Nov. 2012), pp. 2642–2655.
- 39 [189] F William Studier. “Protein production by auto-induction in high density shaking cultures.” In: *Protein expression and purification* 41.1 (May 2005), pp. 207–234. arXiv: NIHMS150003.

Bibliography

- 1 [190] Fusao Takusagawa et al. “Crystal Structure of S -Adenosylmethionine
2 Synthetase ”. In: 271.1 (1996), pp. 136–147.
- 3 [191] Loverine P Taylor and Erich Grotewold. “Flavonoids as develop-
4 mental regulators.” In: *Current opinion in plant biology* 8.3 (June
5 2005), pp. 317–23.
- 6 [192] Martin Tengg et al. “Molecular characterization of the C-methyltransferase
7 NovO of Streptomyces sphaeroides, a valuable enzyme for perform-
8 ing Friedel-Crafts alkylation”. In: *Journal of Molecular Catalysis B:*
9 *Enzymatic* 84 (Dec. 2012), pp. 2–8.
- 10 [193] David J Thomas et al. “Arsenic (+3 Oxidation State) Methyltrans-
11 ferase and the Methylation of Arsenicals”. In: *Experimental biology*
12 and medicine (Maywood, N.J.) 232.1 (Jan. 2007), pp. 3–13.
- 13 [194] Marie Thomsen et al. “Chemoenzymatic synthesis and in situ
14 application of S-adenosyl-L-methionine analogs.” In: *Organic &*
15 *biomolecular chemistry* 11.43 (2013), pp. 7606–10.
- 16 [195] Robert Tibshirani. *Regression Selection and Shrinkage via the Lasso*.
17 1994.
- 18 [196] Dominique a Tobbell et al. “Identification of in vitro folding condi-
19 tions for procathepsin S and cathepsin S using fractional factorial
20 screens.” In: *Protein expression and purification* 24.2 (Mar. 2002),
21 pp. 242–254.
- 22 [197] Jaime Torres-Corzo, Roberto Rodríguez-Della Vecchia, and
23 Leonardo Rangel-Castilla. *Observation of the ventricular system*
24 and *subarachnoid space in the skull base by flexible neuroendoscopy: normal structures*. 1st ed. Vol. 141. 2. New York: Garland Science,
25 2009, pp. 165–168.
- 27 [198] Emmanouil a. Trantas et al. “When plants produce not enough or
28 at all: metabolic engineering of flavonoids in microbial hosts”. In:
29 *Frontiers in Plant Science* 6.January (2015), pp. 1–16.
- 30 [199] Oleg Trott and Arthur J. Olson. “Software news and update
31 AutoDock Vina: Improving the speed and accuracy of docking with
32 a new scoring function, efficient optimization, and multithreading”.
33 In: *Journal of Computational Chemistry* 31.2 (Jan. 2010), pp. 455–
34 461.
- 35 [200] Kouhei Tsumoto et al. “Role of arginine in protein refolding, solu-
36 bilization, and purification.” In: *Biotechnology progress* 20.5 (2004),
37 pp. 1301–1308.
- 38 [201] P. Urban et al. “Characterization of recombinant plant cinnamate
39 4-hydroxylase produced in yeast - Kinetic and spectral proper-
40 ties of the major plant P450 of the phenylpropanoid pathway”. In:
41 *European Journal of Biochemistry* 222.3 (1994), pp. 843–850.

Bibliography

- 1 [202] Alexei a. Vagin et al. “REFMAC5 dictionary: Organization of prior
2 chemical knowledge and guidelines for its use”. en. In: *Acta Crystal-*
3 *lographica Section D: Biological Crystallography* 60.12 I (Nov. 2004),
4 pp. 2184–2195.
- 5 [203] Jacob L. Venzie et al. “Electron-impact and glow-discharge ion-
6 ionization LC-MS analysis of green tea tincture”. In: *Analytical and*
7 *Bioanalytical Chemistry* 387.1 (2007), pp. 321–333.
- 8 [204] J Vidgren, L a Svensson, and a Liljas. “Crystal structure of catechol
9 O-methyltransferase.” In: *Nature* 368.6469 (1994), pp. 354–358.
- 10 [205] Renaud Vincentelli et al. “High-throughput automated refolding
11 screening of inclusion bodies.” In: *Protein science : a publication of*
12 *the Protein Society* 13.10 (2004), pp. 2782–2792.
- 13 [206] Thomas Vogt. “Regiospecificity and kinetic properties of a plant nat-
14 ural product O-methyltransferase are determined by its N-terminal
15 domain”. In: *FEBS Letters* 561.1-3 (Mar. 2004), pp. 159–162.
- 16 [207] Thomas Vogt. “Regiospecificity and kinetic properties of a plant nat-
17 ural product O-methyltransferase are determined by its N-terminal
18 domain”. In: *FEBS Letters* 561.1-3 (Mar. 2004), pp. 159–162.
- 19 [208] Rui Wang et al. “Formulating a fluorogenic assay to evaluate S-
20 adenyl-L-methionine analogues as protein methyltransferase co-
21 factors”. In: *Molecular BioSystems* 7.11 (2011), p. 2970.
- 22 [209] Rui Wang et al. “Labeling substrates of protein arginine methyl-
23 transferase with engineered enzymes and matched S-adenosyl-l-
24 methionine analogues”. In: *Journal of the American Chemical Soci-
25 ety* 133.20 (2011), pp. 7648–7651.
- 26 [210] Williard J. Werner et al. “In vitro phosphinate methylation by PhpK
27 from Kitasatospora phosalacinea”. In: *Biochemistry* 50.42 (2011),
28 pp. 8986–8988.
- 29 [211] Ludger a. Wessjohann et al. “Alkylating enzymes”. In: *Current Opin-
30 ion in Chemical Biology* 17.2 (Mar. 2013), pp. 229–235.
- 31 [212] C M Whitehouse et al. “Electrospray interface for liquid chro-
32 matographs and mass spectrometers.” In: *Analytical chemistry* 57.3
33 (Mar. 1985), pp. 675–679.
- 34 [213] Christine a Williams and Renee J Grayer. “Anthocyanins and other
35 flavonoids.” In: *Natural product reports* 21.4 (2004), pp. 539–573.
- 36 [214] Melissa Swope Willis et al. “Investigation of protein refolding using
37 a fractional factorial screen: a study of reagent effects and interac-
38 tions.” In: *Protein science : a publication of the Protein Society* 14.7
39 (2005), pp. 1818–1826.
- 40 [215] Sophie Willnow et al. “A Selenium-Based Click AdoMet Analogue
41 for Versatile Substrate Labeling with Wild-Type Protein Methyl-
42 transferases”. In: *ChemBioChem* 13.8 (2012), pp. 1167–1173.

Bibliography

- 1 [216] Martyn D. Winn et al. "Overview of the CCP4 suite and current de-
2 velopments". In: *Acta Crystallographica Section D: Biological Crys-*
3 *tallography* 67.4 (Apr. 2011), pp. 235–242.
- 4 [217] Jaclyn M. Winter et al. "Expanding the structural diversity of
5 polyketides by exploring the cofactor tolerance of an inline methyl-
6 transferase domain". In: *Organic Letters* 15.14 (2013), pp. 3774–
7 3777.
- 8 [218] Tomasz Włodarski et al. "Comprehensive structural and substrate
9 specificity classification of the *Saccharomyces cerevisiae* methyl-
10 transferome". In: *PLoS ONE* 6.8 (2011).
- 11 [219] Sebastian Wolf et al. "In silico fragmentation for computer assisted
12 identification of metabolite mass spectra." In: *BMC Bioinformatics*
13 11 (2010), p. 148.
- 14 [220] J.-L. Wolfender et al. "Evaluation of Q-TOF-MS/MS and multiple
15 stage IT-MSn for the Dereplication of Flavonoids and Related Com-
16 pounds in Crude Plant Extracts". In: *Analisis* 28.10 (Dec. 2000),
17 pp. 895–906.
- 18 [221] Eckhard Wollenweber. "On the occurrence of acylated flavonoid
19 aglycones". In: *Phytochemistry* 24.7 (1985), pp. 1493–1494.
- 20 [222] R W Woodard et al. "Stereochemical Course of the Transmethylation
21 Catalyzed by Catechol O-Methyltransferase". In: *The Journal
22 of Biological Chemistry* 255.19 (1980), pp. 9124–9127.
- 23 [223] Ronald W Woodard et al. "Stereochemistry of Indolmycin Biosyn-
24 thesis. Steric Course of C- and N-Methylation Reactions". In:
25 *Journal of the American Chemical Society* 102.20 (1980), pp. 6314–
26 6318.
- 27 [224] B. Xiao et al. "Structure and catalytic mechanism of the human
28 histone methyltransferase SET7/9". In: 421.February (2003).
- 29 [225] Hiroshi Yamaguchi and Masaya Miyazaki. "Refolding techniques for
30 recovering biologically active recombinant proteins from inclusion
31 bodies." In: *Biomolecules* 4.1 (2014), pp. 235–51.
- 32 [226] William C Yee, Susan J Eglsær, and William R Richards. "Confirma-
33 tion of a ping-pong mechanism for S-adenosyl-L-methionine:magnesium
34 protoporphyrin methyltransferase of etiolated wheat by an ex-
35 change reaction." In: *Biochemical and biophysical research commu-*
36 *nications* 162.1 (1989), pp. 483–490.
- 37 [227] E. G. Yordi et al. "Antioxidant and Pro-Oxidant Effects of Polyphe-
38 nolic Compounds and Structure-Activity Relationship Evidence".
39 In: *Nutrition, Well-Being and Health* (2012), pp. 23–48.
- 40 [228] Yoon Youngdae et al. "Characterization of an O-methyltransferase
41 from *Streptomyces avermitilis* MA-4680". In: *Journal of Microbiol-*
42 *ogy and Biotechnology* 20.9 (2010), pp. 1359–1366.

Bibliography

- 1 [229] Changsheng Zhang et al. “Natural product diversification using
2 a non-natural cofactor analogue of S-adenosyl-L-methionine”. In:
3 *Journal of the American Chemical Society* 128.9 (2006), pp. 2760–
4 2761.
- 5 [230] Qi Zhang and Wilfred A van der Donk. “Catalytic promiscuity of
6 a bacterial α -N-methyltransferase.” In: *FEBS letters* 586.19 (Sept.
7 2012), pp. 3391–7.
- 8 [231] Qi Zhang, Wilfred A. van der Donk, and Wen Liu. “Radical-Mediated
9 Enzymatic Methylation: A Tale of Two SAMS”. In: *Accounts of
10 Chemical Research* 45.4 (Apr. 2012), pp. 555–564.
- 11 [232] Xing-Hai Zhang and C. C. Chinnappa. “Molecular characterization
12 of a cDNA encoding caffeoyl-coenzyme A 3-O-methyltransferase
13 of *Stellaria longipes*”. In: *Journal of Biosciences* 22.2 (Mar. 1997),
14 pp. 161–175.
- 15 [233] Jian Min Zhou et al. “Sequential O-methylation of tricetin by a
16 single gene product in wheat”. In: *Biochimica et Biophysica Acta -
17 General Subjects* 1760.7 (2006), pp. 1115–1124.
- 18 [234] Saijie Zhu et al. “Efficient synthesis of eriodictyol from l-tyrosine in
19 *escherichia coli*”. In: *Applied and Environmental Microbiology* 80.10
20 (2014), pp. 3072–3080.
- 21 [235] Chloe Zubieta et al. “Structural Basis for the Modulation of Lignin
22 Monomer Methylation by Caffeic Acid / 5-Hydroxyferulic Acid 3 /
23 5- O -Methyltransferase”. In: *The Plant Cell* 14.June (2002), pp. 1265–
24 1277.
- 25 [236] C Zubieta et al. “Structures of two natural product methyl-
26 transferases reveal the basis for substrate specificity in plant
27 O-methyltransferases.” In: *Nature structural biology* 8.3 (Mar.
28 2001), pp. 271–279.

1 Acronyms

2 Å Ångström, 0.1 nm

3 3O4M 3'-hydroxy-4'-methoxy

4 4CL 4-coumarate:CoA ligase

5 4O3M 4'-hydroxy-3'-methoxy

6 ABPP activity based protein profiling

7 AC-9 anthracene-9-carboxylic acid

8 AI auto-induction 90, *see* ZYP-5052

9 ANOVA Analysis of Variance

10 APCI atmospheric pressure chemical ionisation

11 ATP adenosine triphosphate

12 AUC area under the curve

13 BisTris 2-[Bis(2-hydroxyethyl)amino]-2-(hydroxymethyl)propane-1,3-diol

14 B-PER bacterial protein extraction reagent

15 C4H cinnamate-4-hydroxylase

16 CBD cobalamin binding domain

17 CCoAOMT caffeoyl CoA dependent *O*-methyltransferase

18 CCP4 Collaborative Computational Project No. 4

19 CD circulary dichroism

20 CHI chalcone isomerase

21 CHS chalcone synthase

22 CID collision induced dissociation

23 C-MT *C*-methyl transferase

24 CoA coenzyme A

25 COMT catechol O-methyl transferase

26 Coot Crystallographic Object-Oriented Toolkit

27 CV column volumes

28 dAdo 5'-deoxyadenosyl

29 DMSO dimethyl sulfoxide

30 DNA desoxyribonucleic acid

- 1 DNA-MT** DNA methyl transferase
2 DoE design of experiments
3 DTT dithiothreitol; (2S,3S)-1,4-bis(sulfanyl)butane-2,3-diol
4 EDTA ethylenediaminetetraacetic acid
5 EEC enthalpy-entropy compensation
6 EI electron ionization
7 ESI electrospray ionization
8 F3H flavanone-3-hydroxylase
9 FNS flavone synthase
10 FPLC fast protein liquid chromatography
11 FrFD fractional factorial design
12 FT Fourier transformation
13 FTMS Fourier transform mass spectrometry
14 GdmCl guanidinium hydrochloride
15 GFP green fluorescent protein
16 GOD glucose oxidase
17 GSH glutathione, γ -L-glutamyl-L-cysteinylglycine
18 GSSG glutathione disulfide
19 GST Glutathion S-transferase
20 HCD higher-energy collisional dissociation
21 HEPES 2-[4-(2-hydroxyethyl)piperazin-1-yl]ethanesulfonic acid
22 H-ESI heated-electrospray ionization
23 HIC hydrophobic interaction chromatography
24 HPLC high-performance liquid chromatography
25 HRP horseradish peroxidase
26 IB inclusion body
27 IEX ion exchange chromatography
28 IFS isoflavone synthase
29 IMAC immobilized metal affinity chromatography
30 IPB Leibniz-Institute of Plant Biochemistry
31 IPTG isopropyl-D-thiogalactopyranosid
32 ITC Isothermal Titration Calorimetry
33 LB lysogeny broth
34 LC liquid chromatography
35 LC/MS liquid chromatography coupled mass-spectrometry
36 LC-MS/MS liquid chromatography-tandem mass spectrometry

Acronyms

- 1 *m/z*** mass-to-charge ratio
2 ME-plot main effects plot
3 MES 2-(*N*-morpholino)ethanesulfonic acid
4 MLU Martin-Luther-Universität
5 MMT L-malic acid/MES/Tris
6 MR molecular replacement
7 MS/MS tandem mass-spectrometry
8 MT methyl transferase
9 MTP micro-titer plate
10 MW molecular weight
11 MWCO molecular weight cut-off
12 NADES natural deep eutectic solvent
13 NCE normalized collision energy
14 *N*-MT *N*-methyl transferase
15 nos nopaline synthase
16 NPS nitrogen, phosphate, sulfate buffer
17 NRPS non-ribosomal peptide synthase
18 NTA nitrilo triacetic acid
19 *O*-MT *O*-methyl transferase
20 PAGE polyacrylamide gel electrophoresis
21 PAL phenylalanine ammonia-lyase
22 PBS phosphate buffered saline
23 PCA principal component analysis
24 PCH propane-1,2-diol/choline chloride,natural deep eutectic solvent (NADES)-mixture
26 PCR polymerase chain reaction
27 PDA photo diode array
28 PDB Protein Data Base 44, 45
29 PFOMT phenylpropanoid and flavonoid O-methyl transferase
30 PHENIX Phyton-based Hierachial Environment for Integrated Xtallography
31 PKS poly ketide synthase
32 PMSF phenylmethylsulfonylfluoride
33 P-MT protein methyl transferase
34 QSAR quantitative structure activity relationship
35 rmsd root mean squared deviation
36 RNA-MT RNA methyl transferase
37 ROS reactive oxygen species

Acronyms

- 1 RP** resolving power
2 rRNA ribosomal ribonucleic acid
3 RSMT radical SAM methyl transferase
4 RT room temperature
- 5 SAE** *S*-adenosyl-L-ethionine, (2*S*)-2-amino-4-[[*(2S,3S,4R,5R)*-5-(6-aminopurin-9-yl)-3,4-dihydroxyoxolan-2-yl]methyl-ethylsulfonio]butanoat
6 SAH *S*-adenosyl-L-homocysteine
8 SAM *S*-adenosyl-L-methionine
9 SAMS *S*-adenosylmethionine synthase
10 SAR structure activity relationship
11 SDS sodium dodecylsulfate
12 SeAM *Se*-adenosyl selenomethionine
13 SET suvar3-9, enhancer-of-zeste, trithorax
14 SID surface-induced dissociation
15 smMT small molecule methyl transferase
16 S-MT S-methyl transferase
17 SOMT-2 soy O-methyl transferase
18 SPOUT *SpoU-TrmD*
19 SSG succinate/sodium phosphate/glycine
- 20 TB** terrific broth
21 TCA trichloro acetic acid
22 Ti-plasmid tumor inducing plasmid
23 Tris tris(hydroxymethyl)-aminomethane
- 24 U** enzyme unit; measure for enzymatic activity ($1\text{ U} = 1\text{ }\mu\text{mole/min} = 1/60\text{ }\mu\text{kat}$)
25 UDP uridine diphosphate
26 UHPLC ultra-high performance liquid chromatography
27 UV ultra violet
28 UV/VIS ultra violet/visible (light spectrum)
29 V volume
- 30 ZYP** N-Z-amine, yeast extract, phosphate 37, 160, 161, *see* ZYP-5052

Glossary

2 His₆-tag Hexa-histidine tag commonly used for recombinant protein production.

3 PFOMT Phenylpropanoid and flavonoid O-methyl transferase from *Mesembryanthemum crystallinum*, which was first described by Ibdah et al. in 2003 [85]

5 T7-tag Initial 11 amino acids of the T7 gene 10 protein.

6 Ti-plasmid Commonly found plasmids in *A. tumefaciens* and *A. rhizogenes* that confer virulence

8 Trx-tag Thioredoxin tag used to increase solubility and stability of recombinantly expressed proteins.

10 ZYP-5052 Autoinduction medium developed by Studier [189]. The naming stems from the components N-Z-amine, yeast extract and phosphate. The numbering designates the composition; e.g. 5052 refers to 0.5 % glycerol, 0.05 % glucose and 0.2 % lactose. 160